The search for an ionospheric model suitable for real-time applications in HF radio communications.

Thesis

Submitted in fulfilment of the requirements for the degree of

Master of Science by Research

of Rhodes University.

by

CHRISTOPHER CROSSLEY MERCER

December 1993

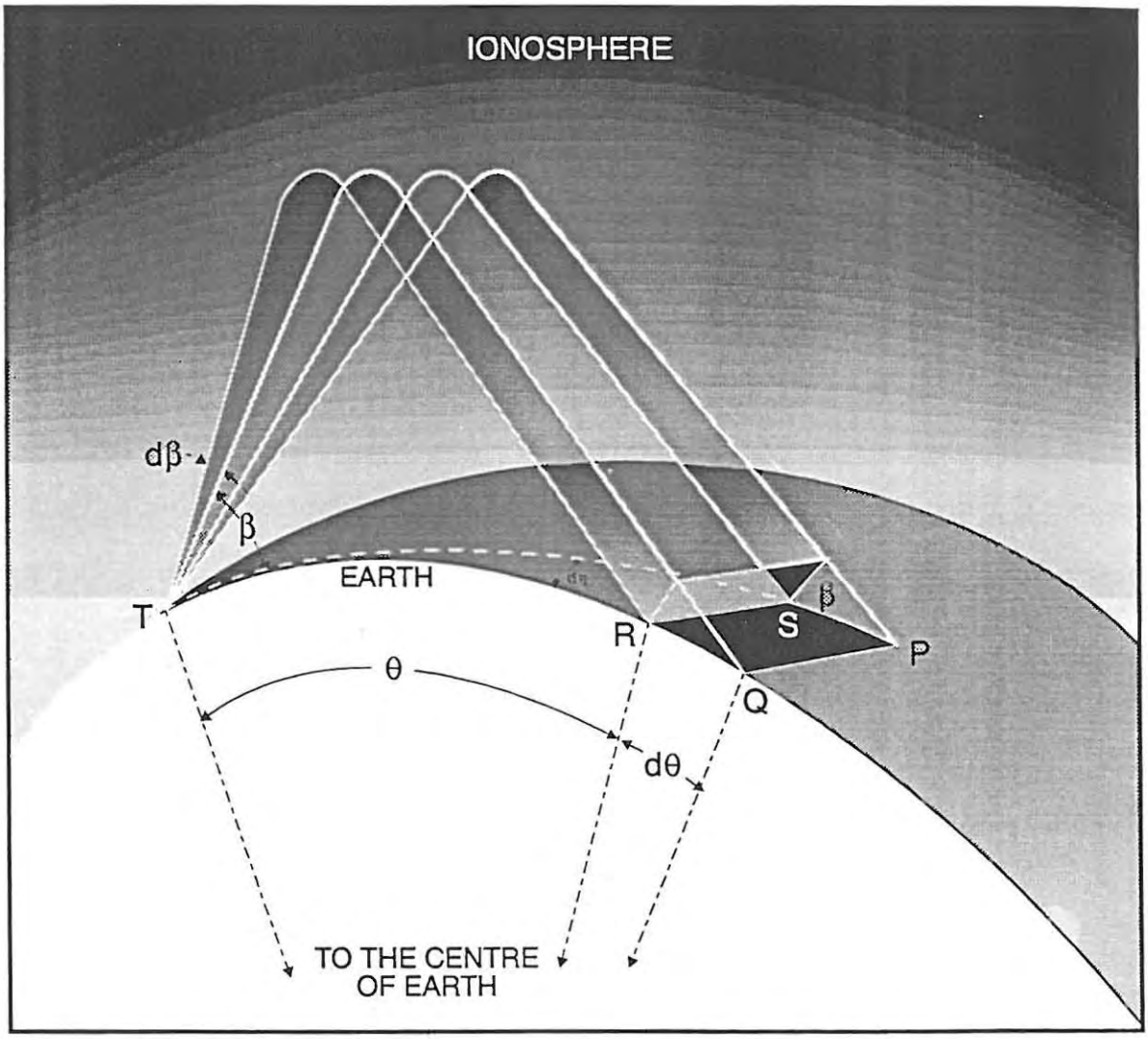

IONOSPHERIC RADIO PROPAGATION OF A HF SIGNAL OVER THE SURFACE OF THE EARTH.

Author's note

It is the belief of the author that the development of an **analytical** model for the F1 ledge condition using multi-quasiparabolic segments (MQPS) constitutes original work. This note of originality refers specifically to the development of;

(a) the gradient algorithm used to determine the location of the point of inflexion, d^2n/dh^2, that is characteristic of the F1 ledge condition.

(b) a mathematical model for the F1 ledge/F2 layer bridging geometry that utilizes only analytical methods.

(c) non-numerical algorithms that permit **real-time** determination of the F1 ledge/F2 layer joining geometry and requiring the following data inputs;

(1) the inflexion point information derived via the gradient algorithm aforementioned in section (a) ,

(2) the ionospheric layer coefficients (A,B,C) embodying the, semi-thickness, critical frequency and height of the electron density maximum for the F2 layer, and

(3) the corresponding (A,B,C) coefficients describing the F1 region modelled as a pseudo-layer,

where the values of (A,B,C) are determined via least squares curve-fitting algorithms applied to ionospheric real height data.

(d) a novel method of implementing Gaussian least squares that allows one to curve fit a quasiparabolic section to a F1 ledge of ionization to within a r.m.s. error of less than 0.5% when using a standard 386 PC, Mercer and Poole (1993).

For Susan

When one door closes, another opens; but we often look so long and so regretfully upon the closed door that we do not see the one which has opened for us.

Alexander Graham Bell

Acknowledgements

I wish to express my gratitude to the Council for Scientific and Industrial Research for giving me the opportunity to submit my research work so that I might gain a higher University degree. I am indebted to my advisor Dr. W.V. Poole, director of HOIA, Rhodes University in Grahamstown for his guidance and encouragement throughout the course of my research project When help was needed Dr Poole gave unstintingly of his time while nevertheless ensuring that I cultivated the ability to develop my own ideas and skills. I thoroughly enjoyed the many thought provoking hours that we spent discussing how one might quantify the vagaries of the ionosphere and it was a slow lesson for me that the results of experimental observation should not give way to the beauty of mathematics!

To my colleague, Mr Erik Eloff, I extend a hearty thankyou for all his efforts during the long hours we spent battling through the endless lines of the "C" code that were to form the backbone of the project, "Real Prop". Erik showed great dedication in his willingness to pursue the task of de-bugging the source code down to the last "byte" and he was always eager to share a challenge.

I would like to thank Mr Andries Delport for his continual support throughout the course of my research work, both in his rôle as financial administrator for the project and as the resident expert in HF direction finding techniques.

It is with pleasure that I acknowledge the assistance given to me by Mr Wim Eek who spent endless hours teaching me the intricacies of Word Perfect and computer graphics. I also wish to thank the Eek family for their warmth and hospitality during the many ocassions

that I banged the night away on Wim's keyboard and for tolerating my presence until the wee hours of the morning!

To Mrs Gale Demmer and Mrs Annette Coetzee I would like to offer my sincere thanks for their Herculean efforts in the "typing department" and for the many laughs we had along the way as we wrestled with Murphy's Laws applied to the word processor.

Finally on a personel note I wish to express my deepest thanks to Susan whose sacrifice and encouragement made the completion of this project possible.

Table of Contents

CHAPTER (1)

INTRODUCTION:

The decision to fund this M.Sc. project was made early in 1991 when Mikomtek, CSIR, decided to re-kindle the research activities of the HF group, then resident within the now defunct Department of Radio Communications. Based upon an in-depth study of the contemporary advances in HF propagation prediction techniques and of the software packages then extant on the South African market, it was realized that CSIR needed to invest in developing the expertise of its radio planning personnel if it was to secure an independent competitive edge in the area of real-time HF frequency forecasting. The research project was given the abbreviated name "Real Prop" and the study was required to address three niche markets within the South African HF radio user community, namely

(a) real time frequency prediction, referred to as "now-casting", for basic HF communications;

(b) the generation of real time ionospheric layer data to provide driver inputs to a HF direction finding single site location (HFDFSSL) system;

and

(c) the development of a dynamic HF spectrum management system for use by the South African frequency allocation body.

STATEMENT OF WORK:

In essence the research work was to focus on the development of an ionospheric model suitable for real time HF frequency prediction and direction finding applications. The modelling of the ionosphere had to be generic in nature, sufficient to ensure that the CSIR could simultaneously secure commercial competitiveness in each of the three niche market areas aforementioned, while requiring only minimal changes to software architecture in the case of each application. A little research quickly showed that the development of an ionospheric model capable of driving a HFDFSSL system in "real time" would result in one having to make only slight re-structuring of the software to facilitate application of the same model in the areas of real time frequency prediction and spectrum management. The decision made at the outset of the project to slant the research toward the development of a model best suited for HF direction finding applications is reflected in the avenues followed during the course of the modelling process.

PLAN OF ATTACK:

To accomplish the end goal of a generic real time ionospheric model it was decided, for the following reasons, that the project should be carried out in three strictly defined stages;

(a) to establish structure and discipline within the sphere of the research activity, by having a defined deliverable goal or milestone at the end of each phase;

(b) that each phase be concluded with a tangible product reflecting the investment of the CSIR either in the form of enhanced expertise and/or a commercially viable software package.

THE THREE STAGES OF THE PROJECT:

STAGE 1: The literature search

The first phase of Real Prop required carrying out a chronological literature survey of the research and development of ionospheric modelling techniques as used in the development of software packages for HF frequency prediction. The main aim of the survey was to establish, from the published literature, the most versatile ionospheric model that would be suitable for real time HF frequency applications. However, it soon came to light that a very large body of the literature on ionospheric research concentrated on the development of synoptic modelling techniques as applied to long and medium term HF forecasting while the issue of real time modelling was addressed only in the most recent of publications. The dearth of information was further compounded by the fact that research projects focused on real time HF propagation assessment are often classified in nature and any published literature reflects sparce detail. In essence the literature survey resulted in a thorough analysis of the results of the real time modelling studies carried out by D.C. Baker et al in South Africa, P.L. Dyson et al in Australia and to a lesser extent L.F. McNamara in the United States, ref: thesis bibliography.

STAGE 2 : **The development of a generic ionospheric model suitable for multi-user applications.**

In the second phase of Real Prop the selected generic ionospheric model had to be matched to observed electron density data and the physical and mathematical accuracy of the modelling process tested using propagation simulation algorithms. It was required that one be able to analytically ray trace through the encoded ionospheric model, the parameters of which had to have been derived from recorded ionogrammetric data gathered by the CSIR, IPS-42 Kel Aerospace ionosonde, sited near Johannesburg. The model simulation of the HF oblique link was to include the ability to determine the typical circuit and model parameters required by a radio user, namely,

(1) maximum usable frequency or MUF under varying conditions of ground range and elevation angle,

(2) graphical display of the HF radio locus and the determination of ray path geometry under varying ionospheric conditions,

(3) synthesis of VI ionogrammes and the comparison with observed h'(f) data, therein providing a measure of accuracy for the modelling process used

(4) graphical presentation of the group delay structure for a synthesized HF radio circuit, and

(5) calculation of the HF energy budget for a simulated radio link. see Appendix [A1]

STAGE 3: **Evaluation of the REAL PROP software using oblique ionogramme simulations and recorded group delay data**

In the final phase of the research project it was hoped to establish a physical HF radio link between CSIR and Rhodes Univesity with the express purpose of evaluating how useful the Real Prop software would be in providing a basis for a real time HF frequency prediction service in addition to its potential as an ionospheric diagnostic tool in HFDFSSL work. The evaluation would be carried out by comparing the observed MUF for the practical link with the values obtained from a simulated ray trace through a model ionosphere whose parameters were to be fixed using observed sounding data recorded at one end of the oblique path. In the event that research funding was to prevent the test link from becoming a reality it was decided that the third stage of Real Prop would be tested in field trials conducted by the CSIR's main potential client. However, the project would still be required to ensure that Real Prop's simulated link algorithms had been tested for self consistency, thoroughly de-bugged and packaged in a generic format for multi-client evaluation. In the absence of measured oblique link data it would be required to synthesize oblique ionogrammes by **analytically ray tracing** through the selected ionospheric model, given its parameters were determined using recorded N-h data, and then to compare the results with those obtained using the **equivalence theorems.** This comparative study would at least check the source code for bugs and incorrect modelling techniques while providing an indication of the value of analytical ray tracing techniques in real time propagation assessment. The predicted MUF values for the various ionospheric layers as determined via each group path synthesis method would have to be compared and due account given of any errors that may reflect poorly on the modelling process. Furthermore, the MUF

results obtained using the analytically synthesized group path profile had to be checked with the values derived via the MUF algorithms developed in phase2 of Real Prop if one were to ensure that both ray tracing algorithms were self consistent.

This concludes the proposed plan of work and the general description of the prescribed milestones that defined the **Real Prop, the "real-time" HF prediction project.**

CHAPTER (2)

THE IONOSPHERE, VERTICAL INCIDENCE SOUNDING, ELECTRON DENSITY PROFILES AND MATHEMATICAL MODELLING OF THE IONOSPHERE.

Nota-bene: SI [Système International] units are used throughout the course of this thesis.

The classical method of obtaining information about the ionosphere is to employ radio waves of a suitable frequency as a probe. A plasma which varies slowly with height will totally reflect a radio wave of frequency f, incident normally, when the ion concentration within the plasma (N) satisfies the equation, Budden [1985],

$$N = \left(\frac{4\pi^2 \epsilon_o m}{e^2} \right) f^2 \qquad (2:1)$$

The eq (2.1) may be transposed to define the resonant frequency of the plasma (f_N) at the point of reflection as

$$f_N = \left(\frac{N\, e^2}{4\pi^2\, \epsilon_o\, m} \right)^{\frac{1}{2}} \qquad (2:2)$$

If the source of radio energy is pulsed then the round trip time of a signal from earth to ionosphere and back can be measured and a profile of the electron concentration as a function of reflection height can be deduced. These principles are embodied in an instrument called an ionosonde which is no more than a pulsed radar operating in the HF band of between 3 and 30 MHz. The frequency sweep of the transmitter is carried out automatically over a period of time, typically in the range, one to five minutes and whose output feeds a wide-band aerial designed to transmit maximum power vertically upwards. A sensitive receiver is held in tune with the transmitter and records both the outgoing and returning pulses. The radar bleeps are displayed on a cathode-ray tube whose time base also shows subsidiary calibration pulses from which the time of flight can be determined. It is usual to divide the time of flight by two and multiply by the speed of light *in vacuo* to give the virtual height of reflection h'(f). The virtual height is, however, only loosely related to the true height of reflection ,h_r, because the ionosphere is not a simple mirror in the optical sense but a thick refracting medium. The echoes displayed on the cathode ray tube are normally photographed by winding a film past the face of the tube giving a continuous record of h'(f) as a function of ,f, up to the frequency which penetrates the ionosphere. The resultant picture or trace is referred to as an h'(f) profile or ionogramme and provides the "radar signature" necessary to deduce the layered structure of the ionosphere.

The relation between virtual height and true height

Suppose a wave of the form $E = E_o \exp[i(\omega t - kx)]$ is propagated vertically upwards into a horizontally stratified ionosphere and consider the earth's magnetic field to be ignored. The group velocity, u, decreases with increasing electron concentration and becomes a minimum at the point of reflection (zero if the collision frequency is negligible). The total time of flight, t, is simply given by the integral

$$t = 2 \int_o^{h_r} \frac{dh}{u} \qquad (2:3)$$

where hr is the height of reflection. From this result it follows that the virtual height is expressible as

$$h' = \int_o^{h_r} \frac{c}{u}\, dh \qquad (2:4)$$

and since c/u is the group refractive index μ' then it follows

$$h' = \int_o^{h_r} \mu'\, dh \qquad (2:5)$$

The relationship between the group and phase refractive indices is given by

$$\mu' = \mu + f \frac{d\mu}{df} \qquad (2:6)$$

and magneto-ionic theory (Ratcliffe, 1962) gives the phase refractive index in terms of the parameters of the plasma and probing frequencies respectively. The general dispersion equation, due to Appleton and Hartree (1931), may be expressed as

$$n^2 = 1 - \frac{X}{1 - iZ - \frac{Y_T^2}{2\,(1 - X - iZ)} \pm \sqrt{\frac{Y_T^4}{4\,(1 - X - iZ)^2} + Y_L^2}} \qquad (2:7)$$

$$X = \frac{Ne^2}{\epsilon_o\, m\, \omega^2} = \frac{\omega_N^2}{\omega^2} \qquad (2:8)$$

$$Y_L = \frac{e\, B_L}{m\, \omega} = \frac{\omega_{HL}}{\omega} \qquad (2:9)$$

$$Y_T = \frac{e\, B_T}{m\, \omega} = \frac{\omega_{HT}}{\omega} \qquad (2:10)$$

$$Z = \frac{\nu}{\omega} \qquad (2:11)$$

where the adopted symbolism is to be interpreted:

ν $\Rightarrow$ collision frequency between electrons and other particles

ω_N^2 $\Rightarrow$ the square of the angular plasma frequency of the medium $(Ne^2/\varepsilon_0 m)$.

f_N $\Rightarrow$ plasma frequency $(\omega_N/2\pi)$.

ω_H $\Rightarrow$ angular gyro-frequency $[(|e|/m)B_0]$, or cyclotron frequency, of the

electrons, that is, the frequency with which they spin in the magnetic field under their thermal motions

$\omega \Rightarrow$ angular frequency of the wave

$X \Rightarrow [\omega_N/\omega]^2$

$\mathbf{Y} \Rightarrow [e/m\omega]\mathbf{B}_0$

$Y \Rightarrow \omega_H/\omega$

$Y_L \Rightarrow Y \cos(\Theta)$

$Y_T \Rightarrow Y \sin(\Theta)$

$\Theta \Rightarrow$ dip angle

$Z \Rightarrow \nu/\omega$

In the upper regions of the ionosphere the collisional frequency is sufficiently small to be neglected, with the result that the Hartree-Appleton equation gives a real as opposed to a complex value for the phase refractive index,

$$\mu^2 = 1 - \frac{2X(1-X)}{2(1-X) - Y_T^2 \pm \sqrt{Y_T^4 + 4(1-X)^2 Y_L^2}} \qquad (2:12)$$

A further simplification can be made if one neglects the effect of the geomagnetic field, to give the well-known result

$$\mu^2 = 1 - X = 1 - \left(\frac{f_N}{f}\right)^2 = 1 - k\frac{N}{f^2} \qquad (2:13)$$

where $k = [e^2/4\pi^2\varepsilon_0 m] = 80.5$ and ,f, is in Hertz. Substitution of the no field/collision free

form of the Hartree-Appleton equation into eq (2.6) yields the simple relation

$$\mu \, \mu' = 1 \qquad (2:14)$$

allowing one to express the virtual height integral in the very manageable form

$$h' = \int_o^{h_r} \frac{dh}{\mu} = \int_o^{h_r} \frac{dh}{\sqrt{1 - \frac{f_N^2}{f^2}}} \qquad (2:15)$$

Inversion of the no-field / collision free form of the virtual height integral

Appleton [1930] and De Groot [1930] independently showed that the group height integral in the field free/collisions ignored case, takes the form of Abel's equation, Budden [1985]

$$h\,(f_r) = \frac{2}{\pi} \int_o^{f_r} \frac{h'\,(f)\,df}{\sqrt{(f_r^2 - f^2)}} \qquad (2:16)$$

and h(f_r) is the <u>true</u> height of reflection corresponding to a frequency ,f_r, defined by

$$f_r \equiv f\,\mathrm{cosec}(\beta) \qquad (2:17)$$

where ,f, is the probing frequency and ,ß, lies in the range zero to ninety degrees. Substitution of the above frequency transformation into Abel's integral gives

$$h\,(f_r\,) = \frac{2}{\pi}\int_o^{\frac{\pi}{2}} h'\,(f_r \sin\,\beta)\;d\;\beta \qquad \text{(2:18)}$$

where the range of integration extends from 0° to 90° instead of 0 to f_r as in eq. (2.16) One can see that by re-graphing the observed h'(f) data using the frequency scale defined by eq (2.17), the area underneath the virtual height curve will be $\pi/2$ times the true height of reflection. The real height profile, $h(f_r)$, can be determined using a numerical integration technique such as Simpson's rule to solve the eq (2.18) for the selected value of probing frequency ,f. The above process is then repeated to obtain the complete range of actual reflection heights corresponding to the sweep of probing frequencies used by the ionosonde. Once the real height profile ,$h(f_r)$, has been determined, one may derive the corresponding electron density using eq (2.1), giving

$$N(h) = \left(\frac{4\pi^2\,\epsilon_o\,m}{e^2}\right) f_r^2 \qquad \text{(2:19)}$$

Inversion of the field included / collision free form of the virtual height integral

To determine the virtual height profile for the case where the earth's magnetic field is included one must use the general form of the Hartree-Appleton equation as given by ,eq (2.12), to calculate the group refractive index. The resultant virtual height integral can not be inverted using Abel's method but the N-h profile may be derived using a numerical technique such as Gaussian quadrature, Budden [1985]. Prior to the advent of high speed computers, the enormous computational difficulties involved in the numerical solution of the

inversion integral severely limited its usefulness but today it is possible to carry out ionogramme inversion with relative ease, even when the complete form of the dispersion equation is used. However, several major practical difficulties prevent one from obtaining accurate N(h) profiles. These problems may be summarized as follows:

(a) The integration requires virtual height information from zero plasma frequency up to the critical frequency of the densest ionospheric layer.

(b) A unique numerical solution only exists if the N(h) profile is monotonic, that is, does not possess a valley region.

(c) The virtual height may become infinite at a critical frequency causing difficulty in evaluating the area under the h'(f) profile.

The aforementioned difficulties associated with ionogramme inversion can be reduced to two basic problems :

(1) The starting problem :

An ionosonde will only record radio echoes beginning at a starting frequency of approximately 1,5 MHz, with the result that one has no physical means of determining where the ionosphere begins. The absence of ionosonde data in the lowest frequency portion of the sweep is due to the heavy attenuation associated with the bottomside of the ionosphere in addition to the inherent inefficiency of an antenna when one operates at long wavelengths. The only way to circumvent the so-called starting problem is to make assumptions as to how the plasma frequency varies below the lower frequency limit of the ionosonde. Titheridge [1985] gives an

empirical method for obtaining the starting height at which the plasma frequency is 0.5 MHz and also details a variable starting frequency model for an ionospheric base height of 90 km. These empirical models are suitable for day-time modelling of the ionospheric starting conditions when one has an absence of ionosonde data. However, at night-time the ordinary and extraordinary ionogramme traces may both be present due to the diminution of ionospheric absorption and if so, can be used to determine an underlying electron density profile consistent with both traces. Titheridge [1985] gives an ionospheric night-time starting model based upon O and X trace data and this is graphically presented as, starting height versus hours after sunset and hours before sunrise.

(2) **The valley problem:**

The identifying and allowing for valleys of ionization between two layers is the single most difficult task in the determination of a N-h profile. Radio echoes do <u>not</u> occur in a region of ionisation depletion and the only way to detect the presence of a valley, from an ionogramme, is to observe the differential refraction that is experienced by the ordinary and extraordinary traces respectively. Currently the main knowledge about valleys has been derived from rocket soundings which show that re-entrant electron profiles have a minimum density of circa 0.9 $N_{MAX}E$ and a width of the order of a few kilometers. Information on the existence of a depletion region can be obtained by making use of both the ordinary and extraordinary virtual height data. If the traces are of the same general form then it is reasonable to assume that the N-h profile is monotonic, however, if the geometries of the $h'(f)_{o\text{-}ray}$ and $h'(f)_{x\text{-}ray}$ are appreciably different one might suspect that an an electron

depletion region is the cause of the observed differential refraction. Titheridge [1985] developed a standard technique to evaluate valley characteristics using three basic steps:

(1) Use the ordinary trace derived from an h'(f) virtual height profile to deduce the equivalent monotonic N-h profile.

(2) The h'(f) curve for the extraordinary wave is then calculated from the monotonic profile and is compared with the observed extraordinary wave trace.

(3) The difference between the observed and calculated virtual heights is attributed to the presence of a valley and by a process of trial and error a N-h profile is found that will remove discrepancies.

A simple reference detailing the above approach may be found in Titheridge [1959]; "The use of the extraordinary ray in the analysis of ionospheric records"

Ionogramme inversion using John Titheridge's POLAN software

When the influences of the Earth's magnetic field and collisions are neglected, then as already discussed, the problem of inverting the group height integral using Abel's method is relatively straight forward, Davies [1969]. In the general case where the magnetic field is included a variety of numerical techniques are available for inversion of the ordinary h'(f) trace to the equivalent monotonic electron density profile, Paul et al [1968]. One of the most comprehensive inversion programmes is Polynomial Analysis, POLAN, developed by Titheridge [1985] and designed for maximum accuracy and reliability. The programme

uses polynomial real height sections of any required degree and fitting any number of data points. The use of the ordinary and extra-ordinary virtual height data makes it possible to estimate the size of the valley between two ionospheric layers, enabling one therefore to analyse re-entrant electron density profiles. Physically unacceptable solutions are rejected by imposing limits on the profile parameters. The new profile coefficients and the least squares fitting error are obtained directly and rapidly from the previous trial solution, allowing repeated iterations until a satisfactory curve fit is found. The iterative loop involves continual calculation of the synthetic ionogramme, comparing the result against the observed h'(f) trace, and repeating the process until the error is minimized. Procedures are included to deal with the unobserved underlying ionization or so-called starting problem. POLAN uses extrapolation and interpolation to fill in gaps in ionogramme scaling, for example data that is often missing in the vicinity of the layer penetration regions of the h'(f) trace. For routine ionogramme analysis POLAN may be used as a black-box with the following inputs: virtual height, frequency, dip angle and gyro-frequency while the output is a true height profile together with the critical frequencies and heights of the maximum electron density for each ionospheric layer plus E/F valley information. In POLAN the group height integral ,eq (2.5), is parameterised in terms of the plasma frequency ,f_N, so that h'(f) may be expressed

$$h'(f) = \int_o^f \mu' \left(\frac{dh}{df_N} \right) \cdot df_N + h(o) \qquad (2:20)$$

It is clear from the form of the integrand in eq (2.20) that the chief output of POLAN is a N-h profile or electron density distribution. A sample electron density profile obtained using POLAN and the observed ionogramme from which the profile was derived are shown below.

(1) quality of the profile match, that is, the model must accurately represent the range of N-h electron distributions encountered in practice; this match should be maintained in the first and second derivatives with respect to height, given that the co-ordinates of a peak or a ledge on the N-h distribution are to be used as anchor points for the model electron profile.

(2) availability and simplicity of the external data required for profile specification.

(3) ray tracing through the model should be a fully analytic process.

There are two approaches to ionospheric modelling, the first, involves the matching of synthetic and observed ionogrammes while the other method utilises curve fitting of an electron density model to an observed N-h profile. It should be noted that one's use of the adjective "observed" when describing an N-h profile is merely to convey that the electron density distribution has been derived via inversion of a recorded as opposed to a synthetic ionogramme.

Indirect method: the matching of observed with synthetic ionogrammes

This method of modelling involves generating a synthetic ionogramme from a general mathematical expression describing the electron density and then determining the constants of the model by adjusting their value until the observed ionogramme matches the synthetically generated h'(f) profile. As the peak heights and thicknesses of ionospheric layers provide one with key descriptions of the structure of the ionosphere, empirical models have been developed to give these parameters explicitly in terms of quantities routinely scaled from ionogrammes. A further criterion is that only ionospheric parameters routinely published by the observatories should be required so that access to original

ionogrammes will not be necessary when using the empirical method. The indirect method has been used extensively by Bradley and Dudeney [1973]; Dudeney [1974]; Dudeney [1978]. A very comprehensive review of empirical models describing the variation of electron density within the ionosphere and their value in radio communications can be found in Dudeney and Kressman [1986]. The main application of empirical models has been in the development of software packages for long term prediction purposes which make use of synoptic ionospheric data bases. A comprehensive list of references coupled with a brief but concise review of the use of empirical modelling techniques in HF propagation assessment can be found in; "Advances in Space Research, Vol II, Number 10, 1991". For a detailed review of the synoptic ionospheric models used in public domain HF prediction programmes, ref: Mercer [1991], "CSIR Report; I MICO - 109". The main drawback to the indirect method is that it is unsuitable for real time determination of the ionospheric layer parameters. To curve fit synthetically generated ionogrammes to observed h'(f) profiles via a process of iteratively adjusting the parameters of a given ionospheric model would involve time consuming numerical algorithms. As the purpose of this research project was to develop an ionospheric modelling approach suitable for real-time applications in HF radio the indirect method was abandoned.

Direct method: curve fitting a model electron density distribution to an observed N-h profile

In this second approach to ionospheric modelling one curve fits an analytical expression for the electron density to an observed N-h profile. This method therefore requires that one first invert an observed ionogramme to obtain the required electron density profile before the modelling process can begin. This task may be carried out using a software package

such as POLAN, Titheridge [1985] which is essentially a computer implementation of the generalized form of Abel's solution discussed by Paul et al [1968]. It is possible to choose a model electron density geometry for which a curve fit to a N-h distribution will result in a mathematical profile that is parameterized in terms of the peak heights, critical frequencies and semi-thickness of the respective ionospheric layers. The direct method of ionospheric modelling has been used extensively by Dyson et al [1988, 1990, 1992] who have shown that the technique is very useful for quasi-real-time applications in HF frequency prediction and direction finding. When implementing the "Direct method" the curve-fitting algorithms operate in real time but the process of ionogramme inversion required to generate the N-h profile takes approximately fifteen minutes to accomplish. In this research project, the description of "accomplished in real-time" is regarded as referring to the process of curve-fitting model profiles to observed N-h data in order to derive the ionospheric layer parameters and/or to the execution time required by the ray-tracing algorithms that are used to determine the HF circuit parameters for such an ionosphere. One pre-supposes the existence of the observed N-h profile and the time required to perform ionogramme inversion is not incorporated in the overall computational time calculated. The focus of the research work is to establish an ionospheric electron density model that will satisfy the aforementioned three yardsticks of a good analytical profile when implemented in the mode of the "Direct method". The CSIR's network of analogue ionosondes were installed in 1982 by Kel Aerospace of Australia and although in 1991 they were upgraded to present the h'(f) data in digital form, one must still use POLAN to obtain the desired N-h profile. Implementation of an ionosonde of the Lowell Digisonde 256 type, Reinisch et al [1989], will give one access to near instantaneous N-h profiles and hence the delivery of observed electron density data in real-time to a "Direct method"

curve-fitting module; CSIR internal communique [1992].

The search for a physically representative and wholly analytical electron density model

The story begins with Sidney Chapman [1931] whose paper on the ionizing effect of monochromatic radiation on the earth's atmosphere is regarded as a classic in the annals of ionospheric physics. The equation of continuity describing the fluid flow inside a region of ionospheric plasma is given by

$$\frac{dN}{dt} = q - \alpha L(N) - Div\ (N\vec{v}) \qquad [2:21]$$

where α is a constant of proportionality and the various terms are identified as

q $\rightarrow$ source

L[N] $\rightarrow$ loss or sink

Div[Nv] $\rightarrow$ transport

Under conditions of quasi-equilibrium the left-hand side of eq [2.21] becomes vanishingly small and assuming altitudes within the ionosphere where the transport term can be neglected, it follows

$$q \cong \alpha L\ (N\ ) \qquad [2:22]$$

If one further makes the assumption that positive and negative ions are present in equal

abundance then the loss term will be quadratic in N, implying

$$N \propto \sqrt{\frac{q}{\alpha}} \qquad (2:23)$$

Chapman showed that the rate of production of ion pairs is given by, Kelso [1964]

$$q = q_0 \exp (1 - Z - \sec \chi \exp (- Z)) \qquad (2:24)$$

where

$\chi \rightarrow$ solar zenith angle

$q_0 \rightarrow$ rate of ion production when the sun is overhead, $\chi = 0$

$Z \rightarrow [h - h_0]/H \rightarrow$ altitude measured in units of scaled height

$H = kT/mg$ defines one scale height.

Substitution of eq (2.24) into eq (2.23) gives the following expression for the electron concentration within the ionosphere, namely

$$N = N_o \exp \frac{1}{2} (1 - Z - \sec \chi \exp (- Z)) \qquad (2:25)$$

This equation provides one with an interesting insight into the form of a suitable analytical expression that might be used to describe the electron density distribution in the vicinity of the peak of an ionospheric layer. The eq (2.25) may be re-written, Kelso [1964]

$$N = N_m \exp (1 - x - \exp (- x)) \qquad (2:26)$$

where the new quantities are defined

$$N_m = N_o \cos^{\frac{1}{2}} (\chi) \qquad [2:27]$$

$$x = Z - \log_e (\sec \chi) \qquad [2:28]$$

The electron density distribution may now be written in the notation

$$N = N_m \, Ch \, (x) \qquad [2:29]$$

where the expression Ch(x) is known as the Chapman function, defined by,

$$Ch(x) = \exp \left\{ \frac{1}{2} (1 - x - \exp (- x)) \right\} \qquad [2:30]$$

and listed in tabular form by Kelso (1964) .

If the expression for Ch(x) is expanded within one scale height of the level of maximum ionization so that $|x| < 1$, it follows

$$N \cong N_m \exp \left\{ \frac{1}{2} \left\{ 1 - x - \left\{ 1 - x + \left(\frac{x^2}{2} \right) \right\} \right\} \right\} \qquad [2:31]$$

$$\cong N_m \exp \left(\frac{- x^2}{4} \right) \cong N_m \left\{ 1 - \left(\frac{x^2}{4} \right) \right\} \qquad [2:32]$$

One now has the simple but elegant result that the electron concentration follows a parabolic variation close to the maximum density in an ionospheric layer which obeys Chapman's law. It is usual to introduce the notion of semi-thickness y_m of a parabolic layer and to express eq (2.32) in the form

$$N \cong N_m \left(1 - \frac{(h - h_m)^2}{y_m^2}\right) \qquad (2:33)$$

where y_m is equivalent to two scale units. The parabolic layer hypothesis was tested by Appleton and Beynon (1940) who compared observed virtual height profiles with synthetic ionogrammes derived assuming a parabolic ionospheric model.

The Appleton-Beynon experiment

Consider a parabolic layer whose maximum electron concentration is ,N_m, at a height ,h_m, and that the semi-thickness of the layer is ,y_m, implying

$$N = N_m \left(1 - \frac{(h - h_m)^2}{y_m^2}\right) \qquad (h_m - y_m) \leq h \leq h_m \qquad (2:34)$$

$$= 0. \qquad \textit{elsewhere}$$

where the base of the ionospheric region is defined by $h_o = (h_m - y_m)$.

If the minimum frequency which just penetrates the layer is ,f_o, then from eq (2.2) a probing frequency ,f, is reflected when

$$f^2 = f_c^2 \left(1 - \frac{(h - h_m)^2}{y_m^2}\right) \qquad o \leq f \leq f_c \qquad \text{(2:35)}$$

If the earth's magnetic field and the effects of collisions are neglected, the phase refractive index for a parabolic distribution of electrons may then be expressed via, eq (2.13),

$$\mu^2 = 1 - \frac{f_c^2}{f^2}\left(1 - \frac{(h - h_m)^2}{y_m^2}\right) \qquad \text{(2:36)}$$

By using the change in variable

$$h_o = (h_m - y_m) \qquad \text{(2:37)}$$

one may re-write eq (2.36) in the more compact form

$$\mu^2 = 1 - \alpha\ (h - h_o) + \beta\ (h - h_o)^2 \qquad \text{(2:38)}$$

where the coefficients are defined as

$$\alpha = \frac{2\left(\frac{f_c}{f}\right)^2}{y_m} \qquad \text{(2:39)}$$

$$\beta = \frac{\left(\frac{f_c}{f}\right)^2}{y_m^2} \qquad (2:40)$$

Recalling the simple reciprocal relationship between μ and μ' for the no-field/collision free case, eq (2.14), one may use eq (2.5) to express the group height for a parabolic electron profile as

$$h' = \int_{o.}^{h_r} \frac{dh}{\left(1 - \alpha\,(h - h_o) + \beta\,(h - h_o)^2\right)^{\frac{1}{2}}} \qquad (2:41)$$

where h_r denotes the height of reflection. From eq (2.13) one can see that at apogee the phase refractive index goes to zero and that one may therefore determine the value of ,h_r, by finding the negative root of the quadratic denominator inside the integrand of eq (2.41), implying

$$h_r = h_o + \frac{\alpha - \sqrt{\alpha^2 - 4\,\beta}}{2\,\beta} \qquad (2:42)$$

The indefinite form of the group height integral, eq(2.41), may be found in the CRC(1985) and inserting the limits of integration, with the aid of eq(2.42), yields

$$h'(f) = \frac{y_m f}{2\,f_c} \log_e \left\{\frac{f_c + f}{f_c - f}\right\} + h_o \qquad (2:43)$$

Whereupon, one can see that for an ionosphere modelled as a single parabolic layer the ionogramme trace ,h'(f), depends only on the semi-thickness ,y_m, the maximum electron density, k(f_c)$^{1/2}$ and its base height, h_o.

Defining a function Φ(x) as

$$\phi\ (x) = \frac{x}{2} \log_e \left(\frac{1 + x}{1 - x}\right) - 1 \qquad (2:44)$$

where the variable x is equivalent to (f/f_c), one may re-express eq (2.44) in the form

$$h'(f) = y_m\ \phi(x) + h_m \qquad (2:45)$$

The above equation (2.45) was derived by Appleton and Beynon in their paper of 1940 and was used to plot observed values of h'(f) against Φ(x). If an ionospheric layer has a parabolic electron density profile then the graph should be a straight line. Results showed that the fit was good for the E layer and fairly good but with more scatter points for the F layer. This would tend to indicate that the E layer of the ionosphere is firmly under solar control whereas the dynamics of plasma flow in the F region are a function of both the transport and solar source terms in the continuity equation, eq(2.21). Using the Appleton-Beynon equation one is able to derive estimates of the semi-thickness and height of the maximum electron density in an ionospheric layer. Examination of eq (2.45) for h'(f) reveals that Φ(x) is zero when x equals 0.834 f_c allowing one to determine the value of ,h_m, using just a single measurement from an ionogramme, Dudeney (1974). It should be noted that under-ionization does affect this rule and although such a perturbation is negligible at night it will, during the daytime, increase the value of h'(f) corresponding to a probing frequency of 0.834 f_c, above that predicted by the single layer assumption. In summary,

it is seen that the parabolic electron density profile is a simple mathematical model with sound physical justification for its use in the modelling of ionospheric structure.

A multi-segmented parabolic electron density model

By introducing the inverse parabolic distribution

$$N = N_m \left(1 + \frac{(h - h_m)^2}{y_m^2} \right) \qquad (h_m - y_m) \leq h \leq h_m \qquad \text{(2:46)}$$

one is able to construct an entire N-h profile, using the reverse curvature property of equation (2.46) to provide a smoothly varying continuous join between adjacent traditional segments. A model electron density profile constructed from multiple parabolic segments satisfies two of the three criteria used to define a successful ionospheric model, ref: pp 18

(1) quality of profile match to real electron density data

(2) availability and simplicity of external data required to anchor the model profile, however, one may <u>not</u> analytically ray trace through the model profile except at vertical incidence.

It is essential that the ionospheric model used for real-time applications in HF communications be analytic when solving the following integral equations

(a) Ground range equation

$$D = 2r_o \int_{r_o}^{r_t} \frac{dr}{r \tan(\beta)} \qquad (2:47)$$

(b) Group path equation

$$p' = 2 \int_{r_o}^{r_t} \frac{dr}{\mu(r) \sin(\beta)} \qquad (2:48)$$

where $r_o \rightarrow$ earth radius, $r_t \rightarrow$ apogee of radio locus, $\beta \rightarrow$ elevation angle made by a ray with respect to the local horizontal, $\mu(r)$ is the phase refractive index expressed as a function of the geocentric ray height. An ionosphere modelled as a single parabolic layer will yield analytical results for ground range and group path provided the earth is regarded as flat, Budden [1985]. However, the determination of the maximum usable frequency over such an HF circuit is not analytically soluble and numerical techniques are necessary to iteratively deduce the skip distance and associated operating frequency. Appleton and Beynon [1940] were able to show that if the earth's curvature is included then an analytical solution to the ground range calculation can still be found provided the base height ,h_o, of the single layer model is considered as very much less than the radius of the earth r_o. However, the calculation of maximum usable frequency and skip distance still requires numerical solution. Appleton and Beynon established transmission curves which give M(3000) as a function of the ratio of semi-thickness to base height, with the peak height acting as a parameter

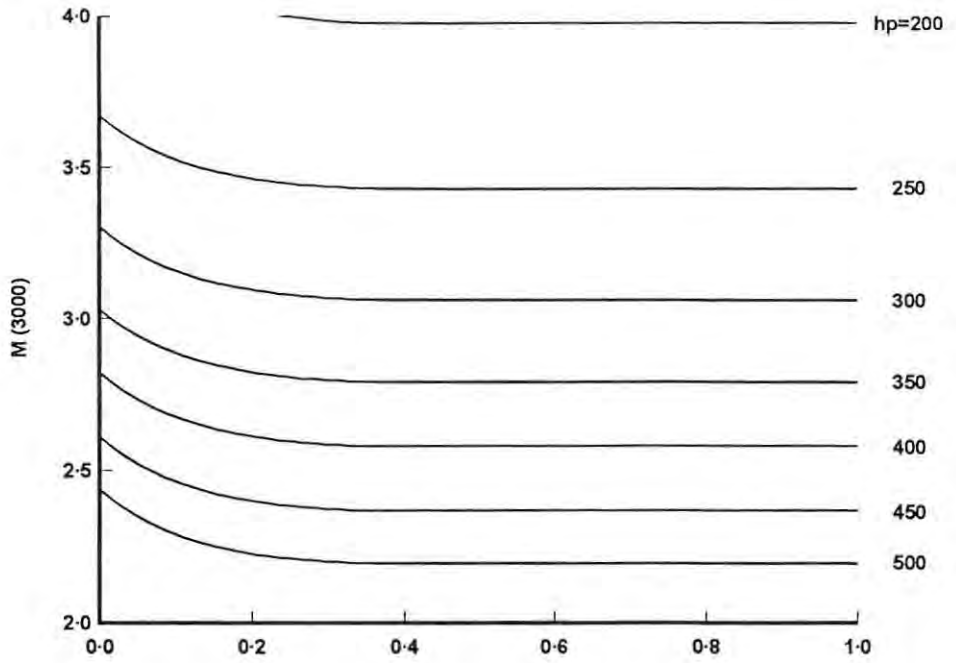

The M(3000) factor as a function of y_P / h_o , parametric in h_P .
(After Appleton and Beynon, 1940.)

Figure (2.3) : The M(3000) factor as a function of ,y_p/h_o, parametric in h_p, after Appleton and Beynon, 1940. (The subscript p denotes maximum).

The quasiparabolic layer and the case of the curved earth

Referring to eq[2.47] for the ground range ,D, of a HF circuit trajectory one may use Snell's law of refraction to express the tan[ß] term as a function of transmitter launch angle ,β_o, and the local refractive index, μ_o, so long as the earth is regarded as flat. However, if earth curvature is to be taken into account, one must first express Snell's law in spherical co-ordinates to give the result known as Bouguer's equation,Davies[1969], before substituting for tan β in terms of ,β_o, and μ_o respectively. The details of the ground range equation are covered in Chapter [4], so for the moment accept that in the curved earth case;

$$D = 2\, r_o^2 \cos \beta_o \int_{r_o}^{r_t} \frac{dr}{\sqrt{r^2\, \mu^2(r) - r_o^2 \cos^2(\beta_o)}} \qquad [2:49]$$

where the phase refractive index ,μ[r], in the absence of the geomagnetic field is given by

$$\mu^2(r) = 1 - \frac{f_{Nmodel}^2}{f^2} = \frac{kN_{model}}{f^2} \qquad [2:50]$$

One can see that the solution to the ground range equation depends on the choice of the electron density model, since the plasma frequency ,f_N, is proportional to the square root of the electron density, N. If the ionospheric model selected is based upon a parabolic distribution the phase refractive index would be given by

$$\mu^2 = 1 - \frac{f_c^2}{f^2}\left(1 - \frac{(h_m - h)^2}{y_m^2}\right) \qquad [2:51]$$

and substitution of eq [2.51] into the ground range integral, eq [2.49], would quickly reveal a non-analytical integral result except in the limiting case of vertical propagation. In 1953, De Voogt proposed a slight perturbation of the parabolic model which would allow one to analytically solve the ground range and group path integrals, without compromising the accuracy of the model's fit to observed N-h profile data. The modified parabolic distribution has come to be known as the quasiparabolic electron density distribution where the term quasi derives from the latin word for "almost". De Voogt gave the mathematical form of this quasiparabola as

$$N_e = \frac{A}{r^2} + \frac{B}{r} + C \qquad [2:52]$$

where N_e is the electron density, r $\rightarrow$ radial geocentric height and the coefficients [ABC] are determined by curve fitting the mathematical form to observed N-h data. De Voogt recognised that a family of ionospheric layers could be constructed using a second degree polynomial in ,1/r, and even went so far as to outline the method that should be followed when computing ray loci in such an ionosphere, but due to the complexity of the procedure the author did not publish exact equations for ground range or group path. However, in 1968 two research workers, Croft and Hoogasian, produced a land mark paper on "Exact ray calculations in a quasi-parabolic ionosphere with no magnetic field". The quasiparabolic model due to Croft and Hoogasian, although mathematically equivalent to the De Voogt

equation, is expressed in the more tractable form

$$N_e = N_m \left(1 - \left(\frac{r - r_m}{y_m} \right)^2 \cdot \frac{r_b^2}{r^2} \right) \quad ; \quad r_b \leq r \leq r_m \left(\frac{r_b}{r_b - y_m} \right) \qquad (2:53)$$

where the quantity r_b is a normalization factor, equivalent to the base height of the layer. Comparing, eq (2.46), describing a traditional parabola with the quasiparabolic geometry expressed in the form of eq(2.53), one sees two differences;

(1) the quasiparabola is perturbed by a multiplying factor $(r_b/r)^2$, and

(2) geometrically the quasiparabolic distribution is asymmetric about its generator axis.

Examination of the graph below due to Croft and Hoogasian [1968] shows that the quasi versus non-quasi geometries are virtually equivalent in the bottom side region of the electron distributions.

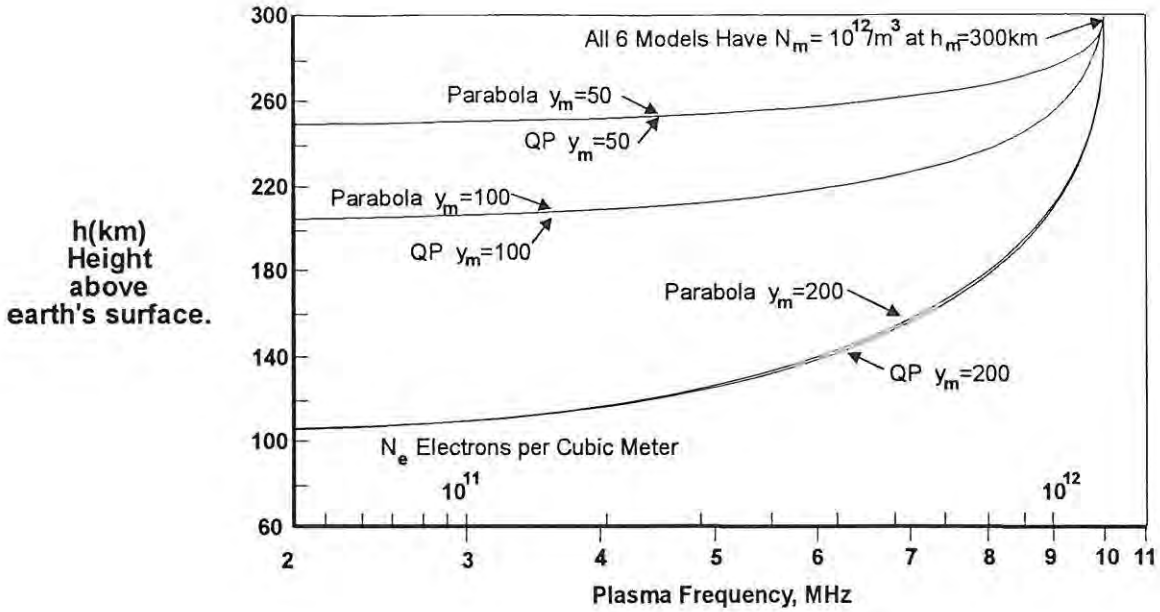

Figure (2.4):Comparison of parabolic and quasiparabolic models of the ionosphere, after Croft and Hoogasian [1968]

Divergence between the two profiles is noticeable in the top-side portion but this region is of no interest when modelling electron distributions except if they should become re-entrant, the details of which are discussed in Chapter 3. Substitution of eq (2.53) into eq (2.50) gives the expression for the phase refractive index corresponding to a quasiparabolic electron distribution under the conditions of zero magnetic field and with electron collisions ignored, namely,

$$\mu^2 = 1 - \frac{1}{F^2}\left(1 - \frac{(r - r_m)^2}{y_m^2} \cdot \frac{r_b^2}{r^2}\right), \quad F \equiv \frac{f}{f_c} \qquad (2:54)$$

where the critical frequency , f_c, equals $(N_m)^{1/2}$.

It should be noted that the position of a point in a quasiparabolic ionosphere is defined by the geocentric radial distance rather than altitude as in the case of a parabolic layer above a flat earth.

Calculation of ground range in a single layer quasiparabolic ionosphere

One may now substitute eq (2.54) into the radical term within the integrand of the ground range equation, eq (2.49) and show that

$$r^2\mu^2(r) - r_o^2\cos^2(\beta_o) = r^2\left\{1 - \frac{1}{F^2} + \frac{r_b^2}{F^2 y_m^2}\right\} - r\left\{\frac{2r_m r_b^2}{F^2 y_m^2}\right\} + \left\{\frac{r_b r_m}{F y_m}\right\}^2 - r_o^2\cos^2(\beta_o) \qquad (2:55)$$

Expansion of the right hand side of eq (2.55) gives a quadratic in ,r, and equating coefficients with respect to a general function of the form

$$R = A'r^2 + B'r + C' \qquad (2:56)$$

gives the ray tracing coefficients , A', B', C',

$$A' = 1 - \frac{1}{F^2} + \left(\frac{r_b}{F\ y_m}\right)^2 \qquad (2:57)$$

$$B' = -\frac{2\ r_m\ r_b^2}{F^2\ y_m^2} \qquad (2:58)$$

$$C' = \left(\frac{r_b\ r_m}{F\ y_m}\right)^2 - r_o^2 \cos^2(\beta_o) \qquad (2:59)$$

Substituting eq(2.56) into eq(2.49) results in eq(2.60) which gives the ensemble ground range covered by a HF signal that propagates over the earth's surface via the ionosphere, as displayed in figure (2.5).

$$D = 2\ r_o^2 \cos(\beta_o) \left\{ \int_{r_o}^{r_b} \frac{dr}{r\sqrt{r^2 - r_o^2 \cos^2(\beta_o)}} + \int_{r_o}^{r_t} \frac{dr}{r\sqrt{A'r^2 + B'r + C'}} \right\} \qquad (2:60)$$

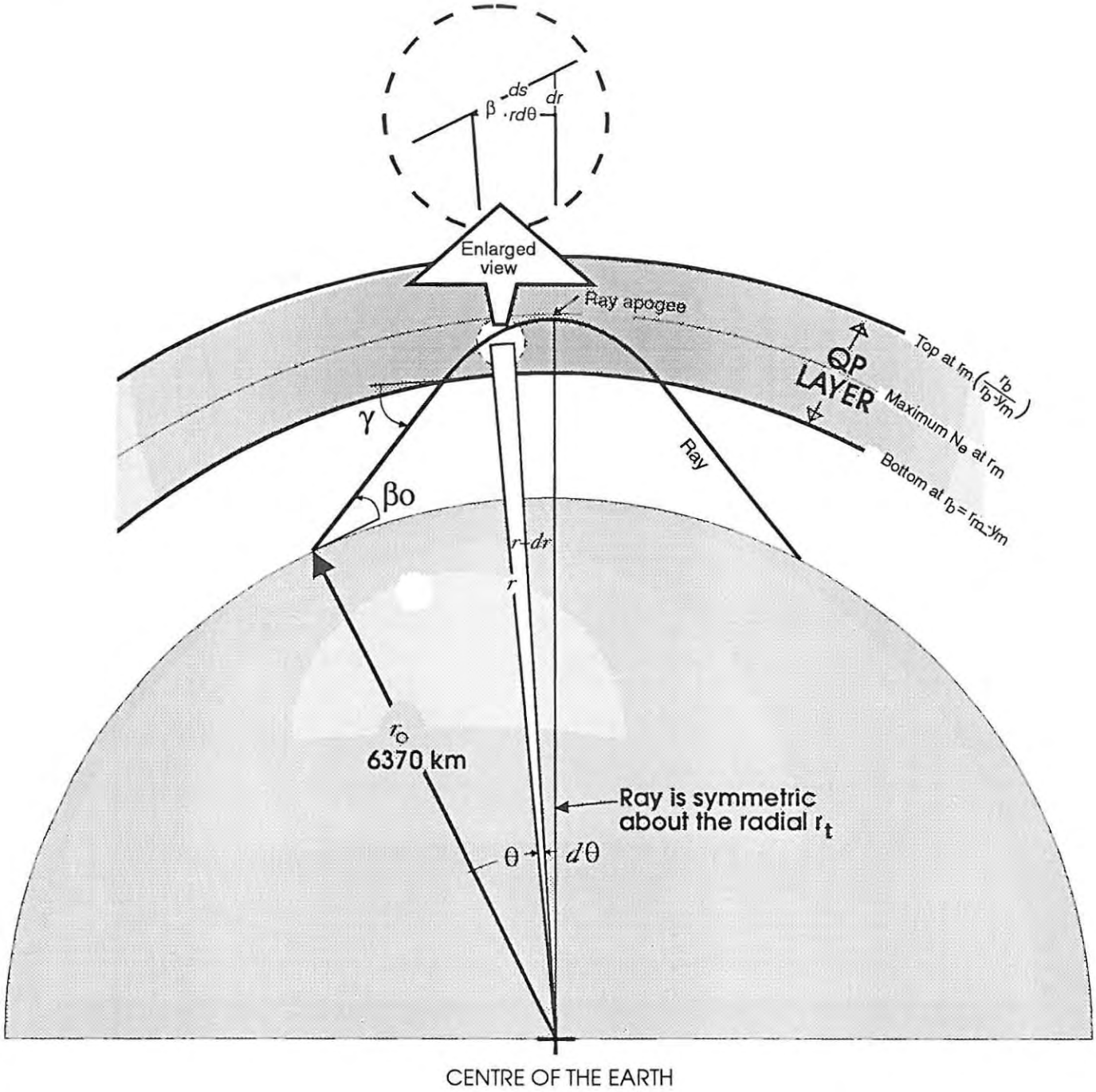

Figure (2.5) : A HF signal propagating through a single layer quasiparabolic ionosphere , after Croft and Hoogasian[1968]

Examination of eq(2.60) shows that the total ground range covered by the trajectory of a HF signal is composed of a free space part and an ionospheric part, shown as two distinct

integral terms. These integrals are analytic and using the CRC handbook [1985] are readily evaluated to give

$$D = 2\, r_o \left\{ (\gamma - \beta_o) - \frac{r_o \cos(\beta_o)}{2\sqrt{C'}} \log_e \left\{ \frac{(B^2 - 4A'C')}{4C' \left\{ \sin(\gamma) + \frac{1}{r_b}\sqrt{C'} + \frac{B'}{2\sqrt{C'}} \right\}^2} \right\} \right\} \qquad (2:61)$$

There are three useful ancillary ray tracing results for the quasiparabolic layer that will be discussed in detail in Chapter 4 and are only quoted here to whet one's appetite.

$$A' r_t^2 + B' r_t + C' = 0 \;\rightarrow\; \textit{apogee equation} \qquad (2:62)$$

$$\cos(\gamma) = \left(\frac{r_o}{r_b}\right) \cos(\beta_o) \;\rightarrow\; \textit{entry angle at bottom of ionosphere} \qquad (2:63)$$

$$r_{tmax} = -\frac{B'}{2A'} \;\rightarrow\; \textit{maximum apogee height} \qquad (2:64)$$

The integral equation describing the group path is also analytic for the quasi-parabolic ionosphere provided the geomagnectic field is ignored, Croft and Hoogasian [1968]. The solution to the group path integral with and without the earth's magnetic field is central to the process of ionogramme synthesis and the details of the required algorithms are to be found in Chapter 6.

The multi-segmented quasiparabolic (MQP) ionosphere, Hill [1978]

The work of Croft and Hoogasian [1968] on ray tracing through a single layer quasiparabolic ionosphere was extended by Hill [1978] to facilitate the modelling of a realistic ionosphere using multiple quasiparabolic segments. Figure [2.6] shows Hill's multilayer model constructed using quasi and inverse quasiparabolic sections so as to provide a smoothly varying electron profile with no discontinuity in gradient.

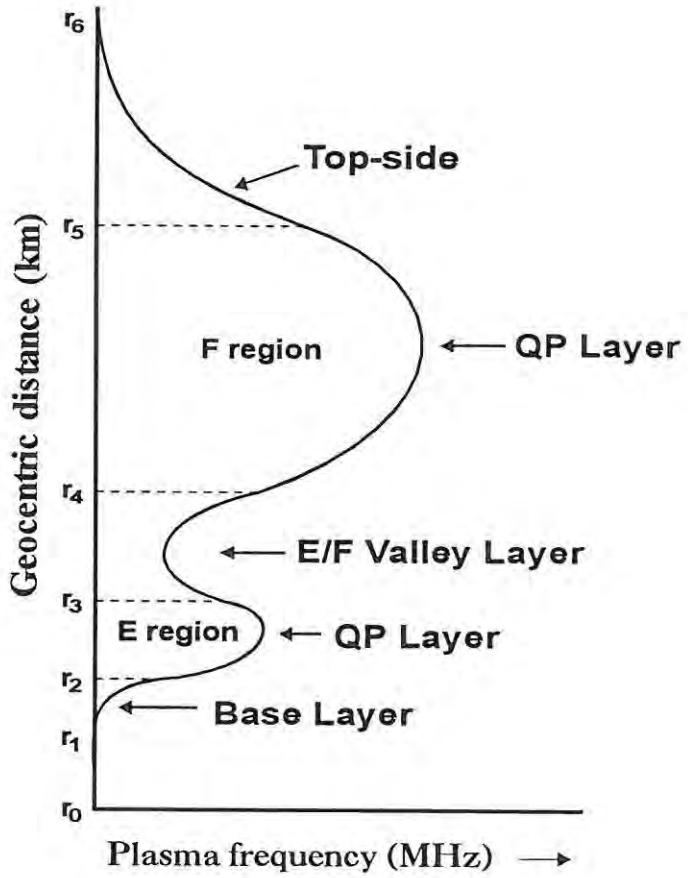

Figure [2.6]: The multi-segmented quasiparabolic [MQP] model due to Hill [1978]

Hill [1978] gives expressions for ground range, as well as group path and shows how one to ray trace through the inverse quasiparabolic construction which is used to provide an

interim or joining section between adjacent quasiparabolic layers. Hill's MQP model has been extended in the course of this research project to include a fully analytic:

(a) MQP E/F1 and/or F1/F2 valley region

and

(b) MQP F1-ledge condition

In Chapter 7 the effect of an E/F_1 valley and a F1-ledge condition upon the calculation of ground range is mathematically simulated and the results compared with those obtained by Baker et al [1992] using numerical methods.

Extension of the Hill ionospheric model, Dyson et al [1988]

The MQP model due to Hill [1978] has been developed further by Dyson et al [1988, 1990, 1992] and involves fitting as many as fifteen QP segments to an observed N-h distribution. Furthermore, the model due to Dyson incorporates the facility to represent an F_1 ledge condition using the MQP geometry. The enhanced MQP model ionosphere due to Dyson et al was developed for use in ground range estimation for HF direction finding single site location (HFDFSSL), however, the details of the algorithms required to implement the generalized ionospheric model are not published and only the results of HFDFSSL field trials are made available to the reader. The purpose of the research work conducted at the CSIR, and described in this thesis, was to independently develop a fully generalized MQP ionospheric model that would be suitable for application in real time HF frequency prediction and HF direction finding single site location (HFDFSSL). In the next chapter the details of ray tracing and MUF algorithms applicable to the MQP ionosphere are developed and derived from first principles.

CHAPTER (3)

A MATHEMATICAL DISCUSSION OF THE MULTISEGMENTED QUASIPARABOLIC (MQP) MODEL USED IN THE REAL TIME HF PREDICTION ALGORITHMS

The ionosphere is modelled using quasiparabolic layers, Hill [1978], to describe the E, F_1 and F_2 regions respectively. The model is constructed by connecting the traditional QP layers via inverse QP joining segments to build a smoothly varying electron density profile. Continuity conditions require that the model N(h) profile and the derivative quantity dN(h)/dh be continuous everywhere, while the quasiparabolic nature of the segments allows one to ray trace analytically through the entire model profile. The mathematical accessibility of the MQP ionospheric profile makes it suitable for many applications such as quasi-real time HF prediction, Lockwood [1983], or Single Site Location (SSL), Chen et al [1990]. Each quasiparabolic layer is independent and is fully described in terms of three parameters, namely (i) the plasma frequency at the peak identifiable with f_oE, f_oF_1 and f_oF_2, (ii) the height at which the maximum electron density occurs, and (iii) the semi-thickness

of the layer. The three layers are therefore completely described by nine parameters. An additional two parameters fix the two inverted joining layers while the valley is constructed using data derived from POLAN.

The construction of the transition layer

In figure (3.1) one sees depicted two traditional quasiparabolic segments connected by an inverse quasiparabolic curve with the constraint that both the electron density and its derivative be continuous at the joining points.

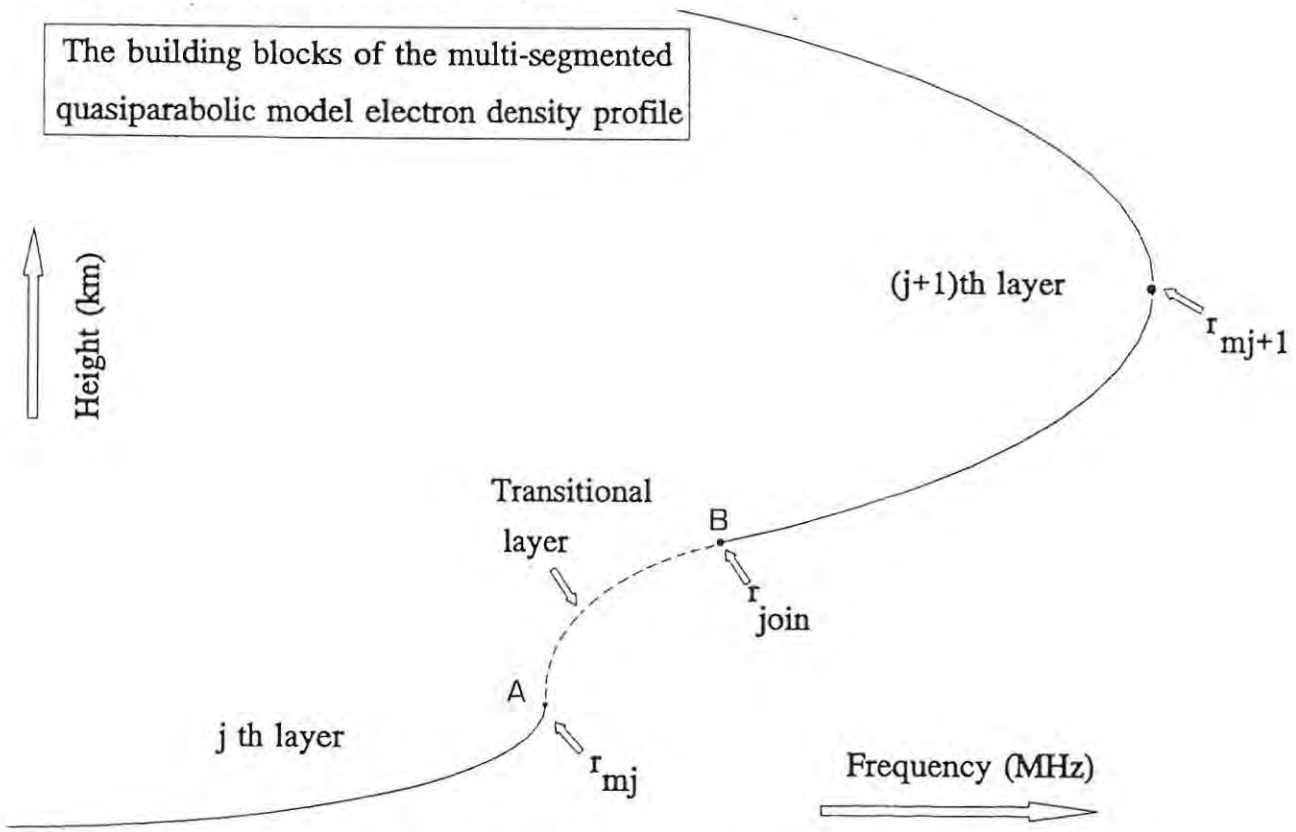

Figure (3.1) The building blocks of a multi-segmented quasiparabolic model electron density profile

Layer one may be mathematically described by the equation

$$N_{e_1} = N_{m_1}\left\{1 - \frac{(r-r_{m_1})^2}{y_{m_1}^2}\right\}\frac{r_{N_1}^2}{r^2} \qquad (3:1)$$

where r_{m1} denotes the height of the electron density maximum, y_{m1} represents the semi-thickness, r_{N1} is a normalization factor and r is the geocentric radius. Note that the factor $[r_N/r]^2$ converts the otherwise conventional parabolic shape into a quasi-parabolic geometry suitable for ray-tracing in a spherical ionosphere. Layer three is likewise described by the equation.

$$N_{e_3} = N_{m_3}\left\{1 - \frac{(r-r_{m_3})^2}{y_{m_3}^2}\right\}\frac{r_{N_3}^2}{r^2} \qquad (3:2)$$

where the symbols have the same interpretation. The inverse quasi-parabolic segment is used purely as a mathematical construct allowing one to connect the QP layers in a smoothly varying fashion. Referring to the figure (3.1) one can see that the inverse layer must satisfy the continuity conditions at points A and B respectively and that the segment must have a sense of curvature opposite to that possessed by the traditional layers. The joining segment may be expressed mathematically by the equation

$$N_{e_2} = N_{m_2}\left\{1 + \frac{(r-r_{m_2})^2}{y_{m_2}^2}\right\}\frac{r_{N_2}^2}{r^2} \qquad (3:3)$$

where the plus sign reverses the curvature of the otherwise quasiparabolic function. Furthermore, the continuity conditions applied at the joining points A and B give four equations

$$N_{1A} = N_{2A} \qquad [3:4]$$

$$\left[\frac{dN_1}{dr}\right]_A = \left[\frac{dN_2}{dr}\right]_A \qquad [3:5]$$

and

$$N_{2B} = N_{3B} \qquad [3:6]$$

$$\left[\frac{dN_2}{dr}\right]_B = \left[\frac{dN_3}{dr}\right]_B \qquad [3:7]$$

Using the above continuity equations one can determine the parameters describing the inverse layer, namely the semi-thickness y_m and the matching height r_t at the point of connection denoted by B. In the interests of simplifying algebra it is wise to express the quasiparabolic equations in the form

$$N = a \mp b\left(1 - \frac{r_m}{r}\right)^2 \qquad [3:8]$$

where the ∓ signs denotes conventional and inverse layers respectively, a is equivalent to N_{max} (maximum electron density) and ,b, represents the quantity $N_m(r_N/y_m)^2$. The three equations describing the connection of two quasiparabolic layers by an interim inverse quasiparabolic segment may now be formulated

$$N_1 = a_1 - b_1\left(1 - \frac{r_{m_1}}{r}\right)^2 \qquad (3:9)$$

$$N_2 = a_2 + b_2\left(1 - \frac{r_{m_2}}{r}\right)^2 \qquad (3:10)$$

$$N_3 = a_3 - b_3\left(1 - \frac{r_{m_3}}{r}\right)^2 \qquad (3:11)$$

The gradient in electron density for each layer may be expressed by the three equations

$$\frac{dN_1}{dr} = \frac{-2r_{m_1}}{r^2} b_1\left(1 - \frac{r_{m_1}}{r}\right) \qquad (3:12)$$

$$\frac{dN_2}{dr} = \frac{2r_{m_2}}{r^2} b_2\left(1 - \frac{r_{m_2}}{r}\right) \qquad (3:13)$$

$$\frac{dN_3}{dr} = \frac{-2r_{m_3}}{r^2} b_3 \left(1 - \frac{r_{m_3}}{r}\right) \qquad (3:14)$$

Assuming that the inverse joining layer is tangent to the lower layer at its maximum, it follows

$$a_2 = a_1 \qquad (3:15)$$

and

$$r_{m_2} = r_{m_1} \qquad (3:16)$$

The equation describing the inverse layer can now be written

$$N_2 = N_{m_1} + N_{m_1} \frac{r_t^2}{y_{m_2}^2} \left(1 - \frac{r_{m_1}}{r}\right)^2 \qquad (3:17)$$

where the normalization constant for the inverse layer is chosen to be transition height at the upper end of the joining segment. Matching the electron density and its gradient at the transition height r_t one obtains the continuity conditions

$$a_1 + b_2 \left(1 - \frac{r_{m_1}}{r_t}\right)^2 = a_3 - b_3 \left(1 - \frac{r_{m_3}}{r_t}\right)^2 \qquad (3:18)$$

and

$$\frac{r_{m_1} b_2}{r_t^2}\left(1 - \frac{r_{m_1}}{r_t}\right) = \frac{- r_{m_3} b_3}{r_t^2}\left(1 - \frac{r_{m_3}}{r_t}\right) \qquad (3:19)$$

Examination of the above two continuity equations shows that with the exception of the quantities b_2 and r_t all other quantities are determined by the characteristics of the traditional layers. Solving eq (3.19) for b_2 gives :

$$b_2 = - \frac{r_{m_3}}{r_{m_1}} \frac{\left(1 - \frac{r_{m_3}}{r_t}\right)}{\left(1 - \frac{r_{m_1}}{r_t}\right)} b_3 \qquad (3:20)$$

where

$$b_2 \equiv N_{m_1} \frac{r_t^2}{y_{m_2}^2} \qquad (3:21)$$

$$b_3 \equiv N_{m_3} \frac{r_{N_3}^2}{y_{m_3}^2} \qquad (3:22)$$

Substitution of the expression for ,b_2, into eq (3.18) gives the joining height, r_t,

$$r_t = \frac{b_3\, r_{m_3} \left\{ \frac{r_{m_3}}{r_{m_1}} - 1 \right\}}{(a_3 - a_1) - b_3 \left\{ \frac{r_{m_3}}{r_{m_1}} - 1 \right\}} \qquad (3:23)$$

where the quantities a_1, a_3 and b_3 are defined

$$a_1 \equiv N_{m_1} \qquad (3:24)$$

$$a_3 \equiv N_{m_3} \qquad (3:25)$$

$$b_3 \equiv N_{m_3} \frac{r_{N_3}^2}{y_{m_3}^2} \qquad (3:26)$$

Expressing eq (3.20) and eq (3.23) in terms of the fundamental quantities that describe the quasiparabolic layers, one obtains the semi-thickness and joining height equations for the inverse section, in the form

$$y_{m_2}^2 = \frac{r_{m_1} (r_t - r_{m_1}) N_{m_1} r_t^2}{r_{m_3} (r_{m_3} - r_t) N_{m_3} r_{N_3}^2} y_{m_3}^2 \qquad (3:27)$$

and

$$r_t = \frac{N_{m_3}\, r_{N_3}^2\, r_{m_3}\left(\frac{r_{m_3}}{r_{m_1}} - 1\right)}{y_{m_3}^2\left[(N_{m_3} - N_{m_1}) + \frac{N_{m_3}\, r_{N_3}^2}{y_{m_3}^2}\left(\frac{r_{m_3}}{r_{m_1}} - 1\right)\right]} \qquad [3:28]$$

It is usual to set the normalization constant of a traditional quasiparabolic layer equal to the height of its base at the point of zero plasma density, therefore

$$r_{N_3} = r_{b_3} = (r_{m_3} - y_{m_3}) \qquad [3:29]$$

Given that the parameters of the quasiparabolic sections used in the above construction are determined by curve fitting such model geometry to an observed electron density profile, it is clear that the geometry of the inverse quasiparabolic joining segment follows mathematically by substituting eqs [3.27] and [3.28] into eq [3.3] where it should be remembered that , $r_{N\,2}$, is equivalent to r_t.

The analysis of a monotonic electron density profile

In chapter [5] the details of the least squares curve fitting algorithms necessary to determine the ionospheric layer parameters are developed from first principles. For the moment a set of sample data, Baker et al [1990], will be used for the sole purpose of demonstrating how a N[h] profile can be constructed using the multisegmented

quasiparabolic model of the type proposed by Hill [1978]. The defining parameters of a three-layer model ionosphere are :

IONOSPHERIC LAYER	CRITICAL FREQ. f_c(MHz)	MAXIMUM HEIGHT OF LAYER r_m(km)	SEMI-THICKNESS OF LAYER y_m(km)
E - layer	3.0	110.00	20.00
F1 - layer	4.2	210.00	80.00
F2 - layer	6.0	320.00	100.00

Table (3.1) : Ionospheric parameters of a three-layer model ionosphere; Baker [1990]

Each quasiparabolic layer is fully described by the three ionospheric parameters (f_c, r_m, y_m) as can be seen from an examination of the terms contained in the equation describing a quasiparabolic electron distribution.

$$f_N^2 = f_c^2 \left(1 - \frac{(r - r_m)^2}{y_m^2} \cdot \frac{r_N^2}{r^2} \right) \qquad (3:30)$$

The normalization constant r_N is by convention made equal to base height r_b of the layer and as previously discussed is given by (r_m - y_m). It is clear that nine parameters in total will be required to describe the three layer structure displayed in table (3.1) but since the distribution is non re-entrant a total of only two inverse joining layers will be needed. The

semi-thickness ,y_m, and the joining height ,r_t, of the inverse quasiparabolae are derived via eqs (3.27) and (3.28), given that the parameters of the ionospheric layers have already been determined. Figure (3.2) shows a plot of the MQP model profile corresponding to the sample ionosphere described in table (3.1). As previously stated the N(h) profile does not have a valley and is therefore described as being monotonic or non re-entrant. The model electron density profile is everywhere continuous and smoothly varying and extends from an altitude of ninety to three-hundred and twenty kilometers.

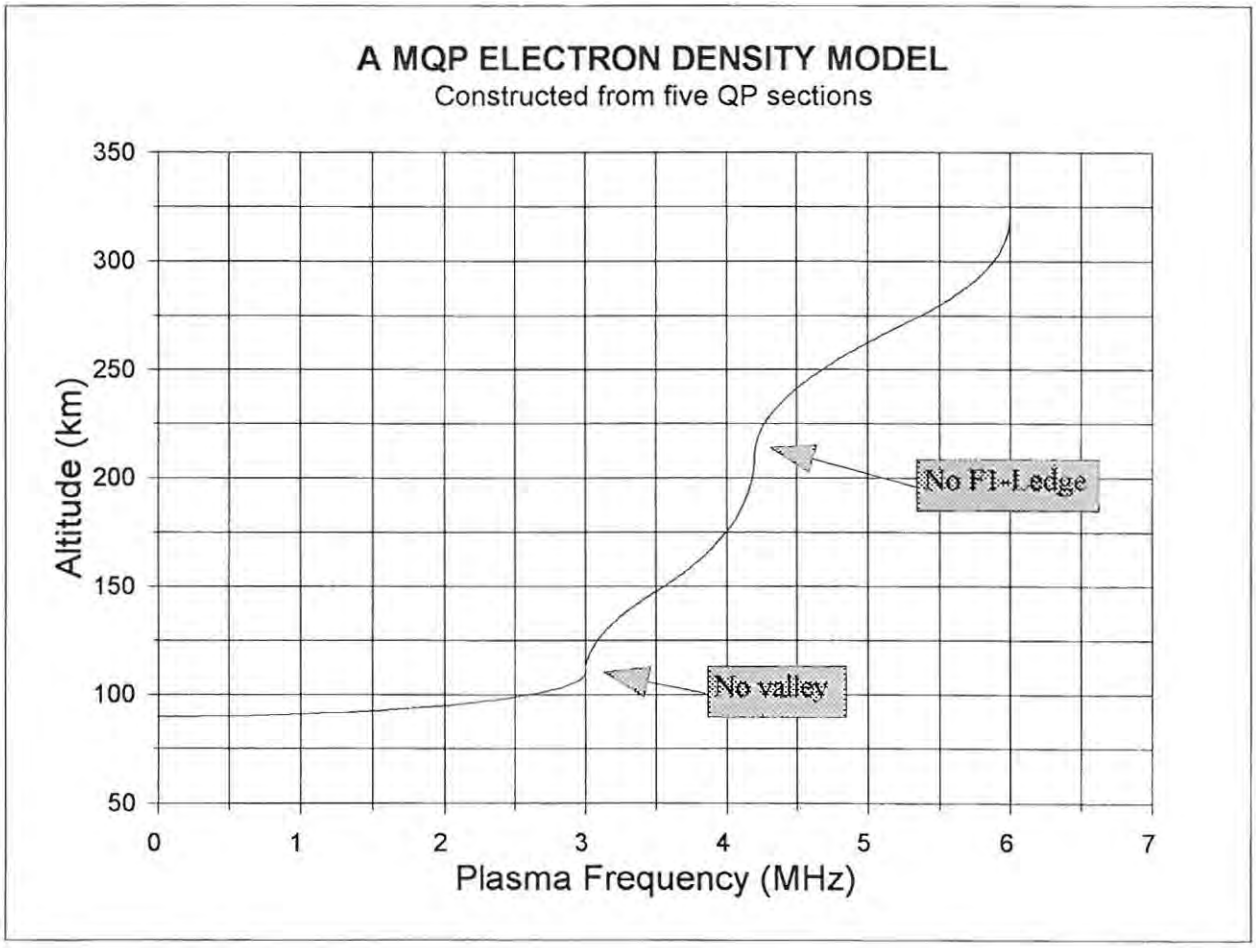

Figure (3.2) Model MQP electron density distribution corresponding to the ionosphere described in table (3.1)

The quasiparabolic description of a non-monotonic electron density profile

If an N-h profile has an ionization depletion region between the maximum electron density in the E layer and the F_1 region, it will be necessary to incorporate an E/F_1 valley. The figure below depicts a valley region constructed from quasiparabolic sections and shows how a re-entrant electron density distribution can be made to smoothly connect the E/F_1 transition.

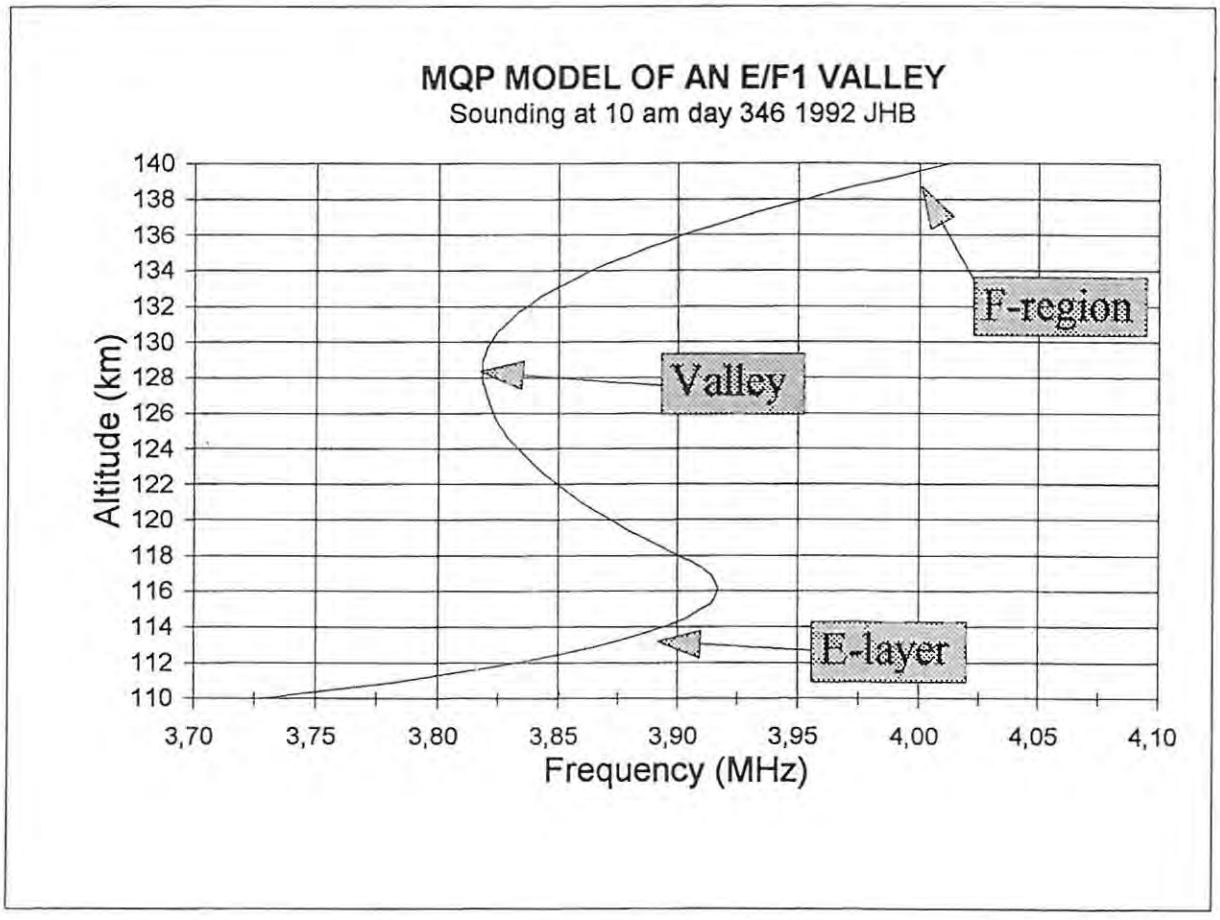

Figure (3.3) Multi-segmented quasiparabolic valley :- an exploded view of the E/F_1 region of the MQP profile displayed in figure (6.4)

An ionogramme inversion program such as POLAN (Titheridge 1986) provides a description of an E/F1 depletion region in terms of the valley's width, W, and its depth δ, while the parameters of the ionospheric layers above and below the valley region are determined via curve fitting to observed N-h data. The above information is sufficient to determine the geometry of the quasiparabolic segments that are needed to construct the E/F_1 valley region. The figure (3.4) below illustrates the geometry of a re-entrant electron density distribution constructed from three quasiparabolic segments with continuity in the concentration and its derivative throughout the valley's extent.

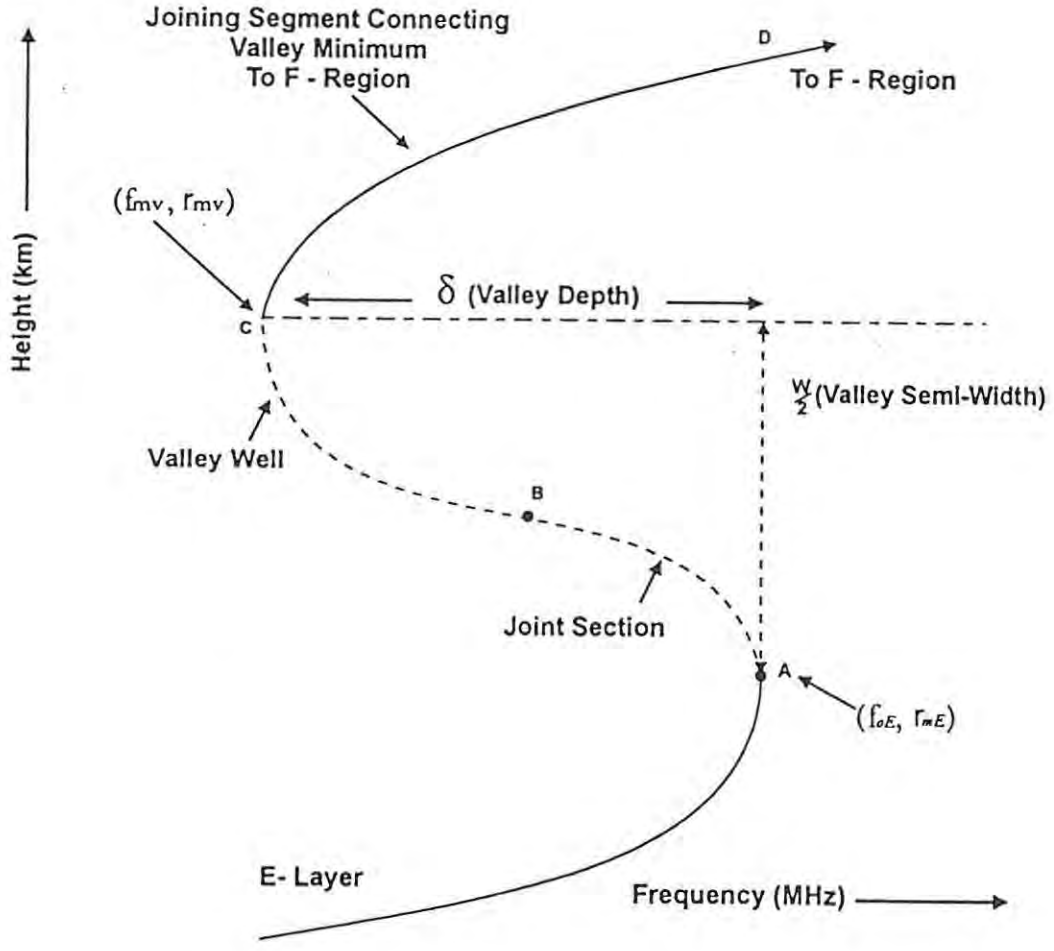

Figure (3.4) Sketch of the geometry required to construct an E/F_1 valley using three quasiparabolic type segments.

The segment BC is an inverse quasiparabola that passes through the valley minimum, (r_{mv}, N_{mv}), and the quasiparabolic section AB connects the top of the E layer to the well of the valley. One must choose a value for the semi-thickness of the re-entrant section, AB, that will ensure a two segment fit between the peak of the E layer and the valley minimum. A third section, CD, is needed to close out the valley and provide a smooth connection to the F-region of the ionosphere. The inverse quasiparabolic curve, CD, must satisfy the continuity conditions at the bottom of the valley and again at the joining height ,r_j, where the electron density distribution becomes monotonic again. The dimensions of the valley are obtained from the ionogramme inversion programme, POLAN, but only the valley depth and the semi-width are used in the construction of the re-entrant geometry.

Default case

In the event that the E/F valley disappears then the depth and width tend to zero so that points A, B and C co-locate, resulting in only one inverse layer being required to smoothly connect the E layer to the F region.

The derivation of the equations needed to build a MQP E/F valley region

Referring to figure(3.4), the segment AB passes through the vertex of the E layer which has co-ordinates (r_{mE}, f_oE) and possesses a traditional parabolic geometry of the form

$$f_v^2 = f_o^2 \left(1 - \frac{r_N^2}{y_m^2}\left(1 - \frac{r_{mE}}{r}\right)\right) \qquad (3:31)$$

where it should be noted that the electron density is proportional to the square of the

plasma frequency. If the valley has a depth ,δ, equivalent to [f_0E] less [f_{mv}], then the plasma frequency at the bottom of the well is

$$f_{mv}^2 = f_o^2 - \frac{f_o^2\, r_N^2}{y_m^2}\left(1 - \frac{r_{mE}}{r^*}\right)^2 \qquad [3:32]$$

where one has chosen to extend the segment AB to determine the co-ordinates of the point [f_{mv}, r^*] given ,r_{mv}, is set equal to [$r_{mE} + \delta/2$]. If the value of r^* is greater than or equal to the height of the valley minimum, r_{mv}, an over-shoot condition exists and one must adjust the value of the factor [r_N^2/y_m^2] until $r^* < r_{mv}$,only then is it possible to insert the inverse section, BC. The value of the normalization height r_N for the section AB is determined using the convention of setting r_N equal to the geocentric radial height at which the quasiparabolic profile gives a zero value for plasma density, in this case the top-side value. On account of the quasiparabolic geometry being asymmetric about its generator axis, one must solve the quadratic in plasma frequency, select the larger of the two roots and obtain the top-side height corresponding to zero electron concentration, implying

$$r_{Ntop\text{-}side} = \frac{r_m\, r_b}{(r_b - y_m)}\,, \quad r_b = (r_m - y_m) \qquad [3:33]$$

Solving eq [3.32] for, r^*, substituting eq [3.33] for the normalization factor and finally applying the overshoot criterion yields the inequality

$$r_{mv} > \frac{r_{mE}}{\left\{1 - \frac{y_m (r_{mE} - 2y_m)}{r_{mE} (r_{mE} - y_m)} \left(1 - \frac{f_{mv}^2}{f_c^2}\right)^{1/2}\right\}} \qquad [3:34]$$

which must be satisfied to ensure a two segment fit from the top of the E layer to the bottom of the valley.

Determination of the joining height of the contiguous QP segments constituting the E/F valley region :

The figure [3.5] illustrates the generic geometry involved in the construction of a re-entrant portion of an otherwise monotonic MQP profile.

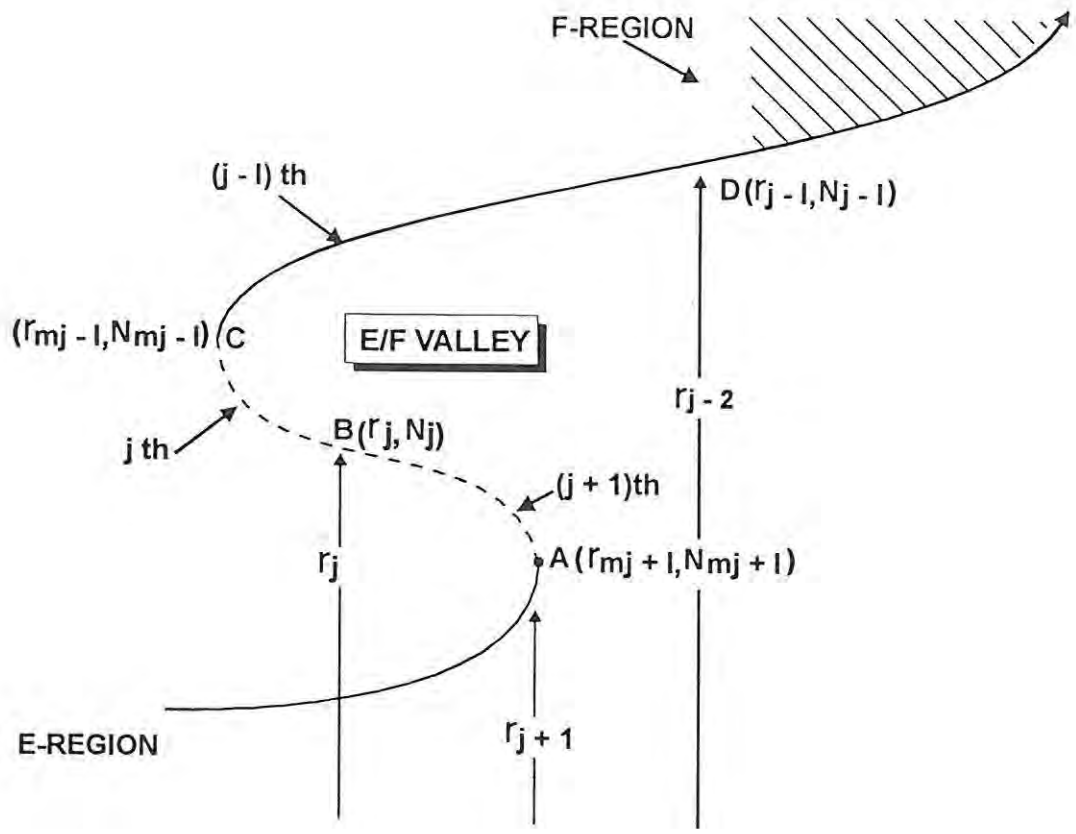

Figure (3.5) The construction of a MQP E/F_1 valley

One can express the, eq (3.28), to give the joining height ,r_j, in terms of the generic co-ordinates shown in figure (3.5), to give

$$r_j = \frac{N_{mj+1}\, r_{Nj+1}^2\, r_{mj+1}\left(\frac{r_{mj+1}}{r_{mj-1}} - 1\right)}{y_{mj+1}^2\left[(N_{mj+1} - N_{mj-1}) + \frac{N_{mj+1}\, r_{Nj+1}^2}{y_{mj+1}^2}\left(\frac{r_{mj+1}}{r_{mj-1}} - 1\right)\right]} \qquad (3.35)$$

a result that can be easily applied to any section of a re-entrant geometry.

Stage (1) : Fitting the (j + 1)th quasiparabolic section of the E/F_1 valley

Based on the valley geometry it is clear that the generic co-ordinates (r_{mj+1}, N_{mj+1}) transpose to (r_{mE}, N_{mE}) while the ratio r_{Nj+1} / y_{mj+1} is determined by the "over shoot" condition discussed earlier. In general the value of the semi-thickness of the section AB will be less than ,y_{mE}, if one is to ensure a two segment fit between the E layer maximum and the bottom of the E/F_1 valley. The appropriate value of the semi-thickness, y_{mj+1}, required to satisfy the over-shoot condition is determined using, eq (3.34), provided the co-ordinates of both the E layer maximum and the valley minimum are known. It was found that in the case of every electron density profile analysed using POLAN, setting y_{mj+1} equal to y_{mE} ensured a two segment fit connecting (r_{mE}, N_{mE}), and (r_{mv}, N_{mv}). This is not surprising given that POLAN'S software models the onset of an E/F depletion region as an extension of a parabolic E layer, the top-side of which intersects a flat bottomed well. If one uses an inversion programme other than POLAN, then eq (3.34) must be implemented to determine the value of top-side semi-thickness ,y_{mj+1}, that ensures the over shoot condition ,$r^* < r_{mv}$, will be satisfied.

Stage (2) : Fitting the j th quasiparabolic section of the E/F_1 valley

The joining height ,r_j, of the connection point for the (j+1)th and jth QP sections of the E/F valley is obtained by substituting the generic equivalents listed below,

$$r_{mj+1} \equiv r_{mE} \qquad (3:36)$$

$$N_{mj+1} \equiv N_{mE} \tag{3:37}$$

$$y_{mj+1} \equiv y_{mE} \tag{3:38}$$

$$r_{Nj+1} \equiv \frac{r_{mE}\,(r_{mE} - y_{mE})}{(r_{mE} - 2y_{mE})} = r_N \tag{3:39}$$

$$N_{mj-1} \equiv N_{mv} \tag{3:40}$$

$$r_{mj-1} \equiv r_{mv} \tag{3:41}$$

into eq(3.35) and then simplifying to yield,

$$r_j = \frac{r_{mE}}{\left[1 - \dfrac{(N_{mE} - N_{mv})}{\dfrac{N_{mE}\, r_N^2}{y_{mE}^2}\left(1 - \dfrac{r_{mE}}{r_{mv}}\right)}\right]} \tag{3:42}$$

The ionospheric parameters (N_m,r_m,y_m) are determined by curve fitting a quasiparabolic section to N-h data describing the E region while the valley co-ordinates (N_{mv},r_v) are derived directly from POLAN. The semi-thickness of the valley segment BC can be found by using the generic form of eq (3.27),namely

$$y_{mj}^2 = \frac{r_{mj-1}\,(r_j - r_{mj-1})\,N_{mj-1}\,r_j^2\,y_{mj+1}^2}{r_{mj+1}\,(r_{mj+1} - r_j)\,N_{mj+1}\,r_{Nj+1}^2} \qquad (3:43)$$

where one substitutes the generic equivalents expressed in eqs (3:36 → 3:41) to yield the result

$$y_{mv}^2 = \frac{r_{mv}\,(r_j - r_{mv})\,N_{mv}\,r_j^2\,y_{mE}^2}{r_{mE}\,(r_{mE} - r_j)\,N_{mE}\,r_N^2} \qquad (3:44)$$

Stage (3) : Fitting the (j-1)th quasiparabolic section of the E/F_1 valley

Knowing the co-ordinates of the valley minimum (r_{mv}, N_{mv}) and the F layer parameters one can fit the (j-1)th section of the valley using the generic joining equations to calculate the transition height ,r_{j-2}, and semi-thickness ,y_{mj-1}. The N(h) profile now becomes monotonically increasing again as one enters the F region of the ionosphere. In the simple case of a single F layer the calculation of the MQP geometry is now complete and a total of five quasiparabolic sections will be sufficient to model the full extent of the ionosphere from the base of the E layer up to the maximum electron density in the Fregion.

Bifurcation of the F region

During the day the ionosphere undergoes a series of photochemical and transport phenomena in the F region and a bifurcation or splitting of this ionospheric stratum

invariably occurs. The two strata into which the F region splits are called the F_1 and F_2 layers respectively and a MQP model profile will now require an additional two quasi-parabolic sections for a complete description of the observed N-h distribution. The figure (3.6) shows a three layer, re-entrant ionosphere constructed from a total of seven quasiparabolic segments.

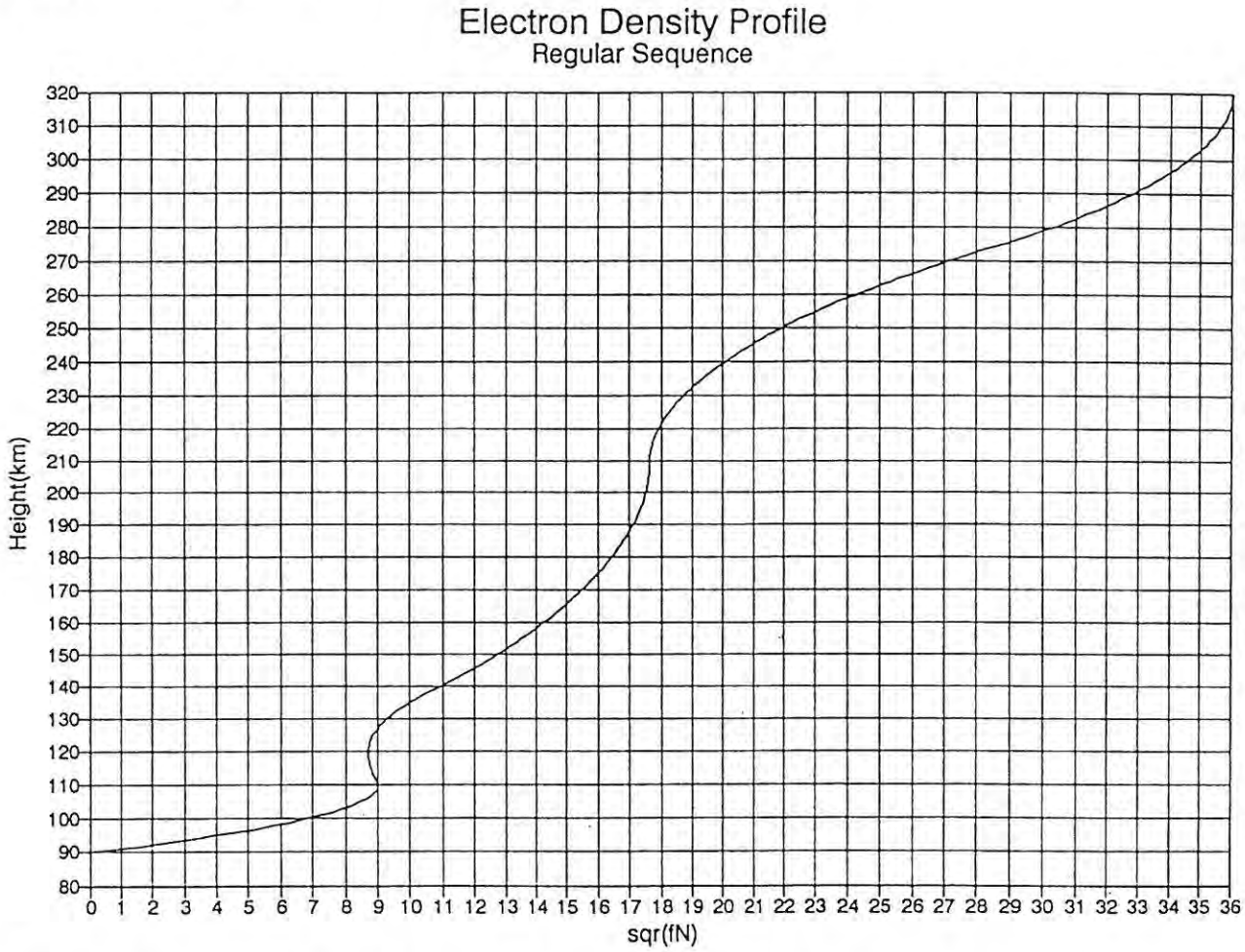

Figure (3.6) A MQP curve fit to a three layered, re-entrant ionosphere constructed from the layer parameters listed in table(3.1), with the inclusion of an E/F1 valley of depth 0.05MHz and width 20km , after Baker (1990).

The F_1 region of the N(h) profile depicted in figure (3.6) is the exception rather than the rule as it is more often the case that the double derivative of the plasma density vanishes

at the top of the F1 layer giving rise to an inflexion condition. The complexities of curve fitting model profiles to the F_1 region when it exhibits a ledge of ionization are discussed in Chapter (5) but suffice it to say that a completely new algorithm must be developed to determine the F_1 ledge / F_2 layer joining height. It should noted in passing that it much easier to implement the De Voogt [1953] rather than the Croft and Hoogasian[1968] formulation of the quasiparabolic profile when determining the mathematical description of a ledge/layer joining section. However, more on these details later! One now has a comprehensive understanding of the joining height equations that ensure continuity of the MQP model electron density and its derivative throughout a monotonic or re-entrant profile, the F_1 ledge condition notwithstanding. The rôle of POLAN in determining the required critical frequencies and heights of the plasma density maxima in the respective ionospheric layers together with the calculation of the E/F1 valley dimensions has been discussed. The next step is to develop the necessary algorithms to curve fit quasiparabolic sections to observed N-h electron density data under both layer and ledge conditions.

CHAPTER (4)

THE ANALYSES OF HF RADIO PROPAGATION THROUGH A MQP IONOSPHERIC MODEL AND THE DETERMINATION OF GROUND RANGE AND CIRCUIT MUF.

In the field of HF communication forecasting it is desirable to use simplified ionospheric models to determine the ray path trajectories of radio waves. Ray- tracing requires extensive computer calculations if the exact details of the electron density distribution, the effects of collisions and the presence of the earth's magnetic field are included. The ionospheric model must be sophisticated enough to embody the radio physics of the propagation path while minimizing the computer time involved in executing its algorithms. In general one may ignore collisions for frequencies lying in the range 3 to 30 MHz if the altitudes are in excess of seventy kilometers and if one elects to ignore the earth's magnetic field it becomes possible to choose an ionospheric model that will yield analytical solutions to the ground range equations. In chapter (2) the parabolic model was discussed

extensively and the quasiparabolic variant of this electron density distribution was introduced to facilitate analytical ray tracing over an oblique radio link. In the current chapter the exact integral solutions to the ground range equations applicable to a spherical earth and concentric ionosphere are derived from first principles, for the propagation conditions describing apogee in or traversal of, either a quasi or inverse quasiparabolic ionospheric layer. Ray-tracing algorithms are developed to determine the maximum usable frequency that may be supported by an HF radio link and simulations are carried out using a multi-segmented quasiparabolic ionosphere of the type described by Hill[1978]. The results are compared with those obtained via a standard F2 layer MUF algorithm developed by Lockwood[1983] and adopted by the CCIR [report 340-6,1991] for use in HF prediction when only the standard URSI scaled ionospheric parameters are available.

Radio propagation through an ionosphere modelled as a single quasiparabolic layer

The figure [4.1] shows the refraction process undergone by an HF radio signal as it propagates through the earth's curved ionosphere in the absence of any horizontal or vertical tilts and ignoring the influence that the earth's magnetic field has upon propagation.

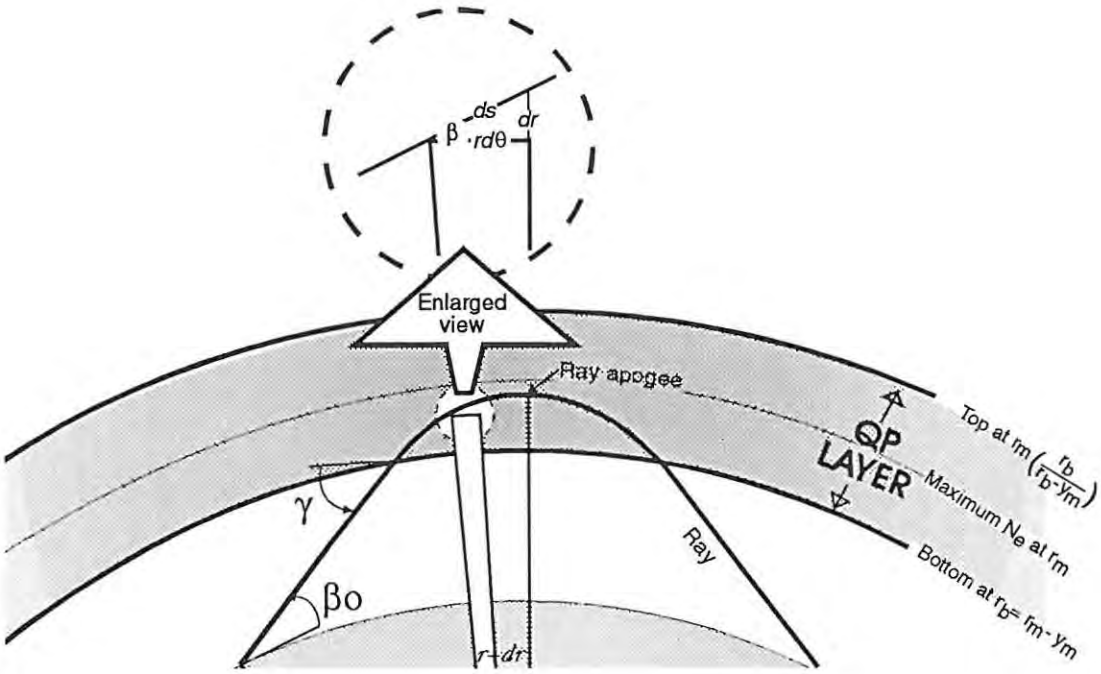

Geometry of radio locus in a quasiparabolic ionosphere.

Figure (4.1): A typical HF radio locus in a quasiparabolic ionosphere.

The law of Snellius, more often associated with optical phenomena, is equally applicable to HF propagation providing suitable account is taken of the curved earth geometry. In making this modification one arrives at Bouguer's rule which states that the product ,rμcos(β),

remains invariant along a radio locus, its ground level value of $r_0\cos(\beta_0)$ being a constant of the propagation path defined by the launch angle ,β_0. Therefore, the equation describing the HF radio locus is given by

$$r_1\mu_1\cos\beta_1 = r_2\mu_2\cos\beta_2 = - - - = r_0\cos\beta_0 \qquad [4:1]$$

where $r_0 \cos \beta_0$ is known as the radio invariant. Applying elementary geometry to the enlarged view of a section of the radio locus displayed in figure (4.1), one can show that in the limit as the arc length becomes infinitesimally small, the sub-sum of the incremental ground range contributions is given by the integral equation

$$D = 2r_0\int_0^{\Theta_t} d\Theta = 2r_0\int_{r_0}^{r_t}\frac{dr}{r\tan\beta} \qquad [4:2]$$

where r_t represents the geocentric height of the radio apogee

Using Bouguer's rule one may express tanβ in terms of the geocentric ray height, phase refractive index and radio invariant, to give:

$$D = 2\int_{r_0}^{r_t}\frac{r_0^2\cos^2\beta_0 dr}{r\left(r^2\mu^2(r) - r_0^2\cos^2\beta_0\right)^{1/2}} \qquad [4:3]$$

If the effect of electron collisions, positive ions and magnetic fields are ignored, one may use the fundamental form of eq(2.13) to express the phase refractive index of an electron gas, as

$$\mu^2 = 1 - \frac{e^2 N_e}{(4\pi^2 m \epsilon_0 f^2)} \qquad [4:4]$$

where e/m $\rightarrow$ charge to mass ratio of the electron

ϵ_0 $\rightarrow$ permittivity of free-space

N_e $\rightarrow$ ionospheric electron density

f $\rightarrow$ radio frequency of propagating signal

It is clear that the mathematical form of the electron concentration ,N, will determine whether or not the ground range integral is soluble in closed form. To ensure an analytical solution when propagating at oblique incidence through a MQP ionosphere one uses the quasi and inverse quasiparabolic electron profiles proposed by Hill [1978]. It follows from eq(2.13) that the phase refractive index of a MQP model ionosphere is given by

$$\mu^2 = 1 - 81\frac{N_{QP|IQP}}{f^2} \qquad [4:5]$$

where the mathematical form of the plasma density for either curvature of QP layer may be expressed

$$N_{QP|IQP} = N_m\left(1 \mp \left(\frac{r - r_m}{y_m}\right)^2\left(\frac{r_n}{r}\right)^2\right) \qquad [4:6]$$

N_m → maximum electron density in the layer

r_m → geocentric height corresponding to N_m

y_m → layer semi-thickness

r_n → normalization factor usually set equal to the geocentric height of the layer base

$\mp$ → quasi / inverse quasiparabolic profile.

Derivation of the ionospheric layer coefficients (ABC) for quasi and inverse quasiparabolic segments

From eq (2.2) it is clear that the plasma frequency of a quasi or an inverse quasiparabolic electron profile has the same functional form as the expression for its electron density, namely

$$f^2_{N_{QP/IQP}} = f_c^2 \left[1 \mp \left(\frac{r - r_m}{y_m} \right)^2 \left(\frac{r_b}{r} \right)^2 \right] \qquad (4:7)$$

where

$$f_c \simeq 9 (N_m)^{1/2} \qquad (4:8)$$

One may also mathematically describe the electron profile of the QP and IQP sections of a MQP model via De Voogt's generalized quadratic in (1/r) ,eq(2.52),

$$f^2_{N_{QP/IQP}} = \frac{A}{r^2} + \frac{B}{r} + C \qquad (4:9)$$

Equating terms in, r^2, r^1, r^0 , one can show that the ionospheric coefficients A,B,C may be expressed

$$A = \mp f_c^2 r_m^2 \frac{r_b^2}{y_m^2} \qquad (4:10)$$

$$B \equiv \pm 2 f_c^2 r_m \frac{r_b^2}{y_m^2} \qquad (4:11)$$

$$C = f_c^2 \mp f_c^2 \frac{r_b^2}{y_m^2} \qquad (4:12)$$

where -/+ denotes (quasi/inverse quasi) parabolic geometry.

Derivation of the ray tracing coefficients A′, B′, C′. for a MQP model ionosphere

The determination of the ground range covered by a HF signal propagating through a MQP ionosphere requires that one solve an integral equation of the form:

$$I = \int \frac{dx}{x\sqrt{X}} \qquad (4:13)$$

where the quantity ,X, inside the radical is a quadratic of the form:

$$X = ax^2 + bx + c \qquad [4:14]$$

The solution to the above equation can be found in any standard mathematical handbook, CRC [1985], and listed below are the cases encountered when propagating through the QP/IQP layers that form the building blocks of the MQP model

Case 1: **apogee / traversal of a quasiparabolic layer**

$$I = -\frac{1}{\sqrt{c}} \log_e\left(2\sqrt{cX} + bx + 2c\right) \;,\; c>0 \qquad [4:15]$$

Case 2: **apogee / traversal of an inverse quasiparabolic layer**

$$I = \frac{1}{\sqrt{-c}} \sin^{-1}\left(\frac{2c + bx}{x(b^2 - 4ac)^{1/2}}\right) \;,\; c<0 \qquad [4:16]$$

The general equation for ground range, eq [4.3], is usually written:

$$D = 2r_0^2 \cos^2\beta_0 \int \frac{dr}{r\sqrt{R}} \qquad [4:17]$$

where the quantity R is known as the ray tracing polynomial, equivalent to

$$R \equiv r^2 \mu^2(r) - r_0^2 \cos^2\beta_0 \qquad [4:18]$$

The phase refractive index ,μ[r], of a QP/IQP ionospheric layer may be expressed as a function of plasma frequency by substituting eq [4.6] into eq [4.5], to give

$$\mu^2(r)_{QP/IQP} = 1 - \frac{f_c^2}{f^2}\left(1 \mp \left(\frac{r - r_m}{y_m}\right)^2 \left(\frac{r_b}{r}\right)^2\right) \qquad [4:19]$$

where one has used the relation, $f_c \approx 9[N_m]^{1/2}$. Substitution of the expression for, $\mu(r)_{QP/IQP}$, into eq (4.18) shows that the ray tracing polynomial is quadratic in ,r, for the case of the quasiparabolic electron profile. One may express the function R in the form

$$R \equiv A'r^2 + B'r + C' \qquad (4:20)$$

where the so-called ray-tracing coefficients (A',B',C') are dependent upon the ionospheric coefficients (A,B,C), the propagation frequency ,f, and the launch angle ,β_0, at the transmitter site. To see this relationship one first combines eq(4:9) with eq(2:13) so as to express the phase refractive index μ in terms of A,B,C and the signal frequency f. If one now substitutes the newly derived form of μ into eq(4:18) it follows from eq(4:20) that equating coefficients in r^2,r,r^0 will give the following relationships

$$B' = -\frac{B}{f^2} \qquad (4:21)$$

$$A' = 1 - \frac{C}{f^2} \qquad (4:22)$$

$$C' = -r_0^2 \cos^2\beta_0 - \frac{A}{f^2} \qquad (4:23)$$

where A, B, C are determined via eqs (4.10), (4.11) and (4.12) respectively.

The determination of ground range when ray tracing through a MQP model.

To determine the distance travelled by a HF signal one must divide the radio locus into free-space and ionospheric sections and then sub-sum the respective projected ground range

contributions.

The evaluation of the free-space ground range component.

The general form of the ground range integral eq (4.17) may be expressed in the form

$$D = 2r_0^2 \cos\beta_0 \int_{r_0}^{r} \frac{dr}{r(A'r^2 + B'r + C')^{1/2}} \qquad (4:24)$$

where the ray tracing coefficients A′, B′, C′, are given by eqs (4:21), (4.22) and (4:23) respectively. Under free-space conditions the phase refractive index μ assumes its in-vacuo value of unity and substituting zero values for the ionospheric coefficients A,B,C into eqs (4.21) to (4.23) yields

$$A'_0 = 1 \qquad (4:25)$$

$$B'_0 = 0 \qquad (4:26)$$

$$C'_0 = -r_0^2 \cos^2\beta_0 \qquad (4:27)$$

where the subscript 0 denotes the non-ionospheric values of the ray tracing coefficients A′, B′, C′ respectively. Examination of eq (4:27) shows that the value of C_0' is less than 0 implying that the integral solution to eq (4:24) under free-space conditions is given by eq (4:16). Substitution of the free-space ray tracing coefficients into the general form of eq (4.16) and integrating from the surface of the earth to the base of the ionosphere yields, upon substitution of the appropriate limits, the result

$$D_0 = 2r_0(\gamma - \beta_0) \qquad [4:28]$$

where ,γ, is seen from figure (4.1) to be the angle at which the radio trajectory enters the ionosphere, given by

$$\gamma = \cos^{-1}\left(\frac{r_0}{r_b}\cos\beta_0\right) \qquad [4:29]$$

To evaluate the ionospheric contribution to the ground range.

Four cases must be discussed if one is to derive ray tracing algorithms capable of calculating the ensemble ground range covered by a radio signal propagating through a multisegmented ionosphere. A MQP model profile is composed of both quasi and inverse quasiparabolic layers and a radio ray can experience, apogee in or traversal of, either type of electron distribution.

Case 1: Apogee in a traditional quasiparabolic layer

One wishes to solve eq (4.24) where the ray tracing coefficients A′, B′, C′ correspond to a quasiparabola and the limits of integration extend from the base of the layer, r_b, up to the apogee height, r_{ap}. To determine the geocentric height of the radio apogee one applies Bouguer's rule ,eq (4.1), at the turning point of the radio locus, where the angle of refraction, β_{apogee}, goes to zero, implying

$$\mu(r)\, r\cos\beta \rightarrow \mu(r_{ap})\, r_{ap} = \mu_0 r_0 \cos\beta_0 \qquad [4:30]$$

It follows, therefore, that under apogee conditions the ray tracing quadratic may be

expressed

$$R_{ap} = A' r_{ap}^2 + B' r_{ap} + C' = \mu^2(r_{ap}) r_{ap}^2 - \cos^2\beta_0 = 0 \qquad (4:31)$$

a result which is known as the null condition. Before embarking on solving the ground range equation for apogee in a traditional layer it is appropriate to introduce the ancillary result, Dyson et al [1988],

$$\frac{B' r_{ap} + 2C'}{r_{ap}} = \sqrt{B'^2 - 4A'C'} \qquad (4:32)$$

which together with the null condition expressed in eq (4.31)

$$R_{ap} = 0 \qquad (4:33)$$

allows one to greatly simplify the form of the solutions to the ground range equation. Mathematically the quasi and the inverse quasiparabolic distributions are distinguished from one another by the algebraic sign of their respective ray-tracing coefficient, C'. The ionospheric coefficient ,A, eq (4:10), may be substituted into ,eq (4.23), enabling one to express the ray tracing coefficient ,C', in terms of the QP/IQP layer parameters, propagation frequency and elevation angle, as follows

$$C' = -r_0^2 \cos^2\beta_0 \pm \frac{f_c^2 r_m^2 r_b^2}{y_m^2} \qquad (4:34)$$

from which it is clear;

C' > 0 defines a quasiparabolic

$C' < 0$ defines an inverse quasiparabolic.

If one refers to the standard integral results in the form of eqs (4.15) and (4.16) it is straight-forward to make the correct selection to solve the ground range by equation

$$D = 2r_0^2 \cos^2\beta_0 \int \frac{dr}{r\sqrt{R}} \qquad (4:35)$$

subject to the condition,

$C' > 0.$

It follows that the ground range covered by a radio locus undergoing apogee in a quasiparabolic layer is given by

$$D = \frac{2r_0^2 \cos^2\beta_0}{\sqrt{C'}} \log_e \left(\frac{r_a\left(2\sqrt{C'R_b} + B'r_b + 2C'\right)}{r_b\left(2\sqrt{C'R_a} + B'r_a + 2C'\right)} \right) \qquad (4:36)$$

where the subscripts ,b, and ,a, derive from the integration limits which extend from the bottom of the QP layer ,r_b, to the top of the ray trajectory ,r_{ap}. Using the ancillary equations, (4.31) and (4.32) describing the apogee condition, one may simplify the above result to give

$$D = \frac{2r_0^2 \cos^2\beta_0}{\sqrt{C'}} \log_e \left(\frac{2\sqrt{c'R_b} + B'r_b + 2C'}{r_b\sqrt{B'^2 - 4A'C'}} \right) \qquad (4:37)$$

The physical interpretation of the roots of the ray-tracing quadratic:

Inspection of eq (4.37) reveals that the logarithm's argument is controlled by the discriminant of the ray tracing quadratic, being variously, real, infinite and complex. Solving eq (4.31) by completing of the square, gives two values for the apogee height, namely

$$r_{ap} = \frac{-B' \pm (B'^2 - 4A'C')^{1/2}}{2A'} \qquad (4:38)$$

where the nature of the roots is determined by the discriminant. One ignores the positive root if propagation is through a quasiparabolic layer and likewise the negative root if the layer has an inverse geometry. Therefore, one retains the bottom-side apogee height in the case of a QP profile, discarding the mirror image root, while the opposite holds true when one has an inverse layer geometry. The physical significance of the radical term in the denominator of eq (4.37) may be summarized as follows:

1. $B'^2 > 4A'C'$, $\Rightarrow$ apogee occurs in a quasiparabolic layer,
2. $B'^2 = 4A'C'$, $\Rightarrow$ apogee occurs at the height of maximum electron density in a quasiparabolic layer,
3. $B'^2 < 4A'C'$, $\Rightarrow$ quasiparabolic layer does not contain the ray.

Case 2: Traversal of a quasiparabolic layer

A QP profile that constitutes a region of under-ionization within a MQP model ionosphere will be traversed by a HF signal if the layer's ray tracing coefficients satisfy the inequalities

$$B'^2 < 4A'C' \qquad (4:39)$$

$$C' > 0 \qquad (4:40)$$

that is, the ray tracing quadratic has complex roots. To calculate the ground range covered

(upper limit)
by the signal, one integrates eq (4.24) from the bottom ,r_b, to the top ,r_m,of the QP layer, to give

$$D = \frac{2r_0^2 \cos\beta_0}{\sqrt{C'}} \log_e \left(\frac{r_m\left(2\sqrt{C'R_b} + B'r_b + 2C'\right)}{r_b\left(2\sqrt{C'R_m} + B'r_m + 2C'\right)} \right) \qquad (4:41)$$

where ,r_m, denotes the height of the maximum electron density

Case 3: Apogee in an inverse quasiparabolic layer

In theory an IQP layer does not experience a maximum in electron density, excepting the value reached at the upper IQP/QP interface, and for this reason the ray tracing coefficients will obey the inequalities

$$B'^2 > 4A'C' \ , \ C' < 0 \qquad (4:42)$$

under conditions of either apogee or traversal. One may use the standard integral result expressed in eq (4.16) to determine the ground range covered for the case of either containment or non-containment of the radio ray, provided one changes the upper limit of integration accordingly. Therefore, if one has apogee conditions in an IQP layer, the ground range is given by

$$D = \frac{2r_0^2 \cos\beta_0}{\sqrt{-C'}} \left(\sin^{-1}\left(\frac{2C' + B'r_a}{r_a(B'^2 - 4A'C')^{1/2}} \right) - \sin^{-1}\left(\frac{2C' + B'r_b}{r_b(B'^2 - 4A'C')^{1/2}} \right) \right) \qquad (4:43)$$

where the subscripts, b, and, a, refer to the bottom of the inverse layer and the apogee height, respectively. Utilising the ancillary condition expressed in eq (4.32), leads to the

simplified result

$$D = \frac{2r_0^2 \cos\beta_0}{\sqrt{-C'}}\left(\frac{\pi}{2} - \sin^{-1}\left(\frac{2C' + B'r_b}{r_b(B'^2 - 4A'C')^{1/2}}\right)\right) \qquad (4:44)$$

where

$B'^2 > 4A'C'$

$C' < 0.$

Case 4: Traversal of an inverse quasiparabolic layer

As mentioned when discussing case three a HF signal will traverse an IQP layer provided the ray tracing coefficients satisfy the inequalities expressed in eq (4.42) and the resultant projected ground range covered by the radio locus is derived from eq (4.16), to give

$$D = \frac{2r_0^2 \cos^2\beta_0}{\sqrt{-C'}}\left(\sin^{-1}\left(\frac{2C' + B'r_t}{r_t(B'^2 - 4A'C')^{1/2}}\right) - \sin^{-1}\left(\frac{2C' + B'r_b}{r_b(B'^2 - 4A'C')^{1/2}}\right)\right) \qquad (4:45)$$

where the limits of integration extend from the base of the region ,r_b, up to the transition height ,r_t, of the IQP/QP upper interface. One should note that the thickness of the IQP joining layer is defined by (r_t - r_b), the value of which depends upon the continuity conditions governing the joining segments used to construct a QP/IQP interface; ref: chapter (3).

The determination of ground range and MUF for a MQP electron density profile

Using the eqs (4.37), (4.41), (4.44) and (4.45), as derived above it is now possible to computer simulate the propagation of a radio signal through a model ionosphere

constructed from traditional and inverse quasiparabolic segments and to calulate the total distance covered by the signal as a sub-sum of the ground range contributions from each section of the MQP profile. In the course of the research at CSIR algorithms have been developed that allow one to ray trace, in real-time, through a MQP model ionosphere under the following propagation conditions:

Algorithm A1 :- given the ground range, D, determine the MUF and the corresponding launch angle β_0 (skip angle)

Algorithm A2 :- given the operating frequency, f, determine the minimum ground range (skip distance) and the corresponding elevation angle β_0 (skip angle)

Algorithm A3 :- given the launch angle, β_0, determine the MUF and corresponding ground range (skip distance).

The schematics describing the flow chart architecture of the three ray-tracing algorithms are displayed in figures (4.2), (4.3) and (4.4) respectively :

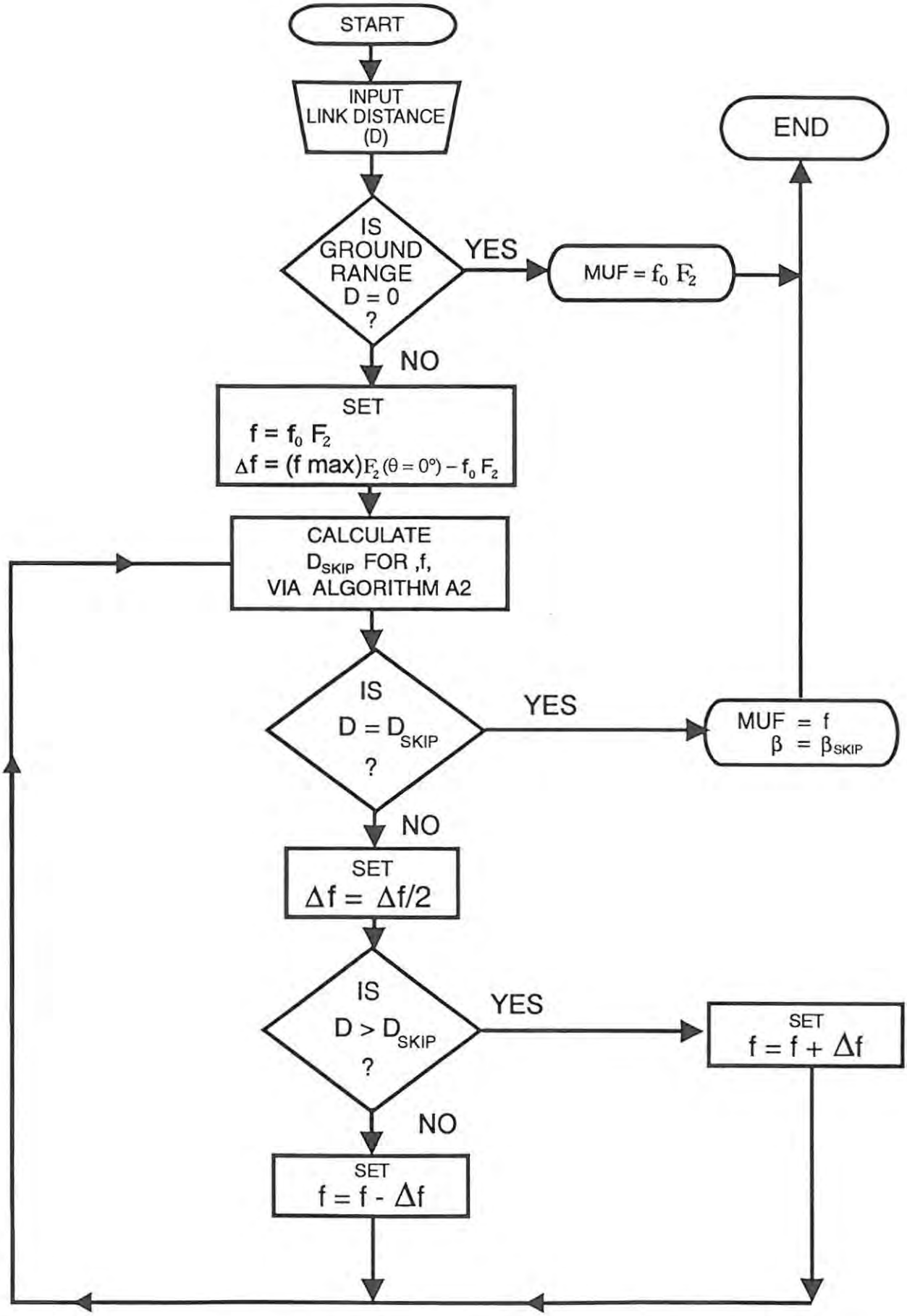

Figure (4.2): Schematic A1; determination of MUF and skip angle (β) given ground range (D)

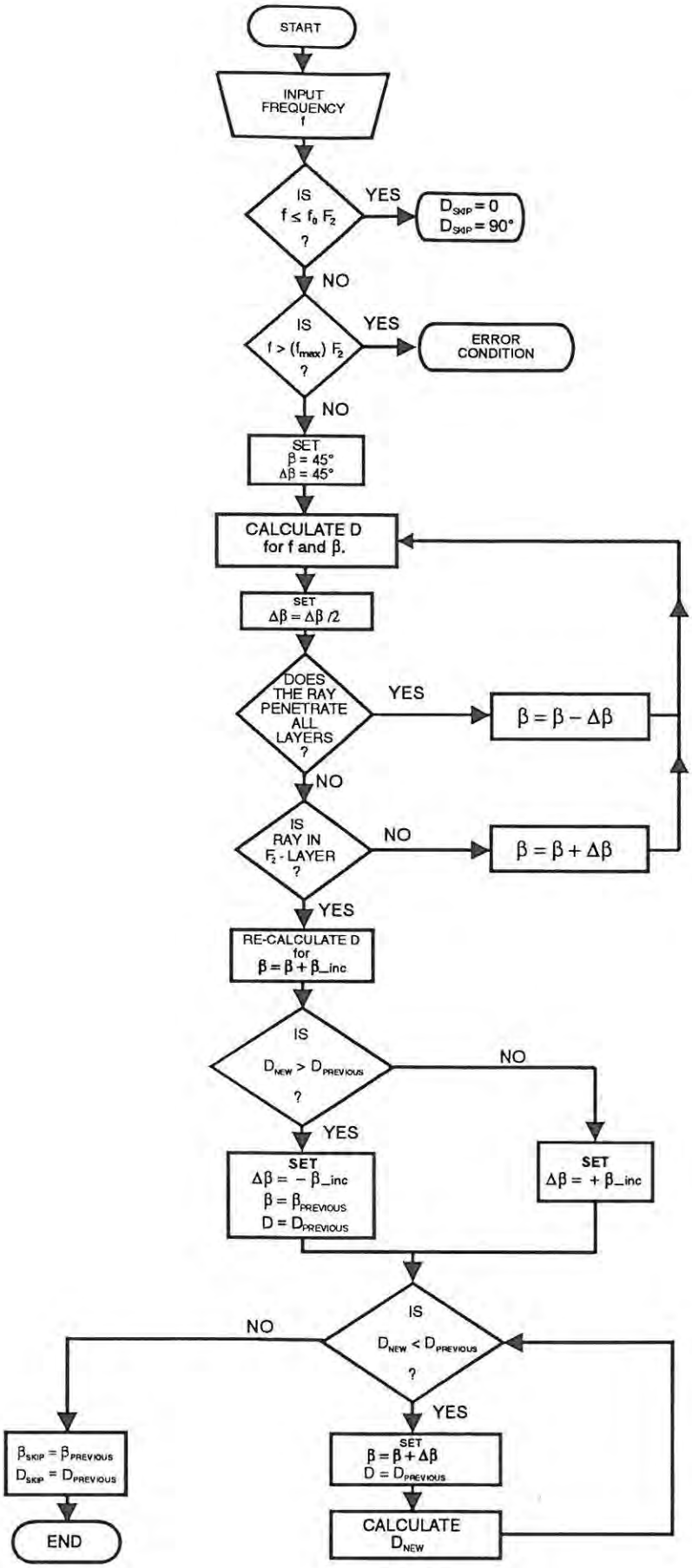

Figure (4.3): Schematic A2; determination of skip distance (D_{skip}) and skip angle (β) given propagation frequency (f).

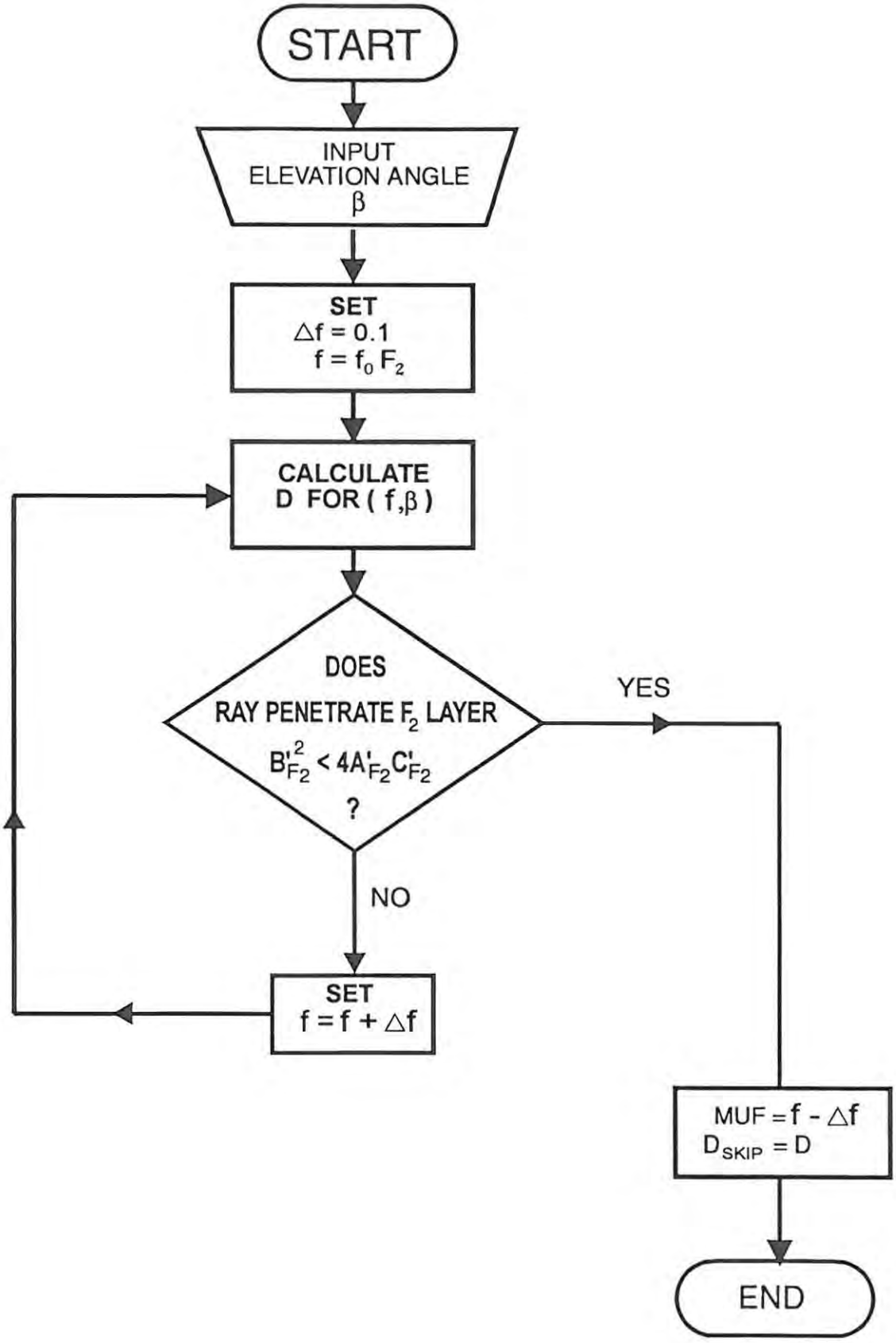

Figure (4.4) : Schematic A3; determination of MUF and skip distance (D_{skip}) given elevation angle (β).

Implementation of the MQP MUF algorithms :

To test the software implementation of the MUF algorithms, A1, A2 and A3, a sample ionosphere was selected and a MQP model profile constructed using the algorithms developed in chapter 3.

Ionospheric layer	Critical frequency f_c (MHz)	Height of max density r_m (km)	Semi-thickness y_m (km)
E	3.0	110	20
F_1	4.2	210	80
F_2	6.0	320	100

Table (4.1): Ionospheric layer parameters (f_c,r_m,y_m), after Baker, D C [1990].

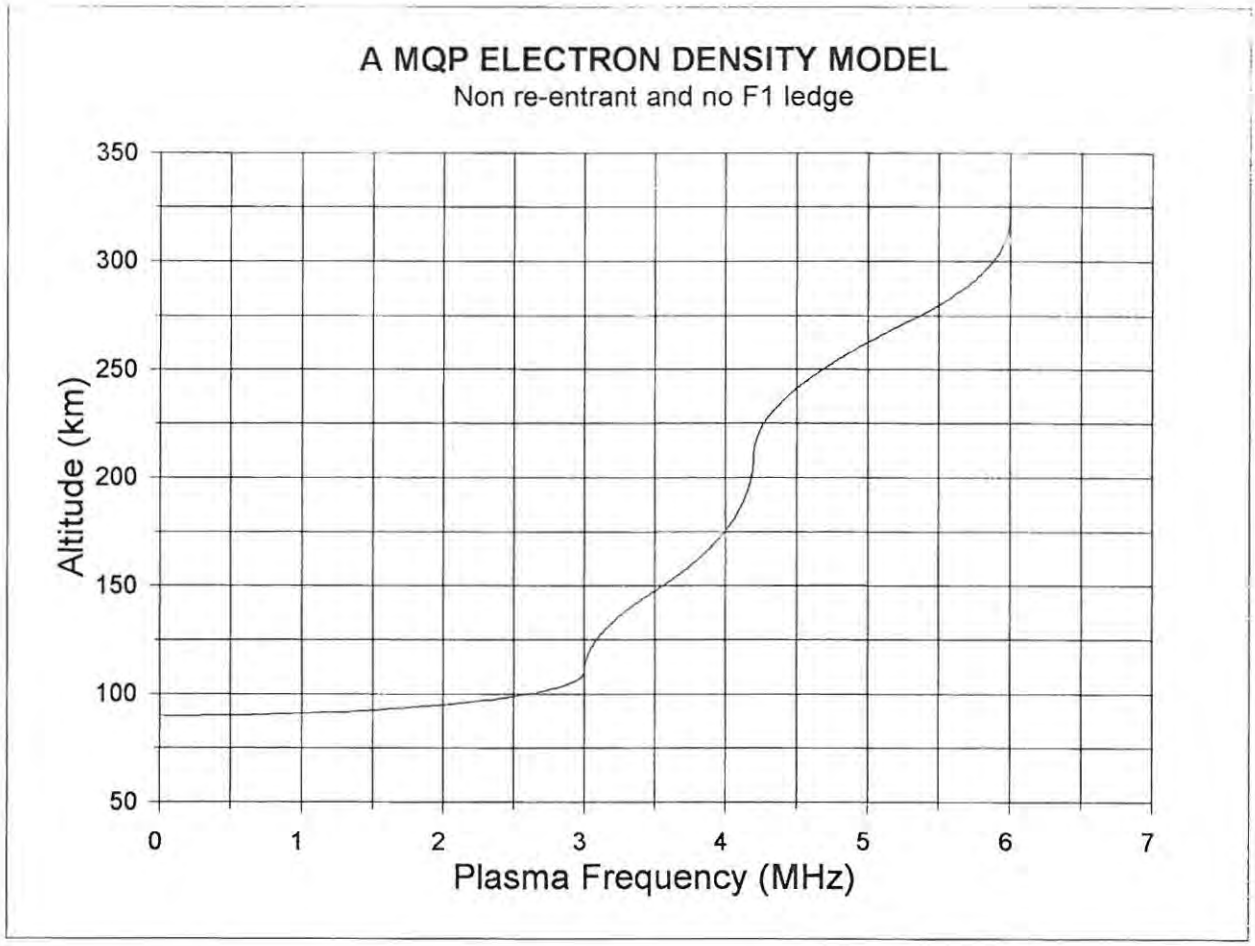

Figure (4.5) : MQP electron density model constructed from the ionospheric parameters displayed in Table 4.1

To determine the MUF(F2) via ray-tracing through a MQP model ionosphere

To initialize the MUF algorithm displayed in figure (4.4), one requires values for the following parameters:

(1) ground range D in km

(2) critical frequency of the F2 layer in MHz

(3) maximum frequency capable of support by the F2 layer.

The values of the ground range covered by an HF signal when utilizing the F2 layer for support are considered to satisfy the inequality, CCIR [1982],

$$0 < D < 4000 \qquad [4:46]$$

given that the propagation frequencies lie in the range

$$f_0F2 < f < f_{max} \qquad [4:47]$$

The maximum frequency ,f_{max}, that may be supported by the ionosphere, ignoring anomalous propagation effects, occurs when one has a transmitter launch angle of zero degrees and if one assumes F2 layer support with under-ionisation neglected, it may be shown that ; Davies [1969],

$$f_{max} = f_0F_2 \left[1 - \left[\frac{R_e}{R_e + h_mF_2} \right]^2 \right]^{-\frac{1}{2}} \qquad [4:48]$$

In practice the presence of under-ionization in the form of E and F1 regions will cause a depression of the frequencies that are predicted using an ionospheric model consisting of only a F2 layer, ref: McNamara [1991].

For the selected ionospheric parameters listed in figure 4.1 the HF radio frequencies that may be supported by the F_2 layer of a MQP model ionosphere will satisfy the inequality

$$6\ MHz \leq f_{MUF} < 19.6\ MHz \qquad [4:49]$$

where the figure of 19.6(MHz) corresponds to the maximum frequency of propagation when the E and F1 layers are ignored. The first stage of algorithm A1; figure(4.2), requires the calculation of the skip distance for a selected frequency ,f, lying in the interval defined by eq (4.46). This level of A1 is executed by making use of the algorithm A2; figure (4.3), as a subroutine that will generate the minimum value of ground range for the given frequency by subjecting the elevation angle ,β, to a Binary Search until ,β_{skip}, has been reached. The value of the skip distance is then returned to algorithm A1 and compared with the input ground range that was selected using eq (4.46). Depending on the outcome, a higher or lower value of frequency is selected and a Binary Search algorithm initiated, followed by successive iterations in a frequency loop, until, the skip distance calculated by algorithm A2 is equal to the link distance used to initialize A1. Displayed in figure (4.6) is a graph of MUF versus skip distance calculated using the computer algorithms A1 and A2 for the MQP model ionosphere shown in figure 4.5.

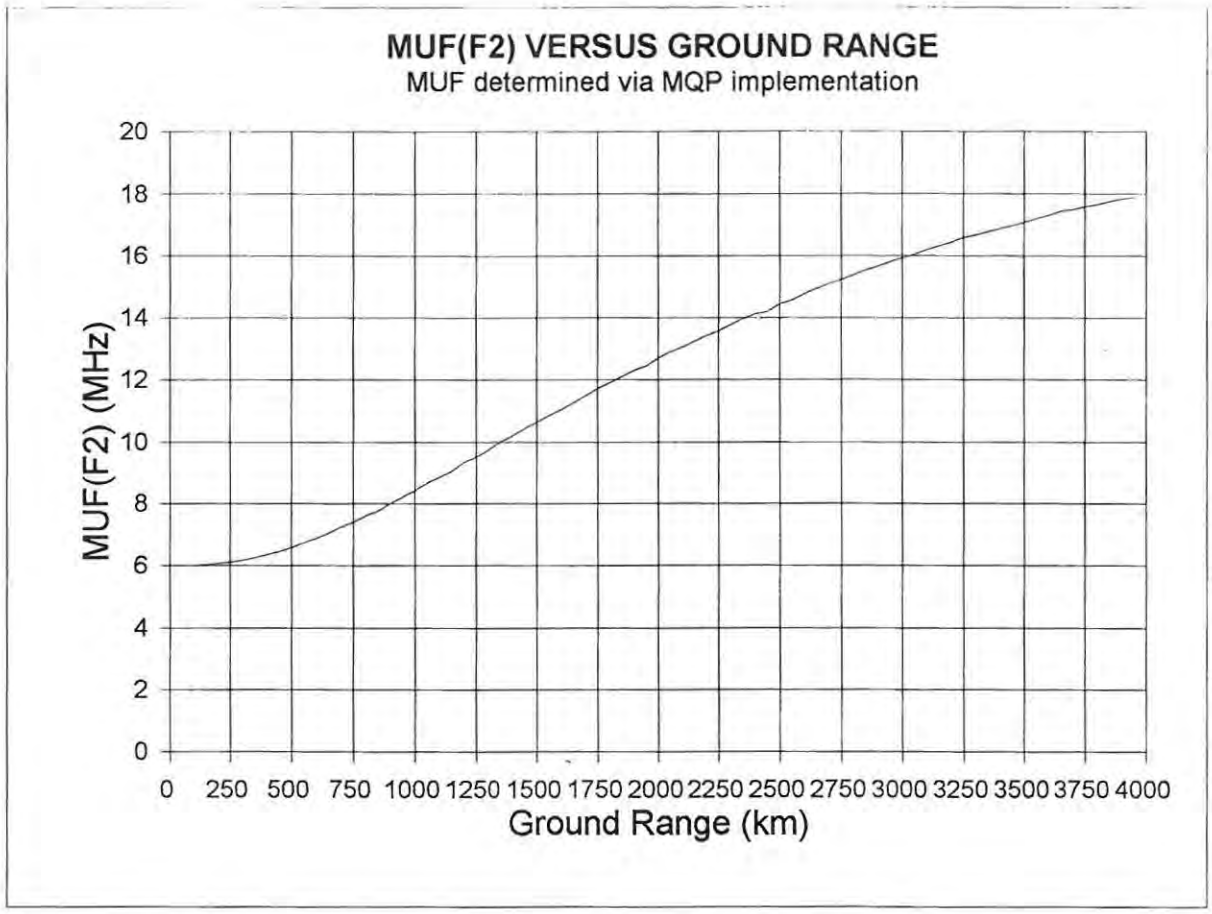

Figure (4.6) : Maximum usable frequency versus skip distance for the MQP ionosphere shown in figure (4.5).

The CCIR MUF(F2) algorithm [1991] due to Lockwood [1983]

For comparative purposes it was thought useful to obtain MUF versus ground range plots using the algorithm developed by Lockwood [1983] and adopted by the CCIR [1990] report 340. Lockwood's algorithm incorporates the Milsom [1977] ionospheric model, displayed in figure (4.7), which makes use of a quasiparabolic geometry to describe the E and F_2 layers

of the ionosphere with the electron density in the F_1 region being assumed to vary in a quasi-linear manner, after Muldrew [1959]. It should be noted that the Milsom profile does not include the option of modelling an E/F_1 valley or a F_1 ledge condition, so for this reason Lockwood's algorithm is of limited use in the prediction of usable HF radio frequencies under typical ionospheric conditions.

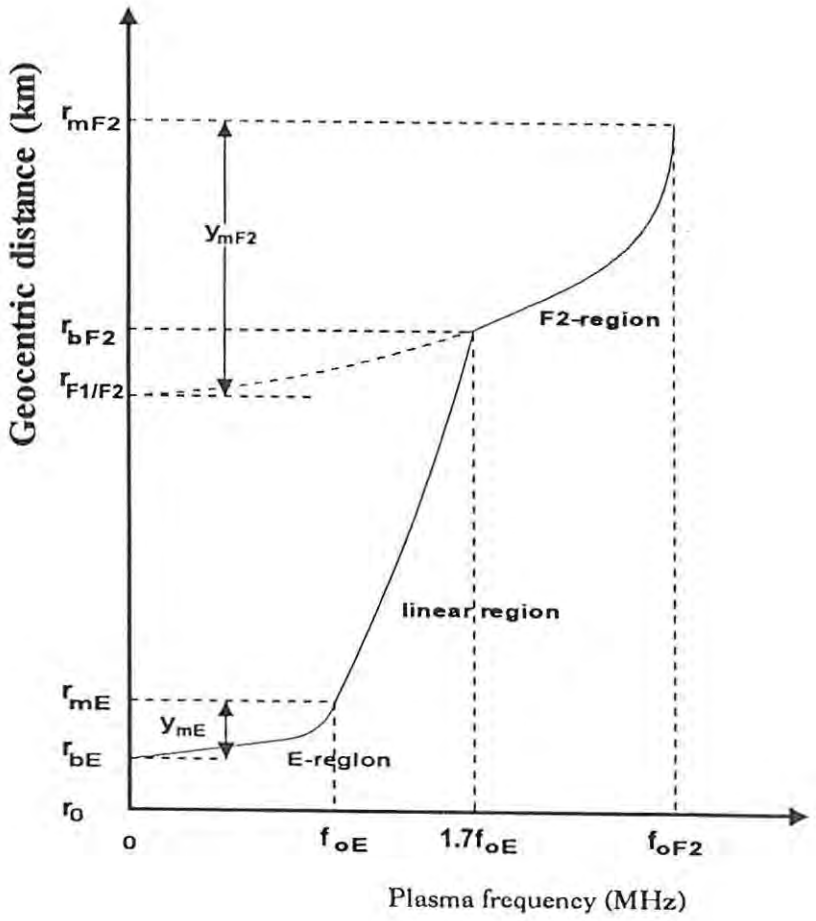

Figure (4.7): The Milsom ionospheric model used in Lockwood's algorithm is described as a "quasi-perturbed" version of the Bradley-Dudeney [1973] ionospheric model. For comparison purposes, the E and F2-region parameters of the Milsom model are identical to those in Table (4.1).

Nota bene: Milsom's use of the "quasi-perturbed" profiles, be it parabolic or linear, allows one to analytically ray trace through the otherwise mathematically intractable Bradley-Dudeney model [1973].

↑ MUF[D]F2

Evaluation of F_2 (D) by computer using Lockwood's algorithm, CCIR [1991]

The following MUF algorithm due to Lockwood [1983] is extracted from report 340, CCIR [1991] and illustrates the required inputs necessary to drive the routines

$$\text{MUF[D]F}_2 = \left[1 + \left[\frac{C_D}{C_{3000}}\right][B - 1]\right] \cdot f_o F_2 \qquad (4:50)$$

where

$$C_D = 0.72 - 0.628z - 0.451z^2 - 0.03z^3 + 0.194z^4 + 0.158z^5 + 0.037z^6 \qquad (4:51)$$

$$z = \left(1 - \frac{2D}{D_{max}}\right) \qquad (4:52)$$

$$D_{MAX} = 3940 + \left[9900 + \frac{15375}{x^2} + \frac{106700}{x^5}\right]\left[\frac{1}{B} - 0.258\right] \qquad (4:53)$$

and

$$B = M(3000)\ -0.124 + (M\ (3000)^2\ -4) * \left(0.0215 + 0.005\ Sin\left(\frac{7.854}{x}\ -1.9635\right)\right) \quad [4:54]$$

given that the quantities D and D_{max} are in kilometers, C_{3000} is the value of C_D when D equals 3000 km and x equals f_oF_2/f_oE, or 2, whichever is the larger. The inputs to the F_2(D) algorithm are:

a) M(3000)F_2 equivalent to MUF(3000)F2 / f_oF2

b) $f_oF_2 \Rightarrow$ critical frequency of the F_2 layer, and

c) $f_oE \Rightarrow$ critical frequency of the E layer.

The required value of M(3000) may be obtained using tables published by the CCIR Report 340; "Atlas of ionospheric characteristics", 1991.

Displayed in figure (4.8) is the variation of circuit MUF with ground range as calculated using the CCIR algorithm and the MQP MUF algorithms A1/A2, respectively.

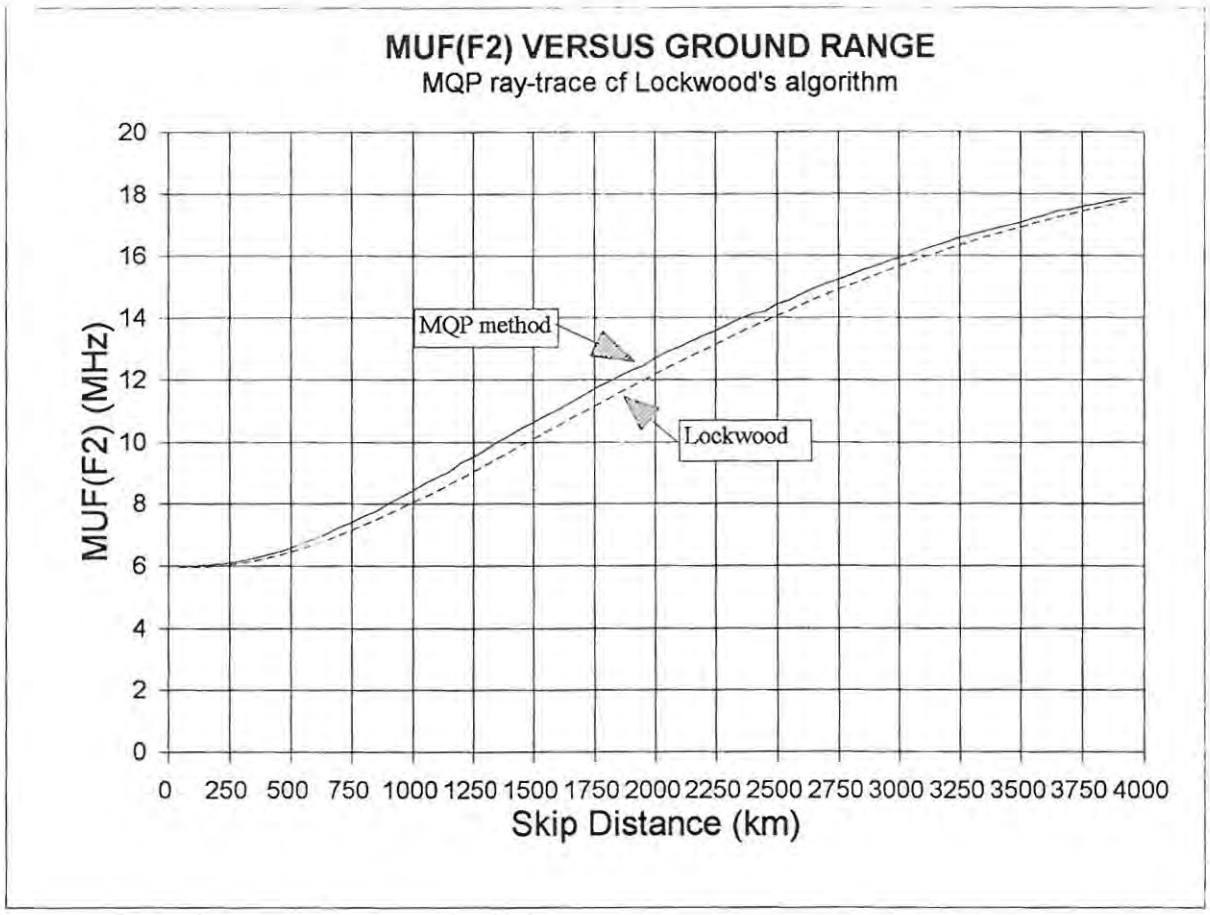

Figure (4.8):- MUF(F_2) versus ground range showing a comparison between the CCIR (Lockwood algorithm) and the CSIR (MQP/MUF algorithms)

Discussion of the results derived from the Lockwood versus MQP/ MUF algorithms.

The Milsom model used in the Lockwood algorithm introduces a slightly higher degree of underlying ionization with respect to the F_2 layer when compared to the MQP electron profile and as a result the CCIR generated frequencies appear in figure (4.8) as marginally depressed with respect to the values obtained via the MQP method. For details of the effect that E/F1 ionization has on the MUF of a HF circuit the reader is referred to Bradley

and Dudeney [1973].

The determination of ground range versus elevation angle with frequency as a parameter

The range equations express the distance ,D, covered by a HF signal in terms of the frequency of propagation ,f, and the elevation angle ,β, that is,

$$D = D(f,\beta) \qquad [4:55]$$

where the mathematical forms of the above function for the MQP model are given by eqs [4.37], [4.41], [4.44] and [4.45]. Figure [4.9] shows the variation of ground range as a function of elevation angle for the cases where the frequency parameter assumes values of 6, 9 and 12 MHz respectively.

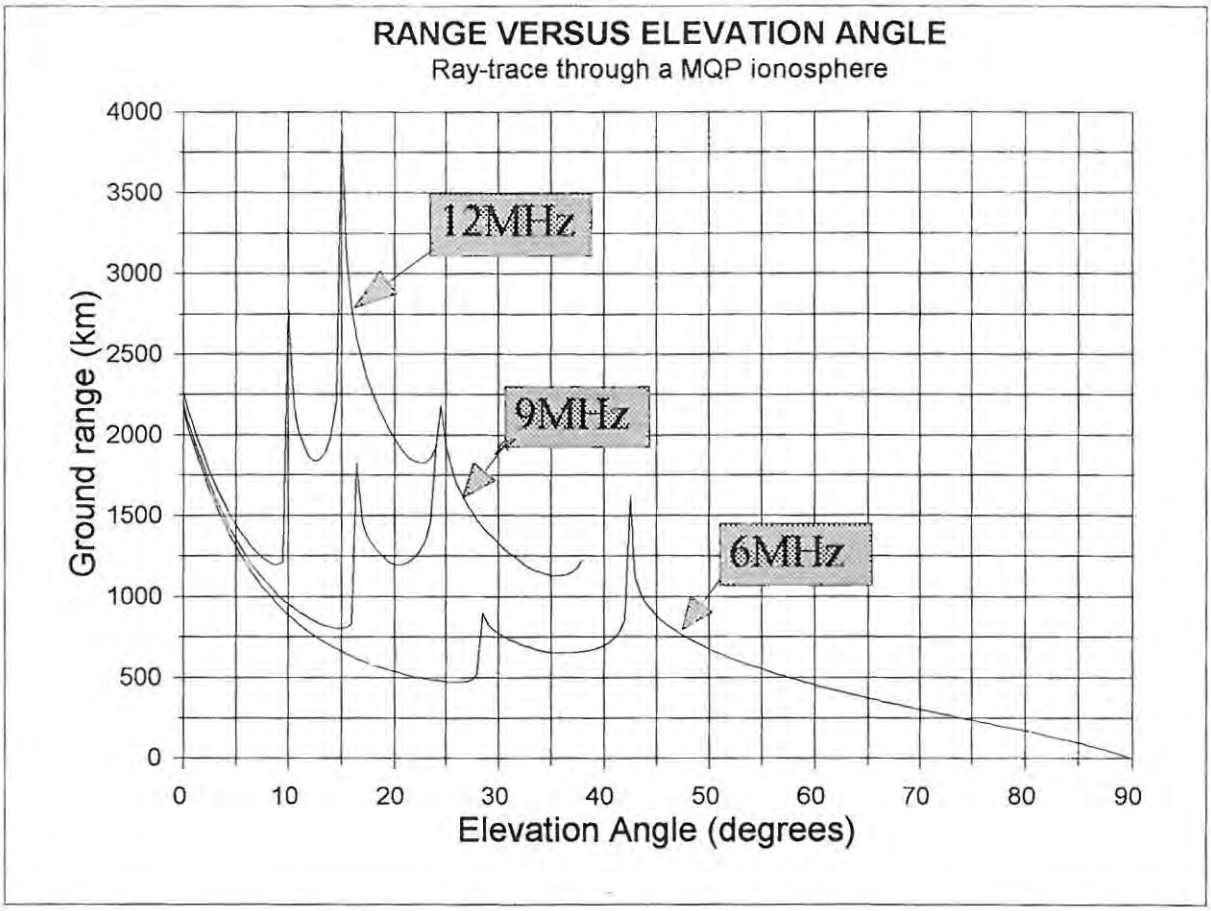

Figure (4.9): Ground range as a function of elevation angle with propagation frequency as a parameter.

There are a number of observations that one should make;

(a) the transmission curves for 6, 9 and 12 MHz indicate E layer support with convergence toward a limiting ground range value of approximately 2250(km) as the elevation angle tends to zero, a phenomenon known as horizon focusing, ref: chapter (8).

(b) with the exception of the 6MHz case one observes penetration of the E, F1 and F2 layers of the model

(c) propagation within a layer, provided $f > f_{critical}$, shows that one can cover a given ground range by either a low or a high angle ray

(d) there is one angle of elevation β_{skip} for which the low and high angle(Pederson) rays superimpose whereupon the frequency of propagation becomes the MUF for the circuit and the ground range, the skip distance

(e) transmission through a layer is associated with a sharp vertical cusp where the Pederson ray appears to shoot off to infinity.

(f) the co-ordinates of the turning points on the D versus β transmission curves, displayed in figure (4.4) give the skip distance, skip angle and layer of support for which the given frequency parameter becomes the MUF. One may directly determine the value of a desired MUF condition by implementing algorithm A3: figure(4.4) and specifying the ionospheric layer that is to be used for propagation support.

(g) The variation of ground range with elevation angle for a given frequency and the specified layer of support provides the essential data needed to generate the plots of elevation angle versus frequency for a fixed link, being essentially the process required to synthesise an oblique ionogramme, ref: chapter 6.

The determination of the variation of ground range with propagation frequency given elevation angle as parameter

In figure (4.10) one sees a graph of ground range versus frequency for elevation angle angles 15, 30, 45 and 60 degrees respectively that has been constructed using the range equations as expressed in eqs (4.37), (4.41), (4.44) and (4.45).

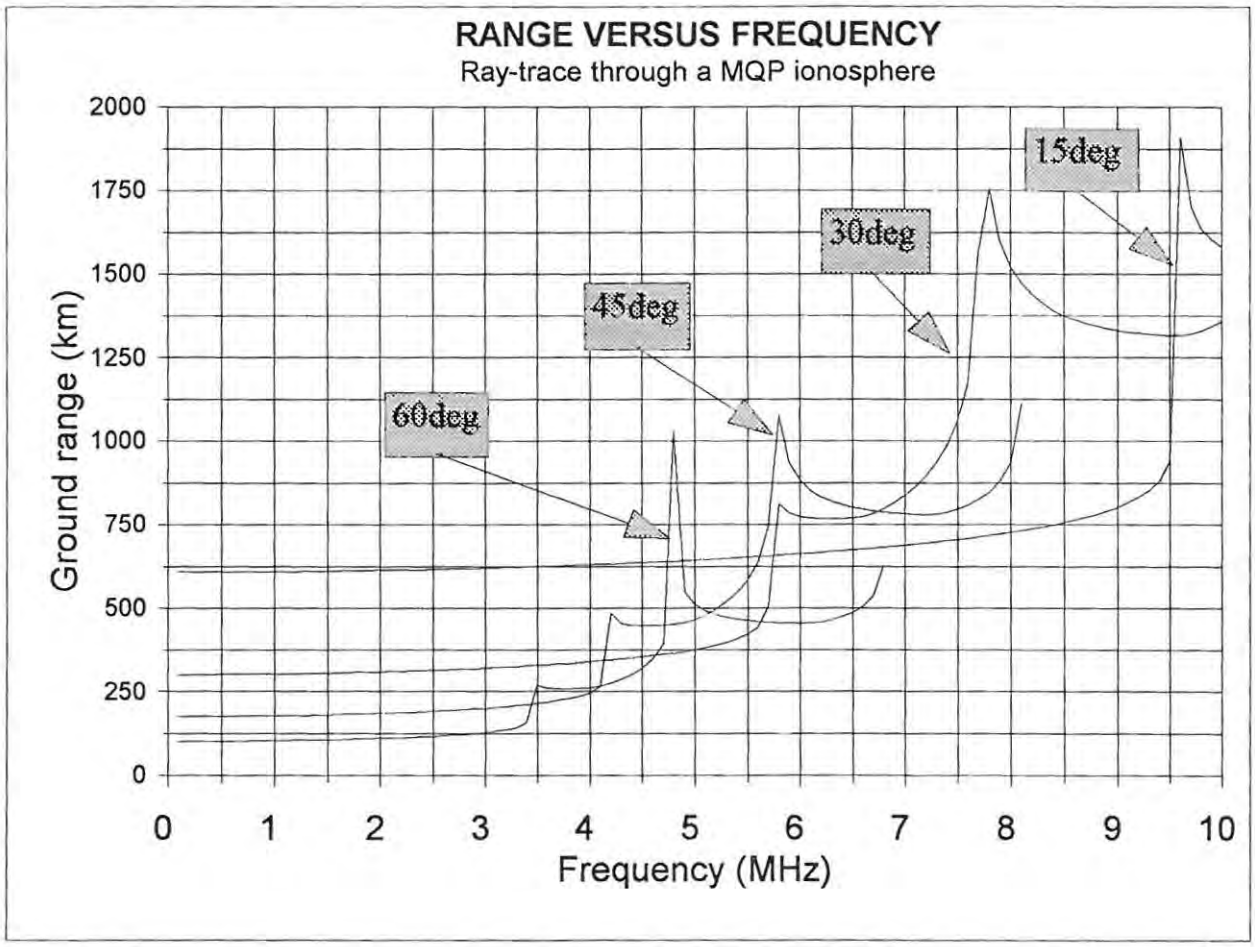

Figure (4.10):- Ground range versus propagation frequency with elevation angle as a parameter.

One should note the following;

(a) for a given ground range lying between 0 and 2000 (km) there is at least one frequency and elevation angle that will ensure successful communications.

(b) either side of a vertical spike one can propagate via adjacent ionospheric layers using the same elevation angle provided one uses different radio frequencies

(c) one can determine the MUF that is capable of being supported by a given ionospheric layer if one implements the algorithm A3 displayed in figure (4.4). Note that the algorithm has been set up to provide the user with MUF(F2) but MUF(F1) and MUF(E) can also be derived by changing the question asked in the decision box accordingly.

This concludes the discussion on the analytical ray tracing algorithms used to construct transmission curves for a MQP model ionosphere. The computer routines and source code have been tested using a given set of ionospheric parameters and results for MUF (F_2) compared with those obtained using a standard CCIR prediction program. The slight offset in the calculated values for MUF F_2 is attributed to increased E/F_1 under-ionisation introduced region by the ionospheric model used in the CCIR algorithm as compared to the equivalent MQP profile.

In the next chapter MQP curve fitting algorithms are developed that will allow one to analytically ray trace through a QP/IQP model fit to an observed N-h electron distribution.

CHAPTER (5)

THE DERIVATION OF ALGORITHMS SUITABLE FOR CURVE FITTING A MQP MODEL PROFILE TO AN OBSERVED N-h DISTRIBUTION

It is appropriate that one should briefly review the subject of ionogramme scaling and inversion before embarking upon a discourse on the special requirements of N(h) profile curve fitting algorithms. An ionogramme is essentially an HF radar scan depicting the variation in the virtual height of reflection as a function of radio frequency, the so-called h'(f) trace. To obtain an electron density distribution corresponding to the virtual height profile one inverts the h'(f) data using an ionogramme inversion programme such as POLAN [1985]. Mathematically the transformation is expressed as

$$(h', f) \Leftrightarrow (h, N) \qquad [5:1]$$

where the co-ordinates (h' , f) on an ionogramme corresponds to a point (h , N) on a real height electron density profile. One can determine the virtual height using the integral result

$$h'(f) = \int_o^{hr} \mu' \, dh = \int_o^{hr} \mu' \frac{dh}{d\Phi} \, d\Phi \qquad [5:2]$$

where the details of inverting eq [5.2] to obtain the N-h profile for a given ionogramme trace have already been discussed in Chapter [2]. Following the approach of Budden [1955] the parameter Φ is considered to represent the plasma frequency, f_N, allowing one to express the inversion integral in the form

$$h'(f) = \int_o^{hr} \mu' \frac{dh}{df_N} \cdot df_N \qquad [5:3]$$

Examination of the virtual height integral gives one considerable insight into the radio physics behind the shape of an ionogramme. For example should the gradient dN/dh of the electron density profile tend to zero, that is the concentration reach a maximum, then according to theory the h'(f) trace should tend to infinity. This phenomena is associated with the peaks of the E and F layers of the ionosphere although in practice attenuation of the reflected signal near to penetration of a given layer causes the expected infinite cusp to become finite in extent. The F region of the ionosphere is wont to bifurcate into two sub-regions, the F_2 and F_1 layers respectively where the latter may be present as either an electron distribution having a pure maximum or in the form of a ledge of ionization known as the F_1 - L condition. Mathematically an F_1 ledge of ionization corresponds to a point of inflexion on a real height profile and a sounding of the ionosphere at the ledge frequency, f_oF_{1L}, will produce a rounded cusp on the corresponding ionogramme. The modelling of an F_1 - L condition is quite tricky and the lack of knowledge concerning the electron density gradient at the ledge height requires the development of sophisticated curve fitting

algorithms in comparison to the routines needed to fit layer conditions. Below is a reproduction of an ionogramme record clearly showing the presence of an E and F_2 layer in addition to the existence of an F_1 ledge condition. One can see the presence of two virtual height profiles referred to as the ordinary and extraordinary traces respectively, with a frequency separation of approximately one-half of the gyro-frequency, having a value of 0,5 MHz for the South African region. It should be noted that the earth's magnetic field causes the ionosphere to behave as a birefringent or doubly refracting medium and as a result a HF signal will split into two components known as the O and X rays respectively.

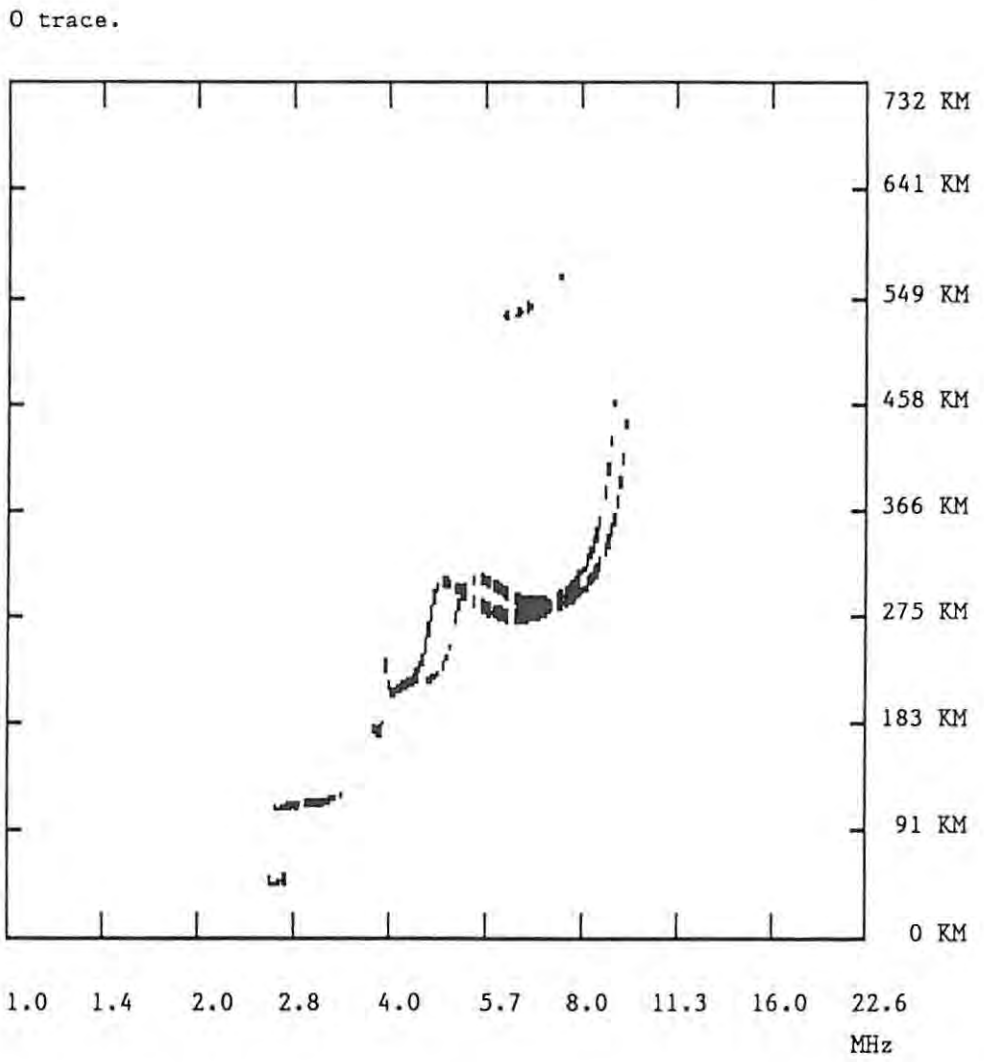

Figure (5.1) Ionogramme recorded at Frankenwald, Johannesburg, sounding at 10 a.m., day 293, 1992.

The virtual height profile displayed in figure (5.1) is inverted using POLAN and the resultant N-h electron distribution is displayed in figure (5.2).

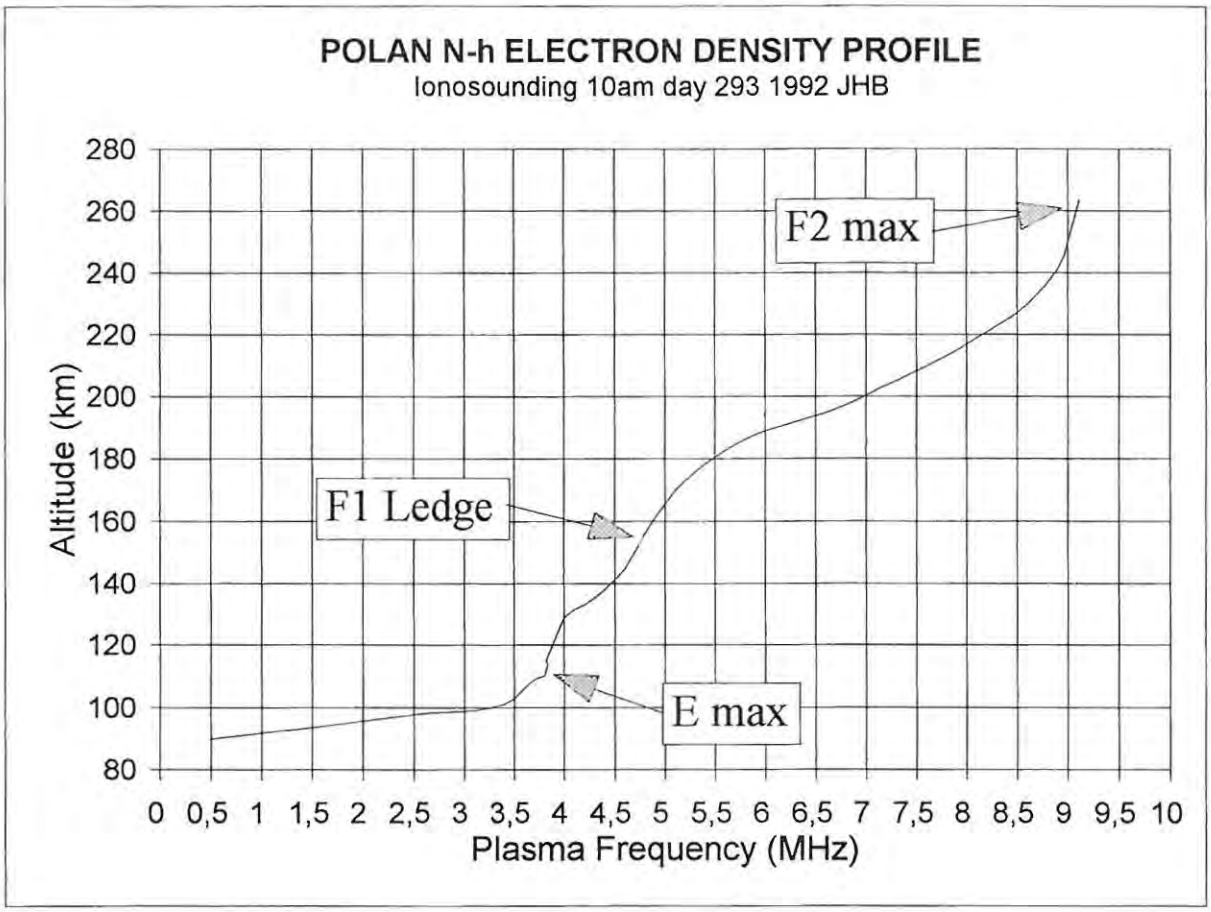

Figure (5.2) The observed electron density profile, obtained via POLAN, from the ionogramme displayed in figure (5.1).

One can clearly see the presence of the E and F_1 layers with their associated maxima in electron density and also the existence of an F_1 ledge condition, characteristically identified by the point of inflexion in the N-h electron profile.

The selection of a modelling approach

The principle behind the modelling approach adopted in this research is to describe each distinct region of the ionosphere using three parameters only;

(a) f_c, the critical frequency of a layer/ledge of ionization

(b) r_{max}/r_{Ledge}, the height of the maximum electron density or the inflexion height of a layer/ledge of ionization and

(c) y_m, the semi-thickness of the layer/ledge region

The basis of the modelling technique is to use the co-ordinates $(f_c , r_m)_{peak}$ or $(f_c , r_L)_{ledge}$ as anchor points for the model electron density profile. Ionogramme scaling and inversion, (POLAN), provides one with the positional information needed to define an ionospheric peak but in the case of an F_1 ledge the values of the co-ordinates $(f_c, r_L)_{ledge}$ as derived from POLAN are at best ambiguous. This deficiency in the selected inversion programme necessitates the development of an algorithm capable of detecting a point of inflexion on an observed N-h profile.

The modelling of an ionospheric layer possessing a maximum in electron density

In the case of an ionospheric layer with a peak in electron concentration one forces the curve fit to pass through the point (f_c , r_{max}) where the gradient in density goes to zero so ensuring that the co-ordinates of the maximum electron density in the layer provides an anchor point for the model profile. The semi-thickness ,y_m, refers to the fitted quasiparabolic segment and is derived from the coefficients (A, B, C) of the model enabling one to replace the observed ionospheric layer by a mathematical curve of the form

$$f_N^2 = \frac{A}{r^2} + \frac{B}{r} + C \qquad (5:4)$$

where y_m is given by

$$y_m = \frac{-2A/B}{1 + \{B^2/\{4AC + B^2\}\}^{1/2}} \qquad (5:5)$$

$$A = \mp f_c^2 \, r_m^2 \, r_b^2 / y_m^2 \qquad (5:6)$$

$$B = \pm 2 f_c^2 \, r_m \, r_b^2 / y_m^2 \qquad (5:7)$$

$$C = f_c^2 \mp f_c^2 \, r_b^2 / y_m^2 \qquad (5:8)$$

$$r_b = (r_m - y_m) \qquad (5:9)$$

The above method of curve fitting is akin to the approach used by Chen, Bennett and Dyson [1990], being essentially a constrained least squares algorithm, in that, the mathematical profile is forced to pass through the peak of the electron distribution at [f_c , r_{max}].

The derivation of a constrained least squares algorithm for a layer with a peak

One wishes to fit an observed N-h profile to a quasiparabolic curve of the form

$$y \triangleq f_N^2 = \frac{A}{r^2} + \frac{B}{r} + C \qquad (5:10)$$

where the values of (A, B, C) are determined using three criteria;

(a) continuity of f_N^2 at the end points of the quasi-parabolic section

(b) continuity of the gradient of f_N^2 at the same end point, and

(c) the method of least squares

Each layer will have its own values for the coefficients (A, B, C) which are determined by the curve fitting algorithm while the inverse quasiparabolic joining sections are simply mathematical constructs, the coefficients of which have values that ensure continuity in concentration and its gradient at the upper and lower joining heights respectively.

Given an ionospheric layer having a maximum electron density at a geocentric height r_j where $d(f_N^2)/dr$ is known, one can initialize the curve fitting procedure by requiring that the model profile begins on the point $(r_j , y(r_j))$. Differentiating with respect to r, the expression for plasma frequency squared, gives

$$\frac{dy}{dr} = -\frac{2A}{r^3} - \frac{B}{r^2} \qquad (5:11)$$

Substituting the initial conditions into eqs (5.10) and (5.11) gives

$$y(r_j) = \frac{A}{r_j^2} + \frac{B}{r_j} + C \qquad (5:12)$$

and

$$\frac{dy(r_j)}{dr} = -\frac{2A}{r_j^3} - \frac{B}{r_j^2} \qquad (5:13)$$

Solving simultaneous the equations in $y(r_j)$ and $dy(r_j)/dr$ one can deduce an expression for the coefficient C,

$$C = y(r_j) + \frac{A}{r_j^2} + \frac{dy(r_j)}{dr} r_j \qquad (5:14)$$

while the equation for $dy(r_j)/dr$ can be re-arranged to give

$$B = -\frac{2A}{r_j} - \frac{dy(r_j)}{dr} r_j^2 \qquad (5:15)$$

The coefficient, A, can be determined using the method of least squares whereupon the values of the coefficients B and C can be obtained using eq (5.15) and eq (5.14).

The method of least squares and the determination of the A coefficient

An ionogramme contains the virtual height information describing the extant state of the ionosphere and an inversion programme converts the h'(f) trace to a plot of altitude versus plasma density, known as a N-h distribution. For the purposes of analysis the N-h data is conveniently expressed as an array of data points,(x_i , y_i), where

$$x_i \equiv (r_i - r_o) \qquad [5:16]$$

$$y_i \equiv f_{N_i}^2 \qquad [5:17]$$

and

$$r_o \rightarrow \textit{radius of the Earth} \qquad [5:18]$$

The least squares condition, Stroud [1992], requires that

$$\frac{\partial}{\partial A}\left[\sum_{i}^{N_{MAX}} \left(y\,(r_i) - y_i \right)^2\right] = 0 \qquad [5:19]$$

where y(r$_i$) refers to the model curve ,y$_i$, to the data points and N$_{max}$ is determined by the maximum tolerable r.m.s. error between the data and fitted points. Substituting the expressions for the coefficients ,B, and ,C, into the form of the model profile yields

$$y(r) = \frac{A}{r^2} + \frac{1}{r}\left[-\frac{2A}{r_j} - \frac{dy}{dr}(r_j)\, r_j^2\right] + y(r_j) + \frac{A}{r_j^2} + \frac{dy}{dr}(r_j)\, r_j \qquad [5:20]$$

Collecting terms and factorizing gives the simplified expression

$$y(r) = A\left(\frac{1}{r_j} - \frac{1}{r}\right)^2 + \frac{dy}{dr}(r_j)\, r_j^2 \left(\frac{1}{r_j} - \frac{1}{r}\right) + y(r_j) \qquad [5:21]$$

One now forms the sum of the squares of the differences between the values of ,y(r$_i$), given by the model and the actual data points ,y$_i$, resulting in the expression

$$\sum (y(r_i) - y_i)^2 = \sum \left\{ A\left(\frac{1}{r_j} - \frac{1}{r_i}\right)^2 + \frac{dy}{dr}(r_j)\, r_j^2 \left(\frac{1}{r_j} - \frac{1}{r_i}\right) + y(r_j) - y_i \right\}^2 \qquad (5:22)$$

Differentiating eq (5.22) with respect to the quasiparabolic coefficient ,A, and setting the result equal to zero yields

$$\frac{\partial}{\partial A} \sum (y(r_i) - y_i)^2 = 2 \sum A \left(\frac{1}{r_j} - \frac{1}{r_i}\right)^4 + 2\sum \frac{dy}{dr}(r_j)\, r_j^2 \left(\frac{1}{r_j} - \frac{1}{r_i}\right)^3 + 2\sum (y(r_j) - y_i) \left(\frac{1}{r_j} - \frac{1}{r_i}\right)^2 = 0 \qquad (5:23)$$

Rearranging the minimization equation gives the value of ,A, which will ensure the smallest r.m.s. error between the fitted and the actual data, subject to the constraint that the curve fit pass through the point (r$_j$, y(r$_j$)) giving,

$$A = \frac{\sum_i \left\{ (y_i - y(r_j)) \left(\frac{1}{r_i} - \frac{1}{r_j}\right)^2 \right\} + \sum_i \left\{ \frac{dy}{dr}(r_j)\, r_j^2 \left(\frac{1}{r_i} - \frac{1}{r_j}\right)^3 \right\}}{\sum_i \left(\frac{1}{r_i} - \frac{1}{r_j}\right)^4} \qquad (5:24)$$

In summary, the eqs (5.24), (5.15) and (5.14) allow one to determine the values of the A, B, C coefficients describing the fitted quasiparabolic section provided that one knows the

values of

$$y(r_j) \tag{5:25}$$

and

$$\frac{\partial y}{\partial r}(r_j) \tag{5:26}$$

at one end of the model curve where the geocentric height is defined as r_i. If one starts the curve fitting procedure at the altitude of the maximum electron density in the F_2 layer, one can then initialize the least squares algorithm using the equivalencies;

$$y(r_j) \equiv (f_0F_2)^2 \tag{5:27}$$

$$\frac{\partial y}{\partial r} = 0 \tag{5:28}$$

since

$$r_j \equiv r_{max}F_2 \tag{5:29}$$

It should be noted that the above procedure is equally valid when curve fitting to the electron density distribution within the E layer of the ionosphere. Furthermore the F_1 region can also be fitted using the constrained version of least squares provided there exists a peak in the plasma density profile, however, in the event of there being a F1 ledge condition then a non-constrained least squares algorithm must be used as neither the slope nor the

plasma frequency can then be specified at the geocentric height ,r_j. In figure (5.3) one can see the inverse quasiparabolic construction which is used to mathematically connect two neighbouring ionospheric layers that have been replaced by quasiparabolic model sections.

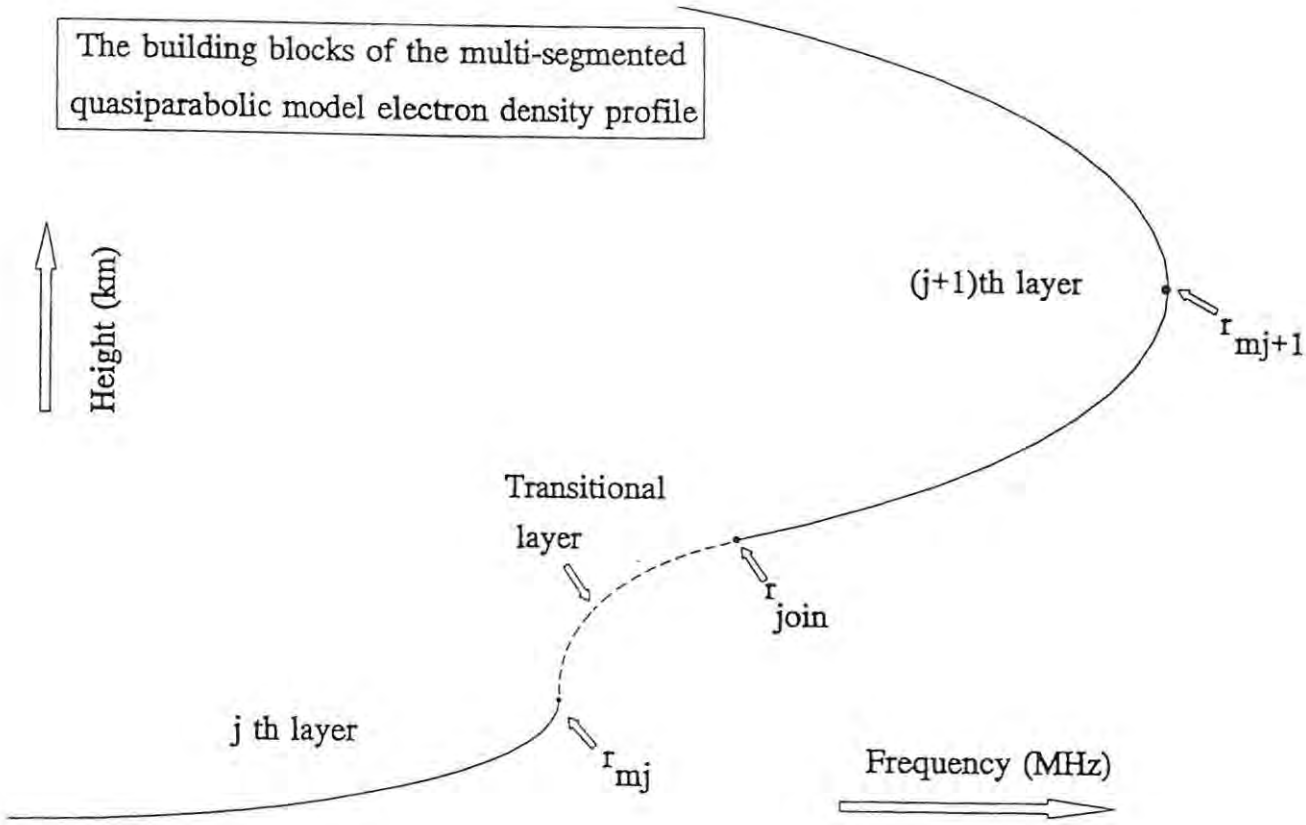

Figure (5.3) The building blocks of the multi-segmented quasiparabolic model electron density profile.

The joining height ,r_j, of the inverse section together with its semi-thickness ,y_m, are determined using the eq (3.35) and eq (3.43) developed in Chapter (3).

One now has the tools to construct the MQP model profile that can mathematically replace an observed N-h distribution that describes an ionosphere which possesses layers with well defined peaks in electron concentration.

The F1 - Ledge Condition

During daytime hours the F_1 region of the ionosphere bifurcates to form two layers F_1 and F_2 respectively. However, the F_1 region very often exhibits an immature layer formation which manifests itself on an observed N-h profile as a point of inflexion or ledge of ionization. Examination of the integrand within the expression for the virtual height ,eq (5.2), shows one that h'(f) will remain finite so long as the electron density gradient dN/dh does not tend to zero. Therefore an F_1 inflexion condition on an observed N-h distribution manifests itself as a finite rounded cusp on the corresponding ionogramme as it is the second not the first derivative in electron density that goes to zero. It is for this reason that the "hallmark" of an F_1 ledge condition is the presence of a finite cusp-like behaviour on the associated virtual height profile. During the course of this research, POLAN was used exclusively to invert ionogrammes and it was found that one cannot rely on this inversion software to provide accurate information regarding the co-ordinates of the F_1 ledge, $(r_L F_1, f_O F_{1L})$. To overcome this difficulty a gradient algorithm was developed to determine if there exists a region on the observed N-h profile where the derivative of electron density gradient approaches zero. Referring to figure (5.2) one can mathematically determine the position of a F_1 ledge of ionization by observing where the curvature of the N-h profile begins to change sign (+/-). Figure (5.4) shows the result of running the electron density data displayed in figure (5.2) through a gradient algorithm designed to iteratively detect small changes in slope.

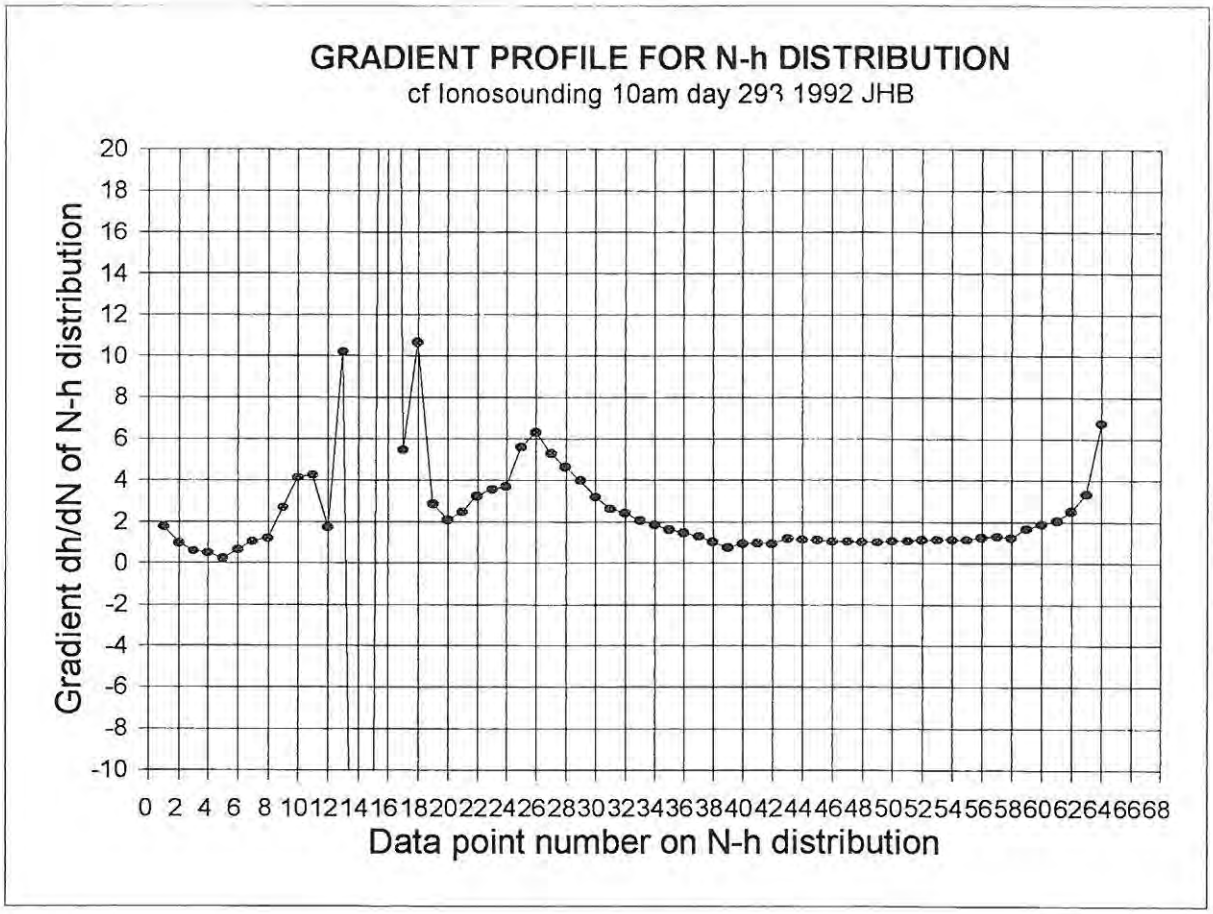

Figure (5.4) The electron density gradient dh/dN variation expressed as a function of data point for the N-h distribution displayed in figure (5.2)

It is clear that at data point number 26 the double derivative of electron density approaches zero giving one the approximate location of the F_1 ledge of ionization, $(r_L F_1, f_0 F_{1L})$.

One is now able to define the F_1 ledge condition in terms of the boundary conditions

$$y(r_L) = (f_0 F_{1L})^2 \qquad (5:30)$$

and

$$\frac{\partial^2 y(r_L)}{\partial r^2} = 0 \qquad (5:31)$$

However, because it is not possible to accurately determine the value of $dy(r_L)/dr$ without using time consuming numerical methods one is unable to satisfy the initial conditions required by the constrained least squares algorithm.

In the next section are derived the mathematical details of a non-constrained least squares algorithm suitable for curve fitting a quasiparabolic curve to a ledge of ionization.

The derivation of a non-constrained least squares algorithm suitable for modelling the F1 Ledge Condition

Given that one has N data points belonging to an observed N-h profile it is required to curve fit a model quasiparabolic electron density distribution of the form

$$y(r_i) = \frac{A}{r_i^2} + \frac{B}{r_i} + C \qquad (5:32)$$

to the data points (y_i , r_i) where the values of the coefficients A, B and C are such that the sum, S, of the squares of the differences between the fitted model and the observed data points ,y_i, is a minimum. Expressed mathematically

$$S = \sum_{i=1}^{N} \{y(r_i) - y_i\}^2 \qquad (5:33)$$

where the least squares condition requires that

$$\frac{\partial S}{\partial A} = \frac{\partial S}{\partial B} = \frac{\partial S}{\partial C} = 0 \qquad (5:34)$$

Substitution of the form of the quasiparabolic profile given by eq (5.32) into the expression for ,S, yields

$$\frac{dS}{dA} = \sum_{i=1}^{N} 2\left(\frac{A}{r_i^2} + \frac{B}{r_i} + C - y_i\right) \cdot \frac{1}{r_i^2} = 0 \qquad (5:35)$$

or re-arranging in coefficient form

$$A \sum_{i=1}^{N} \frac{1}{r_i^4} + B \sum_{i=1}^{N} \frac{1}{r_i^3} + C \sum_{i=1}^{N} \frac{1}{r_i^2} - \sum_{i=1}^{N} \frac{y_i}{r_i^2} = 0 \qquad (5:36)$$

Likewise differentiating the sums of the squares with respect to ,B, gives

$$A \sum_{i=1}^{N} \frac{1}{r_i^3} + B \sum_{i=1}^{N} \frac{1}{r_i^2} + C \sum_{i=1}^{N} \frac{1}{r_i} - \sum_{i=1}^{N} \frac{y_i}{r_i} = 0 \qquad (5:37)$$

and finally the derivative of ,S, with respect to the coefficient ,C, results in the equation

$$A \sum_{i=1}^{N} \frac{1}{r_i^2} + B \sum_{i=1}^{N} \frac{1}{r_i} + C \sum_{i=1}^{N} 1 - \sum_{i=1}^{N} y_i = 0 \qquad \text{(5:38)}$$

Equations (5.36), (5.37) and (5.38) are three equations in three unknowns which may be written in the compact form

$$\begin{aligned} aA + bB + cC + e &= 0 \\ bA + cB + dC + f &= 0 \\ cA + dB + NC + g &= 0 \end{aligned} \qquad \text{(5:39)}$$

where the coefficients a, b, c, d, e, f and g are defined

$$a = \sum_{i=1}^{N} \frac{1}{r_i^4} \qquad \text{(5:40)}$$

$$b = \sum_{i=1}^{N} \frac{1}{r_i^3} \qquad \text{(5:41)}$$

$$c = \sum_{i=1}^{N} \frac{1}{r_i^2} \qquad \text{(5:42)}$$

$$d = \sum_{i=1}^{N} \frac{1}{r_i} \qquad (5:43)$$

$$e = -\sum_{i=1}^{N} \frac{y_i}{r_i^2} \qquad (5:44)$$

$$f = -\sum_{i=1}^{N} \frac{y_i}{r_i} \qquad (5:45)$$

$$g = -\sum_{i=1}^{N} y_i \qquad (5:46)$$

To solve the system of simultaneous equations one sets the determinant of the coefficients of A, B and C equal to zero, to give

$$A\begin{vmatrix} a & b & c \\ b & c & d \\ c & d & N \end{vmatrix} + \begin{vmatrix} e & b & c \\ f & c & d \\ g & d & N \end{vmatrix} = 0 \qquad (5:47)$$

the solution of which may be obtained using, for example, Jordan's method, Stroud [1992].

Expanding the determinants and simplifying, yields

$$A = -\frac{1}{\Delta}\left[\, e\,(cN - d^2) + b\,(gd - fN) + c\,(fd - gc)\right] \qquad [5:48]$$

where the quantity ,Δ, is defined by

$$\Delta \equiv \begin{vmatrix} a & b & c \\ b & c & d \\ c & d & N \end{vmatrix} \qquad [5:49]$$

Similarly the model parameter ,B, may be proved equal to

$$B = -\frac{1}{\Delta}\begin{vmatrix} a & e & c \\ b & f & d \\ c & g & N \end{vmatrix} \qquad [5:50]$$

and likewise the quantity ,C, may be expressed as

$$C = -\frac{1}{\Delta}\begin{vmatrix} a & b & e \\ b & c & f \\ c & d & g \end{vmatrix} \qquad [5:51]$$

This concludes the preliminary derivation of the source code required to implement a **non-constrained** least squares algorithm but it should be noted that the above formulation is not optimal and that it was found necessary to use a computer power in excess of twenty-

five decimal places to prevent the machine accuracy adversely affecting the quality of the attainable curve fit. A reduction of the computer power requirements of the curve-fitting algorithms can be achieved by re-structuring the format of the observed N-h data. The source of the accuracy problem lies in the large change in the value of the plasma frequency that is caused by a small change in geocentric height, that is

$$\frac{\Delta y_i}{y_i} \gg \frac{\Delta r_i}{r_i} \qquad (5:52)$$

where the model plasma frequency corresponding to the geocentric height of the i th data point of the observed N-h profile is given by the quasiparabolic expression

$$y(r_i) = \frac{A}{r_i^2} + \frac{B}{r_i} + C \qquad (5:53)$$

To avoid the effects of eq (5.52) one expresses the geocentric height ,r_i, of the observed N-h data points in terms of a reciprocal variable ,q_i, given by

$$q_i \equiv \frac{1}{r_i} \qquad (5:54)$$

where

$$q_i = q_o + \Delta q_i \qquad (5:55)$$

$$q_o = \frac{\sum_i q_i}{N} \qquad [5:56]$$

and N is the size of the array $[q_i]$. Substitution of the new variable into the equation for the quasiparabolic profile results in

$$y(r_i) = A\,(q_o + \Delta q_i)^2 + B\,(q_o + \Delta q_i) + C \qquad [5:57]$$

Expanding the modified form of $y[r_i]$ yields

$$y(r_i) = Aq_o^2 + Bq_o + C + A(2q_o\,\Delta q_i + \Delta q_i^2) + B\Delta q_i \qquad [5:58]$$

and introducing the coefficient ,D, allows one to express the square of the plasma density as

$$y(r_i) = A(2q_o\,\Delta q_i + \Delta q_i^2) + B\Delta q_i + D \qquad [5:59]$$

where

$$D = Aq_o^2 + Bq_o + C \qquad [5:60]$$

Using the previously derived eq [5.33], for the sums of the squares of the errors between the model and the experimental data yields

$$S = \sum_{i=1}^{N} \left[A\,(2q_o\,\Delta q_i + \Delta q_i^2) + B\Delta q_i + D - y_i \right]^2 \qquad [5:61]$$

Differentiating ,S, with respect to the coefficient ,A, and minimizing

$$\frac{dS}{dA} = 2 \sum_{i=1}^{N} \left\{ (y(r_i) - y_i) (2q_o \Delta q_i + \Delta q_i^2 + q_o^2) \right\} = 0 \qquad (5:62)$$

The expansion of eq (5.62) can be greatly simplified by replacing Δq_i with $(q_i - q_o)$ to yield

$$\frac{dS}{dA} = 2 \sum_{i=1}^{N} \left\{ q_i^2 \left(A (2q_o \Delta q_i + \Delta q_i^2) + B \Delta q_i + D \right) - q_i^2 y_i \right\} = 0 \qquad (5:63)$$

Finally eq (5.63) can be expressed in the compact form

$$Aa + Bb + Dc + j = o \qquad (5:64)$$

where the quantities a, b, c and j are defined

$$a = \sum_{i=1}^{N} (2q_o \Delta q_i + \Delta q_i^2) \, q_i^2 \qquad (5:65)$$

$$b = \sum_{i=1}^{N} q_i^2 \, \Delta q_i \qquad (5:66)$$

$$c = \sum_{i=1}^{N} q_i^2 \qquad (5:67)$$

$$j = - \sum_{i=1}^{N} y_i \, q_i^2 \qquad [5:68]$$

Differentiating ,S, with respect to the ,B, coefficient of the quasiparabolic curve and minimizing

$$\frac{d}{dB} \left\{ \sum_{i=1}^{N} \left(y(r_i) - y_i \right)^2 \right\} = 0 \qquad [5:69]$$

giving

$$2 \sum_{i=1}^{N} \left(y(r_i) - y_i \right) \left(\Delta q_i + q_o \right) = 0 \qquad [5:70]$$

Recognizing that $(\Delta q_i + q_o)$ is equal to q_i and expanding eq (5.70) gives

$$\sum_{i=1}^{N} \left(A \left(2 q_o \, \Delta q_i + \Delta q_i^2 \right) q_i + B \, \Delta q_i \, q_i + D \, q_i - q_i \, y_i \right) = 0 \qquad [5:71]$$

By introducing the quantities d, e, f and k one may express eq (5.71) in the compact form

$$Ad + Be + Df + k = 0 \qquad [5:72]$$

where

$$d = \sum_{i=1}^{N} \left(2 q_o \, \Delta q_i + \Delta q_i^2 \right) q_i \qquad [5:73]$$

$$e = \sum_{i=1}^{N} \Delta q_i \; q_i \qquad [5:74]$$

$$f = \sum_{i=1}^{N} q_i \qquad [5:75]$$

$$k = - \sum_{i=1}^{N} y_i \; q_i \qquad [5:76]$$

Finally differentiating ,S, with respect to the coefficient ,C, and minimizing

$$\frac{d}{dC} \left\{ \sum_{i=1}^{N} \left[y\,(r_i) - y_i \right]^2 \right\} = 0 \qquad [5:77]$$

or

$$2 \sum_{i=1}^{N} \left(y(r_i) - y_i \right) \cdot (1) = 0 \qquad [5:78]$$

Expanding eq [5.78] yields

$$\sum_{i=1}^{N} \left\{ A(2q_o \; \Delta q_i + \Delta q_i^2) q_i + B \; \Delta q_i \; q_i + D - y_i \right\} = 0 \qquad [5:79]$$

Introducing the quantities g, h, i and l, one may re-write eq (5.79) in the form

$$Ag + Bh + Di + l = 0 \qquad (5:80)$$

where

$$g = \sum_{i=1}^{N} (2q_o \, \Delta q_i + \Delta q_i^2) \, q_i \qquad (5:81)$$

$$h = \sum_{i=1}^{N} \Delta q_i \, q_i \qquad (5:82)$$

$$i = \sum_{i=1}^{N} (1) = N \qquad (5:83)$$

$$l = - \sum_{i=1}^{N} y_i \qquad (5:84)$$

One can now formulate the modified form of non-constained least squares in a compact matrix format, expressible as

$$\begin{vmatrix} a & b & c & j \\ d & e & f & k \\ g & h & i & l \end{vmatrix} \begin{pmatrix} A \\ B \\ D \\ 1 \end{pmatrix} = 0 \qquad (5:85)$$

where the coefficients can be determined using the Gauss-Jordan method, Stroud [1992]. Solving eq [5.85] gives the following expressions for the A, B, C coefficients of the quasiparabolic model fit,

$$A = -\frac{1}{\Delta}\begin{vmatrix} j & b & c \\ k & e & f \\ l & h & i \end{vmatrix} \quad ; \quad \Delta = \begin{vmatrix} a & b & c \\ d & e & f \\ g & h & i \end{vmatrix} \tag{5:86}$$

$$B = -\frac{1}{\Delta}\begin{vmatrix} a & j & c \\ d & k & f \\ g & l & i \end{vmatrix} \tag{5:87}$$

$$D = -\frac{1}{\Delta}\begin{vmatrix} a & b & j \\ d & e & k \\ g & h & l \end{vmatrix} \tag{5:88}$$

$$C = D - Aq_o^2 - Bq_o \tag{5:89}$$

In summary the eqs [5.86], [5.87], [5.88] and [5.89] constitute a non-constrained least squares algorithm that is suitable for achieving a satisfactory model fit to a ledge of ionization using an IBM compatible 386 PC. Before applying the constrained or non-constrained least squares curve fitting algorithm to the observed N-h profile displayed in

figure (5.2), one must first derive the form of the joining equations necessary to smoothly fit the inverse quasibarabolic section that is required to connect a F_1 ledge to the F_2 layer above it.

The derivation of the A, B, C coefficients of the joining layer used to bridge a F_1 ledge/F_2 layer transition.

In figure (5.5) one sees the MQP geometry of a bifurcated F region within the ionosphere.

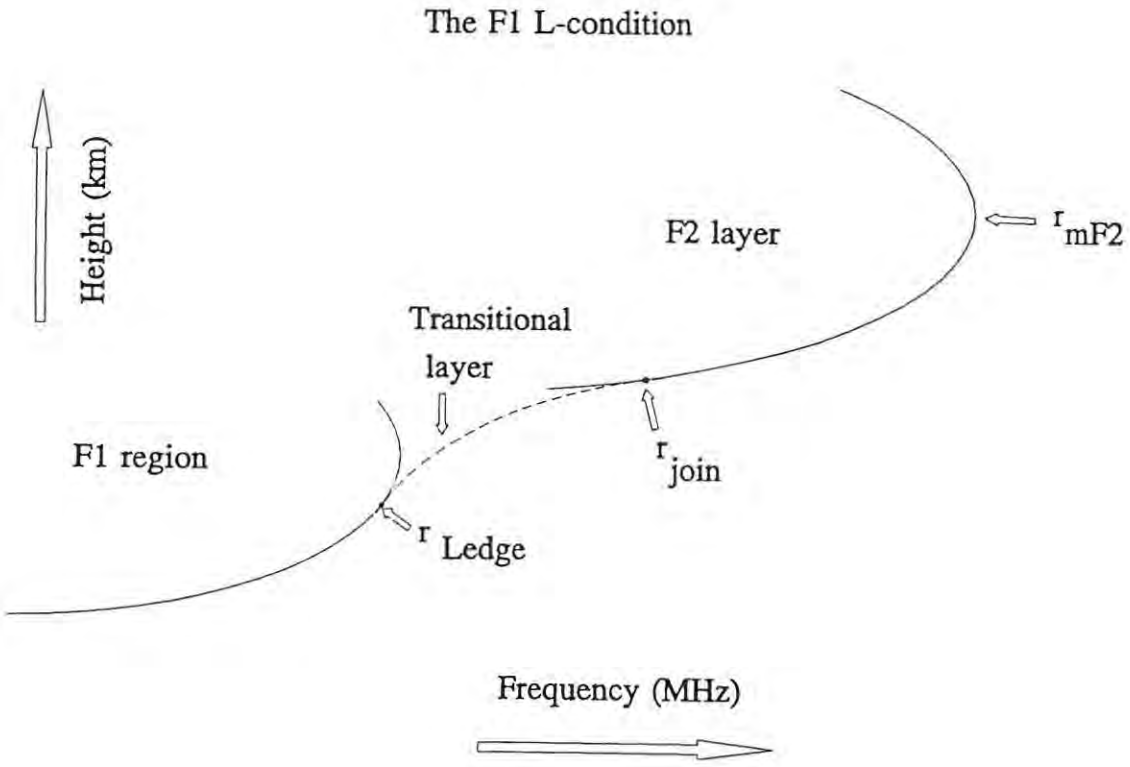

Figure (5.5): A multi-segmented quasiparabolic model for the bridging geometry required to construct a F1 ledge/F2 layer transition. It should be noted that the geocentric heights r_{join} and r_{ledge} as defined in fig (5.5) correspond respectively to the generic notation r_i and r_t that is used in the ensuing mathematical discussion of the F1 ledge condition.

Referring to figure (5.5), the F_2 layer is modelled using the quasiparabolic curve

$$y_{F_2} = \frac{A_{F_2}}{r^2} + \frac{B_{F_2}}{r} + C_{F_2} \qquad (5:90)$$

to describe the electron density as a function of altitude and the F_1 region is similarly described via the equation

$$y_{F_1} = \frac{A_{F_1}}{r^2} + \frac{B_{F_1}}{r} + C_{F_1} \qquad (5:91)$$

Using the constrained least squares algorithm one determines the coefficients (A_{F2}, B_{F2}, C_{F2}) and implementing the non-constrained version of the least squares curve fitting routine one derives the values of (A_{F1}, B_{F1}, C_{F1}). To construct the inverse quasi-parabolic segment constituting the traditional layer, requires the determination of four unknowns namely the coefficients A_{TR}, B_{TR}, C_{TR} and the joining height ,r_j, at the F_1/F_2 interface. Applying the continuity conditions that must exist at each end of the transitional segment, one has four equations from which the four unknowns can be determined by solving simultaneous equations.

The mathematical description of the F_1/F_2 transitional layer

Using eq (5.14) and eq (5.15) one can express the coefficients C_{TR} and B_{TR} via

$$C_{TR} = y_{TR}(r_t) + \frac{A_{TR}}{r_t^2} + \frac{dy}{dr}(r_t)\, r_t \qquad (5:92)$$

and

$$B_{TR} = - \frac{2A_{TR}}{r_t} - \frac{dy}{dr}(r_t)\ r_t^2 \qquad (5:93)$$

The square of the plasma frequency in a transitional region can be determined using eq (5.21) and may be expressed

$$y_{TR}(r) = A_{TR}\left(\frac{1}{r_t} - \frac{1}{r}\right)^2 + \frac{dy}{dr}(r_t)\ r_t^2\left(\frac{1}{r_t} - \frac{1}{r}\right) + y(r_t) \qquad (5:94)$$

The values of $dy/dr(r_t)$ and $y(r_t)$ can be found using eq (5.91) where r_t is taken to be the F_1 ledge height ,r_{F1L}, as determined by the gradient algorithm. Referring to figure (5.5) it is clear that by establishing the continuity conditions governing the electron density and its gradient at the transition height ,r_j, one can solve simultaneous equations to determine the coefficients A_{TR} and r_j respectively.

The continuity equations as applied at the F_1 ledge/F_2 layer interface

a) Continuity in electron density

Assuming that the constrained least squares algorithm has been applied to the F_2 layer, one may express the plasma frequency at the upper transition height by evaluating eq (5.90) at r_j,

$$y_{F_2}(r_j) = \frac{A_{F_2}}{r_j^2} + \frac{B_{F_2}}{r_j} + C_{F_2} \qquad (5:95)$$

Alternatively, the matching value of plasma frequency at the F_1 ledge/F_2 layer interface may be obtained using eq (5.94)

$$y_{TR}(r_j) = A_{TR}\left(\frac{1}{r_t} - \frac{1}{r_j}\right)^2 + \frac{dy_{TR}}{dr}(r_t)\, r_t^2 \left(\frac{1}{r_t} - \frac{1}{r_j}\right) + y(r_t) \qquad (5:96)$$

Applying the continuity condition

$$y_{F2}(r_j) = y_{TR}(r_j) \qquad (5:97)$$

it follows that

$$\frac{A_{F_2}}{r_j^2} + \frac{B_{F_2}}{r_j} + C_{F_2} = A_{TR}\left(\frac{1}{r_t} - \frac{1}{r_j}\right)^2 + \frac{dy_{TR}}{dr}(r_t)\, r_t^2 \left(\frac{1}{r_t} - \frac{1}{r_j}\right) + y(r_t) \qquad (5:98)$$

b) Continuity in the electron density gradient

The gradient in the plasma density at the transition height ,r_j, can be obtained by differentiating the quasiparabolic form of the F_2 layer ,eq (5.90), to give

$$\frac{dy_{F_2}(r_j)}{dr} = -\frac{2A_{F_2}}{r_j^3} - \frac{B_{F_2}}{r_j^2} \qquad (5:99)$$

Similarly the matching gradient in electron concentration at r_j can be obtained by differentiating the equation describing the inverse quasiparabolic joining layer ,eq (5.96), giving

$$\frac{dy_{TR}}{dr}(r_j) = 2\,A_{TR}\left(\frac{1}{r_t} - \frac{1}{r_j}\right)\left(\frac{1}{r_j}\right)^2 + \frac{dy_{TR}}{dr}(r_t)\,r_t^2\left(\frac{1}{r_j}\right)^2 \qquad (5:100)$$

Applying the continuity condition

$$\frac{\partial y_{TR}}{\partial r}(r_j) = \frac{\partial y_{F2}}{\partial r}(r_j) \qquad (5:101)$$

it follows that

$$-\frac{2\,A_{F_2}}{r_j} - B_{F_2} = 2\,A_{TR}\left(\frac{1}{r_t} - \frac{1}{r_j}\right) + \frac{dy_{TR}}{dr}(r_t)\,r_t^2 \qquad (5:102)$$

One can now eliminate the coefficient ,A_{TR}, between the continuity equations, eq (5.102) and eq (5.98), and show that the joining height ,r_j, of the F_1 ledge/F_2 layer interface is given by

$$r_j = -\frac{\left\{\frac{B_{F_2}}{2} + \frac{A_{F_2}}{r_t} + \frac{1}{2}\frac{dy}{dr}(r_t)\,r_t^2\right\}}{\left\{\frac{B_{F_2}}{2r_t} + C_{F_2} - \frac{1}{2}\frac{dy}{dr}(r_t)\,r_t - y(r_t)\right\}} \qquad (5:103)$$

The expression for the A_{TR} coefficient of the joining segment is obtained by eliminating r_j between eq (5.102) and eq (5.103), yielding

$$A_{TR} = - \frac{\left\{ \frac{2A_{F2}}{r_j} + B_{F2} + \left(\frac{dy(r_t)}{dr} \right)_{TR} r_t^2 \right\}}{2\left\{ \frac{1}{r_t} - \frac{1}{r_j} \right\}} \qquad (5:104)$$

The values of the coefficients C_{TR} and B_{TR} are obtained by substituting the expression for A_{TR} into eq (5.92) and eq (5.93) respectively. In summary, one can see that the joining height r_j and the A,B,C coefficients of the inverse quasiparabolic segment required to bridge a F_1/F_2 layer transition can be determined using eq (5.103), eq (5.104), eq (5.93), eq (5.92) respectively, given the following information:-

(i) (ABC) coefficients for the F_2 layer: derived via a constrained version of least squares.

(ii) $y(r_t)$ and $dy(r_t)/dr$: derived by applying a non-constrained least squares algorithm to the F_1 region,

and

(iii) the ledge height r_t: fixed at the point of inflexion on the N-h distribution as determined by the gradient algorithm.

A practical example of the construction of a MQP model to a given observed

electron density distribution

The observed N-h profile displayed in figure (5.2) is used to demonstrate the following:

(a) the constrained least squares algorithm used to fit a layer with a peak,

(b) the non-constrained least squares algorithm developed to model F_1 ledge conditions,

(c) the E/F_1 valley algorithms developed in Chapter (3),

(d) the inverse quasiparabolic joining algorithms used to smoothly and continuously connect two fitted quasiparabolic layers,

and

(e) the joining algorithm used to bridge an F_1 ledge/F_2 layer transition.

One can see from the figure (5.2) that the observed electron density profile possesses the following:

(a) fully developed E layer

(b) E/F_1 valley or ionization depletion region

(c) F_1 ledge condition

(d) distinct F_2 layer.

Using the gradient algorithm one is able to partition the data into sub-sets corresponding to the stratified regions of the ionosphere. In figure (5.4) the gradient of the electron density is plotted as one climbs from the bottom of the E layer to the top of the F region and one can determine the position of points on the observed profile where

$$\frac{dh}{dN} \Rightarrow \infty \qquad (5.105)$$

and/or

$$\frac{d^2h}{dN^2} \rightarrow 0 \qquad [5:106]$$

The gradient algorithm provides one with the ability to check the values that POLAN derives for the heights and the critical frequencies of the ionospheric layers as well as being able to locate the co-ordinates of a possible F_1 ledge condition. In the extended table (5.1) one can see how the partition method is used to stratify the observed N-h data set plotted in figure (5.2).

Ionospheric Region	Data point no.	$f_{critical}$ (MHz)	r_{max} (km)
E layer	13	3.845	113.112
F_1 ledge	26	4.800	155.844
F_2 layer	64	9.119	263.821

Valley	Data Point No.	Depth (MHz)	Width (km)
E/F_1	17	0.009	2.905
F_1/F_2	Not present	N/A	N/A

TABLE (5.1)(a):Anchor point information for the observed N-h profile which is to be used in the construction of the MQP model ionosphere.

Data Point No.	Plasma frequency (MHz)	Altitude (km)
13	3.845	113.11
12	3.811	110.45
11	3.700	109.00
10	3.600	105.89
9	3.500	102.93
8	3.400	101.06
7	3.300	100.24
6	3.200	99.54
5	3.100	99.12
4	2.800	98.70

Ionospheric Model Coefficients (ABC)	Ionospheric Parameters (r_m, f_0, y_m)		
A_E = -4.738989295366479E+13	r_{mE} (km)	f_{0E} (MHz)	y_{mE} (km)
B_E = 1.461723454303836E+10	113.11	3.85	23.40
C_E = -1.127142993557988E+06			

TABLE (5.1) (b) The POLAN and MQP descriptions of the E layer.

Data Point No.	Plasma frequency (MHz)	Altitude (km)
26	4.800	155.84
25	4.700	149.81
24	4.600	144.59
23	4.500	141.21
22	4.400	138.04
21	4.300	135.22
20	4.200	133.10
19	4.100	131.35

Ionospheric Model Coefficients (ABC)	Ionospheric Parameters (r_m, f_0, y_m)		
A_{F1} = -1.137225803419522E+13	r_{mF1} (km)	Pf_{0F1}(MHz)	y_{mF1} (km)
B_{F1} = 3.480817571390137E+09			
C_{F1} = -2.663285910097384E+05	163.25	4.83	60.58

Description of F_1 Ledge Condition	
Ledge Height (km)	Ledge Frequency (MHz)
155.84	4.80

TABLE (5.1)(c):The POLAN and MQP descriptions of the F_1 ledge.

Data Point No.	Plasma frequency (MHz)	Altitude (km)
64	9.119	263.82
63	8.969	245.42
62	8.900	241.28
61	8.800	236.82
60	8.700	233.19
59	8.600	229.90
58	8.500	227.03
57	8.400	224.93
56	8.300	222.75
55	8.200	220.67
54	8.100	218.77
53	8.000	216.88
52	7.900	215.03
51	7.800	213.23
50	7.700	211.53
49	7.600	209.87
48	7.500	208.32
47	7.400	206.79
46	7.300	205.21
45	7.200	203.64
44	7.100	202.03
43	7.000	200.40
42	6.900	198.71
41	6.800	197.39
40	6.700	196.07
39	6.600	194.79
38	6.000	189.04

TABLE (5.1)(d 1):The POLAN and MQP descriptions of the F_2 layer.

Ionospheric Model Coefficients (ABC)	Ionospheric Parameters (r_m, f_0, y_m)		
A_{F2} = -1.616806630061912E+13	r_{mF2} (km)	Pf_{0F2}(MHz)	y_{mF2} (km)
B_{F2} = 4.873700827985901E+09			
C_{F2} = -3.671988570226188E+05	263.82	9.12	98.35

TABLE (5.1)(d 2): The POLAN and MQP descriptions of the F_2 layer.

In summary one can now model the following ionospheric conditions via least squares algorithms of the constrained or non-constrained type, namely,

(a) a ionospheric region possessing a peak in electron density where the derivative of the concentration with respect to geocentric height dN/dh goes to zero,

(b) a ledge of ionization defined by a point of inflexion on the observed N-h profile where the double derivative of the electron density with respect to the geocentric height goes to zero.

Using the constrained and non-constrained curve fitting algorithms to model peak and ledge conditions respectively, the following mean square plots were obtained.

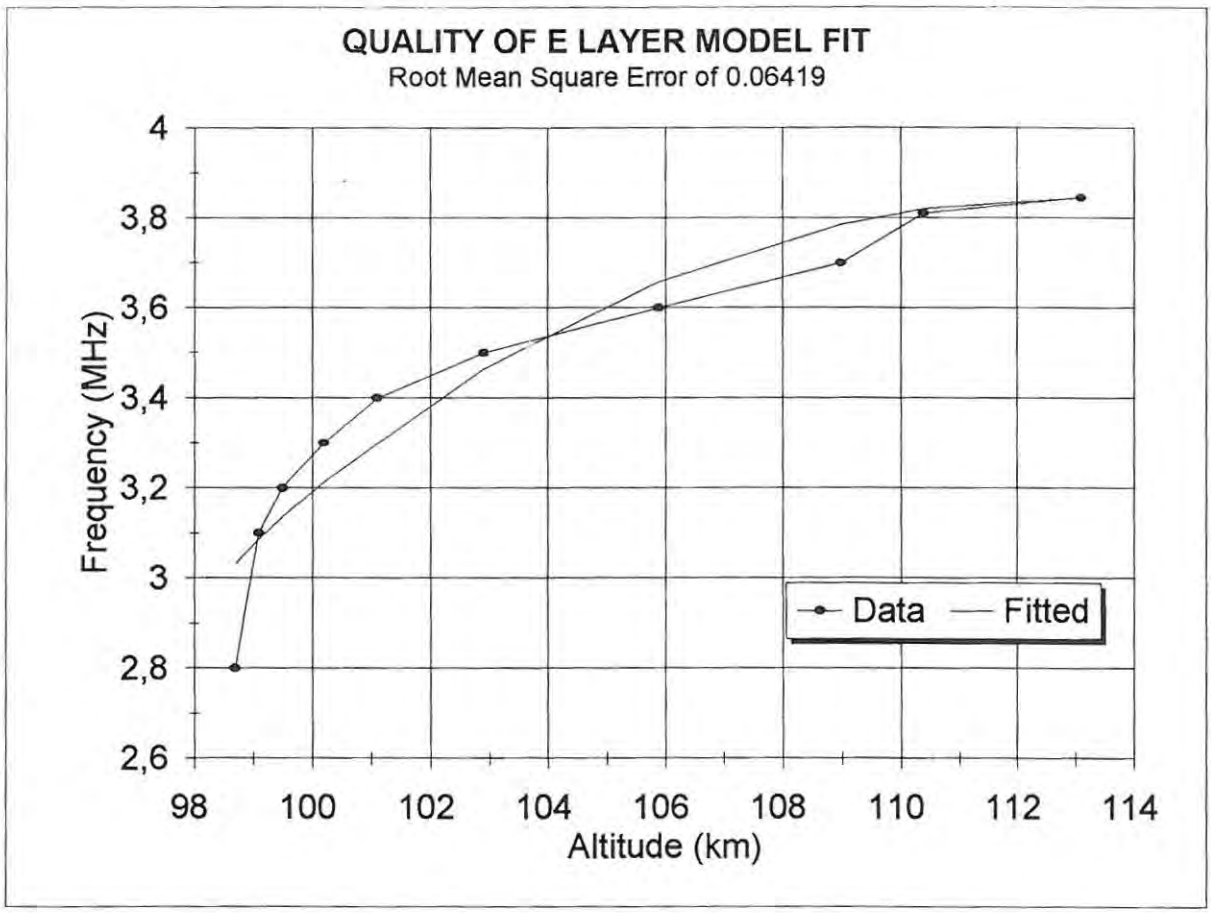

Figure (5.6): Root mean square error for QP curve fit to E layer N-h data.

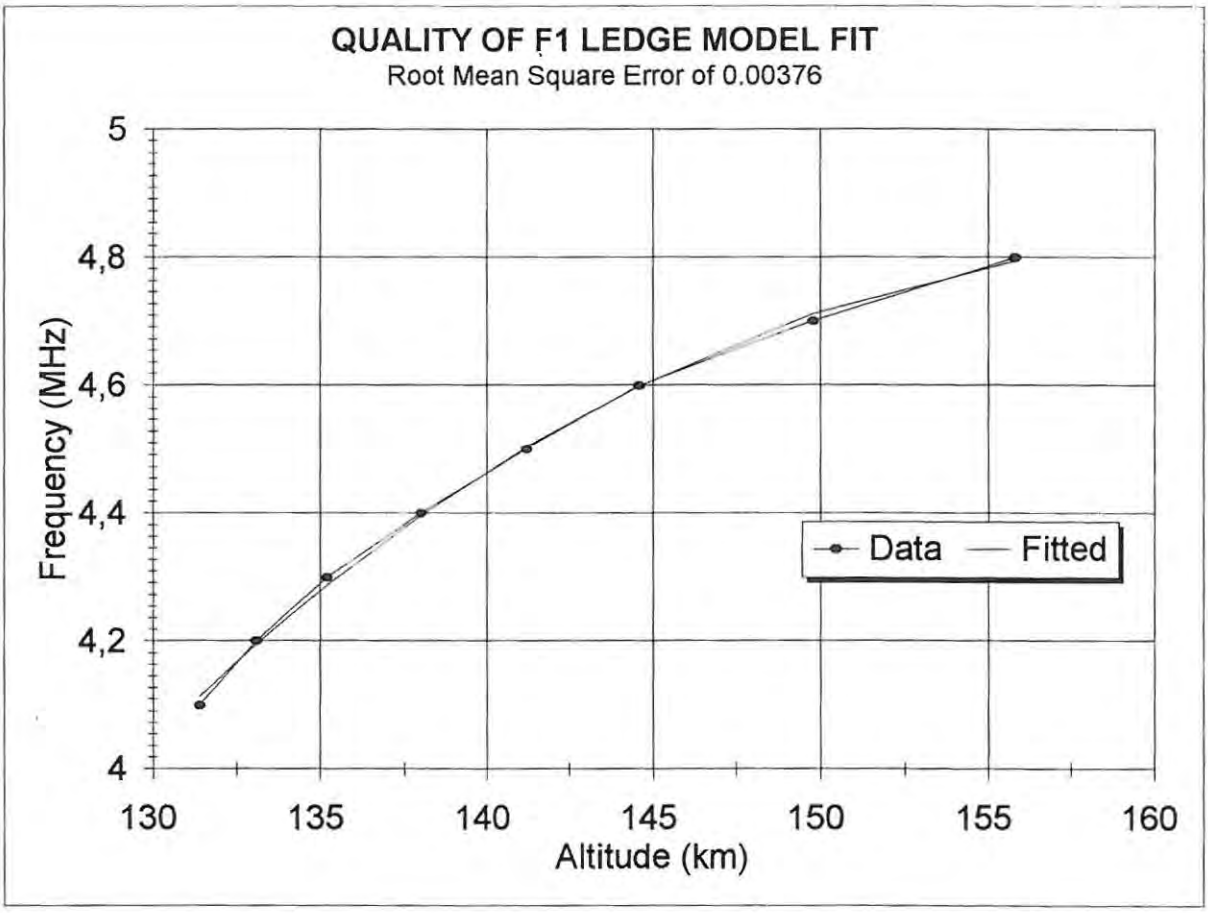

Figure (5.7) Root mean square error for QP curve fit to F_1 ledge N-h data.

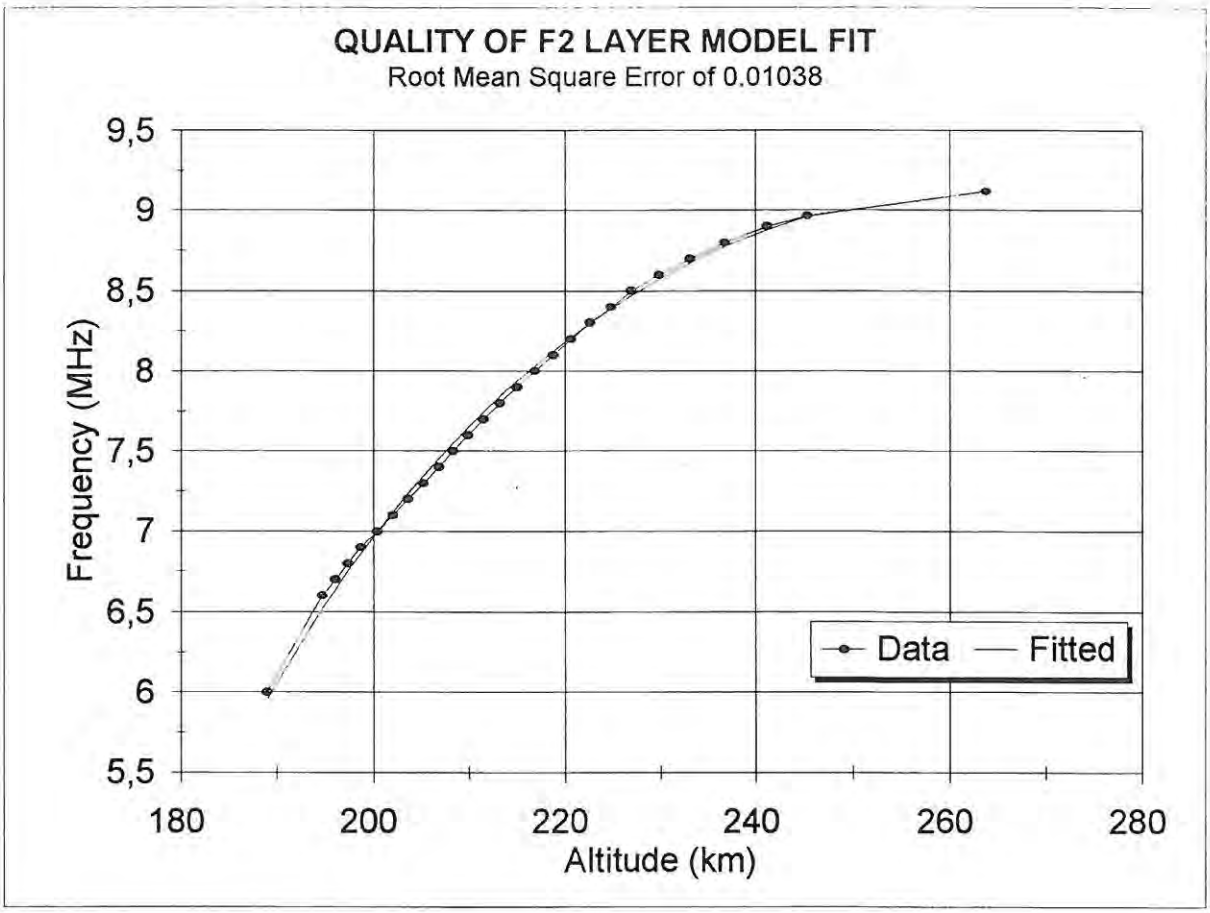

Figure (5.8) Root mean square error for QP curve fit to F_2 layer N-h data.

The root mean square error plotted in figure(5.6),(5.7)and (5.8) is based on a rms value that is calculated using the definition

$$r\,m\,s_{error} = \sqrt{\left[\sum \{ \{ y(r_i) - y_i \}^2 / y_i^2 \} \right]} / (N)^{1/2}$$

where

(1) N is the number of data points in N-h electron density distribution

(2) y_i is square of the plasma frequency of the "ith" data point.

(3) $y(r_i)$ is the square of the plasma frequency corresponding to a point that is located on the quasiparabolic curve fit at the same height as the "ith" data point.

(4) the index "i" runs from one to N.

It should be noted that the absolute minimum r.m.s. error is obtained using the non-constrained version of least squares as the model curve is, in this case, not required to pass through a specific data point. A unique bridging algorithm has been developed to continuously and smoothly connect the QP segment corresponding to a F_1 ledge of ionization with the F_2 region above. The equations used to determine the upper joining height and semi-thickness of the inverse connecting section are thought to represent original work. All algorithms involved in modelling the F_1 ledge/F_2 layer are fully analytic and given the co-ordinates of the inflexion point and the ionospheric coefficients A,B,C describing the F_1 ledge and F_2 layers respectively, it is possible to form a continuous MQP composite section in "real-time". The curve fitting algorithms developed in chapter 3 are used to model an E/F_1 valley region are used to construct the re-entrant portion of the observed N-h distribution displayed in figure (5.2) with a continuum of QP/IQP/IQP sections. In figure (5.9) one sees the composite MQP model ionosphere with which the observed N-h distribution in figure (5.2) may be replaced for the purposes of analytical ray-tracing and HF circuit parameter assessment.

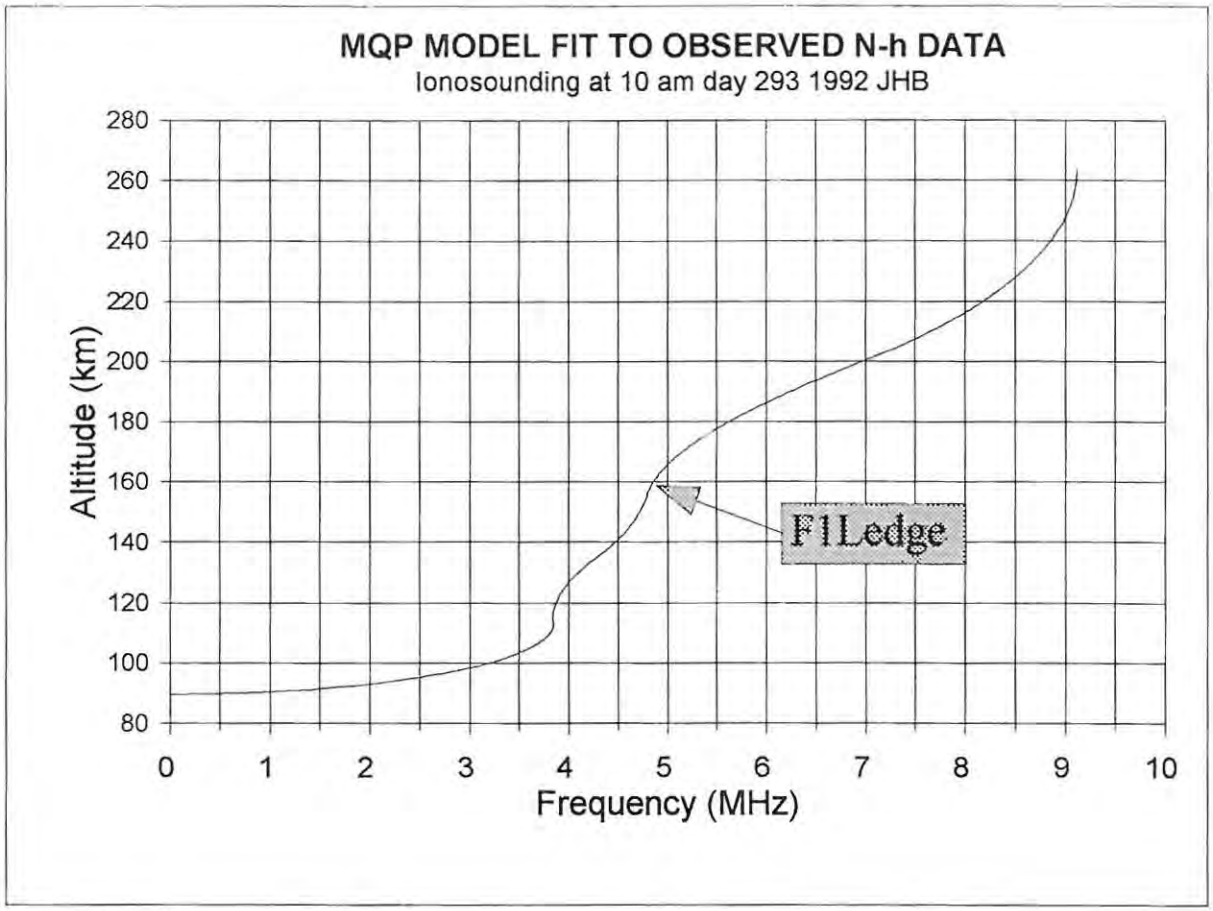

Figure 5.9 The complete MQP electron density profile derived via curve fitting algorithms applied to the observed N-h distribution displayed in figure (5.2)

This concludes the chapter on the quantitative analysis of curve fitting QP segments to a realistic N-h distribution and the replacement of the observed profile with a continuum of QP/IQP building blocks so that one may analytically ray trace through an ionospheric reflection point modelled by a MQP ionosphere.

CHAPTER (6)

REAL TIME SYNTHESIS OF VERTICAL AND OBLIQUE INCIDENCE IONOGRAMMES USING ANALYTICAL RAY TRACING METHODS APPLICABLE TO THE MQP MODEL.

In Chapter 5 a detailed account was presented of the process involved in fitting quasiparabolic curves to observed electron density data, so allowing one to represent the ionosphere, in a realistic way, using a fully analytic model profile. To establish the quality of the model fit to the ionospheric layers, one synthesizes a virtual height profile by vertically ray-tracing through the MQP model ionosphere using a sweep of frequencies and then comparing the synthesized and observed ionogrammes for exactness of fit. In this chapter the algorithms required to synthesize a group path profile with the geomagnetic field included, are derived from first principles for the specific case of a MQP ionosphere. The group path algorithms enable one to generate the following; (a) a group path profile or oblique ionogramme with/without the presence of the geomagnetic field, and

(b) a group height profile or vertical ionogramme with/without the presence of the

geomagnetic field

The Group path integral

Referring to Croft and Hoogasian [1968] the group path integral under conditions of zero magnetic field is given by

$$P' = 2 \int_{r_o}^{r_t} \frac{r\, dr}{\sqrt{r^2\mu^2 - r_o^2 \cos^2 \beta_o}} \qquad (6:1)$$

where

μ → phase refractive index

r_o → radius of the earth

β_o → elevation angle at the transmitter

r_t → maximum height of the HF radio signal

To evaluate eq (6.1) it is necessary to split up the integral into two components, one being the contribution made to the overall group path from the free space portion of the ray's trajectory, P_o, while the other represents the ionospheric portion, P'_i. One can therefore express the group path integral as

$$P' = P'_o + P'_i \qquad (6:2)$$

where

$$P_o' = 2 \int_{r_o}^{r_{base}} \frac{r\,dr}{\sqrt{r^2 - r_o^2 \cos^2 \beta_o}} \qquad (6:3)$$

$$P_i' = 2 \int_{r_{base}}^{r_t} \frac{r\,dr}{\sqrt{r^2\mu^2 - r_o^2 \cos^2 \beta_o}} \qquad (6:4)$$

To solve the group path integrals for a multi-quasiparabolic model ionosphere one recognizes that the term inside the radical within eq (6.4) must be replaced by the ray tracing quadratic

$$R = A'r^2 + B'r + C' \qquad (6:5)$$

where the ray-tracing coefficients A', B', C' are defined by eq (2.57), eq (2.58) and eq (2.59). Using standard integral tables, CRC (1985), the indefinite integral solutions to eq (6.4) for the cases, $A' > 0$ and $A' < 0$, corresponding to the quasi and an inverse quasi-parabolic distributions, are respectively, given by

$$I_1 = 2\frac{\sqrt{R}}{A'} - \frac{B'}{(A')^{3/2}} \log_e \left\{2\sqrt{A'R} + 2A'r + B'\right\} \qquad (6:6)$$

$A' > 0$

$$I_2 = 2\frac{\sqrt{R}}{A'} - \frac{B'}{(-A')^{3/2}} \sin^{-1} \left\{\frac{2A'r + B'}{\sqrt{B'^2 - 4A'C'}}\right\} \qquad (6:7)$$

$A' < 0$

One is now required to solve the general forms of the no-field group path equations, as expressed in eq (6.6) and eq (6.7), for the cases corresponding to, traversal of /apogee in, either a QP or an IQP layer, respectively.

Case 1: Group path contribution given traversal of a quasi or an inverse quasi-parabolic ionospheric layer

In the event that the ray traverses either a quasi or inverse quasi-parabolic layer, the group path contributions are respectively

$$P_i' = 2\frac{\sqrt{R_t}}{A'} - \frac{B'}{(A')^{3/2}} \log_e \left\{2\sqrt{A'R_t} + 2A'r_t + B'\right\} - 2\frac{\sqrt{R_b}}{A'} + \frac{B'}{(A')^{3/2}} \log_e \left\{2\sqrt{A'R_b} + 2A'r_b + B'\right\} \quad \text{(6:8)}$$

for $A' > 0$

$$P_i' = 2\frac{\sqrt{R_t}}{A'} - \frac{B'}{(-A')^{3/2}} \sin^{-1} \left\{\frac{(2A'r_t + B')}{\sqrt{B'^2 - 4A'C'}}\right\} - 2\frac{\sqrt{R_b}}{A'} + \frac{B'}{(-A')^{3/2}} \sin^{-1} \left\{\frac{(2A'r_b + B')}{\sqrt{B'^2 - 4A'C'}}\right\} \quad \text{(6:9)}$$

for $A' < 0$

where the ray tracing coefficient ,A', is positive for a QP section and becomes negative in the case of an IQP joining segment. It is understood that the limits of integration extend from the base ,r_b, to the top ,r_t, of a given ionospheric region.

Case 2: Group path contribution given apogee in a quasi or inverse quasi-parabolic ionospheric layer

If the radio ray undergoes apogee within either a quasi or inverse quasi-parabolic layer then the upper limit of integration becomes, r_{apogee}, and one can make use of the auxiliary ray

tracing equations extracted from Bennett et al [1991], namely,

$$R_{apogee} \equiv A'r_{ap}^2 + B'r_{ap} + C' = 0 \qquad \text{(6:10)}$$

$$(2A'r_{ap} + B') = \sqrt{B'^2 - 4A'C'} \qquad \text{(6:11)}$$

Evaluation of the indefinite integral solutions, eq (6.8) and eq (6.9), using limits extending from the base of a given layer up to the apogee height, followed by simplification using the auxiliary equations (6.10) and (6.11), yields

$$P_i' = -\frac{B'}{2(A')^{3/2}} \log_e \{B'^2 - 4A'C'\} - 2\frac{\sqrt{R_b}}{A'} + \frac{B'}{(A')^{3/2}} \log_e \left\{2\sqrt{A'R_b} + 2A'r_b + C'\right\} \qquad \text{(6:12)}$$

for $A' > 0$

and

$$P_i' = \frac{\pi B'}{2(-A')^{3/2}} - \frac{2\sqrt{R_b}}{A'} + \frac{B'}{(-A')^{3/2}} \sin^{-1}\left\{\frac{(2A'r_b + B')}{\sqrt{B'^2 - 4A'C'}}\right\} \qquad \text{(6:13)}$$

for $A' < 0$

Case 3: The free-space contribution to group path.

An HF radio signal cannot undergo apogee in free space, only traversal, and one may determine P'_0 by simply substituting

$$A' = 1 \qquad (6:14)$$

$$B' = 0 \qquad (6:15)$$

$$C' = -r_o^2 \cos^2 \beta_o \qquad (6:16)$$

in eq(6.6) to give

$$P_0' = 2\left\{\left\{r_b^2 - r_0^2 \cos^2 \beta_0\right\}^{\frac{1}{2}} - r_0 \sin \beta_0\right\} \qquad (6:17)$$

Determination of the group path under magnetic field conditions

The inclusion of the Earth's magnetic field into ray-tracing calculations results in non-analytical solutions to the group path integral, eq (6.4), however, Chen et al [1992] have developed a first order perturbation technique which allows one to analytically determine the group delay experienced by a signal propagating through a MQP ionosphere. The approximate influence of the Earth's magnetic field upon the calculation of group path is taken into account by perturbing the "field free" propagation frequency, so that

$$f_e = f\left\{1 + \frac{1}{2} Y h\right\} \qquad (6:18)$$

where

f_e	→	effective frequency
f	→	unperturbed signal frequency
Y	=	$(eB/mf) \equiv f_H/f$
(eB/m)	=	f_H (gyromagnetic frequency)
h	→	scaling factor

Dyson and Bennett [1979] present graphs of the frequency scaling parameter, h, as a

function of the form

$$h = h\ (W,\ \theta) \qquad (6:19)$$

where

$$W = f\ (f_N^2/f^2\ -\ 1)/f_H \qquad (6:20)$$

and, θ, is the angle between the direction of the wave normal and the geomagnetic field. It was shown that given, $f > f_H$, one may approximate the scaling factor over a wide range of propagation conditions using the results, Chen et al [1992],

$$h \approx \cos^n \theta \qquad \textit{ordinary mode} \qquad (6:21)$$

$$h \approx -\ 1 \qquad \textit{extraordinary mode} \qquad (6:22)$$

The approach used by ,Chen, is to calculate the "no field" group path, P′, using eq (6.4), with a signal frequency , f_{eff}, and then to add a first order perturbation, $\Delta P'$, given by

$$\Delta P' = \frac{1}{2} \int X\ Y\ du \qquad (6:23)$$

where

$$X \equiv \frac{f_N^{\ 2}}{f_e^2} \qquad (6:24)$$

$$Y \equiv \frac{f_H}{f_e} \qquad (6:25)$$

and, du, is the elemental group path elapsed along the Y = 0 ray. In what follows, the various terms that constitute the integrand of eq (6.23) are identified and the group path perturbation term evaluated for the MQP model.

The term ,X, equivalent to ,f_N^2 / f_e^2.

The square of the plasma frequency for a quasiparabolic electron model may be expressed in the form of De Voogt's equation, namely

$$f_N^2 = \frac{A}{r^2} + \frac{B}{r} + C \qquad (6:26)$$

which in turn allows one to define the quantity ,X, as

$$X = \frac{1}{f_e^2}\left\{\frac{A}{r^2} + \frac{B}{r} + C\right\} \qquad (6:27)$$

The term ,du, equivalent to the elemental group path along the un-perturbed ray

The elemental group path, du, by definition, is given by

$$du = 2\mu' \, ds \qquad (6:28)$$

where for the ,Y = 0, (no-field) ray one may replace the group refractive index ,μ', by the reciprocal of the phase index, μ, with the result

$$du = 2\left(\frac{1}{\mu}\right) ds = 2\,\frac{dr}{\mu \sin \beta} \qquad (6:29)$$

given that ,β, is the local elevation angle made by an element of the radio trajectory. Using

Bouguer's rule, eq (4.1), one may re-express eq (6.29) in the form

$$du = 2 \frac{r}{\sqrt{\mu^2(r)r^2 - \cos^2 \beta_o}} dr \qquad (6:30)$$

where the radical term is equivalent to the ray tracing quadratic R as defined in eq (6:5).

The term ,Y, equivalent to f_H / f_e

The effective frequency ,f_{eff}, is given by eq (6.18), where it should be carefully noted that one uses the unperturbed frequency ,f, when determining the value of ,Y, upon which ,f_{eff}, depends. Substitution of eq (6.25), eq (6.27) and eq (6.30) into the expression for the group path perturbation , $\Delta P'$, gives

$$\Delta P' = \frac{f_H}{f_e^3} \int_{r_b}^{r_t} \frac{(A/r^2 + B/r + C)\, r}{\sqrt{A'r^2 + B'r + C'}} dr \qquad (6:31)$$

where the integration path extends from the bottom of the ionosphere to the point of apogee. One should note that eq (6.28) already embodies the factor of two necessary to account for the two legs of the radio locus.

The solution to the group path perturbation equation, $\Delta P'$

The solution to eq (6.31) is readily found by decomposing the integrand into three recognizable standard forms, namely

$$J_1 \equiv \int \frac{dz}{z\sqrt{Z}} \qquad (6:32)$$

$$J_2 \equiv \int \frac{dz}{\sqrt{Z}} \qquad (6:33)$$

$$J_3 \equiv \int \frac{z\,dz}{\sqrt{Z}} \qquad (6:34)$$

$$Z \equiv (az^2 + bz + c) \qquad (6:35)$$

The solutions to the integrals, J_1, J_2 and J_3 can be found in the CRC [1985] handbook and are for ease of application, quoted below

Case 1: Standard integral of type J_1

$$J_1 = -\frac{1}{\sqrt{c}} \log_e \left\{ \frac{2\sqrt{cZ} + bz + 2c}{z} \right\} \quad , \quad c > 0 \qquad (6:36)$$

or

$$J_1 = \frac{1}{\sqrt{-c}} \sin^{-1} \left\{ \frac{bz + 2c}{z\sqrt{b^2 - 4ac}} \right\} \quad , \quad c < 0 \qquad (6:37)$$

Case 2: Standard integral of type J_2

$$J_2 = \frac{1}{\sqrt{a}} \log_e \{2\sqrt{aZ} + 2az + b\} \quad , \quad a > 0 \qquad (6:38)$$

or

$$J_2 = -\frac{1}{\sqrt{-a}} \sin^{-1}\left\{\frac{2az + b}{\sqrt{b^2 - 4ac}}\right\} \quad , \quad a < 0 \qquad (6:39)$$

Case 3: Standard integral of type J_3

$$J_3 = \frac{\sqrt{Z}}{a} - \frac{b}{2(a)^{3/2}} \left\{\log_e \left\{2\sqrt{aZ} + 2az + b\right\}\right\} \quad , \quad a > 0 \qquad (6:40)$$

or

$$J_3 = \frac{\sqrt{Z}}{a} - \frac{b}{2(-a)^{3/2}} \sin^{-1}\left\{\frac{2az + b}{\sqrt{b^2 - 4ac}}\right\} \quad , \quad a < 0 \qquad (6:41)$$

The solution to the group path correction term, ,ΔP′, for the case when the geomagnetic field is included

Four cases occur when calculating the ΔP′ factor for an HF radio signal propagating through a MQP model profile :

Case 1 : Group path correction factor given apogee in a traditional layer;

(A′ > 0, C′ > 0)

Expansion of the eq (6.31) for the group path perturbation, ΔP′, gives the three integral types expressed in eq (6.32), eq (6.33) and (6.34) , that is,

$$\Delta P' = \frac{f_H}{f_e^3}\left\{A\int_{r_b}^{r_{ap}} \frac{dr}{r\sqrt{R}} + B\int_{r_b}^{r_{ap}} \frac{dr}{\sqrt{R}} + C\int_{r_b}^{r_{ap}} \frac{rdr}{\sqrt{R}}\right\} \qquad (6:42)$$

whereupon the solution to ΔP′ follows from direct substitution of the standard intergal

forms. Application of the auxiliary ray-tracing equations, Bennett et al [1991], describing the apogee condition within a quasiparabolic layer, namely

$$R_{ap} \equiv A' r_{ap}^2 + B' r_{ap} + C' = 0 \qquad [6:43]$$

$$\frac{B' r_{ap} + 2C'}{r_{ap}} = (\pm) \sqrt{B'^2 - 4A'C'} \quad , \quad \begin{pmatrix} A' > 0 \\ A' < 0 \end{pmatrix} \qquad [6:44]$$

$$2A' r_{ap} + B' = (\pm) \sqrt{B'^2 - 4A'C'} \quad , \quad \begin{pmatrix} A' > 0 \\ A' < 0 \end{pmatrix} \qquad [6:45]$$

allows one to considerably simplify the definite integral solutions to the perturbation equation, eq [6.42]. The solution to the group path correction equation, in the form of eq [6.42], under apogee conditions within a quasiparabolic layer, [A′ > 0, C′ > 0], is given by

$$\begin{aligned} \Delta P' = {} & \frac{f_H}{f_e^3} \left\{ - \frac{A}{2\sqrt{C'}} \log_e \{B'^2 - 4A'C'\} + \frac{A}{\sqrt{C'}} \log_e \left\{ \frac{2\sqrt{C'R_b} + B'r_b + 2C'}{r_b} \right\} \right\} \\ & + \frac{f_H}{f_e^3} \left\{ \frac{B}{2\sqrt{A'}} \log_e \{B'^2 - 4A'C'\} - \frac{B}{\sqrt{A'}} \log_e \left\{ 2\sqrt{A'R_b} + 2A'r_b + B' \right\} \right\} \\ & + \frac{f_H}{f_e^3} \left\{ - \frac{CB'}{4(A')^{3/2}} \log_e \{B'^2 - 4A'C'\} - \frac{C}{A'} \sqrt{R_b} \right\} \\ & + \frac{f_H}{f_e^3} \left\{ \frac{CB'}{2(A')^{3/2}} \left\{ \log_e \left\{ 2\sqrt{A'R_b} + 2A'r_b + B' \right\} \right\} \right\} \end{aligned} \qquad [6:46]$$

Case 2 : Group path correction factor given traversal of a traditional layer;

$(A' > 0,\ C' > 0)$

$$\Delta P' = \frac{f_H}{f_{eff}^3}\left\{-\frac{A}{\sqrt{C'}}\log_e\left\{\frac{2\sqrt{C'R_t} + B'r_t + 2C'}{r_t}\right\}\right\}$$

$$+\frac{f_H}{f_{eff}^3}\left\{\frac{A}{\sqrt{C'}}\log_e\left\{\frac{2\sqrt{C'R_b} + B'r_b + 2C'}{r_b}\right\}\right\}$$

$$+\frac{f_H}{f_{eff}^3}\left\{\frac{B}{\sqrt{A'}}\log_e\left\{2\sqrt{A'R_t} + 2A'r_t + B'\right\}\right\} \qquad [6:47]$$

$$+\frac{f_H}{f_{eff}^3}\left\{-\frac{B}{\sqrt{A'}}\log_e\left\{2\sqrt{A'R_b} + 2A'r_b + B'\right\}\right\}$$

$$+\frac{f_H}{f_{eff}^3}\left\{\frac{C}{A'}\sqrt{R_t} - \frac{CB'}{2(A')^{3/2}}\left\{\log_e\left\{2\sqrt{A'R_t} + 2A'r_t + B'\right\}\right\}\right\}$$

$$+\frac{f_H}{f_{eff}^3}\left\{-\frac{C}{A'}\sqrt{R_b} + \frac{CB'}{2(A')^{3/2}}\left\{\log_e\left\{2\sqrt{A'R_b} + 2A'r_b + B'\right\}\right\}\right\}$$

CASE 3 : Group path correction factor given apogee in an inverse layer;

(A′ < 0, C′ < 0)

$$\Delta P' = \frac{f_H}{f_{eff}^3}\left\{-\frac{A\pi}{2\sqrt{-C'}} + \frac{A}{\sqrt{-C'}}\sin^{-1}\left\{\frac{B'r_b + 2C'}{r_b\sqrt{B'^2 - 4A'C'}}\right\}\right\}$$

$$+\frac{f_H}{f_{eff}^3}\left\{\frac{B\pi}{2\sqrt{-A'}} + \frac{B}{\sqrt{-A'}}\sin^{-1}\left\{\frac{2A'r_b + B'}{\sqrt{B'^2 - 4A'C'}}\right\}\right\} \qquad (6:48)$$

$$+\frac{f_H}{f_{eff}^3}\left\{\frac{CB'\pi}{4(-A')^{3/2}} - \frac{C}{A'}\sqrt{R_b} + \frac{CB'}{2(-A')^{3/2}}\sin^{-1}\left\{\frac{2A'r_b + B'}{\sqrt{B'^2 - 4A'C'}}\right\}\right\}$$

CASE 4 : Group path correction factor given traversal of an inverse layer;

(A′ < 0, C′ < 0)

$$\Delta P' = \frac{f_H}{f_{eff}^3}\left\{\frac{A}{\sqrt{-C'}}\sin^{-1}\left\{\frac{B'r_t + 2C'}{r_t\sqrt{B'^2 - 4A'C'}}\right\} - \frac{A}{\sqrt{-C'}}\sin^{-1}\left\{\frac{B'r_b + 2C'}{r_b\sqrt{B'^2 - 4A'C'}}\right\}\right\}$$
$$+ \frac{f_H}{f_{eff}^3}\left\{-\frac{B}{\sqrt{-A'}}\sin^{-1}\left\{\frac{2A'r_t + B'}{\sqrt{B'^2 - 4A'C'}}\right\} + \frac{B}{\sqrt{-A'}}\sin^{-1}\left\{\frac{2A'r_b + B'}{\sqrt{B'^2 - 4A'C'}}\right\}\right\} \qquad (6:49)$$
$$+ \frac{f_H}{f_{eff}^3}\left\{\frac{C}{A'}\sqrt{R_t} - \frac{CB'}{2(-A')^{3/2}}\sin^{-1}\left\{\frac{2A'r_t + B'}{\sqrt{B'^2 - 4A'C'}}\right\}\right\}$$
$$+ \frac{f_H}{f_{eff}^3}\left\{-\frac{C}{A'}\sqrt{R_b} - \frac{CB'}{2(-A')^{3/2}}\sin^{-1}\left\{\frac{2A'r_b + B'}{\sqrt{B'^2 - 4A'C'}}\right\}\right\}$$

Summary of the algorithms used to calculate the no-field/field included group path for the case of a MQP model electron density profile

The earth's ionosphere has been modelled as a multi-segmented quasiparabolic electron density distribution and the analytical solutions to the "no-field" group path integrals have been derived. Furthermore, following the work of Chen et al [1990] the effect of the geomagnetic field upon the group path (delay) has been incorporated as a first order perturbation to the field-free results, that is

$$P' = \int \left\{1 - \frac{1}{2} XYh\right\} du \qquad (6:50)$$

where

$\Delta P'$ = $1/2 \int X\,Y\,h\,du$

h $\cong$ $\cos^n \theta$ (ordinary mode)

$h \equiv -1$ (extraordinary mode)

For the case of a MQP electron density model of the ionosphere one can solve eq(6.50) analytically with the result that one can calculate group path and virtual height structure in real time.

The synthesis of an h'(f) trace by ray tracing through a MQP model

To evaluate the accuracy of the MQP ionospheric modelling process it was necessary to synthesize a vertical incidence ionogramme by analytically ray tracing through an QP/IQP electron profile, constructed from curve fits to observed N-h data. Using eq (6.51) it is possible to include the birefringent effect of the earth's magnetic field upon HF propagation, enabling one to compare both the ordinary and extraordinary synthetic virtual height traces with the observed ionogrammetric data. To achieve this end a mid-morning ionogramme was recorded by the Frankenwald ionosonde at 10am on day 346, 1992 and the electron profile corresponding to the observed h'(f) trace subsequently derived via the POLAN inversion programme. The figures (6.1), (6.2), (6.3) and (6.4), shows the sequential process involved in determining the ionospheric layer parameters (A, B, C), see table (6.1), from which the MQP model profile is constructed

KEL Aerospace IPS-51 Ver 2.16

C.S.I.R. Remote Control
Station: Frankenwald - 120
Sounding at 1000 hrs, on day 346, 1992.
10 soundings per channel, 40 uS pulse width, threshold at 20%.

O trace.

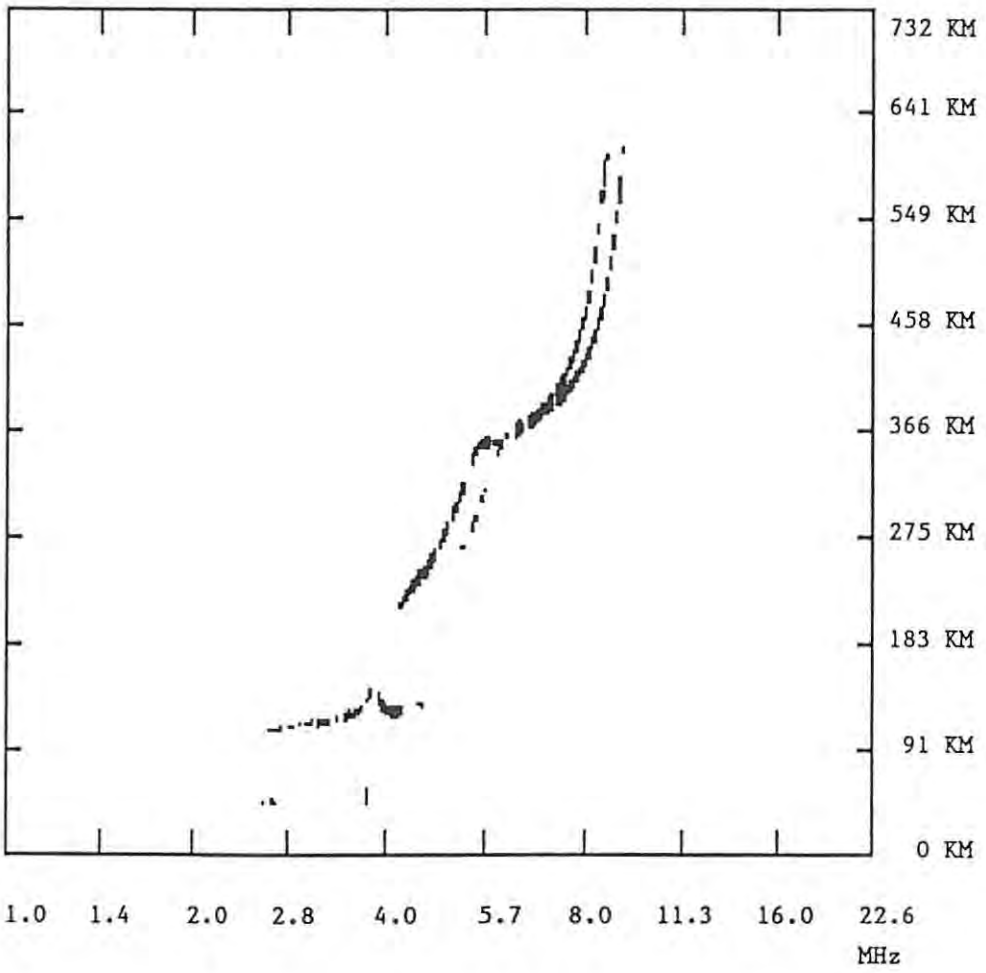

Figure (6.1): Ionogramme recorded 10 am day 346 1992 Frankenwald, Johannesburg, RSA.

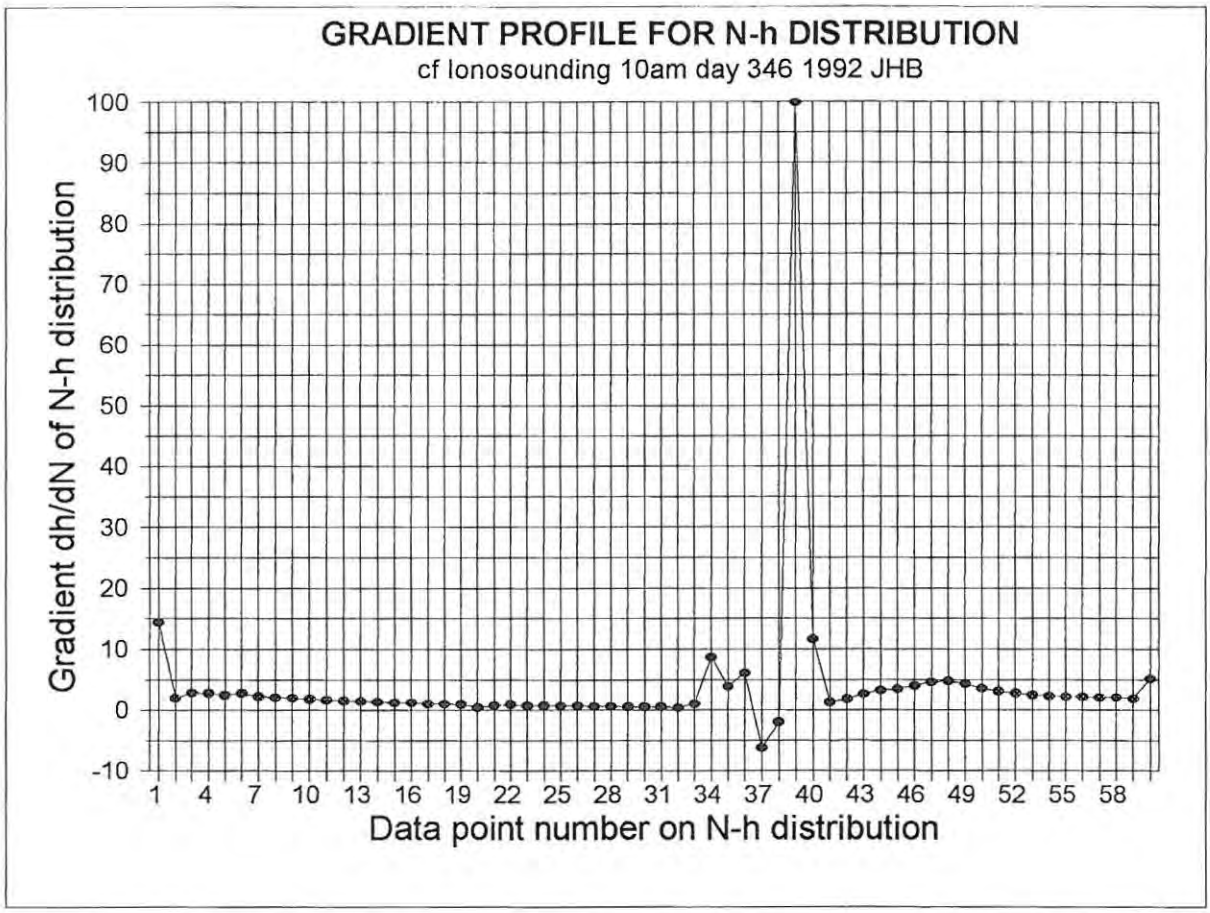

Figure (6.3): Plot of the electron density gradient for the N-h distribution displayed in figure (6.2).

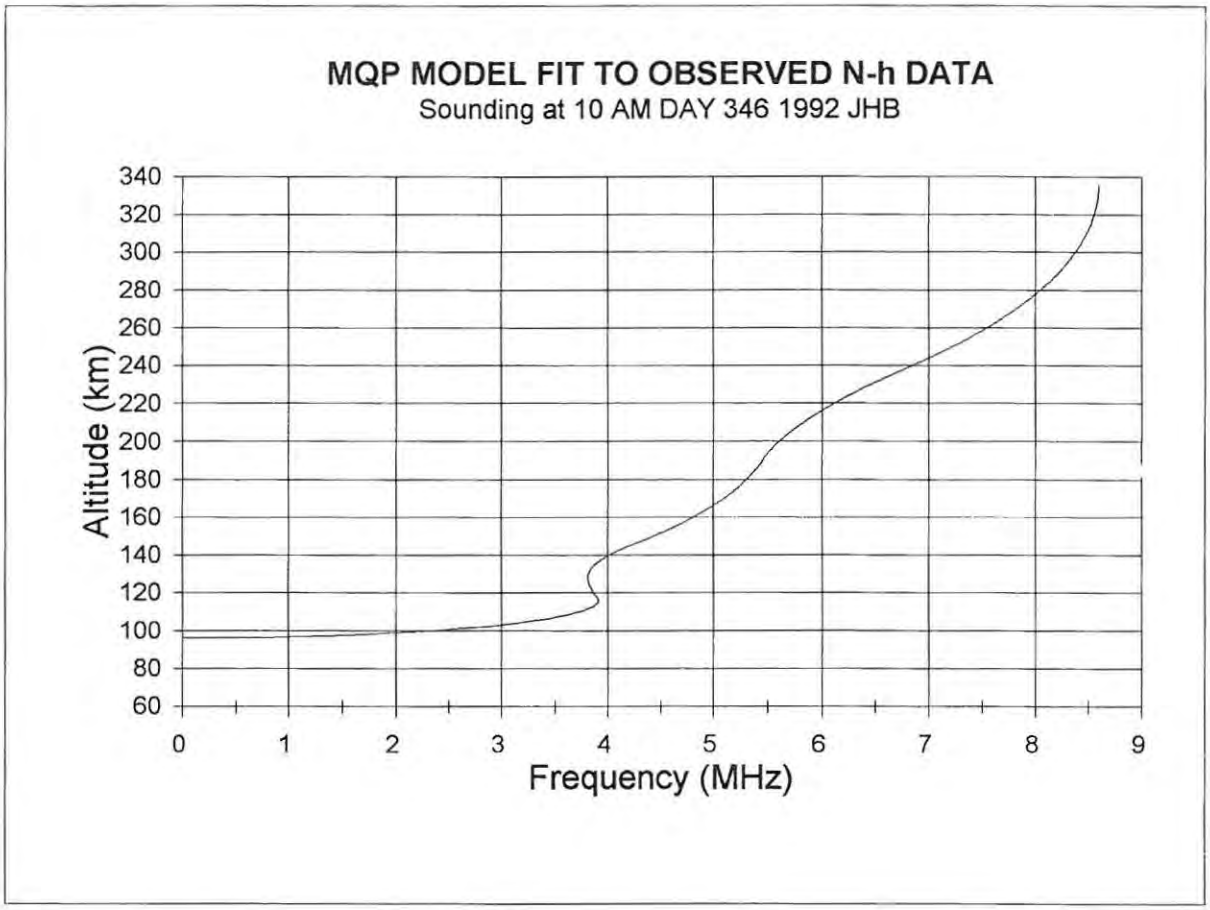

Figure (6.4): MQP model ionosphere used to replace the observed N-h electron distribution in figure (6.2).

	Type	Description	A	B	C
1	Traditional	E-layer	-6,718742225E+13	2,071397106E+10	-1,596520819E+06
2	Traditional	Valley	-6,718742225E+13	2,071397106E+10	-1,596520819E+06
3	Inverse	Valley	1,035064825E+13	-3,185069652E+09	2,450395369E+05
4	Inverse	Valley	2,067922883E+13	-6,363348708E+09	4,895421015E+05
5	Traditional	F1-ledge	-5,700145990E+12	1,732108756E+09	-1,315532809E+05
6	Inverse	F1/F2	1,970000000E+02	-2,449494082E+09	1,871178698E+05
7	Traditional	F2-layer	-5,805787895E+12	1,731269976E+09	-1,289910602E+05

Layer	fm (MHz)	Max. Height (km)	Semi-thickness (km)
E	3,917	116,16	20,048162
F1	5,975	210,74	99,655023
F2	8,598	335,97	156,764650

E/F1 Valley dimensions	
Depth MHz	0,099
Width km	24,64

F1 Ledge co-ordinates	
Ledge freq. MHz	5,48
Ledge ht. km	190

MQP model description of an observed N-h profile corresponding to an ionospheric sounding at 10 AM DAY 346 1992 JHB.

Table (6.1): MQP ionospheric layer coefficients used to construct the QP/IQP model profile in figure (6.4).

The next step is to derive the mathematics necessary to synthesize a virtual height trace given the MQP model parameters listed in table (6.1).

Derivation of group height from the group path equations

The expression for the synthetic h'(f) trace derived from a multi-segmented quasiparabolic electron model is obtained by substituting a launch angle of ninety degrees into the group path equation, eq (6.4), remembering to include a multiplicative factor of one half,

consistent with the calculation of group height. The field-free expression for group (virtual) height is therefore

$$h'(f) = (r_b - r_o)_{free\text{-}space} + \int_{r_b}^{r_t} \frac{r\,dr}{\sqrt{A'r^2 + B'r + C'}} \qquad (6:51)$$

where

r_o → Earth's radius

r_b → geocentric height of the base of the ionosphere

r_t → apogee height of the radio trajectory

$(r_b - r_o)$ → free-space contribution to the group height

(A',B',C') → MQP ray-tracing coefficients evaluated for normal incidence and a given frequency

Inclusion of the magnetic field

It has already been discussed that the double refraction experienced by a HF signal propagating through the ionosphere is caused by the presence of the geomagnetic field and Chen et al (1992) have shown that its first order effect on the group path profile may be

derived using, eq (6.31). The form of virtual height perturbation factor, $\Delta h'$, follows directly from eq (6.31), that is

$$\Delta h' = \frac{1}{2}\frac{f_H}{f_e^3}\int_{r_b}^{r_t}\frac{(A/r^2 + B/r + C)r}{\sqrt{A'r^2 + B'r + C'}}\,dr \qquad (6:52)$$

where

f_H	→	gyro-frequency,≈1.0 MHz, for South Africa
(A',B',C')	→	MQP ray-tracing coefficients, as in table (6.1)
f_{eff}	→	effective frequency is calculated using eq (6.18)

For the case of vertical incidence sounding in mid-latitude regions one may assume quasi-transverse propagation with respect to the geomagnetic field lines and according to Chen et al (1990) under such conditions one may approximate the frequency shift parameters, $h_{o\text{-}ray}$ and $h_{x\text{-}ray}$, with the values that they assume under orthogonal conditions provided that the angle ,θ, between the direction of the wave normal and the earth's magnetic field is in excess of thirty degrees. It follows therefore from eq (6.21) and eq (6.22) respectively that under quasi-transverse conditions the ordinary ray will not be perturbed by the presence of the geomagnetic field whereas the extraordinary ray undergoes a relative frequency shift of, $f_H/2$. One can therefore safely describe the frequency shift parameters under vertical sounding conditions in South African latitudes by the equations

$$h_{o\text{-}ray} = \cos^n \theta \rightarrow 0 \qquad (6:53)$$

$$h_{x\text{-}ray} = -1 \qquad (6:54)$$

Referring to the ionogramme displayed in figure (6.5) one can clearly see the birefringent nature of the ionosphere and that the observed frequency seperation at the layer critical frequency corresponding to the O and X traces is 0,5 MHz consistent with vertical propagation in the South African region.

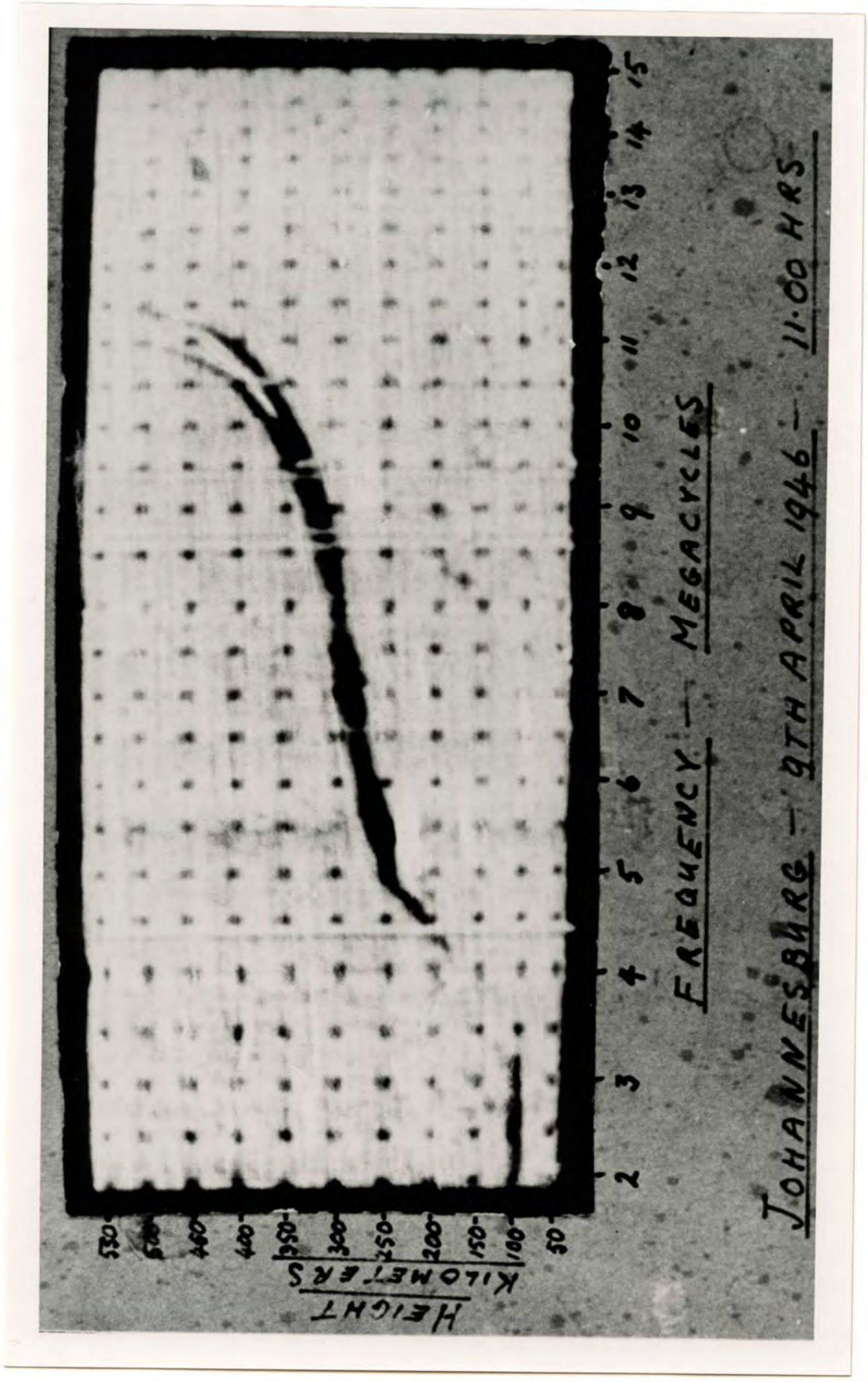

Figure (6.5): First ionogramme recorded with the Wadley ionosonde at the University of Witwatersrand, RSA, on the 9th April 1946.

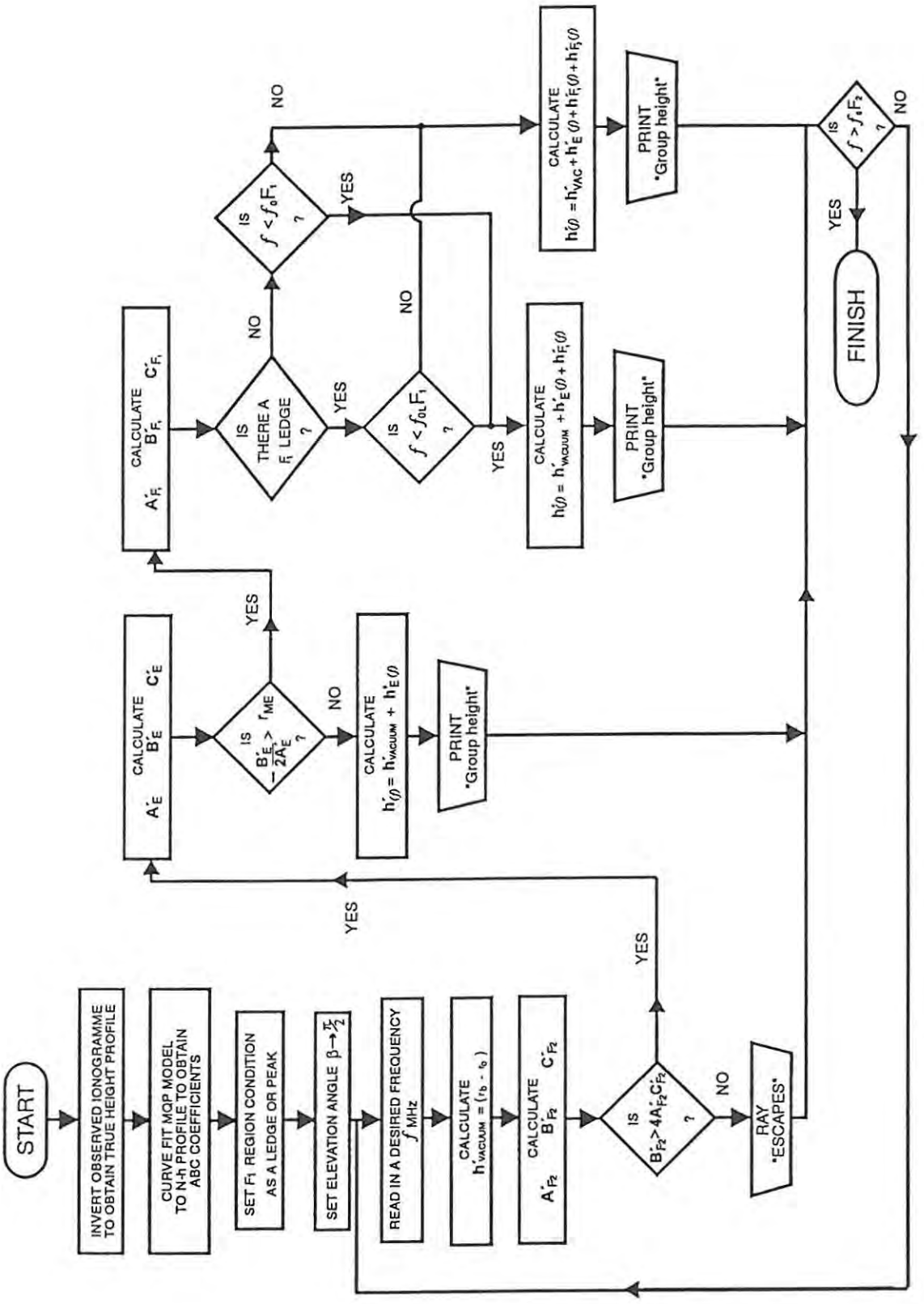

Figure (6.6): A schematic of the logical processes used in group height [VI] synthesis

Actual calculation of h'(f) for a MQP model profile

The flow chart on the preceding page, figure (6.6), illustrates the logical processes involved in synthesizing a virtual height profile when one is provided with the MQP ionospheric layer parameters, { A, B, C }. The analytical expressions for the virtual height contributions from the QP/IQP sections of the MQP model follow directly from the already derived group path equations as does the calculation of the magnetic field induced perturbation term, $\Delta h'$.

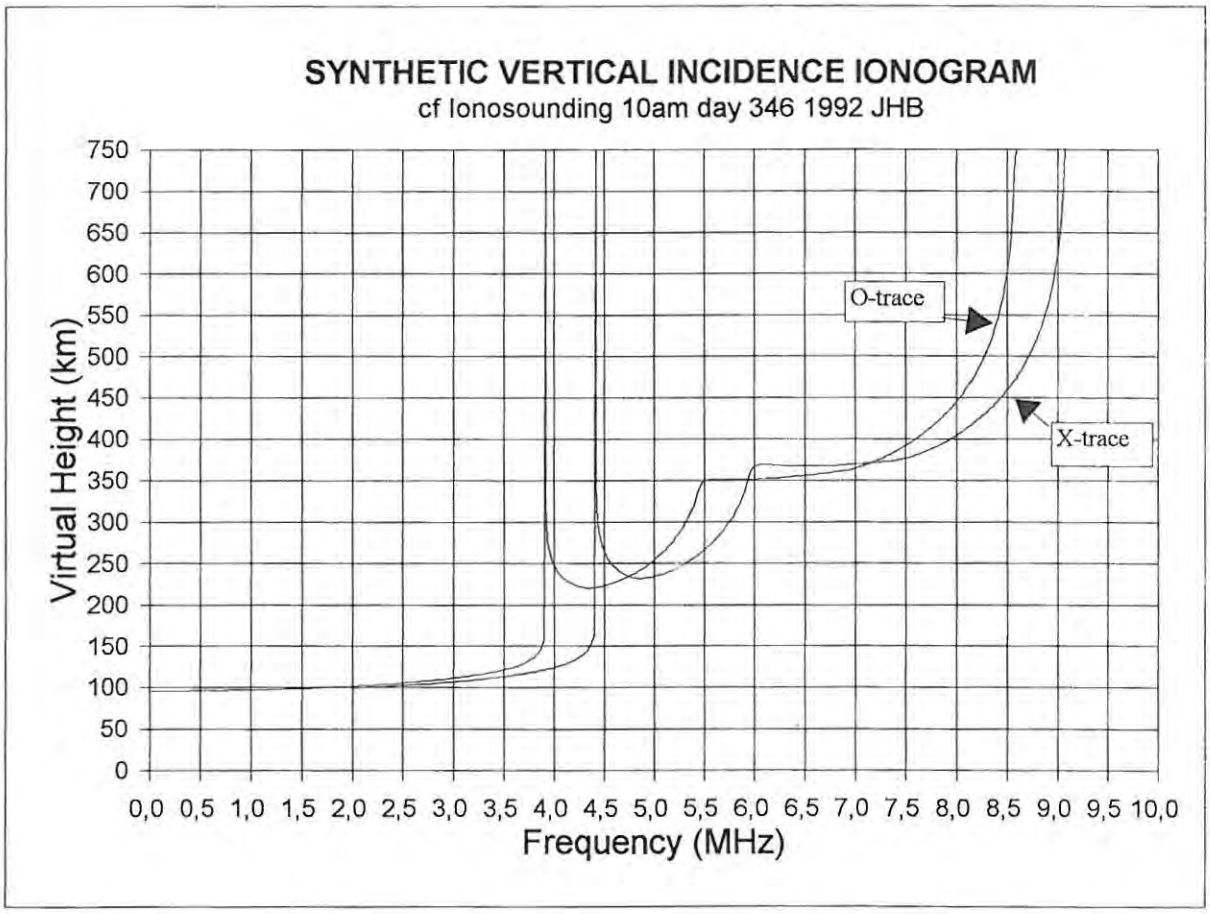

Figure (6.7): Vertical incidence ionogramme synthesized from a MQP electron density derived from curve fits to the observed N-h data displayed in figure (6.2)

The figure (6.7) shows the synthetic virtual height obtained when one re-inverts the MQP model electron distribution, depicted in figure (6.4), using a computer synthesizer package designed using the logic architecture displayed in figure (6.6). One can clearly see two infinite virtual height cusps, corresponding to penetration of the elecron density maxima that occur in the E and F_2 layers respectively, while the F_1 region displays a finite cusp in its virtual height profile, indicative of an inflexion condition at the point of F1/F2 bifurcation.

Synthesized ionogrammes for different F_1 ledge heights

Figure (6.8) shows the effect of artificially altering the F_1 ledge height from its determined value of 190 km and one can see that the F_1 virtual height cusp evolves from a "step-like" geometry towards an infinite spike as the ledge height approaches the altitude of the "pseudo" - maximum of the F_1 region.

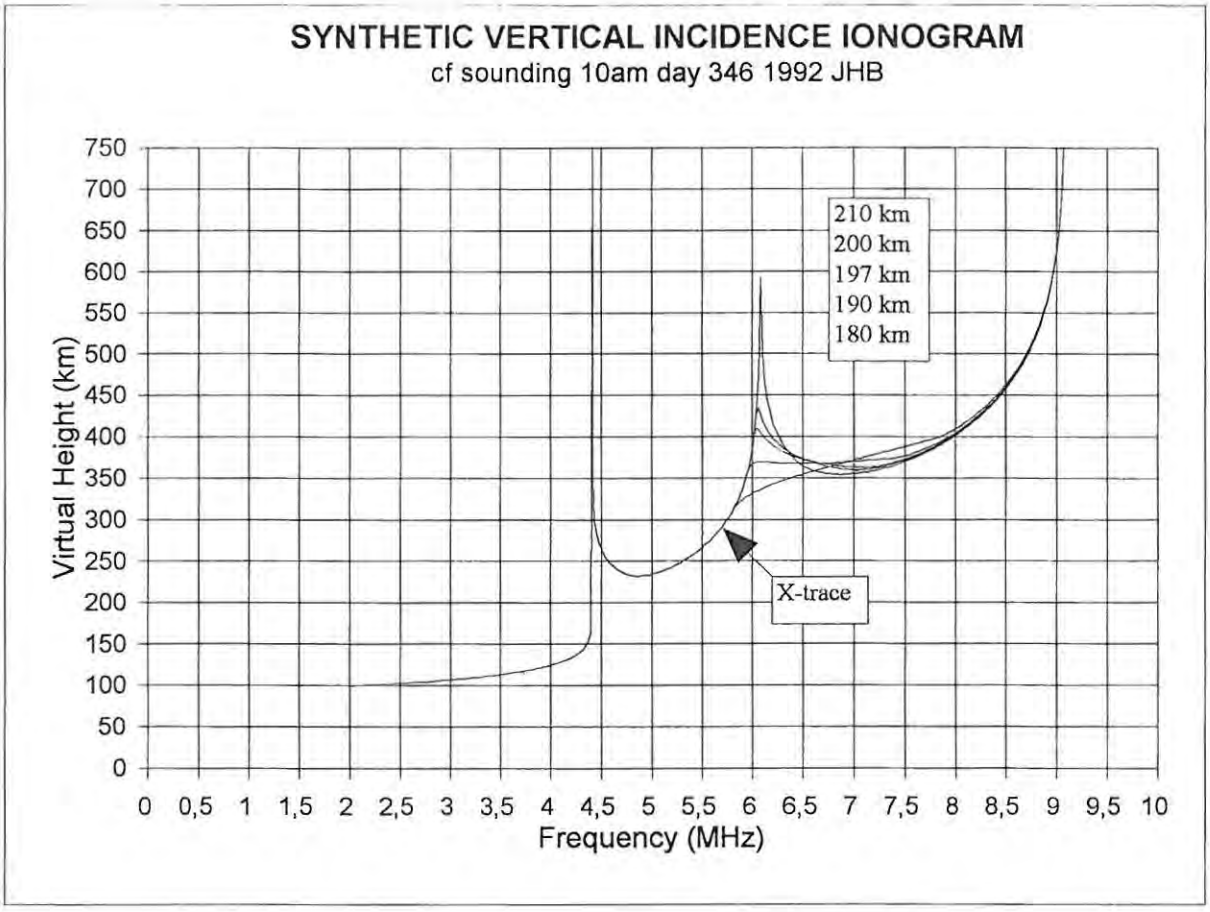

Figure (6.8): A graph illustrating the evolution of the X-trace F1 layer cusp as the ledge height is artifically increased until a pseudo maximum occur

Comparison of synthetic with observed ionogrammes

Comparison of figure (6.7) with the recorded virtual height trace displayed in figure (6.1) reveals excellent agreement between observed and synthetic ionogrammes over the range of scanning frequencies extending from zero up to the cut-off frequency of the F_2 layer. One should examine the following detail when judging the quality of the MQP modelling process;

(a) the cut-off frequencies, f_0E, f_0F1 and f_0F2 must correspond on both the synthetic and observed ionogrammes.

(b) the E and F layer cut-off frequencies on the synthetic virtual height profile must be identifable with the **infinite** cusp-like behavior displayed by the observed ionogramme

(c) an observed F1 ledge condition when modelled using QP/IQP segments is required upon re-inversion, via the synthesizing algorithms, to replicate the **finite** cusp-like behavior exhibited by the observed ionogramme.

(d) the frequency separation of the O and X traces on the synthetic ionogramme be approximately ,0.5MHz (RSA), or half the gyro-frequency.

(e) the overall shape of the synthetic virtual height profile should match the observed ionogramme.

Simulated oblique propagation and synthesis of a group delay profile

The principle of oblique sounding of the ionosphere

The traditional method used to measure the delay structure of HF radio signals transmitted over an oblique link is to implement an oblique ionosonde circuit which utilizes transmitter and receiver sites at opposite ends of the path. This measurement process is more difficult to perform than vertical sounding and requires at minimum partial duplication of equipment for each additional radio path that is studied. It is for this reason oblique sounding is not as widespread as the use of vertical sounders to determine ionospheric morphology. The electron profile obtained from a vertical incidence [VI] sounder can be regarded as extending homogeneously out to a range of some six hundred kilometers, provided the propagation is via the F_2-layer, McNamara [1991]. Adhering to this correlation criterion, ignoring the effects of the geomagnetic field and any horizontal gradients in the ionosphere, it is reasonably straight forward to synthesize the desired

oblique ionogramme from a vertical sounding recorded at one of the end points of the oblique path. The principle assumption used in the above analysis is that the vertical structure of the ionosphere at the control point of the radio link is identical to that recorded by a VI sounder located at one end of the path. Provided that the reflection point lies within the radius of the vertical ionosonder's circle of correlation one may assume homogeneity of the ionospheric structure within the layer being used for propagation support. The synthesis of an oblique ionogramme essentially requires the calculation of the group path, P'(f), of all radio rays capable of ionospheric support over some fixed ground range, D. The group path equations depend upon elevation angle and radio frequency, for a given MQP model structure and it is clear that one must determine the precise elevation angle (s) that define the point(s) of intersection, if any, of a fixed base line with the plot of range versus launch angle for the specified signal frequency.

The "Binary Search" algorithm

An oblique ionogramme is described as a plot of group path delay versus signal frequency for all the rays capable of "homing-in" to a fixed end point. Displayed in figure (6.9) is a schematic illustrating the logical processes involved in the synthesis of an oblique ionogramme.

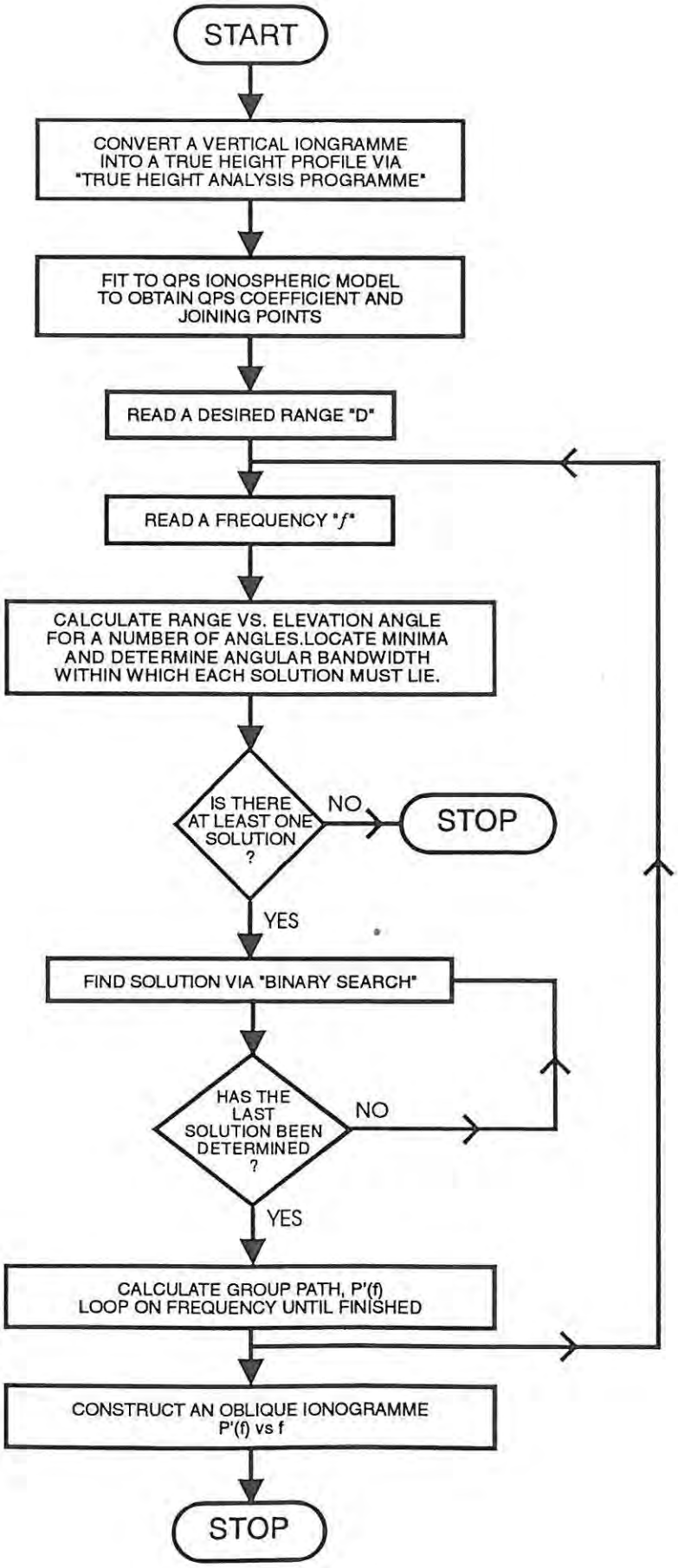

Figure (6.9): A schematic of the logical processes used in group path (OBI) synthesis.

In the first stage of the synthesis one must generate a graph of ground range versus elevation angle, for each signal frequency, before determining the approximate location of possible point(s) of intersection with respect to a base line defining the fixed link distance. Recalling the geometry of the transmission curves derived in chapter 4, it is clear that the group path equations can have two solutions for a given ionospheric layer of support. One must, therefore, be able to identify the possibility of low/high radio rays, having first secured the precise position of the range minima, where the group path solutions become single valued. To determine the exact location of the points of intersection of the base line and a given transmission curve one uses the "Method of Bisection" or as it is better known, the "Binary Search algorithm", the details of which are to be found in any standard text on Numerical Analysis', Burden [1989]. The figure (6.10) shows the variation of group delay with the frequency of propagation for a fixed path length of 1225 km, resulting from re-inverting the MQP model profile shown in figure (6.4) using the OBI synthesis algorithm displayed in figure (6.9).

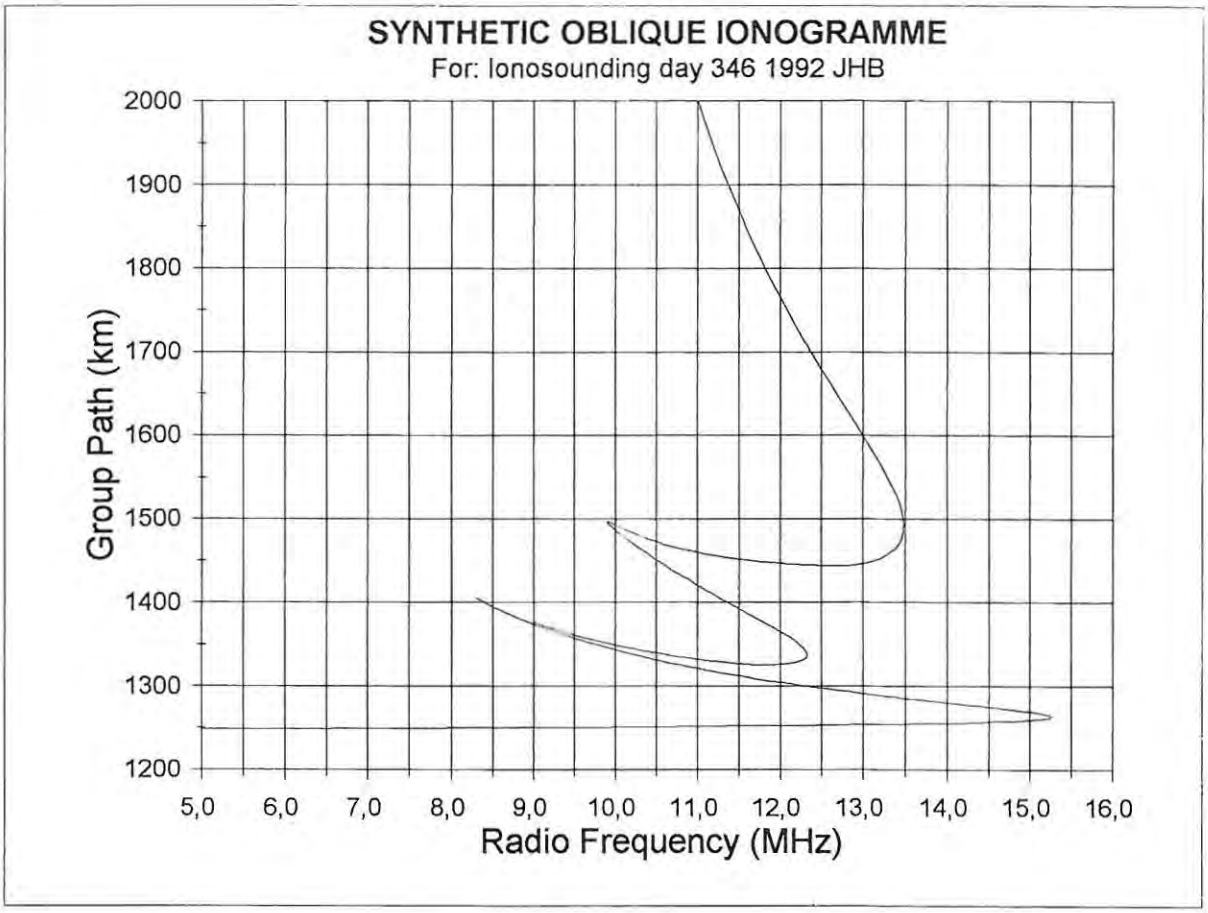

Figure (6.10): Synthetic oblique ionogramme obtained by re-inverting the MQP model fit to the N-h data displayed in figure (6.2).

Each nose of the oblique ionogramme shown in figure (6.10) defines the maximum usable frequency for each of the three layers supporting HF propagation and table (6.1) displays the corresponding group path structure.

LAYER	MUF (MHz)	SKIP DIST (km)	SKIP AGLE (Deg)	GROUP PATH (km)
E	15,265	1225	9,214°	1263,90
F_1	12,325	1225	19,09°	1338,72
F_2	13,489	1225	30,175°	1495,00

table [6.1](a) HF Circuit parameters obtained from synthetic group delay profile displayed in figure (6.10).

It should be noted that the selected base line of 1225 km was chosen in anticipation of measured group delay data from a CSIR/Rhodes oblique sounder link. For the sake of completeness a graph of elevation angle versus radio signal frequency for a simulated oblique propagation between CSIR and Rhodes is shown in figure (6.11) and it is clear that a HF radio signal can travel from the transmitter to the receiver via up to six possible trajectories if one utilizes both the low and high (Pederson) ray that can be supported by each ionospheric layer. Furthermore, the noses of each of three lobes give the maximum usable frequencies corresponding to the E, F_1 and F_2 layers respectively for which 1225 km becomes the skip distance, as listed in table (6.1) (a).

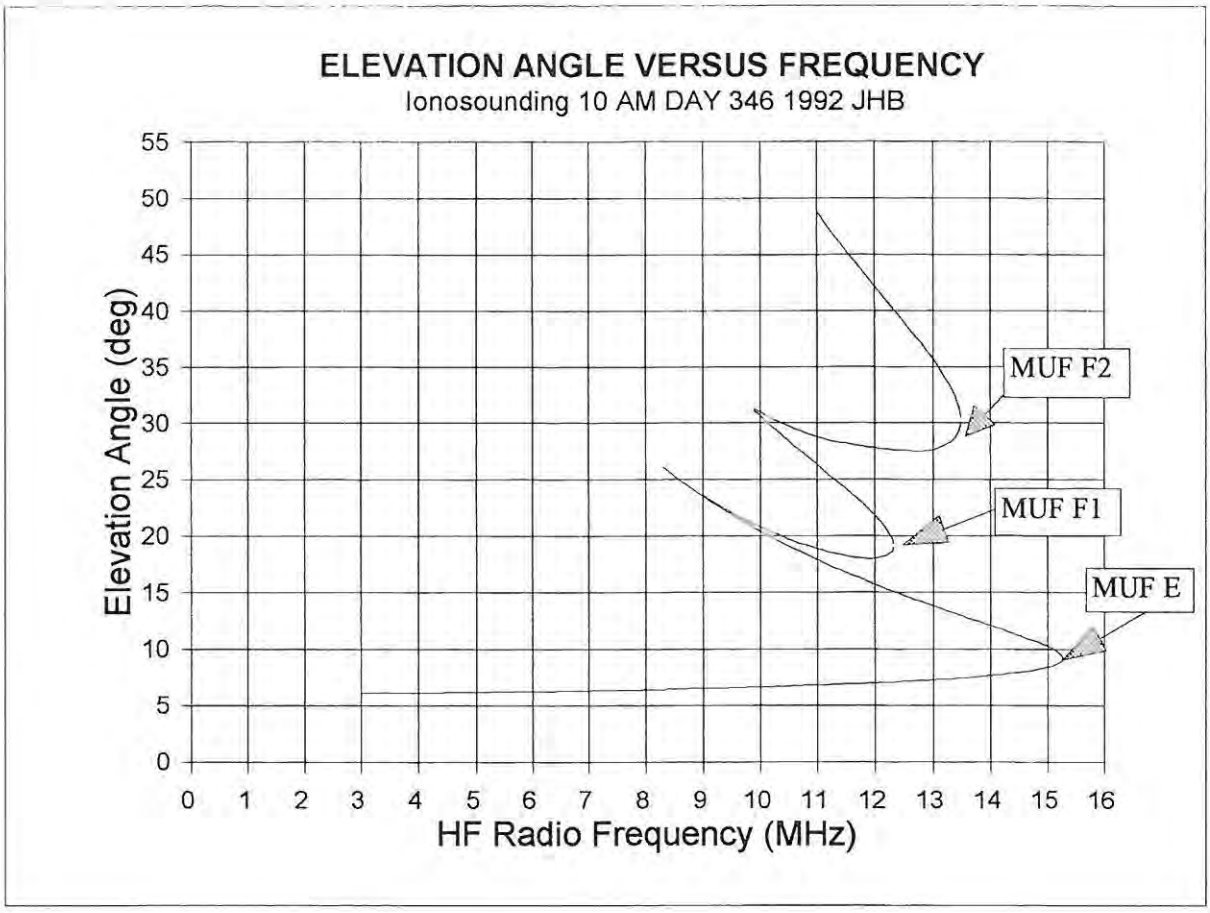

Figure (6.11): Elevation angle versus signal frequency derived by analytical ray tracing through the MQP model ionosphere displayed in figure (6.4).

To test the accuracy of the BINARY SEARCH algorithm used in the group path synthesis programme it was decided to compare the value of MUF(F2) obtained from the group delay structure tabulated in table (6.1) with the maximum usable frequency derived via the MQP/MUF algorithm(A1) in figure (4.2). In figure (6.12) one sees the results of applyiing the algorithm(A1) to a simulated single hop oblique link of variable ground range given that the reflection point of the circuit is described by the MQP electron density profile displayed in figure (6.4).

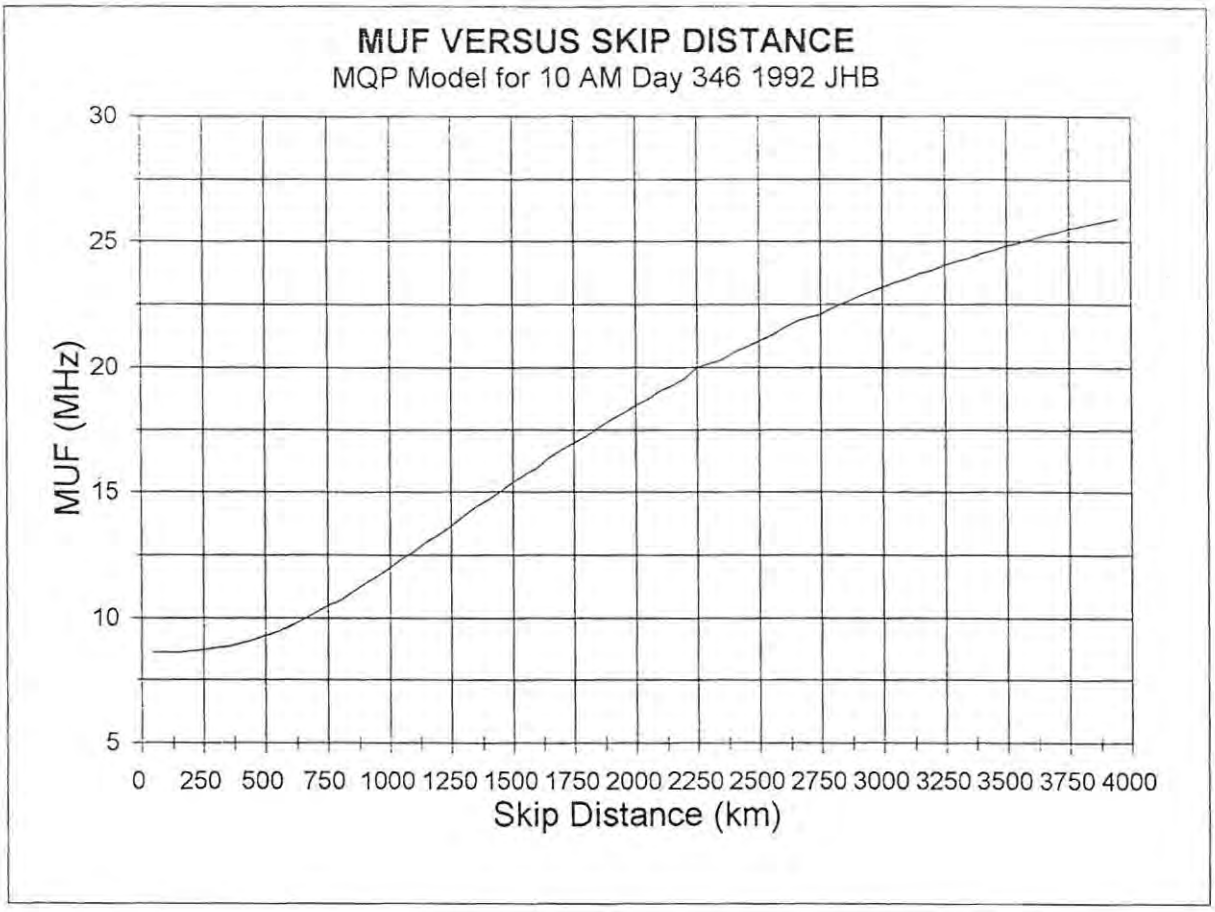

Figure (6.12): Maximum usable frequency(MUF) versus skip distance for the MQP model profile displayed in figure (6.4), determined using the "A1 MUF algorithm" displayed as schematic A1 in figure (4.2)

The co-ordinates of the point on the knee of the MUF(F2) versus ground range curve displayed in figure (6.12) corresponds to the F2 layer nose of the group path structure depicted in figure (6.10) and comparison of the respective results as displayed in tables (6.1) and (6.2) shows that there is excellent agreement between the MUF(F2) values that are derived via the MQP/OBI synthesis programme versus the MUF/MQP (A1) algorithm.

Ionospheric Layer	Ground Range (Km)	Skip Angle (°)	MUF (F2) (MHz)
F2	1225	30,416	13,475

TABLE (6.2): Referring to figure (6.12); MUF (F2) results derived via the MQP/MUF (A1)algorithm, ref: figure (4.2), for a simulated HF circuit of ground range 1225 Km and having a relection point described by the MQP electron density profile displayed in figure (6.4).

The above comparison serves to demonstrate that there is consistency in the algorithmic structure of the software implementation and also that the BINARY SEARCH algorithm provides the user with accurate convergence values. It should be noted that the "GOLDEN SECTION METHOD", Chen et al [1992], converges much more rapidly than does the BINARY SEARCH algorithm and for this reason the former numerical technique is regarded as more suitable for those who require near real-time ionogramme synthesis given the existence of a MQP electron density profile.

Synthetic ionogrammes and the "Classical Method"

As a result of an absence of measured group delay data for the CSIR/Rhodes oblique link it was a required in the Real Prop contingency plan that one compare and contrast the MQP synthesized OBI data displayed in figure (6.10) with the synthetic oblique ionogramme

derived via the so-called classical method, which is based on the application of the equivalence theorems, Davies [1969] to the VI ionogramme data. Synthesis of an oblique ionogramme using the "Classical Method" involves mapping the virtual height domain, defined by the co-ordinates $(h'(f_v), f_v)$, onto the group path plane, defined by the co-ordinates, $(P'(f_{ob}), f_{ob})$. The mathematical relationships governing the co-ordinate transformation

$$(h'(f_v), f_v) \leftrightarrow (P'(f_{ob}), f_{ob}) \qquad [6:55]$$

can be derived for the general case of a curved earth and concentric ionosphere, using the Secant Law together and the theorem of Breit and Tuve [1926]. The figure (6.13) shows that the geometry of a radio trajectory as it propagates over a flat earth via a plane ionosphere.

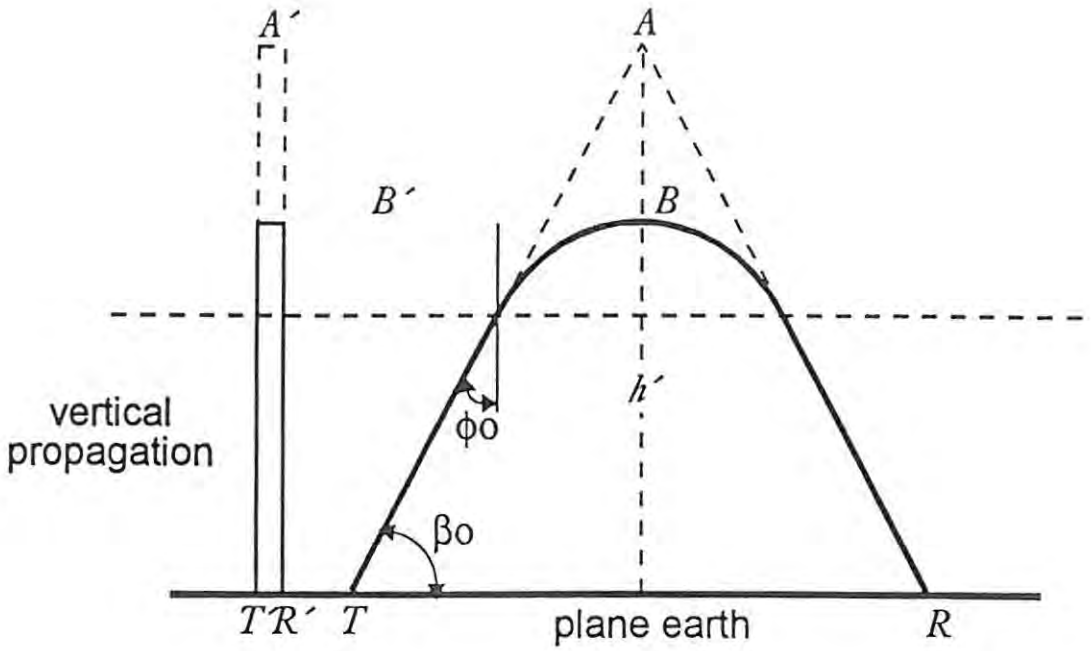

Figure (6.13): The demonstration of the "Secant Law" as applied to the case of a flat earth and a plane ionosphere.

Calculation of the oblique propagation frequency, f_{ob} .

The "Secant Law" states that the oblique propagation frequency, f_{ob}, is related to the equivalent vertical incidence frequency, f_v, through the relationship, Davies [1969]

$$f_{ob} = f_v \sec \phi_o \qquad (6:56)$$

provided both the earth and the ionosphere are modelled as flat. If the ionosphere is modelled as concentric with the surface of a real earth, one must modify the "Secant Law" so as to take into account the effect of ionospheric curvature, something that can be accomplished by introducing a "sec Φ_o" correction factor, k, giving

$$f_{ob} = k f_v \sec \phi_o \qquad (6:57)$$

The value of "k" is a function of the ground range covered by the signal and the real height of reflection of the ray trajectory, Davies[1969]. It is difficult to determine the appropriate value of correction factor to use, U.S. Dept of Commerce [1965], but for most practical situations involving F2 layer propagation, the range is given by

$$1.0 \leq k \leq 1.2 \qquad \text{(6:58)}$$

Referring to figure (6.14) one can use elementary geometry to express the "sec ϕ_0 "term in eq (6.57), as a function of the virtual height of reflection and the ground range, D, enabling the oblique frequency to be expressed

$$f_{ob} \cong k f_v \left\{ 1 + \frac{\sin^2(\alpha)}{[1 - \cos(\alpha) + h'/r_o\,]^2} \right\}^{1/2} \qquad \text{(6:59)}$$

where the angle ,α, equals ($D/2r_o$).

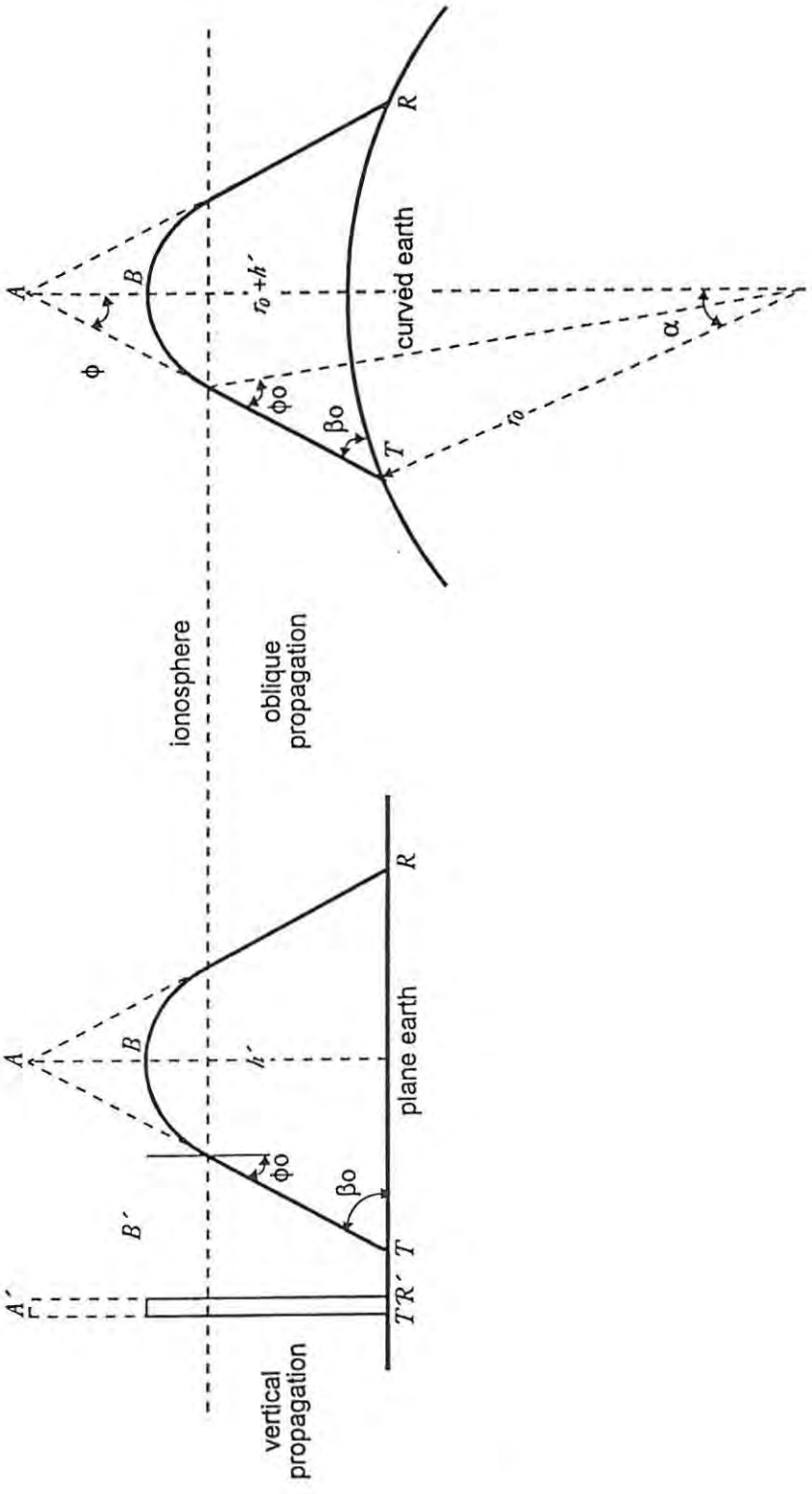

Figure (6.14): The "Secant Law" applied to the case of the curved earth/ionosphere, after Chen et al[1992]

Given a fixed ground range, D, a virtual height profile, $(h'(f_v), f_v)$ and the appropriate choice of the correction factor, k, one can quickly determine the corresponding oblique propagation frequency, f_{ob} .

Calculation of the group path, $P'(f_{ob})$

One can easily derive an expression for the group path, $P'(f_{ob})$, by applying the Sine rule to the ray geometry depicted in figure (6.14), giving

$$P' = \frac{2 \sin\left(\frac{D}{2r_0}\right)}{\cos(\beta_0)} (r_0 + h') \qquad (6:60)$$

where the elevation angle, β_0, is determined from a knowledge of the virtual height, h', via the result

$$\tan(\beta_0) = \frac{\left(\cos (D/2r_0) - \frac{r_0}{(h' + r_0)}\right)}{\sin (D/2r_0)} \qquad (6:61)$$

Using eqs (6.59), (6.60) and (6.61) one is now able to synthesize an oblique ionogramme from a virtual height profile expressed as a data set, $(h'(f_v), f_v)$. Figure (6.15) shows the group path profile obtained as a result of applying the classical method of ionogramme synthesis to the observed $h'(f_v)$ trace depicted in figure (6.1) for a ground range of 1225 km. It should be noted that the curvature factor, K, is set equal to unity for E layer support but in the case of F region propagation assumes the value of 1.038 because of the higher altitudes involved.

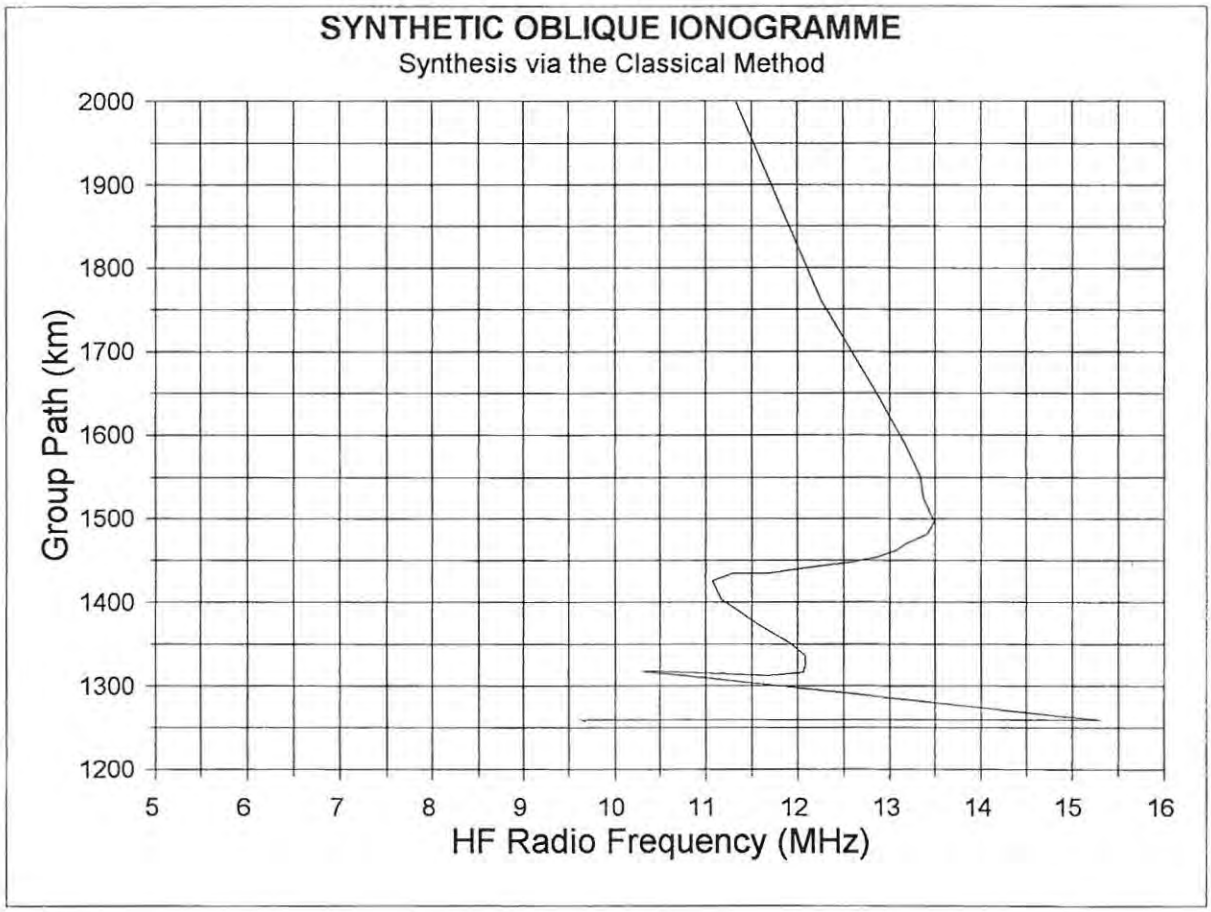

Figure (6.15): Oblique ionogramme synthesized by applying the "Classical Method" to the $h'(f_v)$ trace displayed in figure (6.1) for a ground range of 1225 km.

Table (6.3) displays the calculated co-ordinates for the values of the MUF for the E, F1 and F2 layers respectively.

LAYER	MUF (MHz)	SKIP DIST (km)	GROUP PATH (km)
E	15,3	1225	1259,49
F_1	12,09	1225	1336,21
F_2	13,49	1225	1496,92

Table (6.3): Circuit parameters obtained from a synthetic oblique ionogramme generated via the "Classical Method"

A comparison of the MUF results displayed in table (6.1) and table (6.3) shows excellent agreement and it is especially note worthy that this statement applies to the F1 nose. If a vertical ionogramme possesses a distinct F1 trace, as is the case with the, $h'(f_v)$, profile depicted in figure (6.1), the classical method produces a corresponding, well-defined oblique ionogramme trace because each data point in the $h'(f_v)$ plane is directly transformed onto the oblique $P'(f_{ob})$ space. However, if the F1 layer is not very distinct on the true height profile, the effect on the oblique ionogramme as predicted by the MQP model will be less pronounced than achievable via the classical method. It can be seen that the N-h distribution displayed in figure (6.2) does not have a pronounced F1 region and were it not for the accuracy of the gradient algorithm used to locate the co-ordinates a F1 ledge of ionization, ref:chapter 5, the mapping of the MUF(F1) frequencies using the the MQP model synthesis might not have been so successful.

It was a deep source of regret that financial cut-backs within the CSIR prevented the completion of the installation of a CSIR/Rhodes oblique sounder link as this has resulted in one being unable to compare simulated with measured group delay data. In the meantime one must be content with the success of the MQP modelling process as determined using VI ionogramme data and with the wealth of real time ray tracing algorithms that have been developed, all of which have passed rigorous tests for self consistency and correctness of implementation.

Chapter (7)

COMPUTER SIMULATION OF AN OBLIQUE HF RADIO LINK TO INVESTIGATE THE EFFECTS OF AN IONIZATION DEPLETION REGION AND A F_1 LEDGE CONDITION UPON GROUND RANGE CALCULATIONS.

To obtain the radio locus of a HF signal propagating through a MQP model ionosphere it is necessary to invert the general solutions of the ground range equation, eq (4.24), for the case of both the quasi and the inverse quasi-parabolic layers as expressed in the form of eq (4.15) and eq (4.16) respectively. Armed with the locus equations one is the able to plot the path taken by a HF signal as it propagates through a MQP model ionosphere and hence examine the effect that a re-entrant electron profile and/or a F1- ledge condition can have on the accurate calculation of ground range, a matter of considerable concern in HF direction finding single site location,(HFDFSSL). The Pretoria to Rhodes simulated oblique link data derived in Chapter 5 will be used to quantitatively demonstrate the effect that ray tracing through a E/F1 valley region has on the apogee height of the signal's path

and on the total ground range covered. A qualitative discussion is given of the possible ranging errors that can occur when performing a HFDFSSL measurement when the ionosphere possesses a F1-ledge of ionization. A comparative study is carried out using results published by Baker et al [1992], in which the fully analytic MQP F1 ledge model developed in chapter 5 is tested against Baker's numerical F1 ledge algorithm, under identical ray tracing conditions.

Derivation of the equation of the ray locus for a traditional quasiparabolic layer

Using eq (4.15), the projected ground range covered by the portion of a radio locus lying within in a quasiparabolic layer may be expressed,

$$D(r) = r_o(\gamma-\beta_o) + \frac{r_o^2 \cos\beta_o}{\sqrt{C'}} \log_e\left(\frac{r\,(2C' + r_bB' + 2\sqrt{C'R_b})}{r_b\,(2C' + rB' + 2\sqrt{C'R})}\right) \qquad [7:1]$$

where the quantity R denotes the ray tracing quadratic,

$$R = A'r^2 + B'r + C' \equiv r^2\mu^2 - r_o^2\cos^2\beta_o \qquad [7:2]$$

and the term $r_o(\gamma - \beta_o)$ represents the projected ground range contributed by the free space portion of the ray's trajectory. It is expedient to define the ground range covered in free space as a reference datum

$$D_0 = r_0(\gamma - \beta_0) \qquad [7:3]$$

so that the contribution to the overall range from the ionospheric portion of the radio

trajectory is given by

$$\Delta D = D(r) - D_o \qquad [7:4]$$

One may now re-express eq [7.1] in terms of ΔD to give

$$\frac{r\,(2C' + r_b B' + 2\sqrt{C'R_b}}{r_b\,(2C' + rB' + 2\sqrt{C'R}} = \exp\left(\frac{\sqrt{C'}\,\Delta D}{r_o^2 \cos\beta_o}\right) \qquad [7:5]$$

Inverting, eq [7.5], the geocentric height ,r, of a point on the radio locus may be compactly expressed as

$$r = \frac{4\,C'\,V}{(V - B')^2 - 4\,C'A'} \qquad [7:6]$$

where the quantity V is defined by the auxiliary equations

$$V = \frac{(2C') + r_b B' + 2\sqrt{C'R_b})}{r_b \exp(u)} \qquad [7:7]$$

$$u = \frac{\sqrt{C'}}{r_o^2 \cos\beta_o}\left[\, D(r) - r_o\,(\gamma - \beta_o)\,\right] \qquad [7:8]$$

$$\gamma = \left[\cos^{-1}\left(\frac{r_o}{r_b}\right)\cos\beta_o\right] \qquad (7:9)$$

The application of eqs (7.6), (7.7), (7.8) and (7.9) allows one to plot the radio locus of a HF signal propagating through a single layer quasiparabolic ionosphere of the type described by Croft and Hoogasian (1968) AND DISPLAYED IN FIGURE(7.1)OVERLEAF

Figure (7.1) A HF radio signal propagating through a single layer ionosphere.

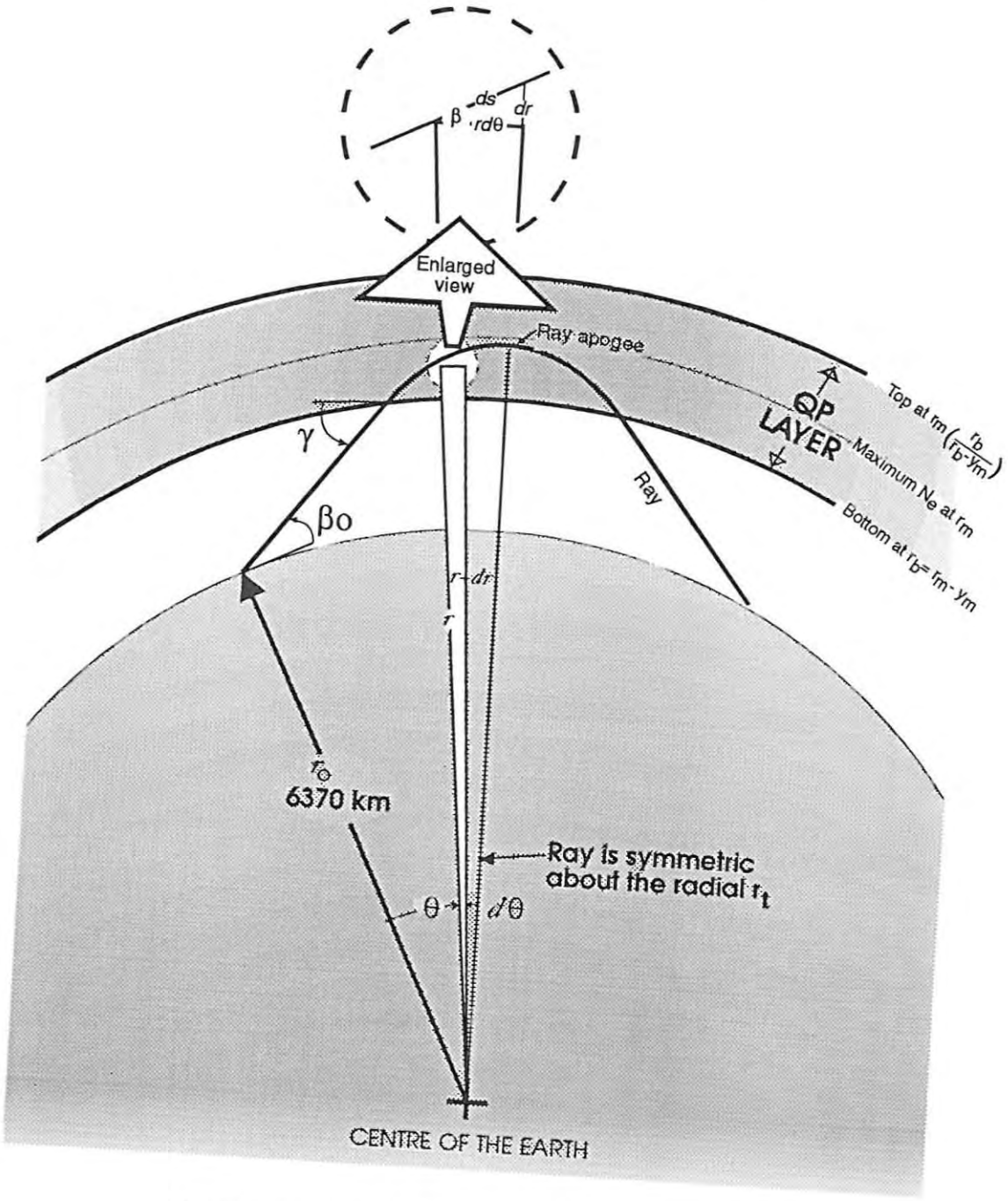

The global geometry describing a HF radio link over a curved earth and through a concentric ionosphere.

To extend the single layer QP model to a fully generalized MQP structure as proposed by Hill[1978] one must derive the radio locus equation applicable to a IQP joining section.

Derivation of the locus of a HF radio ray travelling through an inverse quasiparabolic layer

Recalling, eq (4.16), the projected ground range contribution from a section of a radio locus that lies in an inverse quasiparabolic layer may be expressed in the form,

$$D = \frac{r_o^2 \cos \beta_o}{\sqrt{-C'}} \sin^{-1} \left[\frac{2C' + B'r}{r\,(B'^2 - 4A'C')^{1/2}} \right]_{r_b}^{r} \qquad [7:10]$$

where the limits of integration extend from the base of IQP joining segment ,r_b, to some height ,r, which is less than or equal to the geocentric altitude of the upper IQP/QP interface. Having inserted the limits, one may proceed to invert eq (7.10) and solve for the geocentric height ,r, of an arbitrary point on the radio locus, to give

$$r = \frac{2C'}{(B'^2 - 4A'C')^{1/2} \sin \left\{ \frac{D(r)\sqrt{-C'}}{r_o^2 \cos \beta_o} + \sin^{-1} \left\{ \frac{2C' + B'r_b}{r_b\,(B'^2 - 4A'C')^{1/2}} \right\} \right\} - B'} \qquad [7:11]$$

In summary one can use eq (7.5) and (7.11) to construct the radio locus of a HF signal propagating through a MQP model ionosphere, provided one has a knowledge of the following:

(a) the ionospheric parameters, (f_c, r_m,y_m) and hence the (A,B,C) coefficients for

each QP/IQP section of the MQP model ionosphere.

(b) the transmitter launch angle ,β_o, and the propagation frequency ,f, required to cover a specified ground range, D.

(c) the value of the ray-tracing coefficients, (A', B', C'), derived via eq (4.21), eq (4.22) and eq (4.23), using the data from (a) and (b) above,

and

(d) the ground range contribution ,D(r), from the individual QP/IQP sections of the composite MQP profile.

A practical example of ray tracing through a fitted MQP ionosphere

To test and demonstrate the radio locus algorithms it was decided to plot the trajectory of a HF signal propagating via a simulated link between CSIR and Rhodes, for which an oblique ionogramme was synthesized in chapter 5. In the interests of clarity some of the graphs appearing in the above mentioned chapter will be displayed herewith. One assumes single hop propagation and that the ionosphere at the control point of the HF circuit may be represented by the MQP model ionosphere shown in figure (7.2). It should be noted that observations of the ionosphere made with a vertical incidence ionosonde can be regarded as valid out to a range of about 300 to 600 km in the case of the F2 layer, depending on the time of day, station location, and season, whereas the circle of temporal/spatial correlation for the E layer has a radius of only 100 to 200 km, McNamara (1992). Therefore, to ensure a realistic simulation of HF propagation over a ground range of 1225 km one should use F2 layer support in the absence of having observed oblique ionogramme data. The figure (7.2) shows the MQP model ionosphere derived via curve fitting to an observed N-h electron distribution, obtained from inversion of a vertical incidence

ionogramme that was recorded near one end of the simulated HF radio link between CSIR and Rhodes.

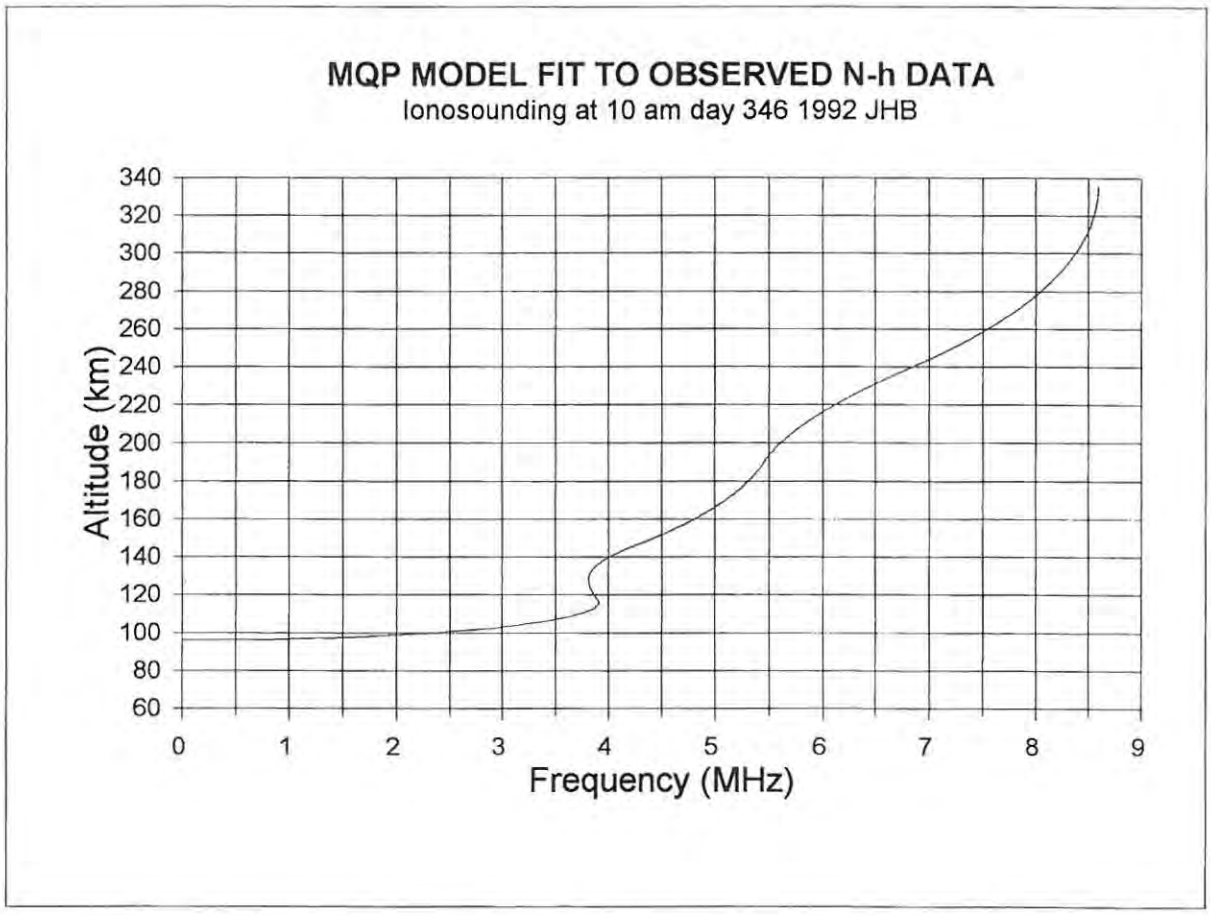

Figure(7.2): MQP model ionosphere derived via curve fitting QP sections to observed N-h data obtained by inverting an ionogramme recorded at 10 am day 346 1992, Frankenwald, Johannesburg, RSA.

The radio locus for the simulated HF link is determined under the following conditions;

(1) the ground range is 1225(km), being the distance between Pretoria and Grahamstown

and

(2) propagation is via the F2 layer of the ionosphere

In figure (7.3) one sees a plot of group path versus propagation frequency for a simulated HF link between CSIR and Rhodes, for the MQP model ionosphere displayed in figure(7.2) while the figure (7.4) shows the required transmitter launch angle for a given signal frequency over the same circuit.

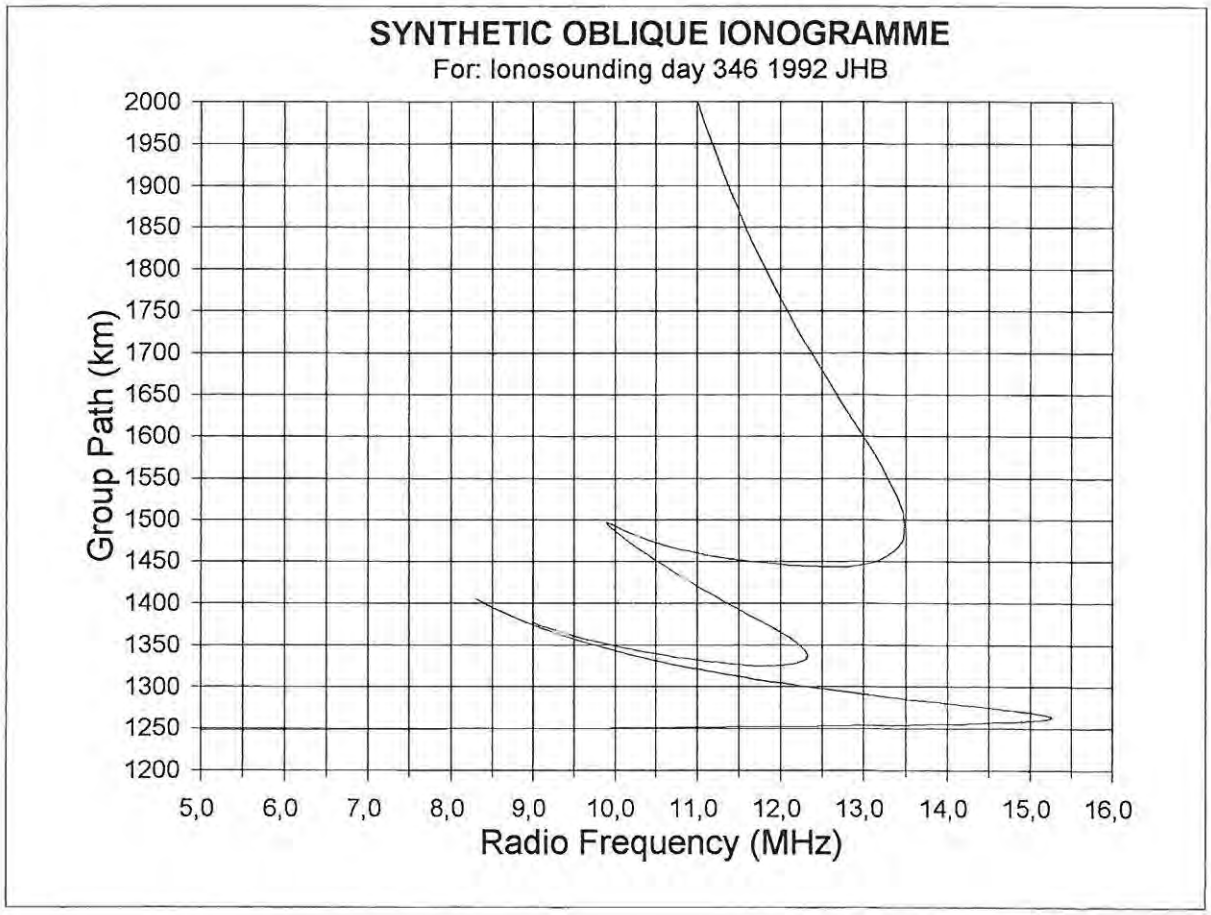

Figure(7.3): Group path versus propagation frequency for a simulated oblique link between Pretoria and Grahamstown, synthesized by ray-tracing through a MQP model ionosphere. The parameters of the QP layers were derived via curve-fits to observed N-h data obtained by inverting an ionogramme recorded at 10 am day 346 1992, Frankenwald, Johannesburg, RSA.

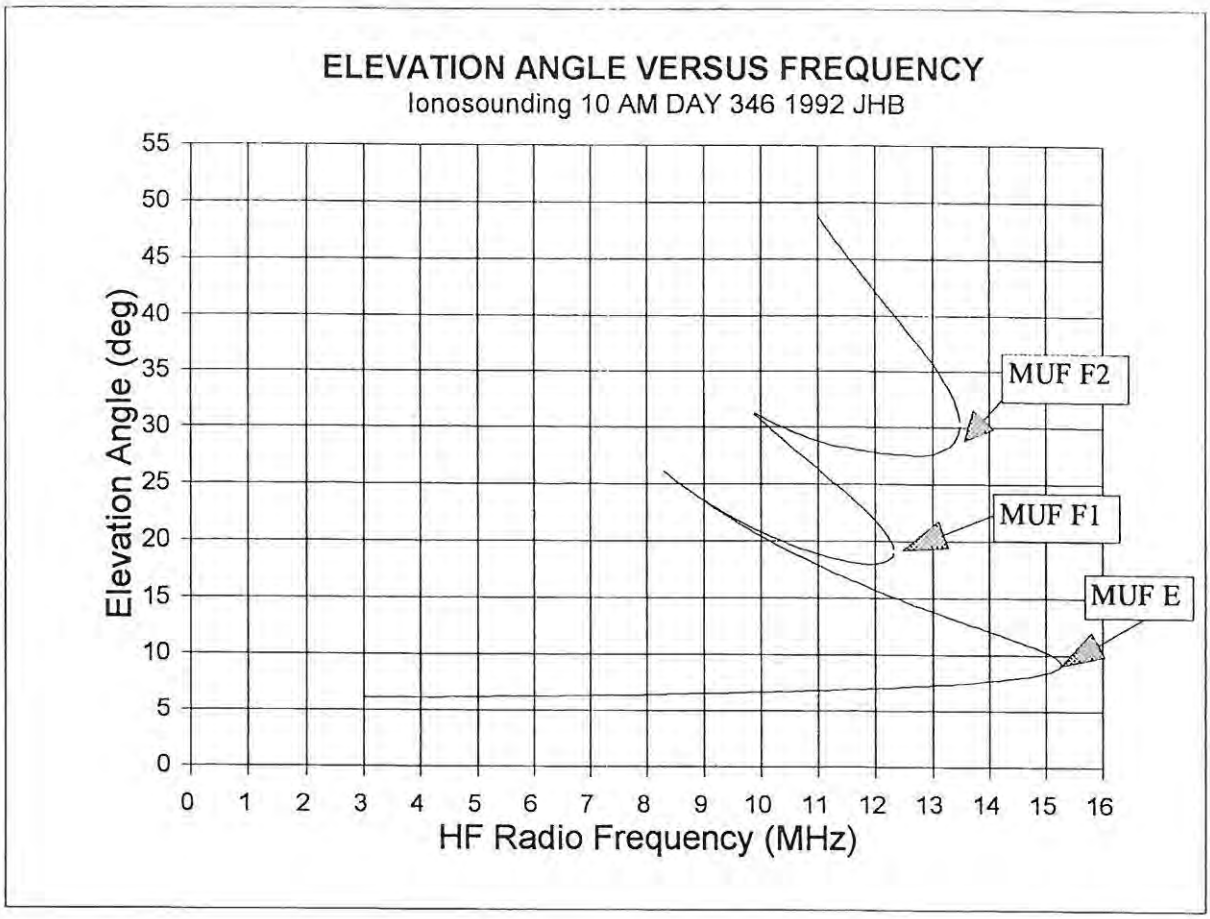

Figure(7.4):Transmitter launch angle versus propagation frequency for a MQP HF circuit simulation between CSIR and Rhodes.

Inspection of figure (7.3), (7.4) and referring to table (6.2) shows that F2 layer support over a ground range of 1225 km is possible if;

(1) the propagation frequency is less than 13.489 MHz

and

(2) the transmitter launch angle is greater than 27.5 degrees

In figure (7.5) one sees a plot of geocentric height versus ground range covered for a HF

signal propagating through the MQP model ionosphere displayed in figure(7.2), utilizing F2 layer support across a great circle distance of 1225 km, given a signal frequency of 13.489 MHz and a transmitter launch angle of 30.175 degrees.

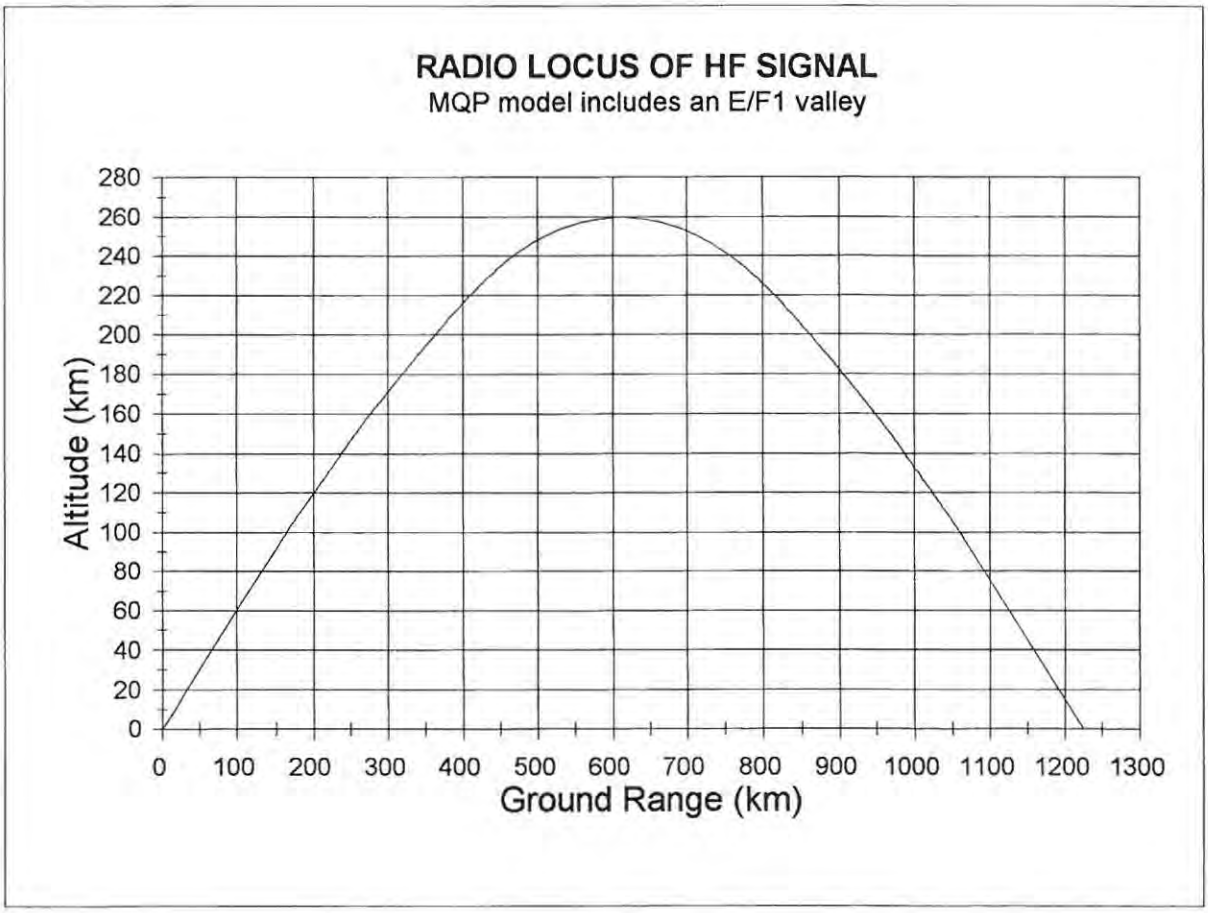

Figure (7.5): Locus of a HF signal propagating through the re-entrant MQP model ionosphere displayed in figure (7.2), given a ground range of 1225km, a propagation frequency of 13.489 MHz and a transmitter launch angle of 30.175 degrees.

Nota bene: An exploded view of E/F1 valley region of the N(h) profile illustrated in figure(7.2) is displayed in figure(3.3).

The determination of the apogee height of the radio locus

To determine the apogee height of a HF radio trajectory one must solve the ray tracing quadratic, eq (7.2), for the apogee condition R=0 given that the A′, B′, and C′ coefficients describe the layer in which

the locus reaches its maximum height. The value of the relevant ray tracing coefficients is determined using eq (4.21), eq (4.22) and eq (4.23), assuming that the corresponding ionospheric coefficients have been calculated via eq (4.10), eq (4.11) and eq (4.12). The ray tracing quadratic has in general two solutions, however, if apogee occurs in a QP layer, only the negative root is physically meaningful. Calculation shows that for the radio trajectory displayed in figure (7.5) the apogee height reached by the HF signal is 259,68 km.

The effect of an E/F_1 valley region on ground range calculations

To determine the effect of the E/F_1 valley on the geometry of a HF signal trajectory, a ray trace was performed through a monotonic version of the MQP model ionosphere depicted in figure (7.2). New circuit parameters are required to achieve the same ground range of 1 225 km as the list below shows :

(1) ground range, 1 225 km

(2) radio frequency, 13,47511 MHz

(3) elevation angle, 30,416 degrees

and

(4) apogee height 259,85 km.

The figure (7.6) overleaf shows the radio locus for the HF signal propagating through the modified monotonic MQP profile.

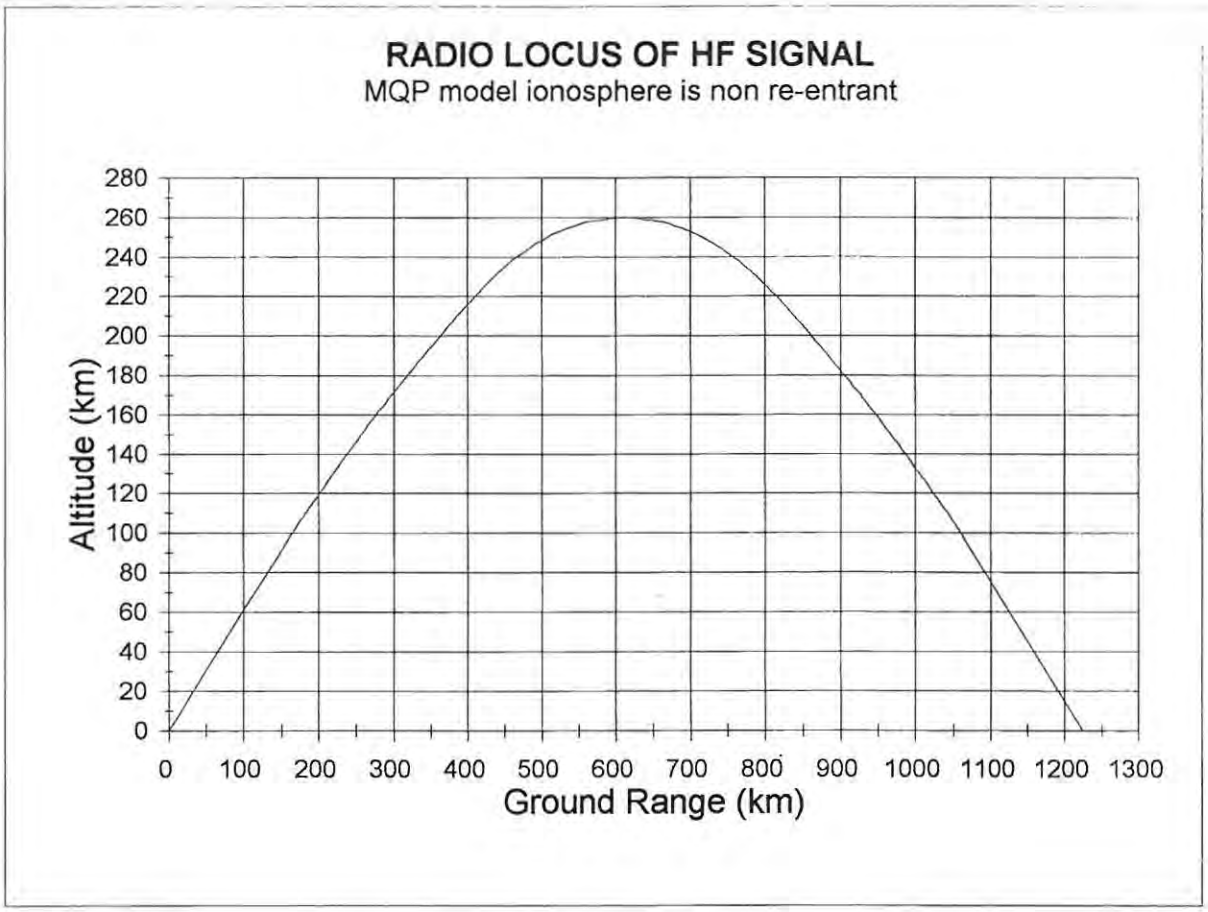

Figure (7.6): Radio locus through the MQP model ionosphere displayed in figure(7.2) but with the E/F_1 valley replaced by a single IQP joining section.

It is seen from table (7.1) that for the fixed ground range of 1225 km the effect of an ionization depletion region on the propagation characteristics is to decrease the frequency of the HF signal and to raise its launch angle only slightly. The ray trace was now repeated through the original re-entrant version of the MQP profile, figure (7.2), using a frequency of 13,47511 MHz and a launch angle of 30,416 degrees and it was found that the ground range was reduced to a value of 1222,82 km while the apogee height increased in the third decimal place. It is clear that the choosing of a propagation frequency right at the limit

of F2 layer support namely, ~13,5 MHz, minimizes the effect of altering the E/F1 region from a monotonic to a re-entrant state.

E/F_1 valley condition	Range	Apogee	Freq. (MHz)	Elev.Angle
No valley	1225.00	259.85	13.47511	30.416
Valley (same distance)	1225.00	259.68	13.48998	30.339
Valley (same frequency & elevation angle)	1222.82	259.85	13.47511	30.416

Table (7.1): Perturbation of HF circuit parameters caused by the presence of an E/F_1 valley region (long range case)

Worst case scenario for the range error caused by an E/F_1 valley.

To examine the conditions under which an E/F_1 valley would appreciably affect HF propagation a very much shorter trajectory of ground range 726,63 km was simulated utilizing F1 layer support so that the radio apogee occurs close to the top of the E/F_1 re-entrant region. The table (7.2) shows the results of ray tracing calculations carried out under conditions of constant signal frequency and launch angle, with/without the inclusion of an E/F1 valley region. One can clearly see the dramatic effect that a re-entrant portion within an otherwise monotonic profile has upon ranging errors when the radio apogee is close to the top of the valley region.

HF Circuit parameters	Valley	No Valley
Apogee(km)	153.24	152.86
Range (km)	726.63	768.52
Elevation Angle °	30.416	30.416
Frequency (MHz)	8.473	8.473

Table (7.2): Perturbation of HF circuit parameters caused by the presence of an E/F_1 valley region (short range case).

The figures (7.7) and (7.8) display the shape of the radio locus under re-entrant and non re-entrant conditions and one can clearly see that the effect of the valley is to decrease the ground range very considerably ($\approx$ 40 km) although the increase in apogee height remains slight.

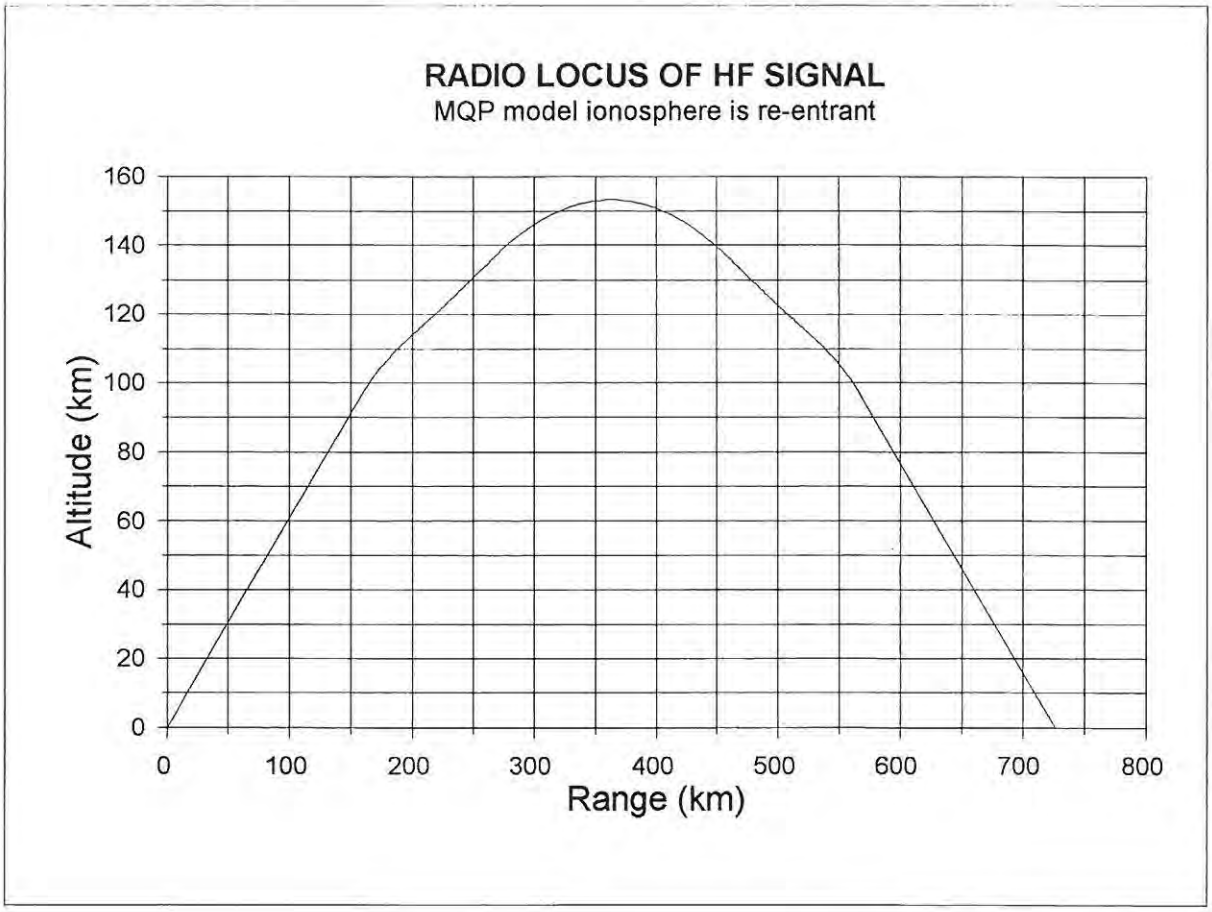

Figure (7.7) Radio locus when propagating through the MQP model ionosphere displayed in figure(7.2), short range case and with apogee close to the top of E/F1 valley.

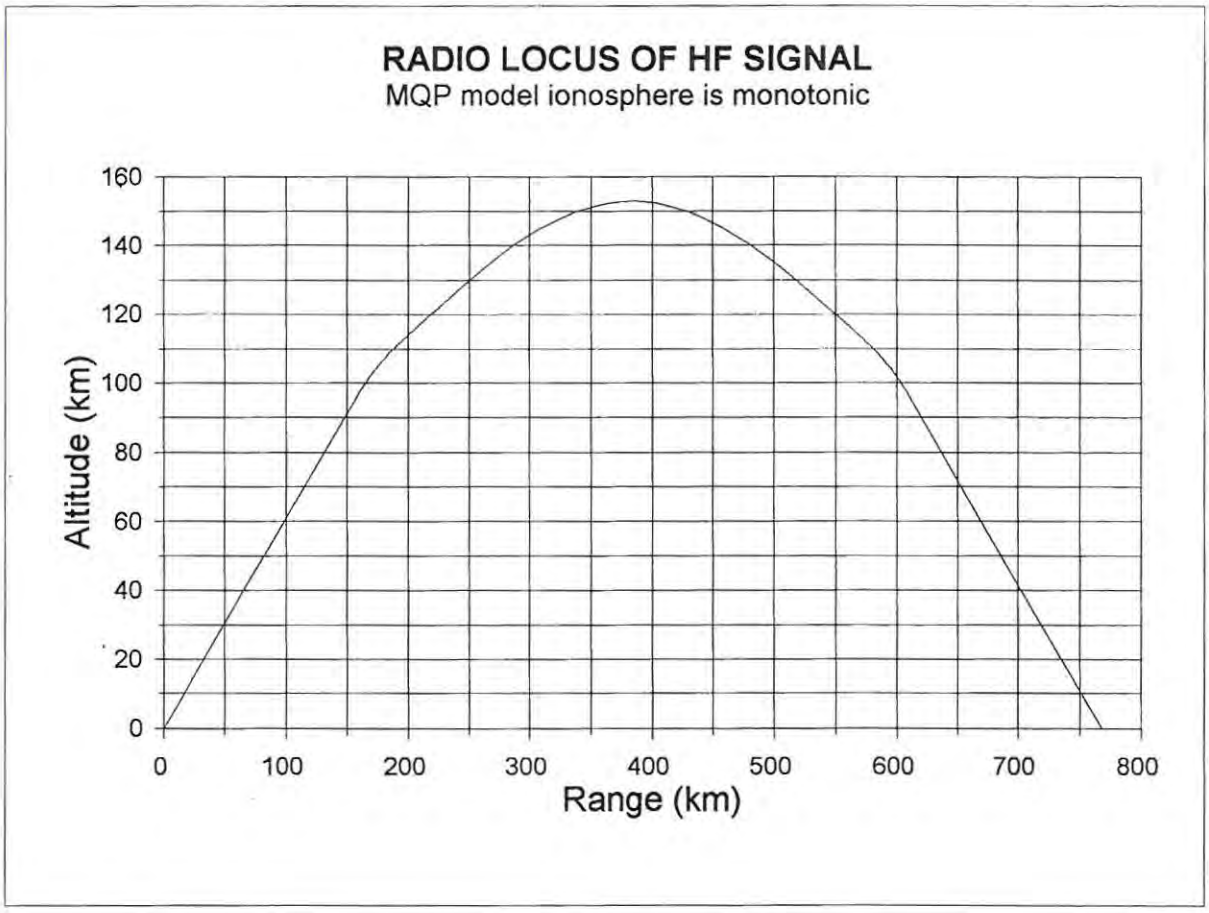

Figure (7.8) Radio locus when propagating through the MQP model ionosphere displayed in figure(7.2), short range case, with the E/F1 valley replaced by a single IQP joining section.

It can be seen in conclusion therefore, that it is important to model the E/F1 valley carefully and that if possible one should avoid HF trajectory geometries where the height of the radio apogee lies close to a N-h depletion region.

Explanation of the perturbing influence of an ionization depletion region upon ground range calculations

From the results of simulated oblique propagation with and without an E/F_1 valley present, it is clear that the depletion region causes the apogee of the radio's trajectory to become raised in height and the ground range covered by the signal to become reduced in value. To explain this phenomenon it is necessary to understand how the phase refractive index contols the degree of bending experienced by a radio ray and the effect that depletions in electron density have upon the refraction mechanism. If one substitutes the Hartree-Appleton equation, eq (2.13), into Bouguer's rule, eq (4.1), then it can be shown

$$\beta = \cos^{-1}\left[\frac{r_0 \cos(\beta_0)}{r\left[1 - \frac{kN(r)}{f^2}\right]}\right] \qquad (7:12)$$

where

$\beta \Rightarrow$ angle of refraction

$r_o\cos(\beta_o) \Rightarrow$ radio invariant

$r_o \Rightarrow$ earth radius

$\beta_o \Rightarrow$ launch angle

$r \Rightarrow$ geocentric height in the ionosphere

$N(r) \Rightarrow$ electron density

Referring to eq (7.12) one can see that a radio signal encountering a region of ionization depletion will experience a reduction in the value of N(r) which in turn causes the angle of refraction β to increase and hence the ray normal to point more vertically. For this reason a HF radio trajectory will, upon traversing an E/F_1 valley, undergo apogee at a greater height than if the ionosphere's N-h distribution were non re-entrant. Furthermore, the ground range covered by the signal's trajectory will be shortened, being symmetrically decreased on both the upward and downward legs of the oblique path.

The influence of the F_1 ledge condition on the accuracy of ground range calculations

It has already been seen that a miscalculation in the height of an F_1 ledge results in a dramatic change in the shape of the F_1 cusp on a synthetic ionogramme as can be seen from figure (6.8). This phenomenon gives one an indication of the possible ranging error that could result if one were to operate an oblique link with the radio apogee point close to the height of an F_1 ledge of ionization. Baker et al [1992] have presented a qualitative evaluation of the ranging errors that can occur in a single site location HF direction finding system (SSL HFDF) due to the F_1 ledge condition. To demonstrate the power of the fully analytic MQP F_1 ledge model developed described in chapter 5, the effects of ranging error upon SSL HFDF were investigated and compared with those numerically deduced by Baker et al [1992]. The ionospheric parameters of the MQP model profile used by Baker are listed in table(7.3) below and the corresponding MQP ,N(r), distribution is displayed in figure (7.9).

IONOSPHERIC LAYER	Critical Freq. f_c (MHz)	Maximum r_m (km)	Semi-thickness y_m (km)
E-layer	3.0	110.00	20.00
F_1-layer	4.2	209.68	112.19
F_2-layer	6.0	320.00	100.00

Valley: Width - 20.00 km Depth - 0.05 MHz

Table (7.3): Ionospheric parameters describing a three layered re-entrant ionosphere as used by Baker et al [1992]

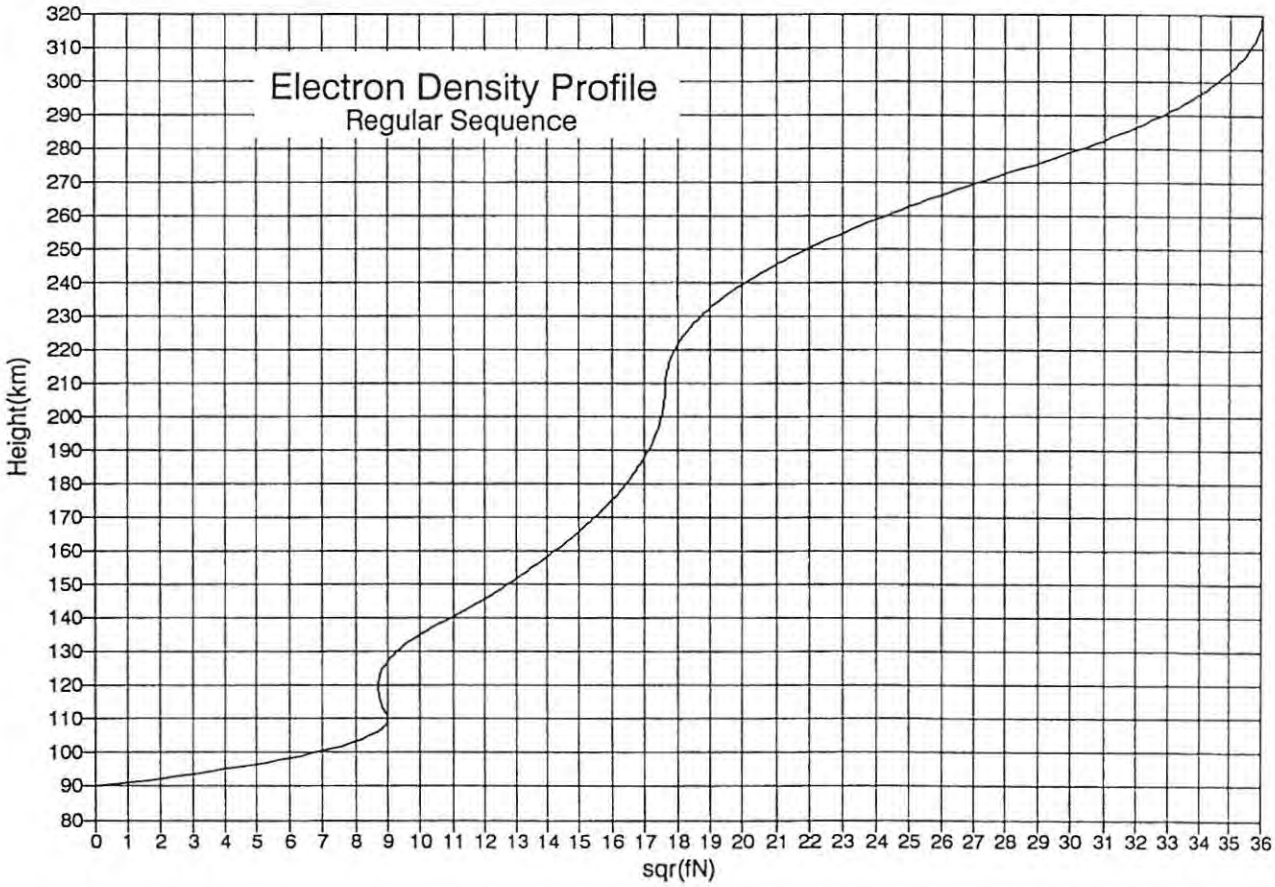

Figure (7.9): MQP electron density profile with an E/F_1 valley and a F1 maximum (regular sequence), constructed using the ionospheric parameters listed in table (7.3).

Ray Tracing through a MQP ionosphere with a F_1 ledge condition present

Using a propagation frequency of 6 MHz and a range of elevation angles extending from 30° to 55° one is able to ray trace through the F1 region of the MQP ionosphere displayed in figure (7.9), with the apogee height lying in the vicinity of, $r_m F1$, namely (209,68 km). A F_1 ledge condition is now artificially introduced by lowering the joining height ,r_j, in figure (7.9), from 209,68 (km) to 200 km and finally to 184 km. The two MQP model profiles with artificial F_1 ledge conditions are shown in figures (7.10) and (7.11).

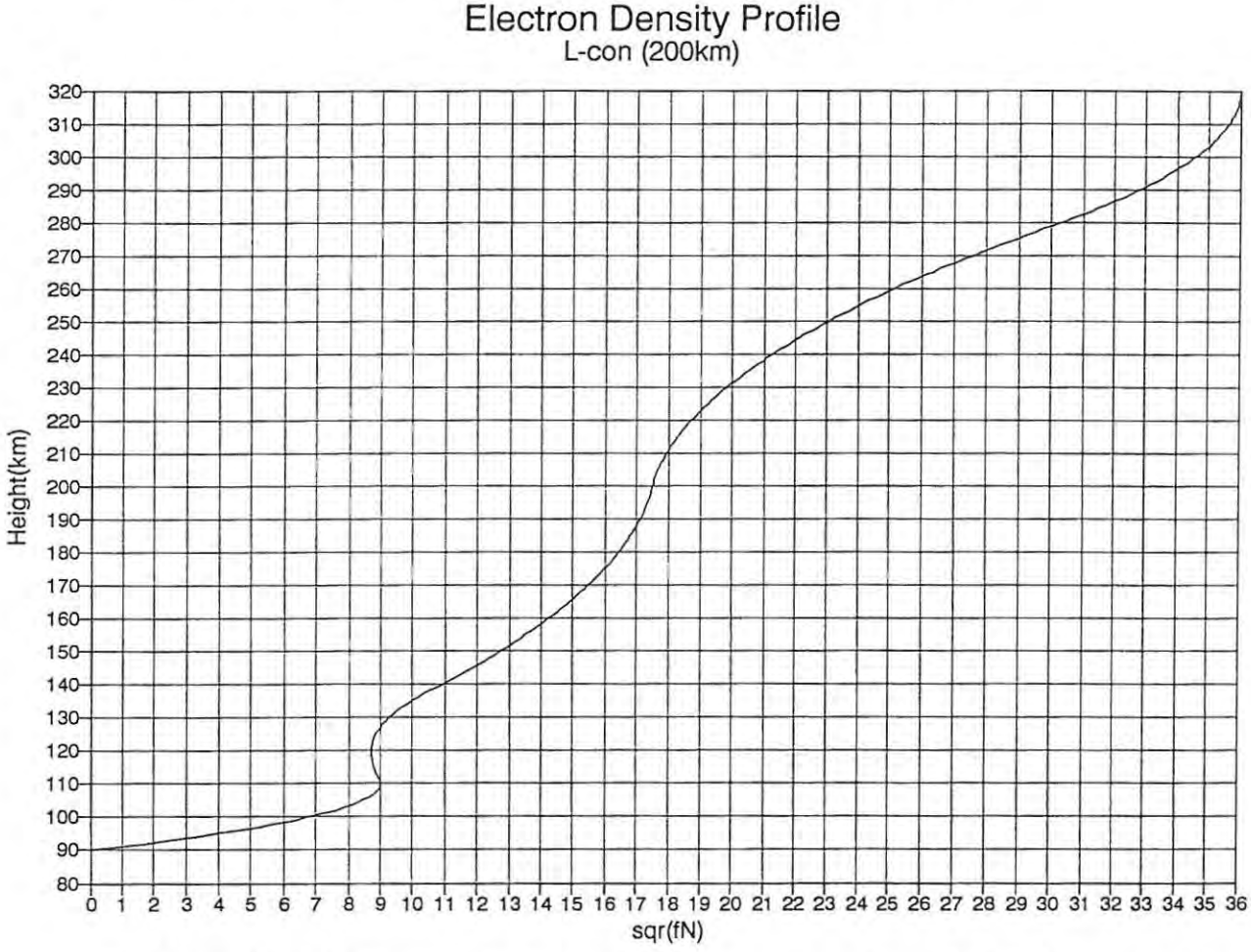

Figure (7.10): MQP electron density profile with a E/F_1 valley and F_1 ledge condition, inflexion height 200 km.

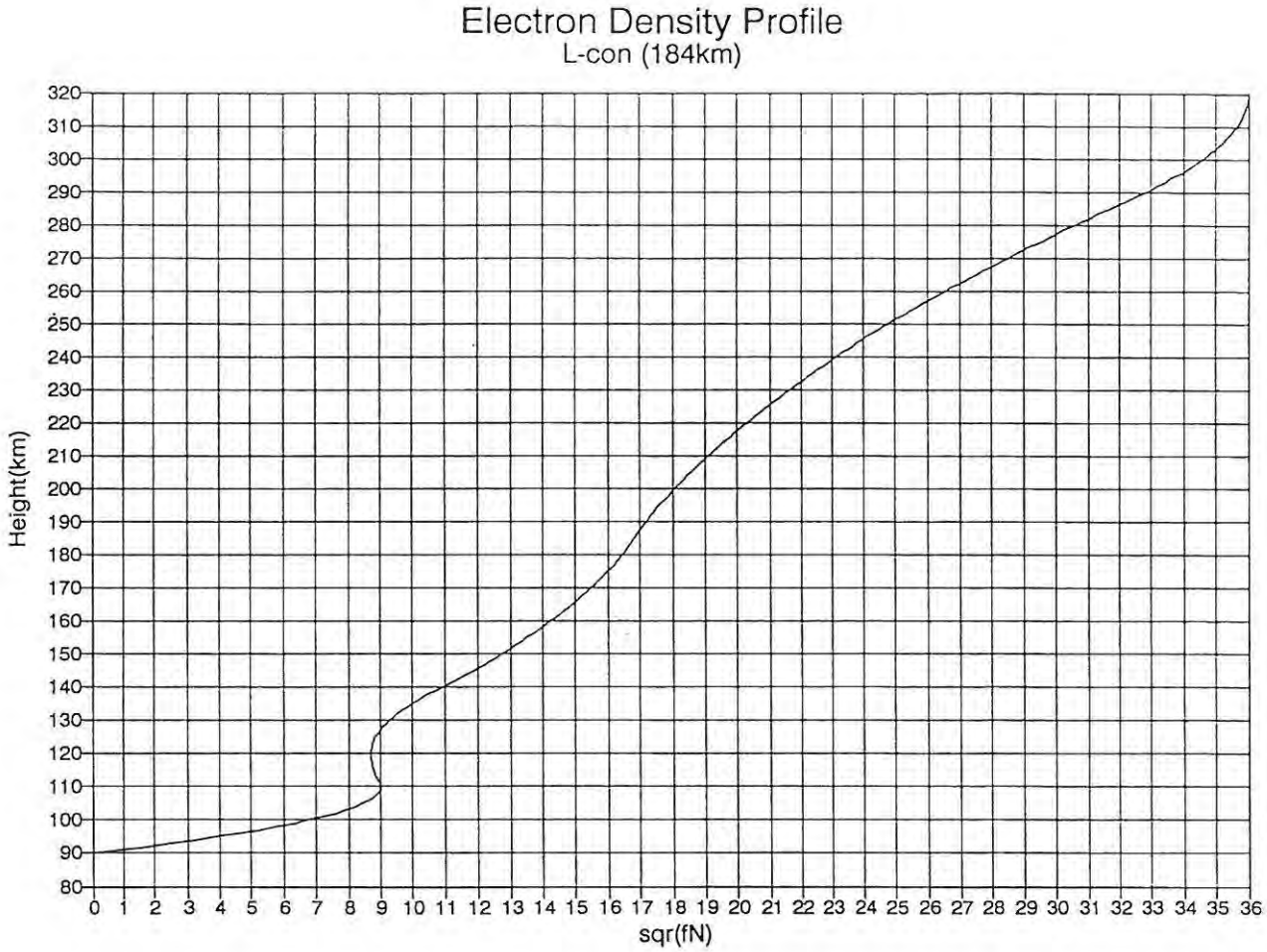

Figure (7.11): MQP electron density profile with a E/F_1 valley and F_1 ledge condition, inflexion height 184 km

Once more a ray trace was performed using a propagation frequency of 6 MHz over a bandwidth of elevation angles extending from 40° to 50° and one can see from figure (7.12) that the F_1 range cusp shrinks from being a spike to becoming a smooth rounded shape as the F_1 ledge condition becomes more pronounced.

In conclusion it can be said that large ranging errors will occur when operating a SSL HFDF system if the radio apogee is close to a F_1 ledge of ionization unless the ledge height has been accurately determined during the construction of the MQP model ionosphere.

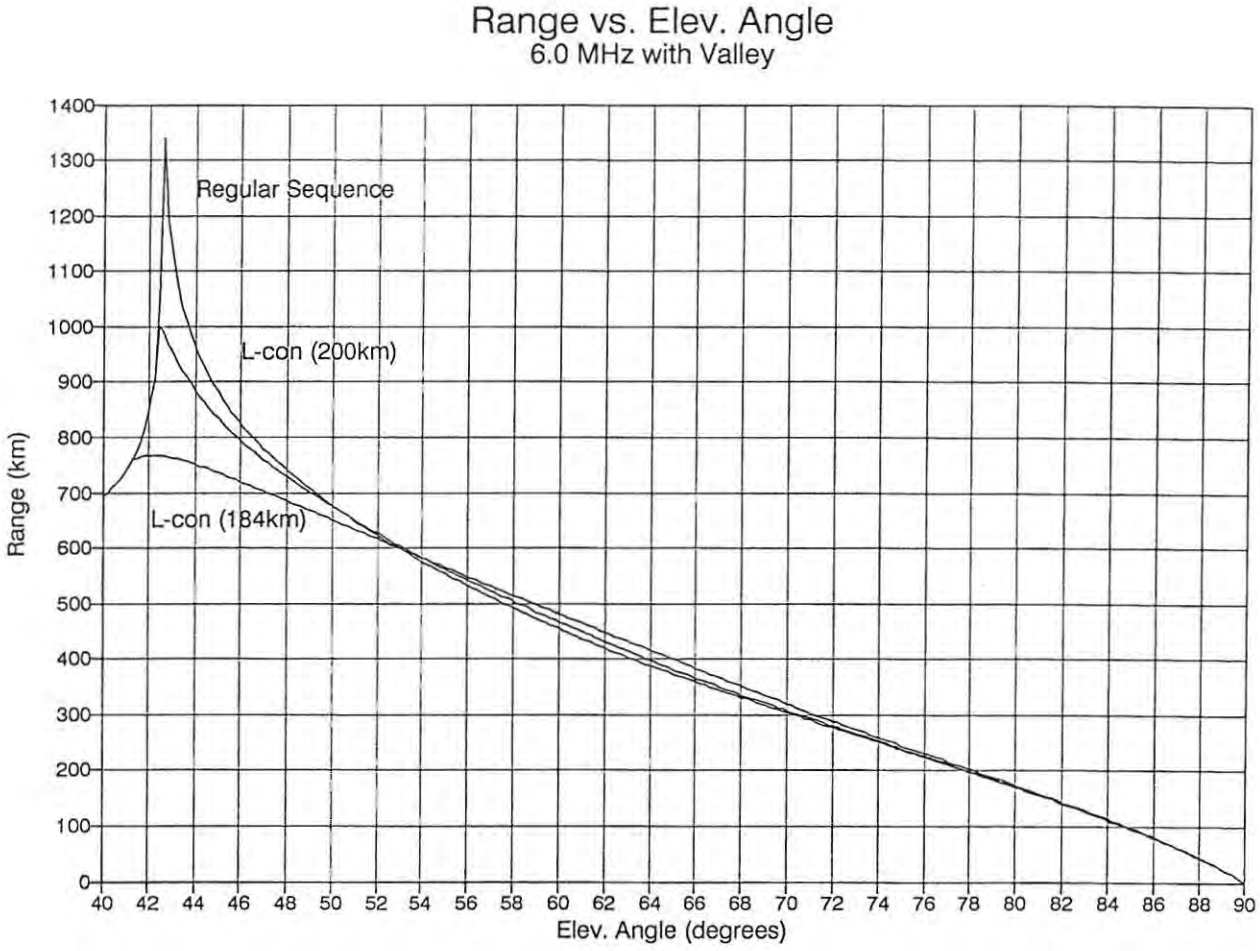

Figure (7.13): The effect of a F_1 ledge condition on the calculation of ground range as seen from a real fully analytic ray trace through the F1 region of the MQP ionosphere displayed in figure(7.2), with height as a variable.

For the purposes of comparison the graphical results of the Baker et al [1992] non analytical study of the F_1 ledge condition and its rôle in ranging errors are shown in figure (7.14).

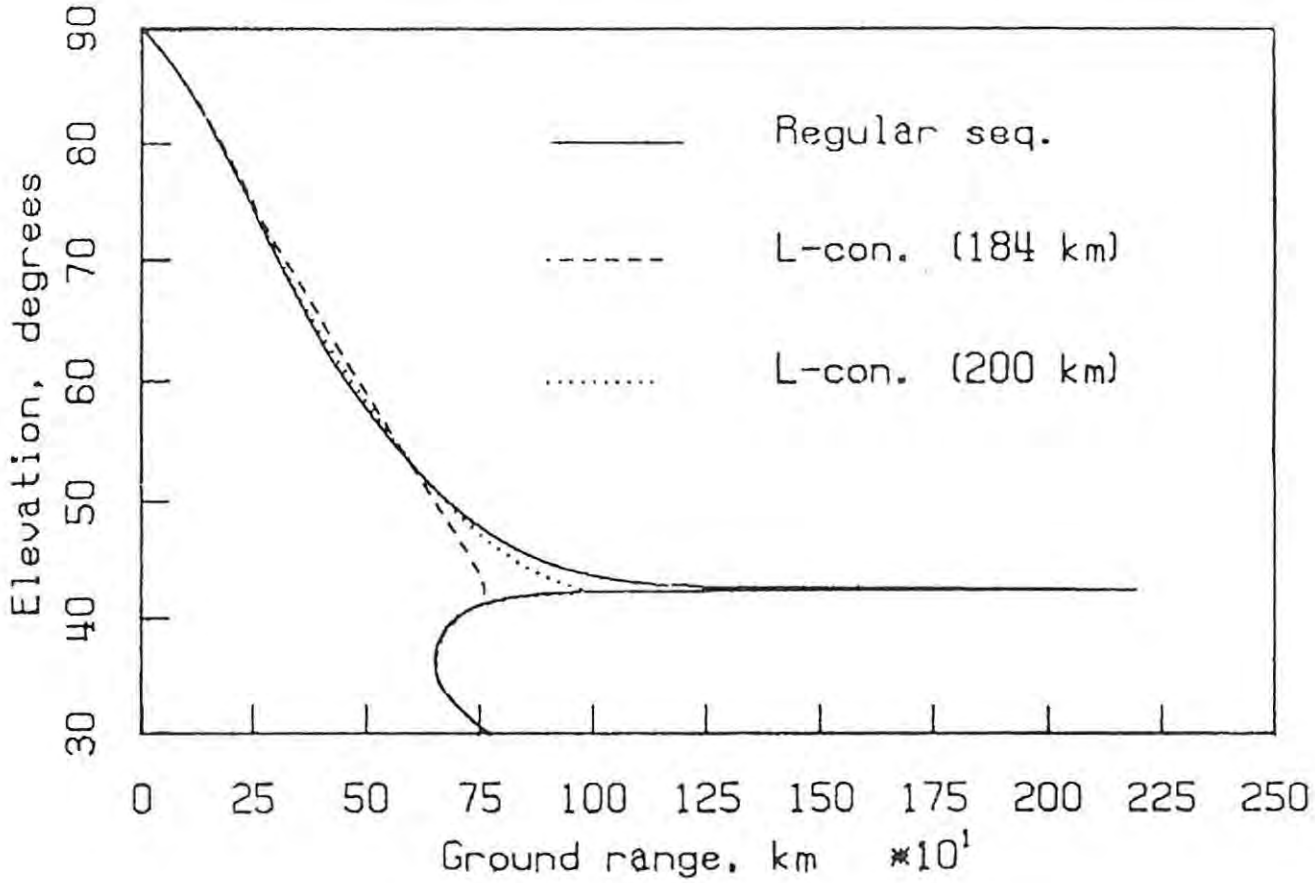

Figure (7.14): "Comparison of ranging estimates as a function of ray elevation angle for a regular sequence of conventional and inverted quasiparabolic segments and two cases of F_1 ledge conditions. The lower transition heights for the F_1 ledge are set at 200 and 184 (km), respectively as compared to a peak height of 209,68 (km)" after Baker et al (1992).

CONCLUSION AND SUMMARY

The conclusion to the Real Prop project will present a general overview of the key result areas, defined at the outset of the research work and detailed in Chapter 1. One should regard the conclusion as an overview or summary of the research results and the reader is referred to the relevant thesis chapters for a detailed account of the findings of a particular body of work. Each chapter is assembled on a "stand alone" basis with the results being presented and discussed in the form of a conclusion at the end.

PHASE 1: THE SEARCH FOR A SUITABLE REAL TIME ANALYTICAL IONOSPHERIC MODEL

The first stage of Real Prop was to carry out an extensive literature survey to identify the major research publications in the field of real time ionospheric modelling, especially in the area of HFDFSSL. The findings of the literature study were published in an internal CSIR report at the conclusion of 1991 and remains proprietary information. However, Chapter 2 contains an overview of the chronological background to ionospheric modelling, both for synoptic and real time applications. In essence the research work conducted in Australia

by Dyson, Bennett and Chen was targeted as being the most relevant to the interests and goals of the Mikomtek HF research team. Peter Dyson and his co-workers have published results on real time modelling of the ionosphere on an almost annual basis since 1988 and they have slanted their research work toward application in HF direction finding applications rather than frequency prediction. Baker et al in South Africa have presented results largely of academic interest and their research findings do not appear to have addressed the fundamental issue of developing analytical modelling algorithms. Baker relies on application of iterative/numerical techniques and uses a version of the "indirect method", discussed in Chapter 2, to determine the ionospheric layer parameters. This approach was used extensively by Dudeney [1985] to develop synoptic ionospheric models for long term forecasting, but the inherently non-analytic nature of the modelling procedures renders the "indirect method" unsuitable for real time (now casting) applications. The decision was made to follow the path already beaten out by Dyson et al, especially their research on real-time HFDFSSL propagation assessment using fully analytic modelling algorithms to describe the ionospheric support medium. It should be noted that although the Australian research team published reasonably prolifically, the details of algorithms or source code were invariably couched in a format that made it quite difficult to avoid "re-inventing the wheel" in the investigative studies carried out at CSIR, a situation that was further exascebated by the failure of Dyson et al to report their Mathematics accurately in their publications.

DEFINITIVE RESULTS CONCERNING THE GENERIC IONOSPHERIC MODEL SUITABLE FOR MULTI-PURPOSE APPLICATION IN REAL TIME HF FREQUENCY ASSESSMENT.

It was clear from the contemporary literature reviewed that the multi-segmented

quasiparabolic electron density model as proposed by Hill [1978] and implemented by Dyson et al [1988] is an excellent candidate for the rôle of a generic multi-purpose ionospheric model in real time HF propagation assessment. The model permits analytical ray tracing and accurately represents the true N-h distribution of a well behaved ionosphere, including the possibility of a re-entrant region as well as F region bifurcation.

PHASE 2 : ASSESSMENT OF THE MQP IONOSPHERIC MODEL.

Analytical ray tracing algorithms were developed to calculate trajectory traces through model MQP profiles using layer parameters determined via curve fits to observed N-h distribution data. The potential users of the Real Prop software required the following circuit parameters;

(1) maximum usable frequency (MUF)

(2) permutations of the circuit parameters ground range, elevation angle and radio frequency

(3) radio apogee height

(4) transmission curves for propagation assessment, and

(5) link budget analysis and radio locus plots, see Appendix [A1]

The above list of HF circuit descriptors must be derivable via analytical ray tracing algorithms applied to a MQP model ionosphere using the layer parameters that have been determined from ionogrammetric data by a sounder located at one end of the simulated radio path. It should be noted that the validity of the computer simulated HF circuit pre-supposes that the reflection point for the assumed single hop propagation falls within the

circumference of the spatial/temporal coherence circle of the sounder, for example in the case of F2 layer support this distance would extend down range some 600 km, McNamara [1991].

NON-MONOTONIC AND BIFURCATED IONOSPHERES

The re-entrant ionospheric conditions derived by the presence of an E/F_1 valley region were modelled using MQP segments and the effects of propagation through an ionization depletion region were investigated using simulated oblique links. It was found that the perturbing effect of an ionization depletion region was greatest when;

(a) propagating over a short ground range

and

(b) the radio apogee is close to the top of the E/F_1 valley portion of the ionosphere.

The quantifying of the refractive influence of a valley segment upon ranging errors is a matter of intense research interest to the users of HFDFSSL systems, McNamara [1991]. There is a detailed discussion in chapter 7 of the effects of a re-entrant electron density profile upon ground range calculation and results are derived via a simulated HF circuit for the ranging errors that occur when the radio apogee is close versus well removed from the top of a E/F1 valley region. Further studies were carried out on the influence of the F_1 ledge condition upon the range versus elevation angle transmission geometry. First it was required to model a ledge of ionization or a point of inflexion on an observed N-h distribution via the use MQP segments and analytic curve fitting routines. It was found that

due to the failure of POLAN, the ionogramme inversion programme, to provide a user of electron density data with accurate information describing the critical frequency and height of a F1 ledge of ionization, one was forced to develop elaborate curve fitting algorithms to match a quasiparabolic segment to the observed F1 region distribution. In addition a rather complicated analytical routine was required to determine the geometry of IQP joining section used to bridge the F1-ledge/F2-layer interface. The success of the curve fitting process was certainly demonstrated in the less than 0.5% root mean square error that was found obtainable when running the "F1 ledge least squares algorithms" on a standard 386 PC. The achieving of such a high degree of accuracy with a limited machine accuracy can be attributed to the subtle re-formatting of the expression for a QP model profile so that the inherent effect of small changes in geocentric height causing large changes in plasma frequency does not require the use of excessive computer power. The F_1 ledge algorithms developed in the course of Real Prop are thought to be unique and tests involving synthetic VI ionogrammes reveal a high level of accuracy in the curve fitting/modelling of the F_1 ledge/F_2 layer region of the ionosphere. The research carried out at CSIR, using MQP sections to model a bifurcated F region has been presented in a poster session at URSI, Kyoto, Japan in August 1992. In response to the URSI conference presentation, **The Centre National d'Etudes des Telecommunications, France Telecom,** considered world experts in "now casting", have requested interest in the F1-ledge modelling technique used. In the course of the research work carried out at CSIR ray-tracing algorithms were implemented to simulate propagation through a F1 ledge of ionization so that its effects on ground range calculation could be assessed in a quantitative manner. Propagation frequencies were selected to ensure apogee occurred close to the F_1 point of inflexion and a sequence of transmission curves, parameterized in ledge height,

were generated for a narrow bandwidth of transmitter launch angles corresponding to reflection either side of the point of F1/F2 birfurcation. This investigation served to show the importance of modelling the F_1 ledge condition accurately, as large ranging errors were found to occur when a ledge of ionization is inadvertedly modelled as a peak in electron density. A comparative study was conducted using data obtained by Baker et al [1992] who used numerical techniques to model a F1 ledge condition followed by ray tracing through the point of inflexion. The results from Real Prop agree perfectly with Baker's work ,however, the non-analytical nature of that author's F1 ledge algorithms are impractical for use in even quasi "real-time" frequency assessment, GST[1993]. The results of the Real Prop F1 ledge study have been presented to a manufacturer of HFDFSSL systems in South Africa and considerable interest in the research has been stirred as a result.

The final phase: SIMULATED VERSUS MEASURED OBLIQUE DATA

The final phase of the Real Prop research involved established a physical HF radio link between CSIR, Pretoria, and Rhodes University, Grahamstown. The proposed project stipulated the installation of two chirp ionosondes (frequency modulated continuous wave HF radar) at each end of a oblique path and the suitable siting of two sloping inverted vee aerials with which to transmit and receive. A FMCW oblique network sounder uses a synchronised transmitter and receiver but unlike the pulse ionosonde, a low-level frequency sweep is transmitted. The sweep frequency generated at the transmitter can be linear or logarithmic in form and can extend over the whole or part of the HF spectrum while a replica of the transmitted sweep is generated at the receiver for use as a local oscillator input. The signal received via the ionospheric path is mixed with the receiver generated sweep and the resultant beat signal is subject to spectral analysis. Multiple radio paths

give rise to multiple sweeps with each linkage being characterized by a unique received signature defined by a signal amplitude and its relative propagation delay. The spectral analysis provides one with the desired oblique ionogramme data in the form of a group time delay versus signal frequency plot, also known as an oblique ionogramme. Valiant attempts were made to establish the oblique sounder link and although radio communication could be claimed to have occurred for a short interval of time, the project had to be abandoned in its early stages of implementation. Regretably, Mikomtek made the decision to close down the HF research facility ,in line with the financial streamlining policy that the division was forced to adopt in the wake of major recession in South Africa. However, as stipulated in the original definition of goals for the Real Prop project, the algorithms and source code had to be thoroughly de-bugged and tested using **simulated circuit techniques**, in the event of there being no measured data available for an oblique link. To test the MQP ray tracing algorithms for self consistency and to further evaluate the quality of the modelling process comparisons were made using synthetic oblique ionogrammes (group path plots) generated via MQP based algorithms versus a variant of the URSI slider technique known as the classical method . In fact a considerable wealth of information , detailed in chapter 6, was derived from synthetic group path analysis by comparing the group delay structure derived from ray tracing through a fitted a fitted MQP model ionosphere versus mapping the observed h'(f) data onto the oblique frequency plane using a spherical implementation of the equivalence theorems. The Chen perturbation equation [1992] allows one to incorporate the first order effect of the geomagnetic field upon group path calculations via the addition of a fully analytic integral dependent upon the ray tracing coefficients and evaluated for an effective frequency that embodies the gyromagnetic effect. The Chen formulation was successfully implemented in the case of vertical propagation as evidenced

by the high quality of fit between the synthetic and observed ionogrammes analyzed in chapter 6. The generalized case where one synthesizes an oblique ionogramme from a MQP model with the geomagnetic field included, has been derived from first principles and left in algorithmic form. The classical method used to synthesize a group delay profile does not provide one with extraordinary ray data on account of the algorithm's dependence upon the equivalence theorems which are only valid under field -free conditions. If measured group delay data had been available one could have assessed the accuracy of Chen's first order calculation although it should be pointed out that the required determination of the frequency scaling factor ,h, for the case of oblique incidence is a tedious business and the reader is referred toChen et al [1992]for a comprehensive discussion on the assessment of the perturbing effect of the geomagnetic field upon oblique HF propagation. The inclusion of the field perturbation term in the group path calculation should be regarded as a pleasing refinement to the fully analytic MQP based oblique ionogramme synthesis module, however, it should be noted that this would constitute a mini-project of its own.

THE FUTURE PLANS FOR RESEARCH AND DEVELOPMENT

The proposed installation of a network of digisonde sounders in South Africa will make the availability of electron density data in real time a reality and this could allow the Real Prop curve fitting and ray tracing algorithms to be used as the nucleus of a "now casting" frequency prediction module. Furthermore, the completed MQP ionospheric model and its generic software implementation is still of major interest to the purveyors of HFDFSSL systems and the availability of the Lowell digisonde "real-time" N-h profiles would allow such a client to carry out field trial evaluation of the Real Prop software. The proposed digisonde network would also provide the South African academic community with a facility capable

of conducting oblique HF radio studies, especially the opportunity to establish spatial and temporal correlation data on a country wide basis. This project could be accomplished by ray tracing through MQP models of the ionosphere derived from VI(vertical incidence) ionosonde records and then comparing the corresponding synthetic oblique ionogrammes with measured group delay data to determine the dimension of the sounder correlation circle. Using three or more chirp sounders one could eventually map the South African ionosphere and create a synoptic data base of general use to the HF radio community. The possibility of carrying out investigative studies into the effects of ionospheric tilts upon HF propagation and of the establishing a synoptic data base remains of interest to the manufacturers of HFDFSSL systems although it has long been determined that the quantifying of ionospheric plasma gradients is a somewhat intractable problem, Davies[1990]. It is hoped that the digisonde network will become a reality in South Africa and that Real Prop will provide a firm basis for the development of a "now casting " facility for general use by the HF radio community. Furthermore it would be exciting to see the results obtained from HFDFSSL field trials if one were to use the Real Prop ionospheric model to drive the direction finding system, given the availability of the Lowell digisonde 256 real time N-h profiles. Let's wait and see.

APPENDIX (A1)

THE ANALYTICAL DETERMINATION OF IONOSPHERIC FOCUSING GAIN FOR THE MULTI-SEGMENTED QUASIPARABOLIC ELECTRON MODEL AND ITS RôLE IN THE CALCULATION OF AN H.F. LINK BUDGET

The schematic in figure (A.1) shows the various sources of power loss of an HF signal as it travels from a transmitter to a receiver and represents a typical HF link budget.

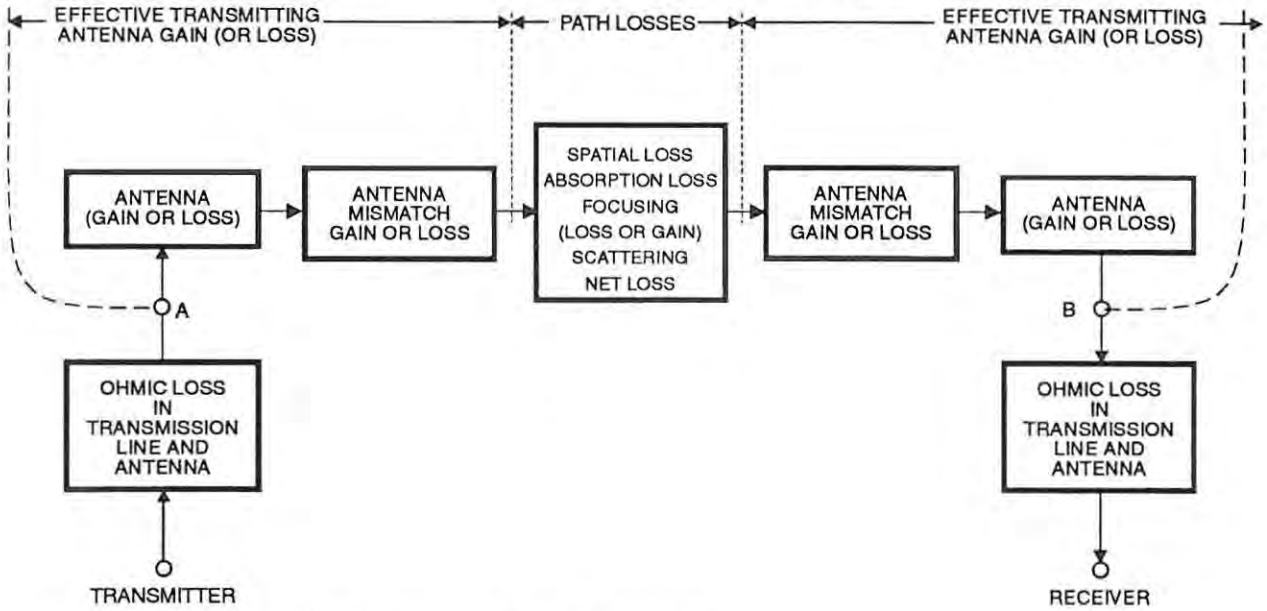

Figure(A.1): Schematic of a typical HF link budget.

If a power, P_{Tx}, is supplied to the transmit side of a radio link and if the signal strength available at the receiver is, P_{Rx}, then one can define the system loss as

$$L_{sys} = -10\ Log_{10}\ \frac{P_{RX}}{P_{TX}} \qquad \text{(A:1)}$$

The ensemble "system loss" is a sub-sum of the component losses depicted in figure (A.1) where it is seen that all but the path losses originate in the circuit equipment. One can lump the equipment losses together under, L_{eq}, and consider the propagation losses as given by

$$L_{prop} = L_{sys} - L_{eq} \qquad \text{(A:2)}$$

where all quantities are assumed expressed in decibels.

The calculation of the propagation losses

After the radio signal has left the transmitting antenna it undergoes the following;

(a) a simple inverse distance spreading loss denoted by L_d in decibels;

(b) absorption in the D layer of the ionosphere, L_{ab} in decibels;

(c) and focusing or defocusing of power, denoted by, L_f, which may be a positive or negative quantity.

The **total path loss** is then the sub-sum of the above loss terms, that is

$$L_p = L_d + L_{ab} + L_f \qquad \text{(A:3)}$$

where it is assumed that all quantities are measured in decibels. The various terms in eq [A:3] are now discussed in more detail :

Spatial loss

As a radio wave expands out from a point source the power flux falls off inversely as the square of the distance "d" from the source of the radiation, expressed mathematically by

$$L_d = 20 \log_{10}(d) \qquad \text{[A:4]}$$

Absorption losses

An excellent review of the subject of ionospheric absorption is to be found in the CCIR supplement to report 252-2 [1978] and various empirical models used to estimate both deviative and non-deviative absorption losses are discussed in detail. Bennett et al [1991] developed an analytical model for the calculation of D layer absorption (non-deviative type) using exponential and quasiparabolic segments, the coefficients of which are determined using electron density data derived from the International Reference Ionosphere, Rawer et al [1987]. It is possible to analytically ray-trace through Bennett's model for the D region of the ionosphere, but unless one is operating a radio link at frequencies low enough for absorption to become significant it is quite reasonable to omit a D layer from the MQP electron profile. Furthermore, since refraction in this region is minimal, omission of a D region from a MQP model will not result in ground range errors and for this reason one may safely ignore the D region of the ionosphere when constructing a MQP model that

is suitable for driving a SSL HFDF, system.

Focusing

The field strength produced at a distance by a radio transmitter in free space is inversely proportional to the transmission range, but for signals travelling via the ionospere, in general ray-path focusing or defocusing takes place. There are three principal conditions under which reflected signals are focused, namely;

(a) when one is operating an HF circuit close to the MUF for the link, then the Pederson and low angle rays superimpose, leading to the phenomenon known as **skip distance focusing.** One should note that the benefits of this type of focusing are usually short lived due to the rapid changes in the skip distance that are caused by fluctuations in the real ionization profile. This problem is circumvented by operating the HF circuit at the Optimum traffic frequency(OTF), the value of which is based on statistics of the ionosphere.

(b) when one has radio signals emanating from a transmitter at low angles of elevation then **horizon focusing** occurs on account of the curvature of the Earth's surface and the lower boundary of the ionosphere

(c) for the ideal case of a concentric, spherical earth and ionosphere, the phenomenon of **antipodal focusing** will occur at the antipode of a transmitter location. However, the degree of focusing, although measurable, Wait[1963], is very sensitive to ionospheric deformations and should not be expected to occur on a regular basis.

Except in the case of propagation to the antipodes, where the ground range by definition is half the circumference of the Earth, both skip distance and horizon focusing can take place over a wide range of path lengths.. In order to quantify the process of focusing one is required to have a detailed knowledge of the ionosphere along the ray path and a sophisticated ray tracing programme. It is first necessary to understand the physics behind the focusing mechanism before discussing the actual ray tracing algorithms required to determine the degree of focusing or defocusing.

Effective path length

The effect of focusing can be described in terms of a, so-called, effective path length, s_e, and the physical meaning of this quantity can be seen from the following argument. In the absence of all other forms of energy loss the power flux at a distance s_e from an isotropic radiator, which radiates a total power p_{Tx} is given by

$$\Phi = \frac{P_{Tx}}{4\pi s_e^2} \qquad \text{(A:5)}$$

where the flux is seen to fall off as the inverse square of the distance from the source. Referring to the figure (A.2) one sees the artificial introduction of a defocusing condition where, s_e, is the distance from the antenna at which the area covered by the defocused ray is the same as that for unperturbed radial flow.

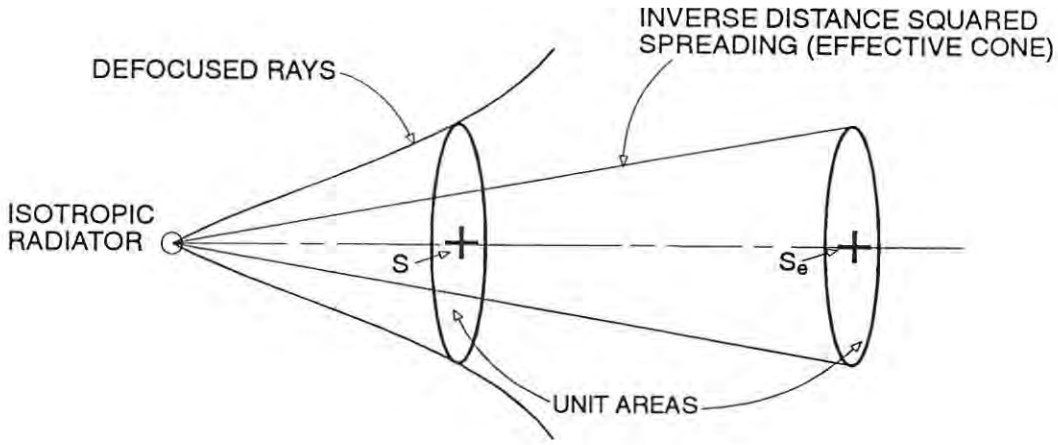

Figure (A.2): Illustration of the concept of effective path length, used to take into account focusing or defocusing within the ionosphere.

Thus the defocusing can be taken into account by replacing the true distance ,s, of the receiver by an effective distance ,s_e, allowing one to combine the spatial loss and focusing losses in the single expression

$$L_d + L_f = 20 \log_{10} s_e \qquad \text{(A:6)}$$

It should be noted that ,s_e , is greater than ,s, for defocusing and less than ,s, for focusing. Using the concept of the effective distance it is clear that ,s_e^2 , is equal to the ratio of the cross-section of the effective cone, which is equal to the actual defocused cone, to the cross-section at unit distance from the source of radiation. The figure (A.3) shows a typical HF radio link and illustrates the azimuthal and zenithal spreading of the beam for a spherically stratified ionosphere.

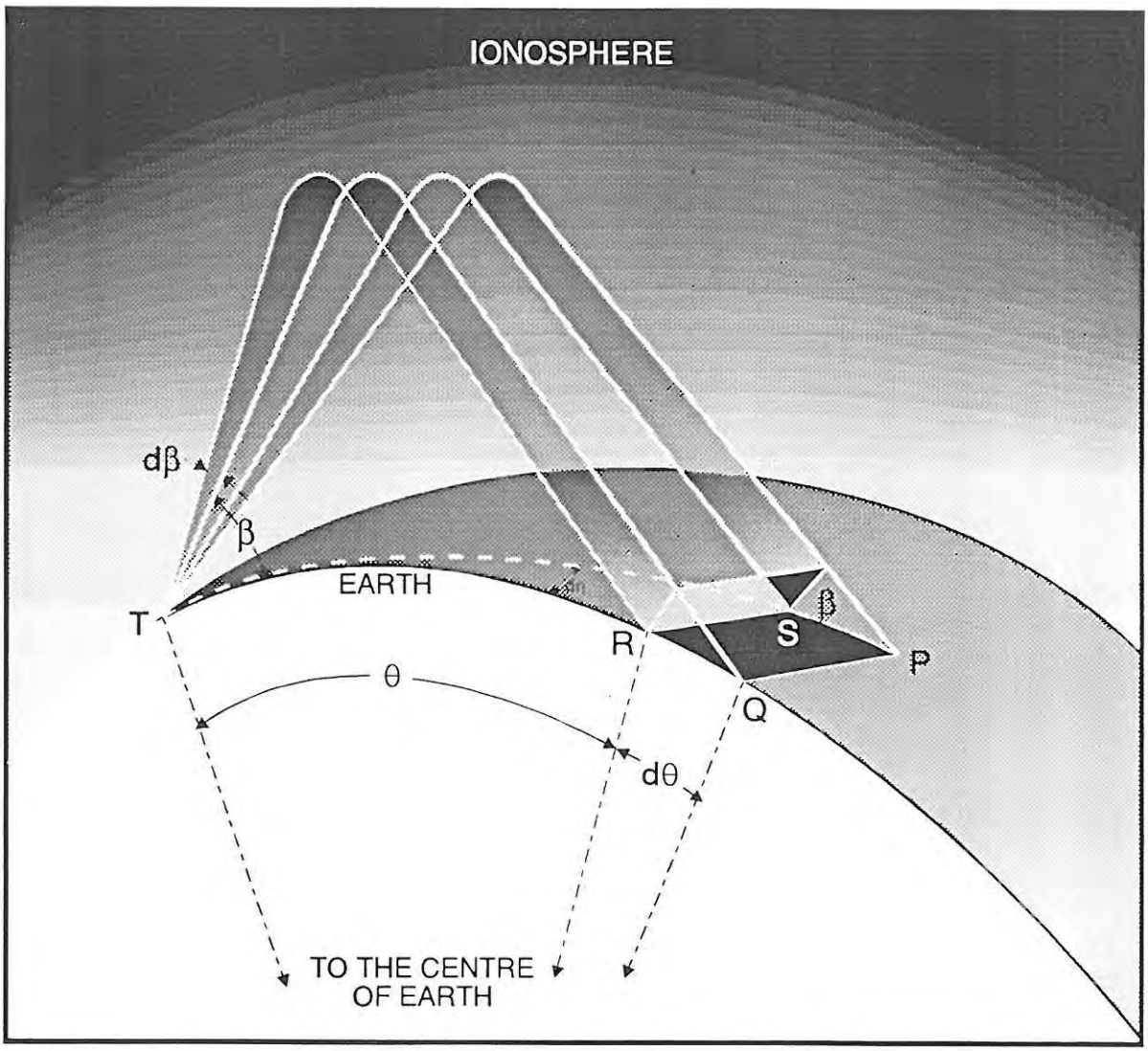

The divergence of a HF radio beam for a curved earth.

Figure (A.3): The divergence of a HF radio beam propagating over a curved earth.

One can see the expanding beam geometry in more detail in figure (A.4) where a rectangular flux pipe of vertical width dβ, of horizontal angular width dη and elevation angle describes the energy flow at unit distance from the transmitter

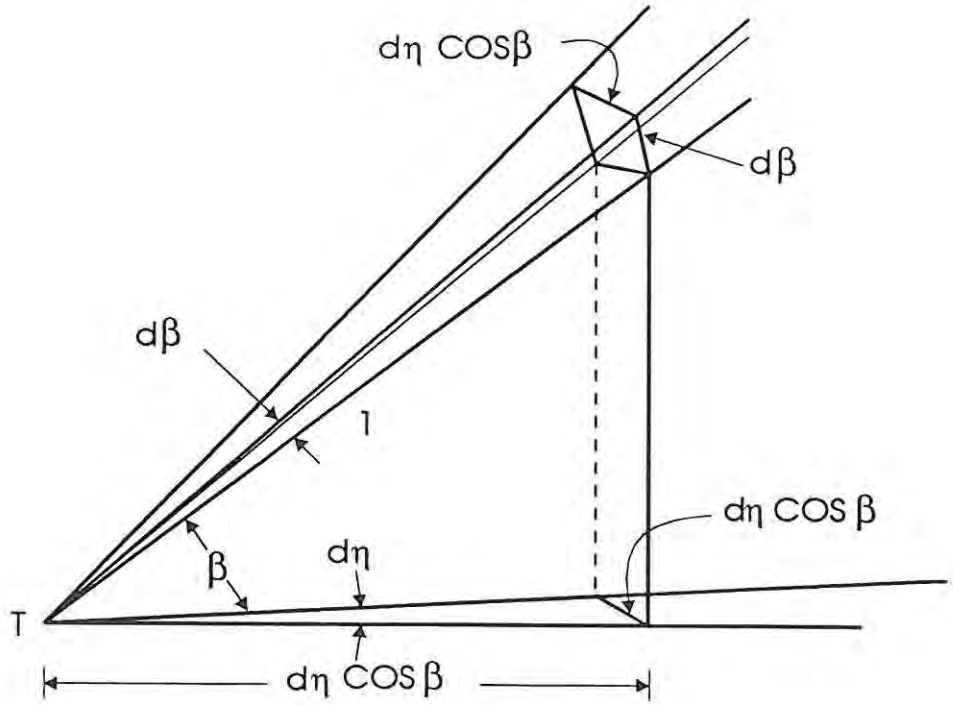

Figure (A.4): Enlarged view of the HF radio beam as the rays emanate from the transmitter

From the figure (A.4) it is clear that the area of the flux pipe at unit distance from the transmitter is dβ (dη cos β) while from figure (A.3) one sees that the area of the beam at the receiver is given by (RQ)(RS sin β). The value of RQ is easily determined being the radius of the earth r_o times the elemental angular substence dΘ, however, to determine the element RS one must establish a new geometrical construction as illustrated in figure (A.5) below.

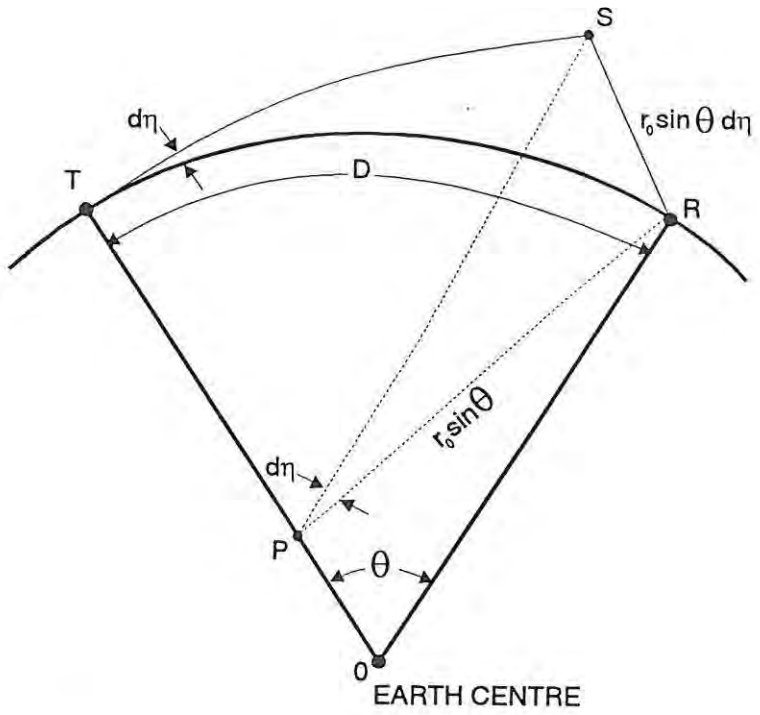

Figure (A.5): Azimuthal spreading of a HF radio beam as it propagates over the Earth's surface.

Given that the construction lines SP and RP are perpendicular to TO, that is,

$$SP = RP = r_0 \sin\theta \qquad \text{(A:7)}$$

then it follows

$$RS = r_0 \sin\theta\, d\eta \qquad \text{(A:8)}$$

The cross section of the beam at the receiver is therefore given by

$$dA = (r_0\, d\,\theta)\,(r_0 \sin\theta\, d\,\eta)\,(\sin\beta) \qquad \text{[A:9]}$$

hence the effective distance s_e may be expressed

$$s_e^2 = r_0^2 \sin\theta \tan\beta \left(\frac{d\theta}{d\beta}\right) \qquad \text{[A:10]}$$

It is more convenient to replace the derivative $(d\Theta/d\beta)$ by the rate of change of ground range with respect to elevation angle using the relationship

$$\frac{dD}{d\beta} = r_0 \frac{d\theta}{d\beta} \qquad \text{[A:11]}$$

to give for s_e^2

$$s_e^2 = r_0 \sin\theta \tan\beta \left(\frac{dD}{d\beta}\right) \qquad \text{[A:12]}$$

Substitution of the above expression for effective distance squared into the eq [A:5] for received radio flux yields the result

$$\phi_{Rx} = \frac{P_{Tx}}{4\pi\, r_o \sin\left(\frac{D}{r_o}\right) \tan(\beta^o) \left(\frac{dD}{d\beta}\right)} \qquad \text{[A:13]}$$

From eq [A.13] one may determine the received flux strength for a given ground range, D,

elevation angle, β°, and $dD/d\beta$. To evaluate the derivative function $dD/d\beta$ requires that one establish a model ionosphere through which to ray trace and the next section is devoted to the derivation of the algorithms necessary to determine the focusing gain for a MQP electron profile.

Ionospheric focusing gain and the multi-quasiparabolic model profile

In excellent review article on ionospheric focusing due to refraction through a single parabolic layer can be found in Bradley [1970] together with prediction curves providing one with the focusing gain as a function of, elevation angle, using the ratio of the propagation to the critical frequencies as parameter. The CCIR [1978] supplement to report 252-2 presents a short discourse on the calculation of focusing gain and recommends the use of the Bradley curves for horizon focusing of rays of low elevation angle for the E and F modes. Various recipes are given in the CCIR [1978] to calculate the focusing effect of the ionosphere but the influence of a multi-layered electron profile is not addressed. The paper by Dyson and Bennett [1988] introduces the topic of ray divergence and field strength calculation when the ionosphere is modelled as a continuum of quasiparabolic segments and the authors derive expressions for the power returned in a back scattered pulse sounding. In the research work carried out at CSIR the interest was in developing algorithms to calculate the ionospheric focusing term in a HF link budget analysis, eq (A.3) when the propagating medium is modelled as a MQP continuum.

Determination of the energy flux equation for the MQP model

The analysis requires that one be able to determine the focusing gain ,L_f , defined in decibels as $10 \log \left\{ 4 \pi S_{Rcvd} / P_{Tx} \right\}$ where the received flux is calculated using the result

$$S_{R_{cvd}} = \frac{P_{Tx}}{4\pi\ r_o \left(\frac{\partial D}{\partial \beta}\right) \tan(\beta) \sin\left(\frac{D}{r_o}\right)} \qquad \text{(A:14)}$$

given

S_{Rcvd} → energy flux reaching the F receiver

P_{Tx} → power transmitted

β → elevation angle at the HF transmitter

D → ground range

r_o → earth radius

As proved in chapter 4 the ground range covered by a HF signal propagating through a MQP model ionosphere is given by

$$D = 2r_o \left\{ (\gamma - \beta) + r_o \cos \beta_o \sum_n (\sqcup_n - L_n) \right\} \qquad \text{(A:15)}$$

where

γ = $\cos^{-1}[r_o/r_b \cos \beta_o]$, entry angle of radio ray at ionosphere's base

r_b → base height of the ionosphere

r_o → radius of earth

β_o → elevation angle at transmitter

and the quantities $\sqcup_n$ and L_n represent the upper and lower limit values of the integral, I,

defined by

$$I \equiv \int_{r_L}^{r_U} \frac{dr}{r\sqrt{R}} \quad , \quad R \equiv A'r^2 + B'r + C' \qquad \text{[A:16]}$$

To obtain the rate of change of ground range with respect to elevation angle it is necessary to partially differentiate eq [A.15] with respect to β, giving

$$\frac{\partial D}{\partial \beta} = 2r_o \left\{ \frac{\partial \gamma}{\partial \beta} - 1 - r_o \sin \beta \sum_n (\sqcup_n - L_n) \right\} + 2r_o^2 \cos \beta_0 \sum_n (\sqcup_{n\beta} - L_{n\beta}) \qquad \text{[A:17]}$$

where the derivative $\partial\gamma/\partial\beta$ can be expressed as

$$\frac{\partial \gamma}{\partial \beta} = \left(\frac{r_o}{r_b}\right) \frac{\sin \beta}{\sin \gamma} \qquad \text{[A:18]}$$

The ensemble value of $\partial D/\partial\beta$ is the sub-sum value of the contribution from each section of the MQP profile. It is required therefore that one obtain expressions giving $\partial D/\partial\beta$ for the following four cases; apogee/traversal of a traditional/inverse quasi-parabolic electron profile. The integral expression, I, given by eq [A.16] has been evaluated in chapter 4 for each of the four cases mentioned above and it remains only to take each of required

integrals and differentiate under the integral sign.

Determination of $\partial D/\partial\beta$ for the quasiparabolic layer

In Chapter 4 the ground range contribution for a ray travelling through a quasi-parabolic layer was proved to be equal to

$$I_1 \equiv \int \frac{dr}{r\sqrt{R}} = -\frac{1}{\sqrt{C'}} \log_e \left(\frac{2\sqrt{C'R} + B'r + 2C'}{r} \right), \quad C' > 0 \qquad \text{(A:19)}$$

where the ray-tracing coefficients A′ and B′ are both independent of elevation angle at the transmitter while the coefficient C′ is given by

$$C' = -r_o^2 \cos^2 \beta - \frac{A}{f^2} \qquad \text{(A:20)}$$

Differentiating eq (A.19) with respect to β and substituting the derivative of eq (A.20) above, yields

$$\frac{\partial I_1}{\partial \beta} = \left\{ \frac{1}{2C'^{3/2}} \log_e T - \frac{1}{T\sqrt{C'}} \left\{ \frac{1}{r} \left\{ \sqrt{\frac{R}{C'}} + \sqrt{\frac{C'}{R}} + 2 \right\} \right\} \right\} C'_\beta \qquad \text{(A:21)}$$

where the quantities

$$C'_{\beta} \equiv \frac{\partial C'}{\partial \beta} = r_o^2 \sin(2\beta) \qquad \text{[A:22]}$$

$$T = \frac{(2\sqrt{C'R} + B'r + 2C')}{r} \qquad \text{[A:23]}$$

Likewise, the corresponding gradient in ground range for the case of an inverse layer is found by differentiating, eq (4.16), namely

$$I_2 \equiv \int \frac{dr}{r\sqrt{R}} = \frac{1}{\sqrt{-C'}} \sin^{-1}\left\{\frac{B'r + 2C'}{r\sqrt{q}}\right\}, \quad C' < 0 \qquad \text{[A:24]}$$

where $q \equiv (B'^2 - 4A'C')$. After some manipulation it can be shown that,

$$I_{2\beta} \equiv \frac{\partial I_2}{\partial \beta} = \left\{\frac{\sin^{-1}(Y)}{2(-C')^{3/2}} + \frac{2}{\sqrt{-C'q(1-Y^2)}}\left\{\frac{AY}{(q)^{1/2}} - \frac{1}{r}\right\}\right\} C'_{\beta} \qquad \text{[A:25]}$$

where the quantities

$$C'_{\beta} \equiv \frac{\partial C'}{\partial \beta} = r_o^2 \sin(2\beta) \qquad \text{[A:26]}$$

$$Y \equiv \frac{(B'r + 2C')}{r(q)^{1/2}} \qquad \text{[A:27]}$$

It is now necessary to determine the forms of $\partial I_1/\partial\beta$ and $\partial I_2/\partial\beta$ given the corresponding ground range equations describe the apogee condition.

To determine $\partial I_1/\partial\beta$ given apogee, $C' > 0$

The ground range equation for a quasi-parabolic layer evaluated at some apogee height ,r_{ap}, yields the result

$$\sqcup_{n_{ap}} \equiv I_{1_{ap}} = -\frac{1}{2\sqrt{C'}} \log_e (q) \quad , \quad C' > 0 \qquad \text{[A:28]}$$

where $q \equiv [B'^2 - 4A'C']$. To obtain the value of the derivative of ground range with respect to β under conditions of apogee one differentiates eq [A.28], to give

$$\sqcup'_{n_{ap}} \equiv \frac{\partial I_{1_{ap}}}{\partial\beta} = \frac{1}{\sqrt{C'}} \left\{ \frac{\log_e (q)}{4C'} + \frac{2A'}{q} \right\} C'_\beta \quad , \quad C' > 0 \qquad \text{[A:29]}$$

where the quantities

$$q = (B'^2 - 4A'C') \qquad \text{[A:30]}$$

$$C'_\beta = r_o^2 \sin (2\beta) \qquad \text{[A:31]}$$

To determine $\partial I_2/\partial\beta$ given apogee, $C' < 0$

One must determine the value of the ground range equation given $C' < 0$ and conditions of apogee, namely

$$\sqcup_{n_{ap}} \equiv I_{2_{ap}} = \frac{\pi}{2\sqrt{-C'}} \quad , \quad C' < 0 \qquad \text{(A:32)}$$

To obtain the value of $(\sqcup'_n)_{ap}$ one must differentiate eq (A.32) to give

$$\sqcup'_{n_{ap}} \equiv \frac{\partial I_{2ap}}{\partial\beta} = \frac{\pi}{4(-C')^{3/2}} \cdot C'_\beta \quad , \quad C' < 0 \qquad \text{(A:33)}$$

where the quantity

$$C'_\beta = r_0^2 \sin(2\beta) \qquad \text{(A:34)}$$

The above equations for the calculation of focusing gain may be applied to a simulated HF radio link where a MQP model ionosphere is used as the support medium. The required input parameters to the ionospheric focusing algorithms are listed below in addition to a recipe that will allow one to create a three dimensional plot of focusing gain versus elevation angle and propagation frequency:

Input parameters necessary to drive the MQP ionospheric algorithm

(1) define the ground range ,D, of the simulated HF circuit

(2) assign a value in (dB) for the gain, G_{Tx} , of the transmitter antenna

(3) establish the effective iosotropic radiated power , P_{Tx} , for the transmitter

(4) determine the MQP model ionosphere for the selected simulated HF link by curve fitting QP sections to observed N-h data recorded at either end of the oblique path

(5) using the synthetic oblique ionogramme data for the HF circuit derived in (4), one selects a suitable layer for support, and establishes the appropriate propagation frequencies and elevation angles.

(6) the focusing gain is determined using eq (A.13) coupled with the auxiliary equations, eq (A.15—A.35), needed to evaluate the ground range ,D, and its derivative, $dD/d\beta$, under conditions of apogee/traversal in a QP/IQP layer.

Milsom [1977] gives the following values for ionospheric focusing gain that the author obtained via ray tracing through a "quasi-perturbed" version of the Bradley-Dudeney[1973], displayed in figure (4.7). It should be remembered that in Milsom's ionospheric model the E and F layers have each got quasiparabolic electron profiles but the E/F1 region is modelled as a quasilinear distribution.

REGION	FOCUSING GAIN (dB)	CONCLUSION
Low angle E (β = 1°)	+8	"horizon focusing"
Tip of E "nose"	+7	focusing
High angle E	-2	Pederson rays defocusing
Very low angle E	+1	slight focusing
Medium angle F1	+18	strong focusing
Low angle F2	-3	defocusing
Tip of F2 "nose"	+20	skip distance focusing
High angle F2	-4	Pederson ray focusing

Table(A.1): Ionospheric focusing gain for quasi-parabolic/linear ionosphere, Milsom [1977].

BIBLIOGRAPHY

Advances in Space Research, Special Issue, "Enlarged space and ground database for ionospheric modelling" Vol. 11, No. 10, 1991.

Appleton, E V and W J G Beynon : " The application of ionospheric data to radio communication problems" Part 1, Proceedings of the Physics Society, 52, Number 4, 518-33, 1940.

Baker D C ,J J Burden : " Qualitative evaluation of ranging errors in SSL HFDF systems due to the E/F1valley and the F1-layer L-condition". IEEE/SAIEE AP/MTTS-92 Proceedings 1992.

Baker, D C and Burden, J J: "The multisegmented parabolic model for ionospheric electron density distribution: A convenient model for HF engineering applications", Proceedings of the Fifth International Conference on HF Radio Systems and Techniques, Edinburgh, IEE Conference Publication Number 339, 22 - 24 July, 1991.

Baker, D C and Lambert, S: Multi-parabolic Ionospheric Model for SSL Application Electron Letters, 24, pp 425-426, 1988

Baker, D C and Lambert, S: Range Estimation for SSL HFDF systems by means of a Multi-quasiparabolic Ionospheric Model, Proc IEE, 136 H, No2, 120 (1989).

Baker, D C and Lambert S : A simple contiuous Multiparabolic Model of ionospheric Electron Density Distribution for use in Certain HF Communications Applications", Transactions, SAIEE, Vol.81, pp. 16-22, 1990.

Barghausen, AF, Finney, J W, Proctor, L L and Schultz, L D : "Predicting long term operational parameters of high-frequency sky-wave telecommunication systems", ESSA Technical Report 110-ITS 78, USA Government Printing Office, Washington, HFMUFES,1969.

Bennett, J A , Chen J and Dyson P L : "Analytic ray tracing for the study of HF magneto-ionic radio propagation in the ionosphere", The Applied Computational Electromagnetics Society Journal, special issue summer Vol. 6, No. 1, 1991

Bradley, P A : "Computer procedure for the deriving ionospheric characteristic M(3000)F_2 from h'(f) data", Electron letters, 10, (15), pp 323-324, 1974,

Bradley, P A and Dudeney, J R : A simple model of the vertical distribution of electron concentration in the ionosphere. Journal of Atmospheric Terrestrial Physics, 35, pp 2131-2140, 1973

Bradley, P A : "Focusing of Radio Waves Reflected from the Ionosphere at Low Angles of Elevation", Electronics Letters, Vol. 6, 15, 1970.

Breit, G and Tuve, M A : " A test of the existence of the conducting layer ", Phys-Rev. 28, 554, (1926) .

Budden, K G : Radio waves in the ionosphere, Cambridge University Press, 1966.

Budden, K G : The propagation of radio waves, Cambridge University Press, 1988

Burden, R L and Faires J D : Numerical Analysis, fourth edition, PWS-KENT Publishing Company Boston, 1989.

CCIR (supplement) to Report 252-2, 1978 : "Second CCIR computer-based interim method

for estimating sky-wave field strength and transmission loss at frequencies between 2 and 30 MHz"

CCIR "Atlas of ionospheric coefficients" : CCIR report 340-4, 1982

CCIR: "Definitions of maximum transmission frequencies" CCIR Recommendations, 373-4, 1982

CCIR: "Atlas of ionospheric characteristics", Report 340, Parts 3 and 12, Geneva, 1990

CCIR : "Propagation in ionized media", annex to Vol. 6, 1990

CCIR : Short-term forecasting of critical frequencies, operational maximum usable frequencies and total electron content, Report 888, Geneva, 1990.

Chapman , S : " The absorption and dissociative or ionizing effect of monochromatic radiation in an atmosphere on a rotating earth", Proceedings of the Physics Society 43, 26, 1931.

Chen, J , Bennett, J A and Dyson, P L : Automatic fitting of quasiparabolic segments to ionospheric profiles with application to ground range estimation for single-station location, Journal of Atmospheric and Terrestrial Physics, 52, pp 277-288, 1990

Chen et al : " Synthesis of oblique ionograms from vertical ionograms using quasi-parabolic segment models of the ionosphere ", Journal of Atmospheric and Terrestrial Physics, Vol 54 Number 3/4 , pp 323-331, 1992.

CRC : Handbook of Mathematical Tables, Chemical Rubber Company, 1985.

Croft, T A and Hoogasian, H : Exact ray calculations in a quasiparabolic ionosphere with no magnetic field, Radio Science, 3, pp 69-74, 1968

Davies, K : Ionospheric Radio Propagation, United States Department of Commerce, National Bureau of Standards, Monograph No. 8, 1965

Davies, K : Ionospheric radio waves, Blaisdell Publishing Company, 1969

Davies, K : " Ionospheric radio", Pub; Peregrinus, London, 1990.

De Voogt, A H : "The calculation of the path of a radio ray in a given ionosphere", Proceedings Institute of Radio Engineer, 41, pp 1183-1186, 1953

Dudeney, J R: "A simple empirical method for estimating the height and semi-thickness of

the F_2-layer at the Argentine Islands, Graham Land", British Antarctic Survey, Scientific Reports, No. 88, 1974

Dudeney, J R : "An improved model of the variation of electron concentration with height in the ionosphere", Journal of Atmospheric Terrestrial Physics 40, 195, 1978.

Dudeney, J R and Kressman R I : "Empirical models of the electron concentration of the ionosphere and their value for radio communications purposes" Radio Science, Volume 21, Numbers 3, Pages 319-330, May-June 1986

Dyson P L and Bennett J A : "General formulae for absorption of radio waves in the ionosphere" Journal of Atmospheric and Terrestrial Physics, Vol 41, pp 367-377, 1972

Dyson P L and Bennett J A : "A model of the vertical distribution of the electron concentration in the ionosphere and its application to oblique propagation studies, Journal of Atmospheric and Terrestrial Physics, Vol 50, No.3, pp 251-262, 1988

Dyson, P L and Bennet, J A : "Exact ray path calculations using realistic ionospheres", IEE proceedings-H Vol 139, No:5, October,1992

Goodman, J M : HF Communications - Science and Technology, Van Nostrand Reinhold, ISBN 0-442-00145-2, 1992

GST : Grinaker Systems Technology, Pretoria, RSA, private communication, 1993.

Gulyaeva, T L, Titheridge, J E and Rawer, K : Discussion of the valley problem in N(h) analysis of ionograms, Advanced Space Research 10, #8,123, 1990.

Haydon, G W and Lucas, D L : Predicting Ionospheric Electron Density Profiles, Radio Science, Vol. 3 (New Series), No. 1, January 1968.

Hill, J R : "Exact ray paths in a multi-segmented quasiparabolic ionosphere", Radio Science, 14, pp 855-861, (1978)

Hitney, H V : " Ionospheric propagation assessment programme, software and user's

manual", IONOPROP, (1990).

International Reference Ionosphere : IRI 1979, World Data Center A for solar Terrestrial Physics, Boulder, Colorado, Report VAG-82, 1981

Kelso, J M (1964) : Radio Ray Propagation in the Ionosphere, McGraw-Hill book, Co. Inc., New York, N.Y.

Kelso, J M : "Ray-tracing in the ionosphere", Radio Science, Vol.3, No.1, January 1968

Lockwood, M : "Simple M-factor algorithm for improved extimation of the basic maximum usable frequency of radio waves reflected from the ionospheric F-region", IEE Proc.F., Communications, Radar and Signal Processing, 130, pp 296-302, 1983

Lockwood, M: Simplified estimation of raypath mirroring height for HF radiowaves reflected from the ionospheric F region, Proceedings IEE, 131 F, #2,117, 1984.

McNamara, L F: The Ionosphere: Communications, Surveillance, and Direction Finding, Orbit Foundation Series, Krieger Publishing Company, ISBN 0-89464-040-2, 1991

McNamara, L F: "Ionospheric modelling in support of single station location of long range transmitters", Journal of Atmospheric and Terrestrial Physics, Vol. 5 pp. 781 - 795, 1988.

Mercer C C and Poole A W V : " A Novel Least Squares Algorithm to Facilitate Analytical Modelling of a F1 Ledge Condition Using a Quasiparabolic Electron Profile", URSI 24th General Assembly of the International Union of Radio Science, Kyoto, Japan, August 25 - September 2, 1993.

Milsom, J D : "Exact ray path calculations in a modified Bradley / Dudeney model ionosphere", IEE Proceedings, H 132, pp 33-38, 1985

Milsom, J D : " Exact ray-tracing through the Bradley/Dudeney model ionosphere" , The Marconi Review, 3rd Quarter, pp 172-196, 1977.

Milsom, J D : Frequency management of HF sky-wave circuits in Europe, Communication

and Broadcasting, 7, #3,24, 1982.

Muldrew, D B : "An ionospheric ray-tracing technique and its application to a problem in long distance radio propagation", IRE Transactions, AP-7 pp 393-396, 1959

Paul, A K and Smith G H : Generalization of Abel's solution for both magnetoionic components in the real-height problem, Radio Science ,3, pp 163-170, 1968.

Piggott, W R and Rawer, K : "URSI handbook of ionogram interpretation and reduction", US Department of Commerce, National Oceanic and Atmospheric Administration Report UAG-23, 1973

Poole, A W V and Mercer, C C : "Towards a Semi - Automatic Scaling Program to Provide Model Parameters rather than Traditional Scaling Parameters", URSI 24th General Assembly of the International Union of Radio Science, Kyoto, Japan, August 25 - September 2nd, 1993.

Rawer, K et al : " The International Reference Ionosphere", Pub: Pergamon, 1987.

Rawer, K and Bilitza, D : "Electron density profile description in the international reference ionosphere", Journal of Atmospheric and Terrestrial Physics 51, #9/10, 781, 1989.

Reinish, B W, Gamache, R R and Bossy, L G : Ionospheric characteristics for IRI in real time, Advanced Space Research 10, #8,25, 1990

Reinisch, B W and Xueqin, H: "Automatic calculation of electron density profiles from digital ionograms and processing of bottomside ionograms", Radio Science, 18(3), pp. 477 - 492, 1983.

Reilly M H : "Ionospheric true height profiles from oblique ionogrammes", Radio Science, 20, No 3,280 (1985).

Rush, C M and Elkins, T J : An assessment of magnitude of the F-region absorption on HF radio waves using realistic electron density and collision frequency models, Telecommunications Journal 42, #8,476, 1975.

Rush, C M, Miller, D and Gibbs, J : The relative daily variability of foF2 and hmF2 and their implications for HF radio propagation, Radio Science 9, #9/9, 749, 1974.

Shimazaki, T : "World-wide daily variations in the height of the maximum electron density of the ionospheric F_2 layer", Journal Radio Research Laboratory, 2, pp 518-533, 1955

Tedd, B L, Strangeways, H J and Jones, T B : Systematic ionospheric electron density tilts (SIT) at mid-latitudes and their associated HF bearing errors, Journal of Atmospheric and Terrestrial Physics, 47, #11,1085, 1985.

Teters, L R , Lloyd, J L, Haydon, G W and Lucas, D L : "Estimating the performance of telecommunication systems using the ionospheric transmission channel: Ionospheric communications and prediction; programme-user's manual", U.S. Department of Commerce, National Telecommunications and Information Administration, Boulder, Colorado, NITA Report 83-127, IONCAP, 1983

Titheridge, J E : " The use of the extraordinary ray in the analysis of ionospheric records", Journal of Atmospheric and terrestrial Physics, 17, 110, 1959.

Titheridge, J E: "Ionogramme analysis with the generalized programme POLAN", World Data Centre A for Solar-Terrestial Physics, Report UAG-93, 1985

Wait J R : "A note on Antipodal Focusing", N.B.S. Technical Note 182, August 1963.

Westover, D E: "Exact ray path solutions for a quasilinear ionosphere", Marconi Review, 40, pp 172-196, 1970

Wright, J W : Ionogram inversion for a tilted ionosphere, Radio Science, Vol. 26, No. 6, pp 1175 - 1182, November - December 1990.